Piazzi

Final Report

DSE group 20

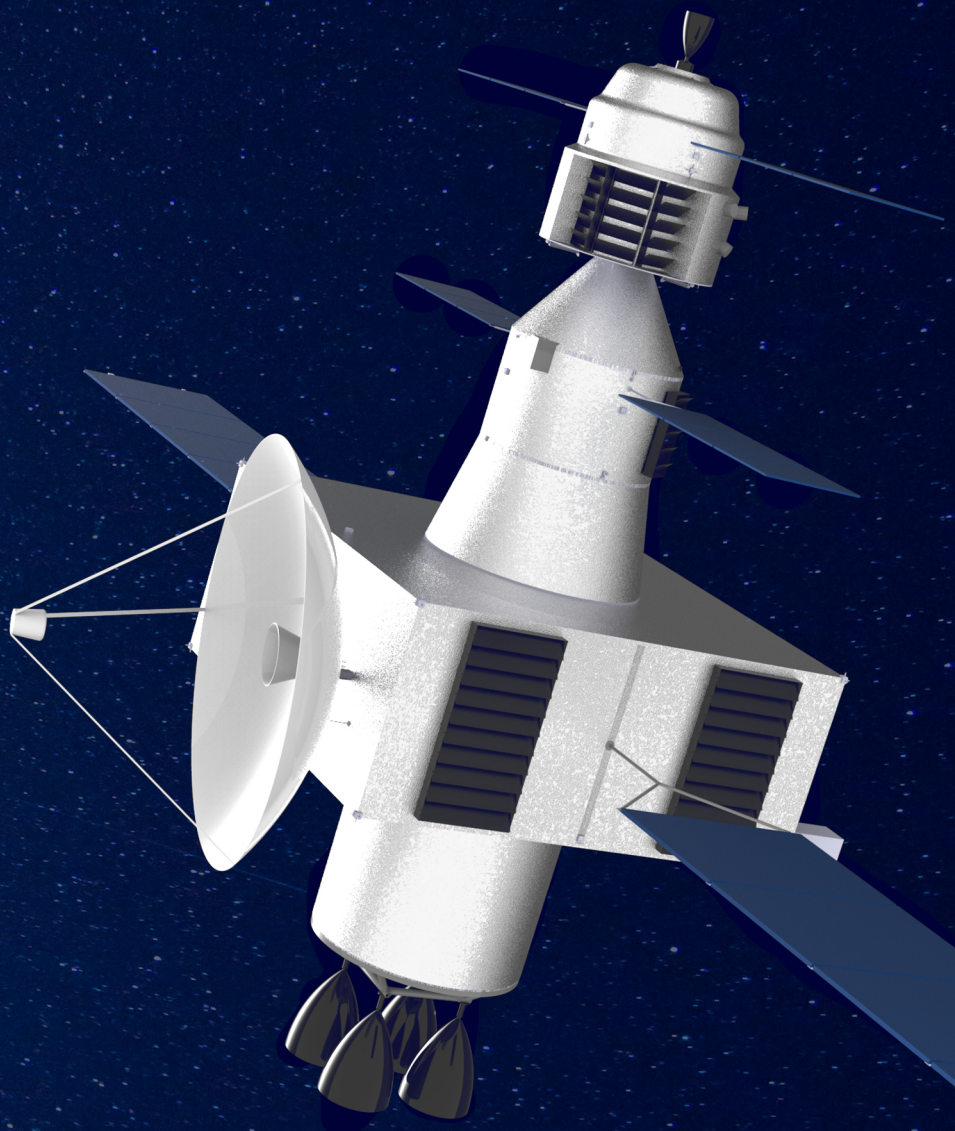

Technische Universiteit Delft

TU Delft

Piazzi

Final Report

by

DSE group 20

to obtain the degree of Bachelor of Science
at the Delft University of Technology.

Group members:	Angyal, Z.	
	Doppenberg, W.	
	den Hertog, K.	
	Kasteel, A.	
	Knoops, S.	
	Losch, L.	
	Lucas, V.	
	Martens, B.	
	de Roos, A.	
	Van den Abbeele, B.	
Project duration:	April 23, 2018 – July 5, 2018	
Tutor:	Schrama, E.	TU Delft, supervisor
Coaches:	Pallichadath, V.	TU Delft
	Lan, H.	TU Delft
Organisation:	TU Delft	
	Faculty of Aerospace Engineering	

Preface

Research into asteroids happens more and more and it has the potential to find answers to fundamental research questions. These include questions about the formation of our Solar System, and whether or not the building blocks of life on Earth originated from outer space. Furthermore, it has practical implications. Near-Earth Objects form a major threat to life on Earth, and in order to effectively protect humanity from this danger, the asteroids have to be studied carefully and their composition determined in detail.

For this reason we set out to develop a space mission which will be able acquire a sample from an asteroid and bring it back to Earth for investigation. The mission was developed using Systems Engineering methodology, and will deliver high-quality result. We came together as part of our bachelor education in the field of Aerospace Engineering, and with this project hope to successfully complete this phase of our studies. Having started the project on the 23rd of April, we went through a planning and a conceptual design phase, upon which we entered the midterm phase of the project, during which concepts were worked out and traded off against each other. In this document the final phase of the DSE project is reported, in which the chosen concept was worked out in more detail. This report marks the end of the project, and serves as the completion of our bachelor Aerospace Engineering at Delft University of Technology.

For this project we have received help from our tutor, coaches and external experts. Therefore we would like to thank Dr Schrama, our project tutor, and our coaches, Dr Lan and Ir Pallichadath, for their guidance, expertise and input on this project. Furthermore, we would like to thank Dr Stam, Dr Müller, Dr Bagnulo, Prof. De Pater, and Dr Cazaux for their input on their respective fields of expertise. We would like to give a special thank you to Dr Schwehm, for giving us valuable insight into the successes and problems of the Rosetta mission, and to Dr Knott, for providing us with contacts and overall support. Finally we would like to acknowledge the organising committee of the Design Synthesis Exercise for the organisation of the project, and the Project Management and Systems Engineering group for their advice in that area.

DSE group 20
Delft, 1 July 2018

Zalán Angyal Wouter Doppenberg Koen den Hertog Arthur Kasteel Stefan Knoops

Lex Losch Valentin Lucas Bruno Martens Andreas de Roos Bert Van den Abbeele

Executive summary

In this report the design of the Piazzi mission is explained. Piazzi is a mission to the 1989 UQ asteroid, with the goal of collecting a sample and returning it to Earth. This will be accomplished by sending a spacecraft to the asteroid, which will consist of three separate spacecraft. Firstly the orbiter, which houses the instruments needed to observe and map the asteroid, and the primary propulsion and communications systems. Then two spacecraft will detach from the orbiter, and each collect a sample in a distinct manner. One, ACSAL, will land on the asteroid, and collect a core sample using a drill. The other, SASH, will hover above the surface, and collect a regolith sample. Both ACSAL and SASH will return to Earth individually, shoot off a reentry capsule with the sample and burn up in the atmosphere themselves.

This report starts with a market analysis, investigating the return on investment that is to be expected. Since Piazzi is a purely scientific mission, this return will not have a monetary value, but rather a scientific one. In order to determine the scientific value, comparable completed, ongoing, and planned missions to asteroids have been analysed. Past missions analysed were NEAR Shoemaker, Deep Impact, Rosetta, and Hayabusa. Ongoing missions analysed were OSIRIS-REx and Hayabusa 2, and planned missions analysed were the Asteroid Redirect Mission and Psyche. From this analysis it could be concluded that the scientific value is high, due to the unique combination of drilling into the surface (Rosetta), gathering more than 50 $[g]$ of material at multiple surface sites and bringing the sample back, allowing more extensive research to be conducted on the sample.

In order to design the Piazzi mission, its need statement and the project objective statement have to be determined. These are, respectively, "Provide an analysis of the composition of Near-Earth Objects in order to assess the threat they pose to humankind." and "Design an unmanned satellite mission whereby you fly to an Earth orbiting asteroid, collect a sample and possibly return it to Earth for further analysis at a cost of 1 billion euros, by 10 students in 10 weeks time." To accomplish this, concepts were created and a trade-off was performed between them, to determine the best concept. The winning concept was to have two separate landers, that each collect a sample in their own way and return to Earth individually. The sample will reenter in a capsule, and the rest of spacecraft will burn up in the atmosphere. The target asteroid was determined to be 1989 UQ, a BC type asteroid, with a radius between 309 and 609 $[m]$, and a maximum separation from Earth of 2.16 $[AU]$.
For every mission it is vital that the requirements are met, and that they are verified and validated. This is shown in a compliance matrix, where for each requirement the verification method is stated, and whether or not it has been met. For the Piazzi mission design, every requirement has been met.

For the design of the Piazzi mission, sustainability has been taken into account for all the phases of the mission. It starts with the phase previous to the launch, where the manufacturing is done in such a way that it produces the least amount of toxic waste possible. For the launch phase, it will be made sure that the upper stage is put in a graveyard orbit, and that it will not collide with the earth or the moon in the future.
For a sustainable space mission, it is vital to comply with COSPAR regulations. First of all, due to the combination of galactic and solar cosmic radiation, high, low or changing temperatures and very high vacuums on very old surfaces, it can be concluded that no life or traces of life can survive on the asteroid, therefore contamination of Earth will not be a problem. Furthermore, the orbiter will be brought into an orbit around the sun, to avoid a possible collision with the asteroid. Reentry is planned in such a way that the ACSAL and SASH will completely burn up in the atmosphere, leaving only the capsules to land on Earth.
Special attention to sustainability is payed in the EPS, where no RTGs will be used, in order to avoid contamination of Earth's atmosphere with a possible launch failure. Finally, a plan has been devised to deal with sustainability in the design, giving a logical sequence of steps to be taken.

The functions that the system will have to perform were analysed, and put into a Functional Flow Diagram. Furthermore, the total mass of the combined spacecraft is estimated to be 1504 $[kg]$, and the combined average power consumption 607 $[W]$. The cost for the Piazzi mission, estimated using the SSCM and QuickCost estimating methods, comes out to 750 [€M] (FY 2018), which includes the 52 million euro launch cost for the Falcon 9, and an operational cost of around 10 million euro per year that the mission is active.

The mission time line spans five years. It starts with the launch on 18 September 2025 and a 67-week transfer to the asteroid. At a distance of 6,000 $[km]$ from the asteroid, the spacecraft will bring its relative velocity with 1989 UQ down, and preliminary mapping will start, which takes 19 weeks. After this, Piazzi will enter orbit around the asteroid, at a height of 600 metres, and

the detailed mapping phase will start, and take a bit more than 2 years. Finally, first ACSAL will detach and collect a sample, and then SASH. On 4 June 2029, the lander and hoverer will start their return to Earth, and the capsule with the sample shall reenter the atmosphere 64 weeks later.
To analyse the astrodynamics of the mission GMAT was used. This program makes accurate simulations of orbits, including finite burns and perturbations. This results in a 441-day inbound journey, with a launch on 18 September. When the spacecraft is at a distance of 5,000 $[km]$ from the asteroid, it will start with preliminary mapping. Over the course of 140 days, the spacecraft will come close to the asteroid, to eventually enter a 600 $[m]$ orbit on 29 April 2027, when the formal observation and mapping phase will start. During this phase the orbiter alternates between mapping, and sending the data back to Earth. Extra attention will be paid to potential sampling sites, in order to prepare the landing and hover. A week before the departure window sample acquiring will take place, afterwards the ACSAL and SASH will return to Earth, on 1 June 2029.
The choice of launcher changed from Atlas V during the midterm phase to Falcon 9 for the final design in this report. This switch was possible because of the lower mass of the spacecraft, leading to lower launch cost.
Reentry of the samples is done with separate capsules, the same as taken on Hayabusa. They were chosen because they meet the dimensional constraints. The reentry of the capsules was simulated using a discrete system of dynamic motion equations, in order to obtain an indication of the landing site of the capsules. It was determined that from the the point of entering the atmosphere at a height of 120 $[km]$, the capsules will travel a distance of approximately 930 $[km]$.

The Piazzi mission consists of three spacecraft that each perform their own mission objectives. The orbiter is used to transport ACSAL and SASH towards the asteroid, and to provide a detailed analysis and mapping of the asteroid. For this tasks, it is equipped with a camera, magnetometers, and spectrometers in different energy regimes: UV, IR-VIS, X-ray, and gamma and neutron rays.
ACSAL will land on the surface of the asteroid, and use a drill to acquire a sample. The drill will collect a core sample of grams, from a depth of 10 centimetres. For the landing it will be equipped with three landing legs, attached to a platform below the main module of the lander. The legs absorb the force of the impact, and with their nail-like feet 'claw' into the asteroid, providing torsional support. In order for the lander to stay on the asteroid, three harpoons will be deployed. They provide the force necessary to keep the lander attached to the asteroid during drilling.
Finally, SASH will hover above the surface, and collect a regolith sample using a grabber mechanism. This mechanism is located at the end of a robotic arm, which lowers the sample collection box to the surface, and secures the sample container into the the return capsule.

The subsystems that make up the busses of the spacecraft are of vital importance to the mission success, and for support of the payload. For each of the subsystem requirements have been set, and every subsystem is designed according to its requirements.
The structural subsystem forms the backbone of the spacecraft. It is designed to safely distribute the launch and propulsive loads throughout the subsystems, without anything failing. It also provides mounting points for all the subsystems, as well as the connectors between the individual spacecraft. The primary structure, which carries the loads, consists of standardised cylindrical sections, made of aluminium. The secondary structure is also made from aluminium, consisting of rigidly connected flat and honeycomb panels.
The electronic power system (EPS), provides power to the payload and the other subsystems. Power generation is done by using solar panels, which have an area of 2.6 $[m^2]$, 0.8 $[m^2]$, and 0.6 $[m^2]$, for the orbiter, hoverer, and lander respectively. The solar panels are sized based on average power consumption. Different operational modes were analysed, and where possible the batteries will provide the additional required power during peak loads, with them being recharged in the intervals between high power consumption.
Propulsion for the orbiter will be performed with four bipropellant engines, capable of providing a total ΔV of 1.1 $[km/s]$. The hover and the lander are both equipped with one monopropellant engine, providing the 0.8 $[km/s]$ needed to return to Earth.
The ADCS system is designed to be as sample, yet effective as possible. The components of the system are the same for each of the three spacecraft. Star sensors and gyroscopes will be used for attitude determination, with coarse sun sensors as a back-up option. Control of the spacecraft's attitude will be done using cold gas thrusters, with reaction wheels taken on the orbiter and hover, since they need to have really accurate attitude control. Orbital determination is done by analysing the time it takes for a dedicated signal to reach the spacecraft and return, and when in orbit around the asteroid additional landmark observation is used. Control of the orbit is done with the main propulsion system for large burns, and small trajectory corrections will be performed by the cold gas thrusters of the ADCS system.
The thermal subsystem is designed to keep the spacecraft internal temperature in a range between 10 and 30 $[°C]$, with a strive temperature of 20 $[°C]$. This is done by coating each of the spacecraft with an insulation coating, and employing a combination of radiators and louvers to radiate excess heat into space. A couple of subsystems need to be cooled exceptionally, for which Peltier cooling systems are used, capable of decreasing the temperature accordingly.
The TT&C system of the orbiter is equipped with a high gain parabolic antenna to communicate with Earth, with a minimum

data rate of 20 [$kbit/s$], and two low gain dipole antennas to communicate with ACSAL and SASH, with a minimum data rate of 1.1 [$kbit/s$], while additionally being for back-up communication with Earth. A much higher data rate can be achieved with the high gain antenna when pointing carefully at Earth. The lander and hover are each equipped with the same low gain antenna as can be found on the orbiter.
On board processing is done by the CD&H system. For the orbiter in total 57 [kB/s] of data is handled, using around 355000 lines of code, and it has a required storage of 3.56 GB, including redundancy the on board storage equals 2 times 7,2 GB. The Cube Computer was chosen as the CPU for this spacecraft, based on the requirements. Since it has a incredibly low mass, cost, and power usage, it is also used in the lander and the hoverer. Some of the tasks that have to be performed by the spacecraft, like landing, need instant feed-back. For this reason, the CD&H system is designed for a high level of autonomy.

Once the spacecraft had been designed, risks could be analysed. The analysis starts with the planning of risk management. After this risks associated with the mission, and each of the individual spacecraft have been identified and given a score between 1 and 4 on probability and severity. This was shown graphically in a risk matrix. Mission risks include technical, cost, schedule, and programmatic risks. For each of the spacecraft, technical, cost and schedule risks were identified. Ones all the risks had been identified and given a score, risk mitigation strategies could be designed. Their aim is to lower the probability or severity (or both) of the risks. Only the most severe or probable risks need to be mitigated.

Connected to risk is the RAMS analysis (reliability, availability, maintainability, and safety). User requirements specify the reliability of the system, therefore this aspect was considered extra careful. The launchers reliability was determined from official data, which gives a 96% reliability. To analyse the reliability of Piazzi a Fault Tree Analysis was performed. They show things that can go wrong, and how this will lead to failure of a system, or the whole mission. Aspects considered in the Fault Tree Analysis are failure modes of the components, its life time, redundancy, and failure rate. This is all combined into a reliability.
Because Piazzi is a interplanetary space mission, maintainability can be neglected. This leads to availability being a function of purely the reliability, meaning this is not elaborated upon.
Safety is mainly taken into account during manufacturing, launch, and reentry. A distinction is made between the safety of human beings, the safety of systems, and the safety of the environment. The first point is the most important, therefore special attention is paid to it.

The spacecraft design itself is not the only thing that has to be considered when designing the Piazzi mission. The first of these additional aspects is the logistics of the project. This starts with manufacturing, where proper planning is of vital importance to make this process as cheap and efficient as possible. The same is true for testing, which has to be done carefully to ensure functioning of all the systems. Furthermore, assembly has to be done on time, and the same is true for the launch preparations. Missing the launch date will lead to a delay of almost 6 years. But planning is not the only aspect of the logistics that has to be considered. For the manufacturing, testing, and operations facilities are needed, that either have to be rented or built. Also, bandwidth on the DSA network has to be reserved for operations. Finally, retrieval of the capsules has to be planned.

For the production of the subsystems different materials are used, of which the main ones are titanium, aluminium, composite, pyrotechnics, and honeycomb. For each of these materials the main problems with their production are explained and dealt with.

Finally the operations for the mission are discussed. For both the preparation of the ground segment and the execution of the mission technicians and engineers are needed, and proper management is of vital importance.

The last part of this report is the planning for the post-DSE time. This is divided into three phases: development, manufacturing, and operations. For each phase multiple workpackages have been set up, that have been subdivided into tasks. The workpackages and tasks are represented graphically in a design & development logic diagram, and are scheduled in a Gantt chart.

To conclude this report the following recommendations were given for the future design process.

- Iterations should be performed on the design.
- Concurrent design strategies should be implemented.
- Industry should be consulted to get more accurate estimates on mass, cost, power, and other design parameters.

Contents

Executive summary iv

List of Tables ix

List of Figures x

List of Symbols xii

List of Abbreviations xv

1 Introduction 1

2 Market Analysis 2
2.1 Completed missions . . . 2
2.2 Ongoing missions . . . 2
2.3 Planned missions . . . 3
2.4 Conclusion . . . 3

3 Project overview and system design 4
3.1 Project definition . . . 4
3.2 Concept trade-off midterm phase . . . 4
3.3 Asteroid 1989 UQ . . . 5
3.4 Verification and validation . . . 5
3.5 Compliance matrix . . . 7

4 Sustainability 13
4.1 Requirements on sustainability . . . 13
4.2 Sustainability in the mission phases . . . 13
4.3 Sustainability in the electrical power system . . . 14
4.4 Sustainability plan . . . 15

5 Final design overview 16
5.1 Functional analysis . . . 16
5.2 Technical Budgets . . . 16
5.3 Cost analysis . . . 16

6 Mission Overview 20
6.1 Astrodynamics . . . 20
6.2 Asteroid mission phase . . . 24
6.3 Launcher . . . 26
6.4 Reentry . . . 27
6.5 Sensitivity analysis . . . 28

7 Spacecraft 31
7.1 Orbiter - Piazzi . . . 31
7.2 Lander - ACSAL . . . 38
7.3 Hoverer - SASH . . . 49

8 The Spacecraft Subsystems 61
8.1 Structural Design . . . 61
8.2 Electronic Power Subsystem . . . 65
8.3 Propulsion . . . 74
8.4 Attitude determination and control system . . . 76
8.5 Thermal control . . . 81
8.6 Telemetry, Tracking and Command . . . 87

8.7 Command and data handling system 91

9 Technical Risk Assessment 97
9.1 Risk planning 97
9.2 Risk identification & assessment 97
9.3 Risk mitigation 99

10 RAMS Analysis 102
10.1 Reliability 102
10.2 Availability, maintainability and safety 107

11 Operations & Production 111
11.1 Logistics 111
11.2 Production plan 112
11.3 Operations 114
11.4 Sensitivity Analysis 115

12 Project design & development 116
12.1 Project design & development logic. 116
12.2 Gantt chart for post-DSE phases 116

13 Conclusion & recommendations 119

Bibliography 120

Appendices A-i

A Appendix Functional flow diagrams and functional breakdown diagrams A-i

B Appendix Work division ix

List of Tables

3.1 Final Trade-Off Matrix . . . 5
3.2 Verification and Validation Methods . . . 6
3.3 Compliance matrix user requirements . . . 7
3.4 Compliance matrix system & subsystem requirements . . . 8

5.1 Mass budget of the Piazzi spacecraft . . . 16
5.2 Power budget of the Piazzi spacecraft . . . 16
5.3 Values used for the first spacecraft cost estimation method . . . 18

6.1 Parameters used in GMAT . . . 24
6.2 GMAT parameters of 1989 UQ . . . 24

7.1 Overview of Instruments on the Orbiter . . . 32
7.2 Overview of the Orbiter . . . 33
7.3 Observation instruments to be used on board of the Piazzi spacecraft . . . 37
7.4 Observation instrument data rate. . . . 37
7.5 Overview of the Instruments on the Lander . . . 39
7.6 Overview of ACSAL's subsystem characteristics. . . . 40
7.7 Properties of the drills . . . 44
7.8 Mass count of the landing mechanism . . . 48
7.9 Overview of the Instruments on SASH . . . 51
7.10 Overview of SASH . . . 53
7.11 Length of mechanism member . . . 55
7.12 Main information about the sample mechanism . . . 59

8.1 Properties for structural materials . . . 63
8.2 Values for EPS sizing . . . 66
8.3 Overview of the power demand per component for the orbiter . . . 68
8.4 Sizing results for EPS components of the orbiter . . . 69
8.5 Sizing results for EPS components of SASH. . . . 69
8.6 Sizing results for EPS components of ACSAL. . . . 71
8.7 Dimensions of the inside tank . . . 75
8.8 Overview of sensors . . . 80
8.9 Cold gas masses and volumes required. . . . 81
8.10 Operational temperature ranges of the lander and hoverer. . . . 82
8.11 Comparable asteroid characteristics . . . 83
8.12 Sizing parameters of the TT&C subsystem for the orbiter, SASH, and ACSAL. . . . 89
8.13 CDHS component requirements. . . . 95

9.1 Probability levels, limits and numbers . . . 97
9.2 Severity of consequences . . . 97
9.3 General mission risk assessment matrix . . . 98
9.4 Spacecraft specific risk assessment matrix . . . 100
9.5 General risk assessment matrix, with mitigation taken into account. . . . 101
9.6 Spacecraft specific risk assessment matrix, with mitigation taken into account. . . . 101

10.1 FMECA Worksheet of the orbiter. . . . 103
10.2 FMECA sorksheet of the lander . . . 106

11.1 Several materials allocated component . . . 112

List of Figures

3.1 Sensitivity Analysis Final Trade-off . . . 5
3.2 Piazzi Mission Overview . . . 5

4.1 Sustainability plan . . . 15

5.1 Cost Breakdown Structure for the total life cycle cost of the Piazzi mission . . . 17

6.1 Mission time line for the Piazzi mission . . . 20
6.2 Trajectory of the Lander Before Reentry . . . 23
6.3 Asteroid Mission Phase . . . 25
6.4 Falcon 9 C3-energy vs. Payload . . . 27
6.5 Hayabusa reentry capsule . . . 27
6.6 Free body diagram of Earth reentry . . . 28
6.7 Velocity vs height for the reentry of the capsule . . . 29
6.8 Height vs horizontal distance for the reentry capsule . . . 29
6.9 Reentry velocity vs time for the model developed for this mission . . . 29
6.10 Reentry velocity vs time (among other trends) for the validation model . . . 29

7.1 Orbiter Architecture (The outer skin has been left out for clarity.) . . . 31
7.2 The Architecture Block Diagram of the Orbiter . . . 34
7.3 The Mission Time line of the Orbiter . . . 34
7.4 Software-hardware collaboration on board of the orbiter. . . . 35
7.5 Lander architecture, the protective skin has been left out for clarity. . . . 38
7.6 Block Diagram of the Lander . . . 41
7.7 Mission profile of the lander . . . 42
7.8 Software-hardware collaboration on board of ACSAL. . . . 42
7.9 Drill mechanism . . . 43
7.10 Drill tower dimensions . . . 45
7.11 Free body diagram of a landing leg. . . . 47
7.12 SASH's architecture, the outer skin has been left out for clarity. . . . 50
7.13 Block diagram of SASH . . . 52
7.14 Mission time line of SASH . . . 52
7.15 Software-hardware collaboration on board of SASH. . . . 54
7.16 Actuators of the sample acquiring mechanism . . . 55
7.17 Retracted mechanism of the SAM. . . . 56
7.18 First procedure of initial positioning of the sample arm. . . . 56
7.19 Second procedure of initial positioning of the sample arm. . . . 56
7.20 Third procedure of initial positioning of the sample arm. . . . 56
7.21 Closed SAM container. . . . 57
7.22 Opened SAM container. . . . 57
7.23 First rotation for placing the sample container in the SRC. . . . 57
7.24 Second rotation for placing the sample container in the SRC. . . . 57
7.25 Container about to enter the SRC . . . 58
7.26 Final position of SAM with respect to the SRC . . . 58
7.27 Crushing disk of SAM . . . 58
7.28 Render of the SRC with the SAM in front. The SRC box is opened, as upon Earth return. One panel is hidden for visibility. . . . 59

8.1 Simplified three-element model for analysis of the primary structure. . . . 63

8.2 Impression of the high gain antenna unfolding mechanism . . . 65
8.3 Power requirements for the operational modes of SASH. . . . 70
8.4 Power requirements for the operational modes of ACSAL. . . . 71
8.5 Electrical Power System Design Options . . . 72
8.6 Electrical block diagram for the orbiter . . . 72
8.7 Electrical block diagram for ACSAL . . . 73
8.8 Electrical block diagram for SASH . . . 73
8.9 Architecture of main propulsion system . . . 75
8.10 Fuel tank dimensions . . . 76
8.11 Graphic representation of the descent trajectory. . . . 78
8.12 Graphic representation of detail of last part of descent trajectory. . . . 79
8.13 Communication diagram of the ground and space segment of Piazzi. . . . 88
8.14 Data rate and signal-to-noise ratio for the uplink between SASH and the orbiter. . . . 90
8.15 Data rate and Signal-to-Noise Ratio for the uplink between SASH and the orbiter . . . 91
8.16 Uplink data rate between SASH and ground station. . . . 92
8.17 Downlink data rate between SASH and ground station. . . . 93
8.18 CDHS architecture of the space segment. . . . 96

10.1 FTA symbols. . . . 104
10.2 Fault tree analysis diagram of the orbiter . . . 105
10.3 Fault tree analysis diagram of ACSAL. . . . 109
10.4 Fault tree analysis diagram of SASH. . . . 110

11.1 Rolling machine . . . 113
11.2 Stretch forming process illustration . . . 113
11.3 Deep drawing process overview. . . . 114

12.1 Block diagram of the project design & development logic . . . 117
12.2 Gantt chart of the schedule of the post-DSE design and development. . . . 118

A-1 Functional flow diagram of the Piazzi mission. . . . A-ii
A-2 Functional flow diagram of the Piazzi mission. . . . A-iii
A-3 Functional breakdown structure of the design of the spacecraft. . . . A-iv
A-4 Functional breakdown structure of the manufacturing process of the spacecraft. . . . A-v
A-5 Functional breakdown of the transport process of the spacecraft. . . . A-v
A-6 Functional breakdown of the launch of the spacecraft. . . . A-vi
A-7 Functional breakdown of the travel process of the spacecraft to the asteroid. . . . A-vi
A-8 Functional breakdown of the rendezvous phase of the spacecraft. . . . A-vii
A-9 Functional breakdown of the scientific research. . . . A-viii
A-10 Functional breakdown of the end of life process of the spacecraft. . . . A-viii

List of Symbols

Symbol	Definition	Unit
α	Eccentric anomaly	rad
	Rotational acceleration	$\frac{rad}{s^2}$
α_{Bond}	Bond albedo factor	–
γ	Flight path angle	rad
ΔV	Delta V	$\frac{m}{s}$
ϵ	Asteroid emittance	–
ζ	Angular position of satellite over orbit	rad
η	Efficiency	–
	NEATM-model parameter	–
η_{DA}	Design & Assembly efficiency	%
η_{deg}	Degradation factor	%
η_{sc}	Solar cell efficiency BOL	%
η_T	Temperature efficiency	%
θ	True anomaly	rad
$\theta_{1/2}$	Halfwidth beam angle	rad
λ	Wavelength	m
μ	Gravitational parameter	$\frac{m^3}{s^2}$
ρ	Density	$\frac{kg}{m^3}$
ρ_{Ast}	Asteroid density	$\frac{kg}{m^3}$
ρ_{Harp}	Harpoon density	$\frac{kg}{m^3}$
σ	Stefan-Boltzman constant	$\frac{W}{m^2K^4}$
σ_y	Yield strength	MPa
σ_z	Normal stress	MPa
τ	Shear stress	MPa
ω	Angular velocity	$\frac{rad}{s}$
a	Semi-major axis	m
a_i	Linear acceleration of ith member	$\frac{m}{s^2}$
A	Bond albedo	–
	Cross-sectional area	m^2
$A_{radiated}$	Radiated surface	m^2
A_{total}	Total area	m^2
B	Bandwidth	Hz
	Ballistic coefficient	–
B_R	Bitrate	dB
c	Speed of light	$\frac{m}{s}$
C	Specific heat capacity	$\frac{J}{mK}$
	Constant	–
	Cost	k$
		k€
C_3	Characteristic Energy	km^2/s^2
$C_{battery}$	Battery capacity	Wh
C_D	Drag coefficient	–
C_L	Lift coefficient	–
d	Diameter	m
	Horizontal offset	m
$d_{sol,max}$	Maximum distance from Sun	AU

D	Diameter	m
	Penetration depth	m
DL	Design lifetime	$months$
e	Eccentric anomaly	–
E	Elasticity modulus	GPa
	Energy	J
f	Frequency	Hz
F	Force	N
	Driving force	N
F_n	Normal force	N
F_{normal}	Normal force	N
F_{view}	Visibility factor	–
FTE_{eng}	Labour cost per engineer	$\$K$
G	Antenna gain	W
G_r	Receiver gain	dB
G_t	Transmitter gain	dB
g	Gravitational acceleration	$\frac{m}{s^2}$
g_0	Earth gravitational acceleration	$\frac{m}{s^2}$
h	Vertical height of leg	m
	Height	m
h_{orbit}	Orbital height of the satellite	m
HB	Brinell Hardness	MPa
I	Area moment of inertia	m^4
J	Mass moment of inertia	kgm^2
I_{sp}	Specific Impulse	$\frac{m}{s}$
J_{Alb}	Albedo irradiance	$\frac{W}{m^2}$
J_{emit}	Radiated energy	W
k	Boltzmann constant	$\frac{J}{K}$
	Bessel differential function	–
	Axial stiffness constant	$\frac{N}{m}$
k_t	Torsional spring constant	$\frac{N}{rad}$
l	Length	m
L	Projectile length	m
L_{atm}	Atmospheric loss	dB
L_{ll}	Line loss	dB
L_s	Space Loss	W
m	Mass	kg
$\dot{m}$	Mass flow	$\frac{kg}{s}$
m_i	Initial mass	kg
m_f	Final mass	kg
M	Mass	kg
	Mean motion	rad
M_{hinge}	Hinge moment	Nm
n	Transmission efficiency battery to load	$\%$
P	Power	W
P_{avg}	Average power	W
P_d	Daytime power usage	W
P_e	Eclipse power usage	W
P_i	Instantaneous power	W
P_{peak}	Peak power	W
P_{sa}	Solar array power	W
P_t	Transmitting power	W
P_x	Feed force	N
P_z	Thrust force	N
Q	Total energy flow	J

	First moment of inertia	m^3
r	Radius	m
	Distance	m
r_{orbit}	Orbit radius	m
r_{planet}	Planet radius	m
r_{sat}	Distance between the satellite and Sun	m
R	Radius	m
R_e	Earth radius	m
$radius_{ast}$	Asteroid radius	m
s	Damper height	m
S	Surface area	m^2
	Solar radiance	$\frac{W}{m^2}$
	Feed	m/rev
S_{min}	Minimum solar flux	$\frac{W}{m^2}$
SI	Surface Irradiance	$\frac{W}{m^2}$
SR	Surface Radiance	$\frac{W}{m^2}$
t	Time	s
	Thickness	m
t_i	Instantaneous time	s
T	Thrust	N
	Temperature	K
$T_{asteroid}$	Asteroid rotational period	h
T_d	Daytime length	h
T_e	Eclipse length	h
T_s	Noise temperature	K
T_{SS}	Subsolar temperature	K
v	Velocity	$\frac{m}{s}$
v_i	Initial velocity	$\frac{m}{s}$
v_e	Exhaust velocity	$\frac{m}{s}$
v_f	Final velocity	$\frac{m}{s}$
V	Velocity	$\frac{m}{s}$
V_0	Initial velocity	$\frac{m}{s}$
X_d	Direct path efficiency for EPS to individual loads	–
X_e	Path efficiency for EPS through batteries	–

List of Abbreviations

Abbreviation	Definition
ACC	Accelerometer
ACSAL	Asteroid Core Sample Acquiring Lander
ADCS	Attitude Determination and Control System
ALM	Asteroid Landing Mechanism
AMP	Amplifier
AMBR	Apogee Monopropellant Booster Rocket
ASRM	Asteroid Sample Return Mission
CAD	Computer-aided design
CAR	Drill bit caroussel
BAT	Battery
CCD	Charge-Couple Device
C&DH	Command and Data Handling
CDHS	Command and Data Handling System
CFC	ChloroFluoroCarbon
CG	Centre of Gravity
CGT	Cold Gas Tank
CMOS	Complementary Metal-Oxide Semiconductor
COGT	Cold Gas Thruster
COSPAR	Committee on Space Research
DECAM	Descent Camera
DoD	Depth of Discharge
DILG	Digital Laser Gyroscope
DIP	Diplexer
DISUS	Digital Sun Sensor
DRL	Sample Drill
DSA	Deep Space Antenna
DSE	Design Synthesis Exercise
EOL	End of life
EPS	Electrical Power System
EELV	Evolved Expendable Launch Vehicle
EOL	End Of Life
FEM	Finite element method
FMECA	Failure Mode, Effects and Criticality Analysis
FTA	Fault Tree Analysis
FY	Fiscal year
GMAT	General Mission Analysis Tool
GRS	Gamma-Ray Spectroscopy
HAR	Harpoon mechanism
HGA	High Gain Antenna
HSS	High Speed Steel
IADC	Inter-Agency space Debris coordination Committee
IFOV	Instantaneous Field of View
IRU	Inertial Reference Unit
IRVS	Infra-Red and Visual Spectrometer
JGM-3	Joint Gravity Model 3
LAS	Sample Assurance Laser
LEO	Low earth orbit
LGA	Low Gain Antenna
LRO	Lunar reconnaissance orbiter
LVR	Louver system
MMH	Monomethylhydrazine
MOTV	Monopropellant Thruster Valve
MRS	Molecule Remote Sensing
NEA	Near-Earth Asteroid
NEO	Near-Earth Object
NS	Neutron Spectrometer
NTO	Nitrogentetroxide
OBC	Onboard Computer
OCC	Orbit Correction Code
ODC	Orbit Determination and Control
OREWH	Orbiter Reaction Wheels
P	Probability
PCDU	Power Control and Distribution Unit
PHE	Pericentre-hyperbola-earth
PLA	Payload Adapter
PLT	Peltier element
PMSE	Project Management and System Engineering
PN	Probability Number
PV	Photovoltaic
RAD	Radiator
RAM	Random Access Memory
RAMS	Reliability, Availability, Maintainability and Safety
RCS	Reaction Control System
REWH	Reaction Wheels
ROM	Read-Only Memory
RTU	Remote Terminal Unit
S	Severity
SAM	Sample Acquiring Mechanism
SAR	Spacecraft-at-return
SASH	Sample Acquiring Surface Hover
SN	Severity Number
SNR	Signal to Noise Ratio
SOI	Sphere Of Influence
SPM	Sample Push Mechanism
SRC	Sample Return Capsule
STAT	Star Tracker
TCM	Trajectory Correction Manouevre
TRA	Transponder
TOD	Transfer-orbit-departure
TOR	Transfer-orbit-rendezvous
TT&C	Telemetry, Tracking and Command
<TBD>	To Be Determined
TRL	Technology Readiness Level
UVS	Ultra-Violet Spectrometer
V&V	Verification and Validation
XRS	X-Ray Spectrometer

1 Introduction

The research on asteroids in the solar system is an ongoing process with previous and ongoing missions such as Hayabusa I and II, Rosetta, and OSIRIS-REx. The scientific value of these missions continues to expand for the scientific community, because they will bring more information about the origin of the solar system and due to the fact that the society on Earth nowadays becomes more aware of the potential threat of asteroids to the life on Earth. This awareness is translated into numerous scientific programs set up by for instance NASA, who track an ever increasing amount of Near Earth Objects (NEOs) and assess their threat to Earth in the coming century. NASA is currently in the design process of an asteroid deflection mission called DART (Double Asteroid Redirection Test) to be able to access the possibility of redirecting an asteroid's orbit. For them to be able to design a suitable mechanism, information about the asteroid, in terms of composition and other physical parameters, is critical. In addition, as said by Carol Raymond, the NASA's Small Bodies Program manager: *"The materials in asteroids represent the building blocks of the planets,"* meaning that the information gathered from asteroids can help scientists to solve this mystery of the origins of our solar system.

Eager to provide scientific value to the scientific community by designing an Asteroid Sample Return Mission, a group of ten students is in the final design phase. During the previous design phase, three preliminary main targets for the Asteroid Sample Return Mission have been identified and five mission concepts were chosen to enter a trade-off. During that stage, the final target asteroid for the mission has be chosen, being 1989 UQ a carbonaceous chrondrite asteroid, together with the final mission concept.

The final concept is composed of one orbiter, a lander and a hoverer. A launcher will launch all three stacked spacecraft up until transfer orbit towards the asteroid. At orbit around the asteroid the lander and hover will detach from the orbiter and continue completing their own mission objectives. The lander - ACSAL (Asteroid Core Sample Acquiring Lander) is designed to collect a core sample while the hoverer - SASH (Sample Acquiring Surface Hover) will collect a surface sample. Once they collected their sample, they have will return to Earth separately, leaving the orbiter behind. At Earth, the individual spacecraft will let go off a capsule containing the sample, and the spacecraft themselves will disintegrate upon reentry.

This report is structured as follows, starting with the market analysis in chapter 2 where the existence of this mission will be justified. Followed by a project overview and system design, where the project mission is given with a summary of the previous phases of this mission. Next to this, chapter 3 includes a description of the verification and validation process followed throughout the design phase together with a compliance matrix with all the project requirements. chapter 4 addresses sustainability, which should be taken into account during the design process. After this a high level final design overview is provided in chapter 5. Later the astrodynamics, which have been determined with the help of a software tool are presented in section 6.1 with the launcher selection and an explanation on the reentry. Chapter 7 provides a detailed overview of the design for the orbiter, the hover and the lander. Chapter 8 describes the different subsystems needed by every spacecraft and gives a detailed overview on every spacecraft's separate subsystems. This is followed by a technical risk assessment and a RAMS analysis in chapter 9 and chapter 10, respectively. After this in chapter 11 the operations and production of the mission will be discussed, followed by chapter 12 the project design and development with a Gantt chart and an explanation on what will be done after the DSE phase. Finally in chapter 13 a conclusion is provided.

2
Market Analysis

Since Piazzi is a purely scientific mission, there is no commercial reward in the sense of a business opportunity. On the scientific market however, there are quite some competitors, including both completed, ongoing and planned missions. Piazzi is thus only a viable mission concept if it has something unique to offer to add knowledge about the solar system or asteroids in particular. This chapter will evaluate completed missions in section 2.1, ongoing missions in section 2.2 and future missions in section 2.3 and justify the existence of this new mission.

2.1. Completed missions

In 2000, NEAR Shoemaker was orbiting Eros attempting to generate compositional maps on both atom (using its XGRS) and, more detailed, on molecular and mineralogical level. Further, it measured the density of Eros and its gravitational and magnetic field. The difference to Piazzi being not only the target (which is a Silicon-type asteroid), but also the absence of subsurface compositional analysis or an attempt to take a sample and return it for further analysis (Holdridge [2002]).

Deep Impact went to visit the comet Tempel I in 2005, mapping the outer surface and releasing an impactor to try to assess what crater size would result and investigate the subsurface composition. Due to the dust caused by the impact, Deep Impact was not able to view the crater itself, only the impact debris could be analysed (Henderson and Blume [2015]).

Another comet mission was ESA's Rosetta, arriving at 67P in 2014, mapping the surface with IR and UV spectrometers and visual systems, revealing the presence of several types of molecules and minerals. Philae was intended to drill into the surface and analyse the sample in detail using mass spectrometry, microscopy and the surface itself using alpha ray spectrometry. Unfortunately Philae was not able to land properly, thus being unable to conduct (sub)surface measurements, leaving an opportunity for other missions. Additionally to all aforementioned research, also comet-specific investigations were performed (for example on the coma), not being relevant comparison for Piazzi [1].

Hayabusa landed on Itokawa, an asteroid in the same size range as 1989 UQ, in 2005, with on the orbiter a X-ray spectrometer (XRS), an IR spectrometer, visual imaging system and a LIDAR system (see Kawaguchi et al. [1999]). Hayabusa took a sample of the asteroid by collecting surface material after an impactor struck the surface and returned these to Earth. Itokawa however is a S-type asteoroid, in contrast with 1989 UQ, which means that Itokawa is more a rocky asteroid and possibly originating from the same area in the pre-solar system as Earth and Mars. The consequence of Itokawa being approximately the same size as 1989 UQ is, that experience of orbiting and landing can be used for development of Piazzi, saving money and the need to reinvent the wheel.

2.2. Ongoing missions

OSIRIS-REx, led by NASA, is due to arrive at Bennu in August of 2018, then starting the mapping phase to first determine the shape of Bennu, after which mapping in the IR spectrum will be conducted. In the final mapping phase, the XRFS will provide a map of the surface in its elemental constituents. Bennu is, just as 1989 UQ, a BC-type asteroid. The additional gain from Piazzi is then not only enhanced mapping of another BC-type body, with in addition a gamma ray and neutron spectrometer as well as an UV spectrometer, allowing more specific determination of the elementary and chemical composition. Additionally, OSIRIS-REx will only collect a sample of the regolith, whereas Piazzi will collect both a surface and a subsurface sample. Furthermore, since the sample collection mechanism of OSIRIS-REx is rather complex, failures might occur, resulting in not being able to collect a sample. Piazzi will incorporate a highly reliable sample collection mechanism to ensure sample return [2].

Hayabusa 2 will arrive at Ryugu, a carbonaceous chondrite asteroid with phyllosilicate minerals, in June 2018 [3], initiating the mapping phase in visual and IR, allowing to see where for instance water is at the surface; it will not be imaging the asteroid using high energy radiation, such as X-ray, so it would be difficult to have a general image of the elemental distribution on

[1] http://sci.esa.int/rosetta/14615-comet-67p/ Accessed June 5, 2018
[2] https://www.asteroidmission.org Accessed June 4, 2018
[3] http://global.jaxa.jp/projects/sat/hayabusa2/index.html Accessed June 4, 2018

Ryugu. Hayabusa 2 will then release 4 rovers that are able to move around the surface, one will research the surface in the IR band and conduct research on the magnetic field; it is also equipped with a camera. The other landers are equipped with thermal sensors to measure the local temperature variation of Ryugu at different places. Further, Hayabusa 2 will take a subsurface sample and return that to Earth for further analysis. The advantage of Piazzi when compared to Hayabusa 2 is, amongst others the taking of material samples on multiple locations, as well as the elemental imaging and extended molecular imaging on Piazzi.

2.3. Planned missions

NASA had planned to launch the Asteroid Redirect Mission in 2020, to bring back a large piece of an asteroid, being Bennu (from OSIRIS-REx), Itokawa (from Hayabusa) or 2008 EV, being returned to Earth by a manned mission. Unfortunately, due to a presidential act, NASA is forced to focus on manned space mission to the moon and Mars, thus abandoning ARM [4]. Psyche (named after the target) is a NASA mission that is planned for launch in 2023 and after launch is going to visit a 250km diameter asteroid that is mainly composed of iron and nickel. The spacecraft will image the surface with GRS and a multispectral imager, allowing a wide range of metals and minerals to be detected. The reason to go to Psyche is to research the formation of Earth-like planets, especially how the core evolved, whereas Piazzi will try to find more on the solar system's lighter planet formation. Further, Psyche will not attempt a landing on the surface, nor return a sample to Earth or analyse it in situ, thus having lower value to the scientific community than Piazzi (Elkins-Tanton et al. [2014]).

2.4. Conclusion

1989 UQ is composed of carbonaceous chondrites, meaning that it is composed of carbon-like rocks that have not undergone physical alterations since their formation. This gives an unique opportunity to study the composition of the early solar system, since all researched material on Earth has had significant alterations due to erosion or suffered from intense thermal stress during atmospheric reentry. Although several missions to asteroids (and other small bodies) have already taken place, are currently in progress, or are in planning, the unique combination of drilling into the surface (Rosetta), gathering more than 50 $[g]$ of material at multiple surface sites and bringing the sample back is a valuable addition for the understanding of the solar system.

[4] https://www.nasa.gov/content/what-is-nasa-s-asteroid-redirect-mission Accessed June 4, 2018

3
Project overview and system design

In this chapter an overview of the project and the Piazzi mission is given, and the system design is outlined. It starts with defining the mission need and project objective in section 3.1. After this, a summary is given of the concepts considered for this mission and the trade-off between them, and the selection of target asteroid is explained. Then, in section 3.4, verification and validation is discussed. Finally, the requirements on the Piazzi mission are stated in a compliance matrix which also indicates whether they have been met.

3.1. Project definition

In this section, the mission need and project objective of the Piazzi mission are stated, which have been defined in the project plan (Van den Abbeele et al. [2018b]).

Mission need statement

The Asteroid Sample Return Mission has the following need statement.

ASRM-MNS Provide an analysis of the composition of Near-Earth Objects in order to assess the threat they pose to humankind.

Project objective statement

The goal of project is to design a spacecraft capable of performing the following objective.

ASRM-POS Design an unmanned satellite mission that flies to a near-Earth orbiting asteroid, collect a sample and possibly return it to Earth for further analysis at a cost of 1 billion euros, by 10 students in 10 weeks time.

3.2. Concept trade-off midterm phase

In the midterm phase different concepts were explored, and a trade-off between those concepts was made. In this section a summary is given. More information can be found in Angyal et al. [2018].

3.2.1. Considered concepts

Four different concepts were considered in the midterm, with concept 4 subdivided in two subconcepts.

Concept 1 involves a hovering approach, during which no landing on the asteroid will occur. The spacecraft will collect a surface sample from the asteroid, upon which it will return to Earth in its entirety. When it arrives at Earth, a small capsule will detach, which will safely reenter the sample. The rest of the spacecraft will burn up in the atmosphere.

Concept 2 is a highly complex mission. It is composed of one mothership with two landers, that each collects a sample independently in a unique way. One of the landers will land on the asteroid and collect a core sample. The other will hover above the asteroid, and collect a surface sample. Once the sample collection is completed the landers will return to Earth separately, and use the same reentry procedure as concept 1.

In concept 3, a lander stage will be used to land on the asteroid and collect a core sample. After the collection of the sample, the lander will take off and return to Earth, leaving the mothership behind at the asteroid. The reentry will be done in the same way as concepts 1 and 2.

Concept 4 is different from the ones above in the sense that the sample will not be returned to Earth, but analysed in situ. There are two versions to concept 4 that differ in the location of analysis. In concept 4.1, the spacecraft travels to the asteroid, where a separate lander will make the landing, collect a sample, and analyse the sample on the asteroid, whereas in concept 4.2, the lander will return to the mothership, and the sample will be analysed aboard the mothership.

3.2.2. Trade-off

The trade-off performed during the midterm phase of this project is based on several criteria. These are:

- Scientific yield (Weight: 40%), based on analysis location, amount of samples, and types of samples.
- Risk (Weight: 20%), based on risk factor and risk mitigation.
- Mass (Weight: 15%)
- Power (Weight: 10%)
- Technological Readiness Level (Weight: 10%)
- Sustainability (Weight: 5%), based on debris near the asteroid, and on debris in Earth orbit.

Using these trade-off criteria, and giving scores to each of the concepts in a quantitative way, concept 2 came out as the most promising concept. An overview of the trade-off can be found in Table 3.1

Table 3.1: Final Trade-Off Matrix

Criterion / Concept	**Scientific yield** (40%)	**Risk** (20%)	**Mass** (15%)	**Power** (10%)	**TRL** (10%)	**Sus.** (5%)	**Final score**
1	0.40	0.33	0.50	1.00	0.50	0.3	0.47
2	1.00	0.33	0.00	0.00	0.00	0.7	**0.50**
3	0.40	0.33	0.50	0.50	0.00	0.7	0.39
4.1	0.00	0.67	1.00	0.50	0.50	0.7	0.42
4.2	0.30	0.33	1.00	0.50	0.00	0.7	0.42

A summary of the sensitivity analysis of the trade-off can be found in Figure 3.1, and in Figure 3.2 a graphical representation of the Piazzi mission is given. In chapter 5, more information on the mission can be found.

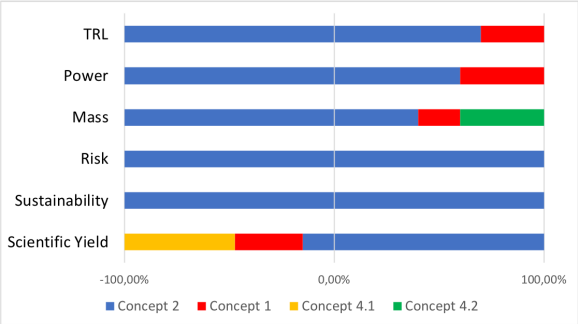

Figure 3.1: Sensitivity Analysis Final Trade-off

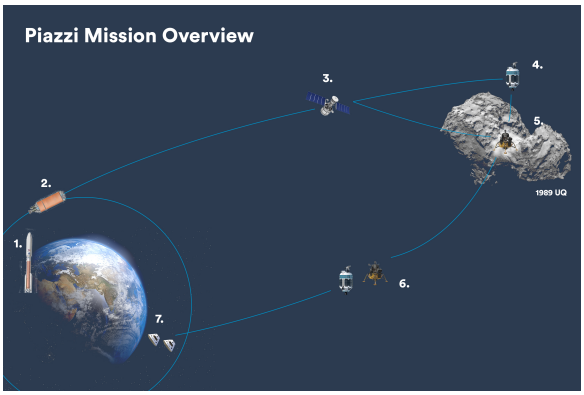

Figure 3.2: Piazzi Mission Overview

3.3. Asteroid 1989 UQ

1989 UQ was the asteroid selected as target for the Piazzi mission. This selection was done based on multiple criteria, including composition, angular velocity, launch window, inbound ΔV and outbound ΔV. These criteria affect the system requirements at a high level since they largely determine the sizing and design for all subsystems. The scientific value of the selected asteroid is of key importance, since this is the return that is at the very core of the mission. Using the NASA Ames Research Center Trajectory Browser (Foster and Frost [2018]) a number of options were found for potential targets that roughly meet the criteria for a potential target asteroid.

A trade-off was performed, based on the criteria explained above, and 1989 UQ came out as the best. It is a BC type asteroid, and based on measurements from infrared spectroscopy it is estimated that it is composed out of hydrogen, iron, nitrogen, and ammonia (Hahn and Mottola [2018]). It has an expected radius between 309 and 609 $[m]$, and is at most 2.16 AU removed from Earth.

3.4. Verification and validation

Verification and validation (V&V) is the process of proving the quality and correctness of a product, and its functionality. In the following sections the V&V process for the Piazzi mission is explained.

3.4.1. About V&V

Verification is the process of checking if a product meets the set of design specifications. It starts during the development phase, where the process is used to make sure the models and simulations used to develop the product are implemented correctly. During the post-development phase, the verification process is used to make sure that the system or subsystem meets the requirements, regulations, or conditions that were set. It specifically checks whether or not the requirements set by the user at the start of the project are met.

Verification is followed by validation. This is the process of ensuring that the product not only meets the requirements, but that it also meets the needs of the user, and that it solves the problem that the project was meant to solve. Validation is also the process that ensures the required accuracy is achieved.

V&V must be done on the lowest hardware and software level possible. The advantage of this is that the process can be simple, and thus that it will cost less. After the individual components or subsystems have been verified and validated, the entire system has to be checked. More on this process will be explained later. The methods that can be used for verification and validation will be explained next.

3.4.2. V&V methods

To verify and validate a product different methods can be used. For verification, these are test, analysis, demonstration, or inspection. To validate, in particular, the requirements, the VALID criteria are used which check if the requirements are Valid, Achievable, Logical, Integral and Definitive. These methods are further elaborated upon in Table 3.2, adopted from Gill [2018]. Two methods for verification are especially useful, namely test and analysis. Testing gives the highest level of certainty, but is almost always the most expensive option. Analysis is a good alternative for testing, except for very complex analyses, such as FEM.

Table 3.2: Verification and Validation Methods

Verification

Test [T]	Test (a representative model of) the product's compliance with requirement under representative conditions
Inspection [I]	Inspect the design documentation or the product to show compliance with the requirement
Demonstration [D]	Establish by operation, adjustment or reconsideration of a test article its compliance with requirement
Analysis [A]	Establish by mathematical or other analysis techniques that the product complies with the requirement

Validation

Verifiable	The requirement is objective, preferably quantified
Achievable	The requirement can be met with available resources
Logical	The requirement is traceable
Integral	The requirement is complete
Definitive	The requirement is unambiguous

For each of the requirements set for this project it will be indicated which method will be used for their verification, by indicating it with the letter respective to the method. Validation of the requirements will be done at their creation. If a requirement is deemed to be not VALID, it will be revisited.

The requirements are not the only features that have to undergo V&V, also the models used for developing the subsystems have to be verified and validated. For models developed by external parties, it has to be checked whether they have been subjected to V&V. If this is not the case, or if the model used has been developed specifically for this project, it has to be verified and validated during this project. Verification can be done by comparing the model with simplified calculations, that give an indication of the scale of the numbers involved. Furthermore, a sanity check can be performed, checking if the numbers make sense, as well as whether or not the response of parameters to variations in other parameters is logical. For this process, it is useful to divide the model into units, and test each unit individually. Once this has been completed, the whole model can be verified, using the same method.
For validation of the model it can be compared to test data, or to an independently validated model, and check if the results are similar. Also, an analysis can be carried out, in order to evaluate potential errors, as well as their impact. Finally the flow of data throughout the model should be evaluated, and at each step it should be checked whether or not the results make sense.

3.4.3. V&V program

Verification and validation for this project will be done in a series of steps. It starts by V&V defining the process, which is done in both this section in this report, and in Angyal et al. [2018]. Then, during the development phase, each individual subsystem, component, and model is verified and validated using the methods described above. The results of this are given in their own respective section of the report.

When production of the components has started its results have to be verified and validated as well. This will be done by acceptance tests, and qualification tests. Acceptance tests check if the product or component is produced to the right standards. It will be subjected to a range of tests, that will determine the quality of the product in different categories, such as thermal or structural performance. Finally the product will be subjected to qualification tests. These test the same elements as the acceptance tests, except for a added margin added to ensure the product can function under even the worst conditions, and to analyse failure modes and weak points in the design.

3.5. Compliance matrix

In order to verify if the design meets all the imposed requirements, two separate compliance matrices are given in Table 3.3 and Table 3.4. First the user requirements are given in Table 3.3 which are all checked with the help of the system and subsystem requirements in Table 3.4. The system and subsystem requirements can be either checked (marked with a ✓), or cannot yet be verified at this stage of the design, these are marked with <TBD>.

Compliance unknown

The requirements which were given a <TBD> are mostly the ones could not have been designed for yet, because for example the testing phase of the concerned systems is still to come. The structure shall be tested on whether it complies with the radiation exposure limits. This is done is the testing phase after the DSE, which is elaborated on in chapter 12. Hence, compliance is still unknown.

Table 3.3: Compliance matrix user requirements (Van den Abbeele et al. [2018a])

Requirement ID	Description	Checked ?
	User requirements	
ASRM-USR-N001	The system shall transfer to the Near-Earth Object.	✓
ASRM-USR-N002	The system shall orbit close to the Near-Earth Object.	✓
ASRM-USR-N003	The system shall analyse the surface composition of the Near-Earth Object.	✓
ASRM-USR-N004	The system shall map the surface of the Near-Earth Object.	✓
ASRM-USR-N005	The system shall provide data to locate a sampling area.	✓
ASRM-USR-N006	The system shall collect a sample from the Near-Earth Object.	✓
ASRM-USR-N007	The design of the system shall be finished within 11 weeks.	✓
ASRM-USR-N008	The design of the system shall be performed by 10 students.	✓
ASRM-USR-N009	The selected Near-Earth Object shall be unique.	✓
ASRM-USR-N010	The system shall survive the launch with a probability of at least 90%.	✓
ASRM-USR-N011	The system shall survive the transfer to the Near-Earth Object with a probability of at least 80%.	✓
ASRM-USR-N012	The system shall be produced according to safe working procedures.	✓
ASRM-USR-N013	The system shall comply with COSPAR regulations (Rummel [2011]) on contamination of Near-Earth Objects.	✓
ASRM-USR-N014	The system shall not make use of radioisotope thermoelectric generators.	✓
ASRM-USR-N015	All systems and subsystems used shall have a Technology Readiness Level of at least 6.	✓
ASRM-USR-N016	The total system cost shall not exceed 1 billion [€] FY18.	✓
ASRM-USR-N017	The budget shall consider 30 years of support by ESA and/or NASA.	✓
ASRM-USR-R002	The system shall return a sample to Earth.	✓
ASRM-USR-R003	The system shall allow for the sample to be retrieved from the system.	✓
ASRM-USR-R004	The system shall return to Earth with a probability of at least 50%.	✓
ASRM-USR-R005	The system shall comply with COSPAR regualations regarding contamination of Earth.	✓

Table 3.4: Compliance matrix system & subsystem requirements

Requirement ID	Description & section	Checked ?
	Sustainability requirements in section 4.1	
ASRM-SUS-001	The spacecraft shall not use radioisotope thermoelectric generators.	✓
ASRM-SUS-002	The mission shall archive which material the spacecraft are made of.	✓
ASRM-SUS-003	The spacecraft shall be passivated at the end of its mission.	✓
ASRM-SUS-004	The mission shall document the spacecraft and debris trajectories.	✓
ASRM-SUS-005	If the spacecraft or orbital stages pass through the LEO region, or have the potential to interfere with the LEO region, they shall be de-orbited.	✓
	ADCS in subsection 8.4.1	
ASRM-ADC-001	The ADCS shall provide a pointing accuracy of 1.6 [°].	✓
ASRM-ADC-002	The ADCS shall be able to determine the attitude of the spacecraft for rotation rates smaller than 5 $[°/s]$.	✓
ASRM-ADC-003	The ADCS shall eliminate jitter sufficiently to avoid blurring of sensor data.	✓
ASRM-ADC-004	The ADCS shall limit spacecraft drift to less than 1 $[°/hour]$.	✓
ASRM-ADC-005	The ADCS shall be able to provide a rotation rate of at least 20 $[°/s]$ around any axis	✓
ASRM-ADC-006	The ADCS shall be able to control the spacecraft's attitude during main engine burns.	✓
ASRM-ADC-007	he ADCS shall be able to rotate the spacecraft over 180 [°] within 90 $[s]$.	✓
ASRM-ADC-008	The ADCS sensors shall have a clear field of view.	✓
ASRM-ADC-009	The ADCS actuators exhaust shall not cause damage to other systems.	
	Structure in section 8.1	
ASRM-ST-001	The structural design of every spacecraft shall be able to withstand the launch loads.	✓
ASRM-ST-002	The structural design of every spacecraft shall enable the mounting of subsystems.	✓
	Propulsion in subsection 8.3.1	
ASRM-PRP-001	The propulsion system shall provide the 1.1 $[km/s]$ ΔV required for orbit matching.	✓
ASRM-PRP-002	The propulsion system shall provide the 0.8 $[km/s]$ ΔV required for returning to Earth.	✓
ASRM-PRP-003	The propulsion system shall allow for multiple actuation cycles.	✓
ASRM-PRP-004	The propulsion system shall have a reliability above 90 [%].	✓
	Observation instruments in subsection 7.1.4	
ASRM-SPL-001	The payload shall determine the age of the 1989 UQ.	✓
ASRM-SPL-002	The payload shall determine the density of 1989 UQ.	✓
ASRM-SPL-003	The payload shall determine atomic composition of 1989 UQ's surface.	✓
ASRM-SPL-004	The payload shall determine molecular composition of 1989 UQ's surface.	✓
ASRM-SPL-005	The payload shall aid in determining the landing site of the landers.	✓
ASRM-SPL-006	The payload shall determine the shape of 1989 UQ.	✓
ASRM-SPL-007	The payload shall detect the presence or former presence of a magnetic field on 1989 UQ.	✓
ASRM-SPL-008	The camera shall map the surface of the asteroid with a resolution of at least 0.075 $[m/px]$.	✓
ASRM-SPL-009	The camera shall be able to view 1989 UQ with a minimum resolution of 4 pixels from a minimum distance of 10,000 $[km]$	✓
ASRM-SPL-010	The camera shall be able to view the entire asteroid in one picture from a minimum distance of 8.5 $[km]$	✓

ASRM-SPL-011	The payload shall estimate the atomic composition of 1989 UQ's surface to a depth of 1 [m].	✓
ASRM-SPL-012	The payload shall determine the atomic composition of the potential sample area with a resolution of six [m].	✓
	Thermal in subsection 8.5.1	
ASRM-THERM-001	The thermal control system shall place each subsystem within its operational temperature range.	✓
ASRM-THERM-002	The thermal control system shall account for eclipse phases during orbit.	✓
ASRM-THERM-003	The thermal control system shall ensure a constant temperature throughout hibernation mode.	✓
ASRM-THERM-004	The thermal control system shall account for different power consumption rates.	✓
ASRM-THERM-005	The thermal control system shall account for changes in solar radiance.	✓
	C&DHS in subsection 8.7.1	
ASRM-CDHS-001	The C&DH subsystem shall perform housekeeping tasks autonomously.	✓
ASRM-CDHS-002	The C&DH subsystem shall be able to identify specific situations with effect on the mission.	✓
ASRM-CDHS-003	The C&DH subsystem shall be able to initialise specific operational modes.	✓
ASRM-CDHS-004	The C&DH subsystem shall be programmable through commands from the ground station.	✓
ASRM-CDHS-005	The C&DH subsystem shall be commandable from the ground station.	✓
ASRM-CDHS-006	The C&DH subsystem shall be able to prioritise commands.	✓
ASRM-CDHS-007	The C&DH subsystem shall allocate storage space for the payload data.	✓
ASRM-CDHS-008	The C&DH subsystem shall shall store payload data until it is downlinked to Earth.	✓
ASRM-CDHS-009	The C&DH subsystem shall delete downlinked data.	✓
ASRM-CDHS-010	The C&DH subsystem shall be in contact with all interfaces.	✓
ASRM-CDHS-011	The C&DH subsystem shall be able to downlink data through the TT&C subsystem.	✓
ASRM-CDHS-012	The C&DH subsystem shall have more than 3.6 [GB] storage.	✓
	EPS in subsection 8.2.1	
ASRM-EPS-001	The EPS shall provide continuous source of electrical power to the spacecraft loads during the mission life.	✓
ASRM-EPS-002	The EPS shall control and distribute power in the spacecraft.	✓
ASRM-EPS-003	The EPS shall provide command and telemetry capability for EPS health and status.	✓
ASRM-EPS-004	The EPS shall allow control by the ground station.	✓
ASRM-EPS-005	The EPS shall be able to function autonomously.	✓
ASRM-EPS-006	The EPS shall protect the spacecraft from failures within the EPS.	✓
ASRM-EPS-007	The EPS shall dissipate excess power.	✓
ASRM-EPS-008	The EPS shall protect the spacecraft payload against failures within the EPS.	✓
ASRM-EPS-009	The EPS shall support a safe mode.	✓
ASRM-EPS-010	The EPS shall support a low-power mode.	✓
ASRM-EPS-011	The EPS shall keep the angle of incidence of the sun rays below 1 [°].	✓
ASRM-EPS-012	The spacecraft shall be able to operate in low-power mode on battery power for one week.	✓
Orbiter	in subsection 7.1.4	
ASRM-ORB-001	The orbiter shall be able to perform a manoeuvre upon rendezvous with the asteroid	✓
ASRM-ORB-002	The orbiter shall be able to study the asteroid	✓
ASRM-ORB-003	The orbiter shall communicate with the landers and Earth	✓

ASRM-ORB-004	The orbiter shall contain a decoupling mechanism	✓
ASRM-ORB-005	The orbiter shall be able to correct its attitude	✓
ASRM-ORB-006	The orbiter shall control its temperature	✓
	TT&C in subsection 8.6.1	
ASRM-ORB-TTC-001	The TT&C subsystem shall be able to send and receive data over a distance of 2.16 [AU].	✓
ASRM-ORB-TTC-002	The TT&C subsystem shall be able to send commands to either SASH or ACSAL with a minimum data rate of 1.1 [$kbit/s$].	✓
ASRM-ORB-TTC-003	The communications link with Earth shall have a maximum bit error rate of 10^{-5}.	✓
ASRM-ORB-TTC-004	The TT&C subsystem HGA of the Orbiter shall use X-band for communication with Earth with a minimum data rate of 20 [$kbit/s$].	✓
	ADCS in subsection 8.4.3	
ASRM-ORB-ADCS-001	The ADCS shall provide enough accuracy to point the telecommunication system.	✓
ASRM-ORB-ADCS-002	The ADCS shall be able to provide a 180 [°] turn in 90 [s].	✓
ASRM-ORB-ADCS-003	The ADCS shall be able to correct the orbit when required.	✓
ASRM-ORB-ADCS-004	he ADCS shall be able to counteract any disturbances.	✓
ASRM-ORB-ADCS-005	The ADCS shall be able to point the instrumentation towards the asteroid.	✓
	Propulsion in subsection 8.3.3	
ASRM-ORB-PRP-001	The propulsion system of the orbiter shall be able to provide enough thrust for a ΔV manoeuvre of 1.11 [km/s].	✓
ACSAL	in section 7.2	
ASRM-ACSAL-001	ACSAL shall be able to touch down on the asteroid.	✓
ASRM-ACSAL-002	ACSAL shall be supported by landing legs.	✓
ASRM-ACSAL-003	ACSAL shall be able to attach harpoons to the asteroid surface.	✓
ASRM-ACSAL-004	ACSAL shall be able to pre-drill a 0.15 [m] hole below the solid surface of the asteroid in basalt-like material.	✓
ASRM-ACSAL-005	ACSAL shall be able to change the drill head of the drill mechanism.	✓
ASRM-ACSAL-006	ACSAL shall be able to acquire a core sample from a depth of 0.20 [m].	✓
ASRM-ACSAL-007	ACSAL shall be able to attempt a backup sample acquisition at a depth of 0.25 [m].	✓
ASRM-ACSAL-008	ACSAL shall be able to seal the acquired sample.	✓
ASRM-ACSAL-009	ACSAL shall be able to place the sealed sample capsule in the reentry capsule.	✓
	EPS in section 8.2	
ASRM-ASCAL-EPS-3	The EPS shall be capable of recharging the energy storage after sample acquisition at a depth ofdischarge of 60 [%] within 3 [hr].	✓
ASRM-ASCAL-EPS-4	The EPS shall be capable of delivering 141 [W] for 900 [s]	✓
	TT&C in section 8.6	
ASRM-ACSAL-TTC-001	The TT&C subsystem of ACSAL shall have a minimum data rate for scientific and housekeeping data of 1.1 [$kbit/s$].	✓
ASRM-ACSAL-TTC-002	The TT&C subsystem of ACSAL shall use S-band.	✓
	ADCS in subsection 8.4.4	
ASRM-ACSAL-ADCS-001	The ADCS shall be able to put ACSAL in the descent orbit.	✓
ASRM-ACSAL-ADCS-002	The ADCS shall be able to point the landing gear towards the asteroid.	✓
ASRM-ACSAL-ADCS-003	The ADCS shall limit the impact velocity to a maximum of 0.4 [m/s]	✓
	Propulsion in subsection 8.3.4	
ASRM-ACSAL-PRP-001	The propulsion system of ACSAL shall fire as soon as ACSAL makes contact with the asteroid. [m/s]	✓
ASRM-ACSAL-PRP-002	The propulsion system of ACSAL shall provide 0.8 [km/s] of ΔV to return back to Earth.	✓
	Landing mechanism in subsection 7.2.5	

ASRM-ACSAL-ALM-001	The landing legs shall unfold when released by pin-puller actuators.	✓
ASRM-ACSAL-ALM-002	The landing legs shall lock into place at a 60 [°] angle with respect to the asteroid surface.	✓
ASRM-ACSAL-ALM-003	The landing legs shall carry the impact load that results from a 0.4 [m/s] impact speed.	✓
ASRM-ACSAL-ALM-004	The landing legs shall carry the thrust load of 445 [N] provided by the thruster during fastening of the satellite to the asteroid.	✓
ASRM-ACSAL-ALM-005	The landing legs shall be able to host the claw mechanism.	✓
ASRM-ACSAL-ALM-006	The landing legs shall provide a nominal ground clearance of 0.15 [m].	✓
ASRM-ACSAL-ALM-007	The landing legs shall be able to carry the combined load of at least 703 [N] under unfolded orientation.	✓
ASRM-ACSAL-ALM-008	The platform shall be able to carry the combined load of at least 703 [N].	✓
ASRM-ACSAL-ALM-009	The platform shall house three harpoon mechanisms.	✓
ASRM-ACSAL-ALM-010	The platform shall release the main satellite module during take-off.	✓
ASRM-ACSAL-HAR-001	ACSAL shall be able to fire the harpoons towards the asteroid surface.	✓
ASRM-ACSAL-HAR-002	ACSAL shall be able to tighten the rope attached to the harpoons.	✓
	Drill mechanism	subsection 7.2.3
ASRM-ACSAL-DRM-001	The drill mechanism shall be able to lift the drill head above the carousel.	✓
ASRM-ACSAL-DRM-002	The drill mechanism be able to unscrew the drill head.	✓
ASRM-ACSAL-DRM-003	The drill mechanism be able to screw on the sample acquisition head.	✓
ASRM-ACSAL-DRM-004	The drill mechanism shall be able to place the sealing head below the drill arm.	✓
ASRM-ACSAL-DRM-005	The drill mechanism shall be able to screw the sample drill bit into the sealing head.	✓
ASRM-ACSAL-DRM-006	The drill mechanism shall be able to fasten the sealed sample capsule in the reentry capsule.	✓
	Sample Return Capsule	subsection 7.2.7
ASRM-ACSAL-SRC-009	The reentry capsule shall be able to return the sample to Earth.	✓
ASRM-ACSAL-SRC-009a	The error for the Entry flight-Path Angle shall be less than 0.08 [°].	✓
ASRM-ACSAL-SRC-009b	The entry attitude shall be less than 10 [°].	✓
ASRM-ACSAL-SRC-009c	The maximum heat rate shall be less than 1200 [W/cm^2].	✓
ASRM-ACSAL-SRC-009d	The attitude at the max heat rate shall be less then 10 [°].	✓
ASRM-ACSAL-SRC-009e	The maximum heat load shall be less than 32 [kJ/cm^2].	✓
SASH		subsection 7.3.1
ASRM-SASH-001	SASH shall be able to perform a hovering sample acquiring manoeuvre.	✓
ASRM-SASH-002	SASH shall be able to perform two practice runs and one actual sample acquiring run.	✓
ASRM-SASH-003	SASH shall be able to move to a different sample acquiring location.	✓
ASRM-SASH-004	SASH shall be able to deflect the thrust required for the descent to prevent contamination of the sample.	✓
ASRM-SASH-005	SASH shall be able to locate the landing site selected by the orbiter from a 100 [m] above the surface.	✓
ASRM-SASH-006	SASH shall be able to track the surface during descent and ascent.	✓
ASRM-SASH-007	SASH shall be able to eject the SRC at the attitude and spin rate required for a safe reentry.	✓
ASRM-SASH-008	SASH shall be able to determine its altitude above the surface of the asteroid.	✓
ASRM-SASH-009	SASH shall provide protection for the critical components of the SRC.	✓
	EPS	subsection 8.2.4
ASRM-SASH-EPS-3	The EPS shall be capable of recharging the energy storage after sample acquisition within 3 [h]. [T]	✓

ASRM-SASH-EPS-4	The EPS shall be capable of delivering 425 [W] for 900 [s] at any point during the mission. [T]	✓
	TT&C	
ASRM-SASH-TTC-001	The TT&C subsystem of SASH shall have a minimum data rate for scientific and housekeeping data of 1.1 [$kbit/s$]	✓
ASRM-SASH-TTC-002	The TT&C subsystem of SASH shall use S-band.	✓
	ADCS	subsection 8.4.5
ASRM-SASH-ADCS-001	The ADCS shall be able to put SASH in the descent orbit.	✓
ASRM-SASH-ADCS-002	The ADCS shall be able to point the sample collection mechanism towards the asteroid.	✓
ASRM-SASH-ADCS-003	The ADCS shall thrust the craft away from the asteroid when collection is completed.	✓
ASRM-SASH-ADCS-004	The ADCS shall limit the impact velocity to a maximum of 0.05 [m/s].	✓
	Propulsion	
ASRM-SASH-PRP-001	The propulsion system of SASH shall provide 0.8 [km/s] of Δ V to return back to Earth.	✓
	Sample mechanism	subsection 7.3.4
ASRM-SASH-SAM-001	The SAM on SASH shall be able to determine whether a sample is acquired.	✓
ASRM-SASH-SAM-002	The SAM on SASH shall be able to collect more than 25 [g] of surface sample from 1989 UQ.	✓
ASRM-SASH-SAM-003	The SAM on SASH shall be able to put the collector into the SRC.	✓
ASRM-SASH-SAM-004	The SAM on SASH shall be able to close the collected sample off hermetically.	✓
ASRM-SASH-SAM-005	The SAM on SASH shall not damage the SRC.	✓
ASRM-SASH-SAM-006	The SAM on SASH shall be able to retract and be stored on the outside of SASH.	✓
	Sample return capsule	subsection 7.3.5
ASRM-SASH-SRC-001	The SRC on SASH shall be able to ensure a safe reentry through the earth's atmosphere.	✓
ASRM-SASH-SRC-002	The SRC on SASH shall be able to carry at most 100 [g] of sample acquiring by the SAM.	✓
ASRM-SASH-SRC-003	The SRC on SASH shall not be damaged during operations until landing on the earth's surface.	✓
ASRM-SASH-SRC-004	The SRC on SASH shall be able to open for the SAM to put in the sample.	✓

4
Sustainability

For any space mission it is inevitable to create space debris, as well as for the spacecraft to be contaminated with small quantities of material from Earth, thereby contaminating the surface of the asteroid as well. This implies that there will be a certain contamination risk on the asteroid. Next to this, since this mission brings a sample from the asteroid back to Earth, a contamination risk of the earth has to be taken into account as well, because it is possible that this sample could possess harmful substances, such as alien DNA. Therefore this section will elaborate on development strategies for sustainability. First, the requirements flown down from sustainability are stated, followed by an explanation on how it is implemented into the different mission phases. A description of the main influence on the EPS subsystem is then given. While working on the sustainability development strategy the team had to make sure to respect Article IX of the UN Space Treaty of 1967, which states the following:

> "Parties to the Treaty shall pursue studies of outer space, including the Moon and other celestial bodies, and conduct exploration of them so as to avoid their harmful contamination and also adverse changes in the environment of the earth resulting from the introduction of extraterrestrial matter, and where necessary, shall adopt appropriate measures for this purpose." Rummel [2011]

4.1. Requirements on sustainability

The following requirement are set, in order to account for sustainability in the design of this mission.

ASRM-SUS-001	The spacecraft shall not use radioisotope thermoelectric generators. [D]
ASRM-SUS-002	The mission shall archive which material the spacecraft are made of. [D]
ASRM-SUS-003	The spacecraft shall be passivated at the end of its mission. [T]
ASRM-SUS-004	The mission shall document the spacecraft and debris trajectories. [D]
ASRM-SUS-005	If the spacecraft or orbital stages pass through the LEO region, or have the potential to interfere with the LEO region, they shall be de-orbited. [A]

4.2. Sustainability in the mission phases

In order to take sustainability into account in a space mission like Piazzi, the mission can be categorised in different phases that have to be to considered. This section will be elaborated on those for the chosen concept. The different phases of the whole mission will be analysed and a sustainable point of view is given.

Manufacturing until launch date

Since some manufacturing techniques are really harmful to the sustainability of the mission, it can already be compromised at the very beginning of the mission design. This needs to be taken care of through simple measures such as cleaner factories, paying special attention to the waste created by the manufacturing process and opting to techniques that create the least amount of toxic waste. Additionally, while choosing materials the spacecraft is manufactured from, attention can be paid to the ecological footprint of the used materials, since some materials require significantly more energy to be produced than others. From this a look can be drawn on the transportation of the components to the launch base in order to make sure it is as sustainable as possible. This is the start of the sustainability plan. The factories, companies and even students working on the project have to be aware of the risk for making a non-sustainable design and the manufacturing process have to be clean.

Launch

Launches are hardly sustainable due to the amount of material that is ejected from the launcher in the atmosphere and in low Earth orbit. It is due to the launch system that produces exhaust gases and a mix of cooling water, sand and dust. Adding to this, during Earth orbit it is possible that the spacecraft releases chemicals which can have harmful effects on the ozone layer. Nevertheless the sustainability for the launch can be taken into account through the manufacturing of the launcher to be as

sustainable as achievable in all fairness. A good sustainability aspect of the chosen launch system is the recovery of the boosters in the sea or at the launchpad. The last stage of the rocket that brings the payload to a transfer orbit towards the asteroid has to be placed into a so-called graveyard orbit. The next step of the sustainability plan is to recover the booster that falls back on Earth and, more importantly, to document the trajectory of the last stage. It is a necessity that the last stage trajectory is proven not to interfere with any celestial body in order to avoid contamination by crashing on one.

Transfer to asteroid
This phase is usually quite sustainable and so less attention should be paid to it. During this period until rendezvous with the asteroid, no space debris will be made, No boosters will be left behind and no harmful substances will be released in space. This phase then is not part of the sustainability plan.

Asteroid rendezvous and departure
Once the mapping of the asteroid is done and the most suitable landing zone is determined, the two landers will be deployed and collect a sample from the asteroid in order to bring it back to Earth. Two sustainability aspects need to be considered here.

The first potential problem that arises is the contamination of Earth with an extraterrestrial pathogenic life form. According to National Research Council [1998], there exists a possibility that conditions on C-type asteroids were once suitable for life to emerge. National Research Council [1998] and Nicholson et al. [2005] state that some known microorganisms are resistant to high vacuum and galactic and solar cosmic radiation, and that they can survive for very long times in dormant state while maintaining a very high survival rate when transferring back to metabolic state. It can thus not be ruled out that microscopic life forms are present on asteroid 1989 UQ. However, the combined deleterious effects of galactic and solar cosmic radiation, high, low or changing temperatures and very high vacuums on very old surfaces, like C-type asteroids, make that the first few meters below the surface have been properly and completely sterilised (Clark [1999], National Research Council [1998]). It can thus be concluded that the return of samples from 1989 UQ, either from the surface or core, does not pose a threat to Earth or the environment and no additional measures have to be taken.

Once the samples are collected and the landers are on their way to Earth, the orbiter is left behind. This could be considered as non-sustainable but measures are taken to make it acceptable. Two solutions can be looked into: one being crashing or attaching the orbiter onto the asteroid. This is considered better than just leaving an inactive spacecraft uncontrolled in the solar system. The other solution is to place the spacecraft into a Sun orbit and use it as a monitoring tool for solar weather. This would induce a slight increase in operational cost but could be a feasible option since no extra instruments have to be brought in order to achieve this change of mission objectives. This last option is then chosen as end-of-life action for the orbiter.

End of life
In the design, the end of life (EOL) phase of the mission should be considered. With EOL, several aspects should be taken into account. Different institutes have set up guidelines for space debris and contamination around Earth. These institutions include DLR, IADC and COSPAR, amongst others. This section will elaborate on how concept design will take into account several regulations regarding aforementioned subjects regarding the end of life of the space craft.

As stated in the previous section, the orbiter will stay behind and so precautions of EOL for spacecraft should be taken into account. This includes tracking of the spacecraft, sending commands for possible impulse if a bad scenario shall occur such as a collision with an unwanted other body. Next to that, the spacecraft needs to be passivated at the end of its mission (4 [2007]). Passivation requires any energy to be disposed of. This may include fuel or electrical energy, but also vents should be depressurised. Reasoning is that when the spacecraft shuts off, these may not be regulated, for example cooling of the fuel system, possibly resulting in exploding fuel tanks or lines, causing lots of debris. The instant the spacecraft will have to be passivated is unknown yet since the solar radiation monitoring mission extension has an undetermined time.

And finally elements returning to Earth need proper design regarding burning up in the atmosphere and contamination. The parts that need to burn up should be designed in a way that burn-up is possible and that no elements may reach Earth's surface, or even worse, populated areas. In contrary, the reentry capsule needs to safely arrive at the surface. Orbit planning should include minimising the chance it landing in populated areas. There is always a non-sustainable aspect of the reentry capsule: since they make use of a process called ablation which is basically making use of the material's heat of evaporation. The material used as coating is said to be evaporating away and dissipating the heat with it. This induces material being spread in the atmosphere that may be toxic, even though the size of the capsule is really small (less than 0.5 $[m]$) and the small amount of material expelled. This step in the sustainability plan is then to determine when to passivate the orbiter and calculations have to be made that the reentry of the spacecraft induce a total burn-up of all components.

4.3. Sustainability in the electrical power system

Special attention with regards to sustainability needs to be paid to the electrical power system. It is a requirement to avoid using radioisotope thermoelectric generators due to the risk it poses on the mission. If one comes to fail during launch, radioactive

elements will be spread through the atmosphere and could have a catastrophic impact on Earth's environment. As for the EPS, solar arrays are the most sustainable solution for this problem. This shows that for some subsystems, the design criteria are not only dictated by the availability but also the sustainability.

4.4. Sustainability plan

In order to give a small overview of the whole sustainability process, a plan is made and is presented here in Figure 4.1.

This concludes the sustainability aspect of the design and how it is taken into account during the whole design and mission process.

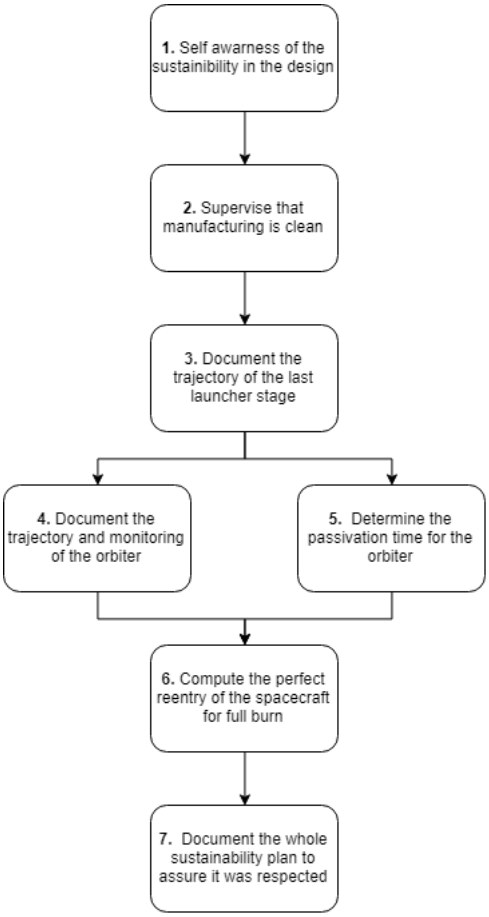

Figure 4.1: Sustainability plan

5
Final design overview

In this chapter a high level overview of the final design is given. It starts with showing an analysis on the functions of the system that have to be performed, and put in a functional flow diagram. Following this, the technical budgets of the design are given, followed by an estimation for the cost of the entire mission.

5.1. Functional analysis

Over this section the functional flow diagram of the whole Piazzi mission is presented. It includes the major steps that have to be taken into account, starting from the design phases until the end of life of each spacecraft. This is then topped by a functional breakdown, describing the steps in the functional flow diagram by a main action. Due to the length of such diagram, it is presented in appendix A.

5.2. Technical Budgets

In this section the mass and power budget of the mission are given, in Table 5.1 and Table 5.2 respectively.

Table 5.1: Mass budget of the Piazzi spacecraft

Item	**Mass [kg]**
ACSAL dry mass	135
ACSAL wet mass	191
SASH dry mass	143
SASH wet mass	203
Orbiter dry mass	1060
Orbiter wet mass	1506
Spacecraft total	1506

Table 5.2: Power budget of the Piazzi spacecraft

Item	**Power [W]**
ACSAL average	37
ACSAL peak	387
SASH average	23
SASH peak	425
Orbiter average	200
Orbiter peak	456

5.3. Cost analysis

The cost estimation for this project is done in four parts. First the operations cost and the cost of the launcher are given. After this the development and production cost of the spacecraft are estimated. For this, two different methods were used and they were compared and combined to get an accurate estimation.

The total life cycle cost of the mission is based on different components. An overview of this can be found in Figure 5.1.

5.3.1. Launcher

The Piazzi mission will be launched on top of a SpaceX Falcon 9, which has a cost of 52 [*M*$] (FY 2018) [1]. This is different compared to the midterm (Angyal et al. [2018]), where the choice was made for an ULA Atlas V. But now that the mass has gone down significantly, the Falcon 9 can be used, more than halving the cost for the launch.

5.3.2. Operations

The operational cost is estimated using the Operations Cost Prediction Model from Wertz et al. [2011]. The model estimates the total operating cost based on several categories, which are given in this section. All costs are given on a per year basis.

[1] http://www.spacex.com/about/capabilities Accessed June 25, 2018

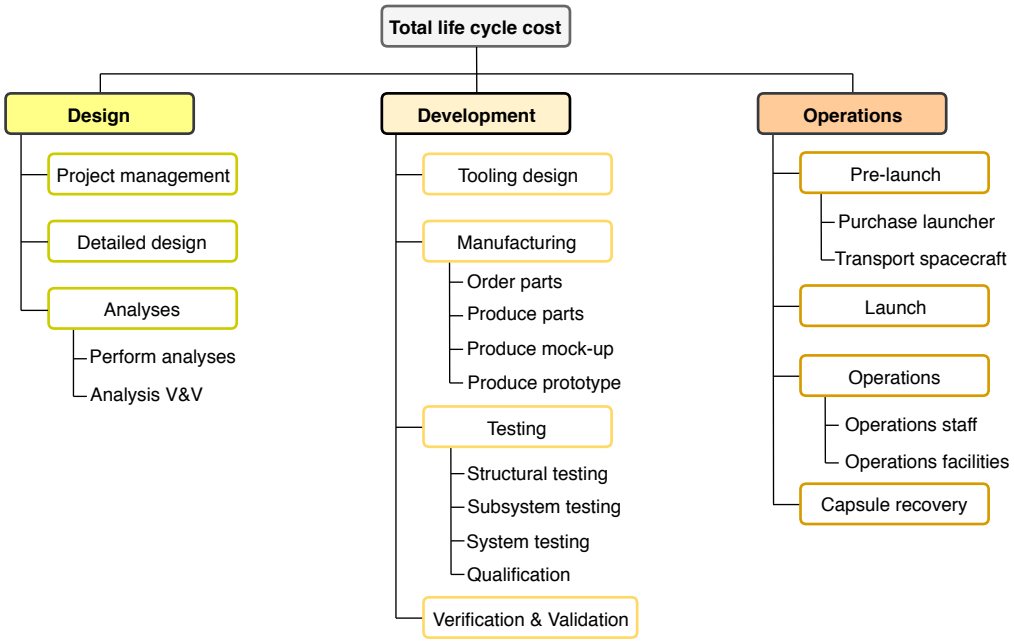

Figure 5.1: Cost Breakdown Structure for the total life cycle cost of the Piazzi mission

Space segment software maintenance
The cost for the maintenance of the space segment software is estimated using Equation 5.1. In this equation, C is the cost [K\$] (FY 2010), and FTE_{ENG} is the labour cost per engineer per year, assumed to be 200 [K\$] (FY 2010). The number of lines of code in the flight software is estimated to be 356,000, as can be found in subsection 8.7.2.

$$C = \frac{\text{Flight Software Lines of Code}}{16,000} \cdot \text{FTE}_{ENG} \tag{5.1}$$

Mission operations
The cost for the mission operations is estimated using Equation 5.2. In this equation, FTE_{TECH} is the labour cost per technician, assumed to be 150 [K\$] (FY 2010) per year. It is estimated that eight engineers and four technicians will be working on the operations staff.

$$C = (\text{Number of engineers}) \cdot \text{FTE}_{ENG} + (\text{Number of technicians}) \cdot \text{FTE}_{TECH} \tag{5.2}$$

Ground segment software maintenance
The cost for the maintenance of the space segment software is estimated using Equation 5.3. An estimated 25,000 lines of code need to be maintained during the operational phase.

$$C = \frac{\text{Ground Software Lines of Code}}{28,200} \cdot \text{FTE}_{ENG} \tag{5.3}$$

Additional costs
Some additional costs added are the ground hardware maintenance cost, facility cost, and PM&SE cost, estimated to be 3, 35, and 20% of the combined cost of the above categories, respectively (Wertz et al. [2011]).

Finally, the costs of the retrieval of the capsules has to estimated. This is based on the cost of renting a helicopter, around 1000 [$] an hour, and the amount of hours it will take to retrieve the capsules, estimated to be 72.

Total operational costs
Applying the method explained above, the following costs for the categories are estimated:

- Space Segment Software Maintenance: 4.4 [M\$] (FY 2010).
- Mission Operations: 2.2 [M\$] (FY 2010).
- Ground Segment Software Maintenance: 200 [K\$] (FY 2010).
- Hardware Maintenance: 204 [K\$] (FY 2010).

Table 5.3: Values used for the first spacecraft cost estimation method

Property	Value
Spacecraft dry mass (M)	887 [kg]
Spacecraft total power (P)	2428 [W]
Data%	70%
Life	61 months
New%	72%
Planetary	1
Year	2025
Instrument Complexity	90%
Team	3

- Facilities: 2.38 [M\$] (FY 2010).
- PMSE: 1.36 [M\$] (FY 2010).
- Retrieval: 72 [K\$] (FY 2010).

This leads to a total cost of 10.8 [M\$] (FY 2010), per year. The mission life of the Piazzi mission is five year, afterwards one engineer will be kept on staff for 25 years, to comply with `ASRM-USR-N017`. This leads to a total operational cost of 60 [M\$] (FY 2010).

5.3.3. Spacecraft cost estimation method one

The first cost estimation method used for estimating the cost of the spacecraft was taken from Wertz et al. [2011], and is called the QuickCost Cost Estimating Method. It uses Equation 5.4 to get a rough estimate of the cost of developing and producing a spacecraft. While taking the same constants as used in the cost estimation during the previous phase, but with an updated cost and power budget from the Angyal et al. [2018].

$$C = 2.829 \cdot M^{0.457} \cdot P^{0.157} \cdot 2.718^{0.171 \cdot Data\%} \cdot 2.718^{0.00209 \cdot Life} \cdot 2.718^{1.52 \cdot New\%} \cdot 2.718^{0.258 \cdot Planetary} \cdot 2.718^{-0.0145 \cdot (Year - 1960)} \cdot 2.718^{0.467 \cdot InstrComp\%} \cdot 2.718^{-0.237 \cdot Team} \tag{5.4}$$

In order perform this estimation, the final updated values of the different spacecraft will be used, given in Table 5.3. From this, a cost of 625 [M\$] (FY 2010) is estimated.

5.3.4. Spacecraft cost estimation method two

The second method used for cost estimation is the Small Space Craft Cost Estimating model (Wertz et al. [2011]). It uses the equations given in Equation 5.5 to estimate the cost of the Piazzi mission. In all of these equations, C is the cost [K\$] (FY 2010), and m is the mass of the respective subsystem [kg], found in Table 7.2, Table 7.6 and Table 7.10, unless otherwise specified. For the payload cost a separate estimating method is used, namely the NCIM Cost Estimating Method for Remote Sensing Instruments (Wertz et al. [2011]). For the cameras and spectrometers (Equation 5.12) and the magnetometers (Equation 5.13), the cost C is in thousands of dollars (FY 2010), P is the instrument total power [W], and DL is the design life in months, which is 48 months.

$$C_{Structure} = 407 + 19.3 \cdot m \cdot \ln(m) \tag{5.5}$$

$$C_{Thermal} = 335 + 5.7 \cdot m^2 \tag{5.6}$$

$$C_{ADCS} = 1850 + 11.7 \cdot m^2 \tag{5.7}$$

$$C_{EPS} = 1261 + 539 \cdot m^{0.72} \tag{5.8}$$

$$C_{Propulsion} = 89 + 3 \cdot m^{1.261} \tag{5.9}$$

$$C_{TT\&C} = 486 + 55.5 \cdot m^{1.35} \tag{5.10}$$

$$C_{CD\&H} = 658 + 75 \cdot m^{1.35} \tag{5.11}$$

$$C_{Instruments} = 328 \cdot m^{0.426} \cdot P^{0.414} \cdot DL^{0.375} \tag{5.12}$$

$$C_{Magnetometers} = 1130 \cdot m^{0.184} \cdot P^{0.238} \cdot DL^{0.274} \tag{5.13}$$

Integration, Assembly, and Test
The costs for the integration, assembly, and testing of the spacecraft are given by Equation 5.14

$$C = 0.139 \cdot \frac{S}{C_{BusTotalCost}} \tag{5.14}$$

Program Level Costs
The program level costs are given by Equation 5.15.

$$C = 0.229 \cdot \frac{S}{C_{BusTotalCost}} \tag{5.15}$$

Aerospace Ground Equipment
The ground equipment costs are given by Equation 5.16.

$$C = 0.066 \cdot \frac{S}{C_{BusTotalCost}} \tag{5.16}$$

Total spacecraft cost for method two
Using the second method, the total cost of the development and production of the Piazzi spacecraft comes out to 4.1 [M\$] (FY 2010). A further 200 [M\$] (FY 2010) is added for the development of the sample acquiring mechanisms, and the sample return capsule. This estimate is based on the fact that the SAMs have to be developed from scratch, giving a significantly higher cost than the other subsystems.

5.3.5. Total mission cost

To determine the total cost for the Piazzi mission, the results of cost estimation method one and two have to be compared against each other, and the weak points of each method have to be taken into account. First, for the QuickCost method, it is valid to use for missions with comparable spacecraft characteristics as the Piazzi mission. Secondly, in order to come up with a better estimate, the second method was used. It is designed for small satellites, with a mass range up to 500 [kg]. It is however a very good estimator for the intended range, having a variance with the actual cost of NEAR Shoemaker of only 1% (Mosher et al. [1999]). When it is used to estimate the cost for the Piazzi mission, it has a much lower result than the QuickCost method. This difference is mainly caused by the fact that the SCCM model does not estimate the cost for original payload, like the SAMs. Furthermore, according to Wertz et al. [2011], smaller spacecraft are less expensive per kilogram, leading to the SSCM model significantly underestimating the cost of the Piazzi mission. In the end, it was chosen to estimate the spacecraft development and manufacturing cost at 650 [M\$] (FY 2010), taking the QuickCost estimating method as guideline, and adding a small margin to deal with any uncertainties.

Adding the 60 [M\$] (FY 2010) results in a cost for development, manufacturing, and operations of 710 [M\$] (FY 2010). Converted to fiscal year 2018 it comes out to 870 [M\$], adding the launcher cost, and converting to euros leads to a total cost for the Piazzi mission of 750 [M€] (FY 2018). It should be noted that when taking the maximum error of estimate (40%), the cost comes out to around 980 [M\$] (FY 2010), which is still below the user requirement. The final cost estimation for the Piazzi mission varies significantly with the estimation made in the midterm phase, which was 923 [M€] (FY 2018) (Angyal et al. [2018]). This is mainly due to the mass, which is around 30% lower. Furthermore, now that the selected launcher has been changed from Atlas V to Falcon 9, the launch cost is halved, to 52 [M\$] (FY 2018). This all results in a lower cost estimate.

6
Mission Overview

In Figure 6.1 the time line of the Piazzi mission is given. Throughout this chapter, more detail on this time line will be given. After the details of the entire mission time line are discussed, a sensitivity analysis on the elements on the time line will be performed.

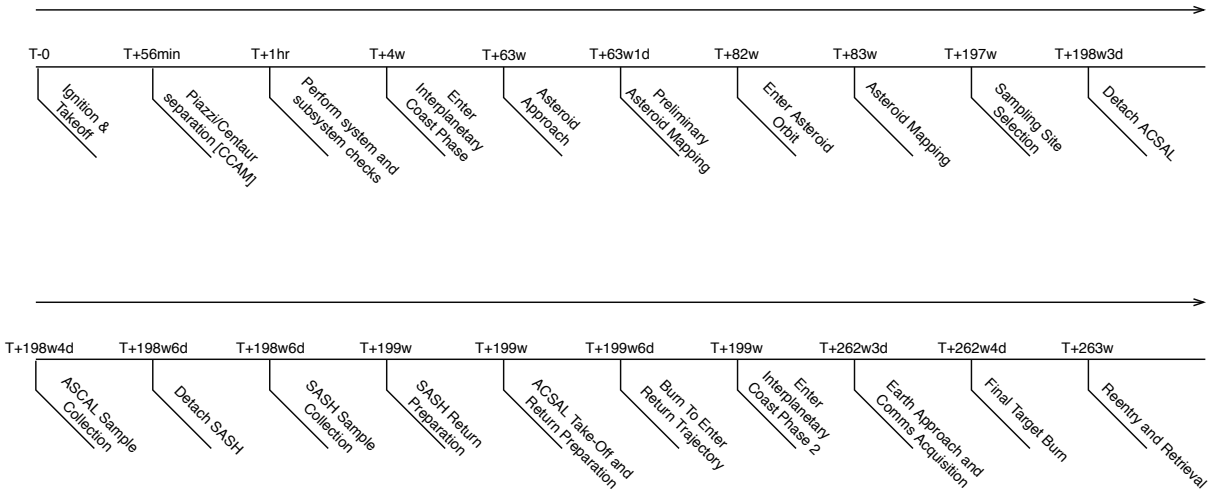

Figure 6.1: Mission time line for the Piazzi mission

6.1. Astrodynamics

In this section the astrodynamics of the Piazzi mission will be discussed. Using GMAT as the tool to perform the simulation, the launch, outbound/inbound trajectory, asteroid orbit phase and reentry up to 100 [km] altitude can be modelled accurately.

6.1.1. GMAT: General Mission Analysis Tool

> "The General Mission Analysis Tool (GMAT) is the worlds only enterprise, multi-mission, open source software system for space mission design, optimization, and navigation. The system supports missions in flight regimes ranging from low Earth orbit to lunar, libration point, and deep space missions. GMAT is developed by a team of NASA, private industry, public, and private contributors and is used for real-world mission support, engineering studies, as a tool for education, and public engagement."[1]

In GMAT an entire preliminary space mission can be designed and simulated including finite burns, the effects of solar radiation pressure and for instance the decay rate of an orbit. For the Piazzi mission this tool has been used to simulate the preliminary space mission from launch up to reentry. First a overview of the software itself will be given, including the possibilities in terms of inputs which can be given to analyse a wide range of space missions. The specific inputs for the Piazzi mission will be discussed while going through the list of inputs for GMAT. After the specific inputs for the Piazzi mission have been given the mission sequence will be discussed, such that if interested, the reader can reproduce the mission in GMAT. Finally, the method that is used to input asteroid 1989 UQ into GMAT is elaborated upon. During this section, all assumptions that are also applicable to this tool will be explained as well as their consequences.

[1] https://software.nasa.gov/software/GSC-17177-1 Accessed June 21, 2018

Force models

In GMAT, the user has to set up so-called force models for the planetary objects that the mission will orbit. In this way the gravity can be modelled in a very accurate manner during the simulation. For the Piazzi Mission force models of Earth, Sun and 1989 UQ have to be put in.

For a force model in general the central body and primary body have to put in. For the primary body, a gravity model has to be inserted into GMAT and can be set to a certain degree and order. If necessary, the user can put in a tide file as well as an atmospheric model to take into account both planet characteristics. Finally, the force model can take into account several point masses (if required any planet in the solar system) and either use or neglect the solar radiation pressure. This solar radiation pressure is calculated based on the distance of the spacecraft with respect to the sun based on an average value for solar flux, being 1,496 $[W/m^2]$. For the Piazzi mission, the following force models are used:

- The force model to simulate the gravitational environment near Earth used for the Piazzi mission is the *Joint Gravity Model 3 (JGM-3)*, which is provided by NASA as part of the GMAT software (Tapley et al. [1996]). This gravity model combines the JGM-1 geopotential coefficients along with the error co-variance and can go up to an degree and order of 70. For the Piazzi mission the gravity model has been set to the 4^{nd} degree and an order of 4. This is based on the fact that only a very small part of the mission is running in the sphere of influence (SOI) of Earth, and using this degree and order GMAT is able to iterate faster. Next to that, an atmospheric model being the *MSISE90* (included in the software by NASA) is used to get a higher accuracy on the orbit close to Earth which is favourable for the launch as well as the return (Picone et al. [2002]). This atmospheric model starts at a 100 $[km]$ altitude and stays highly accurate up to 600 $[km]$, but beyond that, due to the amount of reference data accuracy starts to decrease. The point masses considered are Luna (the moon) and Sun, as the spacecraft is in Earth's SOI in which the influence by other point masses is neglected. Finally, the effect of solar radiation pressure is taken into account.
- The force model to simulate the orbits around the sun is also included in Latex. For the Piazzi mission the sun is set as the central body and all other planetary bodies as point masses. The solar radiation pressure will also be accounted for in the simulation.
- The 1989 UQ force model used for the Piazzi mission is self-engineered. The central body and primary body here are both 1989 UQ and the gravity of the asteroid is put into GMAT by running a gravity file. This gravity file, which goes up to the 2^{nd} degree, is based on the gravitational parameter found for the average estimated radius of the asteroid. More on the parameters of the asteroid will be explained in section 6.2. Next to that, all planetary bodies in the solar system are used as point masses and the solar radiation pressure is also taken into account, to accurately simulate the disturbances the spacecraft will experience in orbit around the asteroid.

Propagators

In GMAT, the user has to set up propagators to use these force models as a function of time. Propagators for the force models of Earth, Sun and 1989 UQ will be used. For these propagators, different types of integrators are used based on the accuracy that can be obtained or is required.

For the propagator in Earth's sphere of influence, the *RungeKutta89* is used along with the earth force model mentioned before, providing an accuracy on the integration of $1.0 \cdot 10^{-13}$. The minimum step size is 0.00001 whereas the maximum is 2700 seconds if required. This propagator keeps track of the accuracy and stops the iterations if the accuracy is violated.

For the propagator in the sun's sphere of influence, the *PrinceDormand78* provides a faster iteration process and is used along with the sun force model mentioned before. This propagator also provides an accuracy of $1.0 \cdot 10^{-13}$ with a minimum step size of 0.001 and 864,000 seconds as it maximum. As with the earth propagator, it will stop if the accuracy is violated during the iterations.

For the propagator in the asteroid's sphere of influence, the *PrinceDormand78* method is used as well. The accuracy of the calculations is again set at $1.0 \cdot 10^{-13}$ with a minimal step size of 0.1 miliseconds and maximum of 86400 seconds. This propagator near the asteroid uses the custom force model of the asteroid as mentioned before.

Solvers

In GMAT, the user has to set up solvers to perform iterations and to either converge or diverge given the solution it has to look for. As the algorithm for this solver, *NewtonRaphson* is used with the *ForwardDifference* (both build in GMAT) as the derivative method. The other options built into GMAT are the *CentralDifference* and *BackwardDifference*. However, the *ForwardDifference* method is the method that converges the fastest and is therefore used. If required, the amount of iterations that GMAT has to perform can be adjusted to increase the accuracy level. If the required accuracy is not met by GMAT, the method of the solver can be changed.

Hardware & burns
In GMAT, the thrusters and propellant tanks can be set up for the spacecraft as well. First, a chemical tank is created where the user can put in the fuel mass, density, temperature, pressure and volume. Next to that, a thruster can be created, for which the coordinate system, thrust direction, fuel tanks to use for the propellant, mix ratio (when bipropellant is used) and the gravitational acceleration (g_0) can be put in. For the thruster the thrust force provided in Newton and specific impulse can be put in as well. In the case of using bipropellant, a mixture ratio for the fuels used can be set. The tanks and thrusters created do have to be 'put' onto the spacecraft, by adding them to the spacecraft folder. For the thruster, the inertial coordinate system is used throughout the simulation of the Piazzi mission which is defined as the VNB coordinate system of the thruster, where the V-axis lies along the velocity vector, the N-axis lies normal to the orbital plane and the B-axis completes the right-handed coordinate system.

These tanks and thrusters are than used for finite burns. A burn can be created in GMAT and for it a previously created thruster can be chosen to execute this burn. The specific directions of the burns or manoeuvres will be calculated during the simulation of the mission sequence, which will be discussed in the following section.

Mission sequence
In the mission sequence of GMAT, the mission that should be executed and simulated by GMAT can be put in. The user can create a target sequence (to target the perigee of the asteroid for example) be setting the following sequence in GMAT:

- Vary Thruster V-Vector
- Vary Thruster N-Vector
- Vary Thruster B-Vector
- Vary Thruster Burntime
- Begin FiniteBurn
- Propagate Burntime
- End FiniteBurn
- Propagate to the Asteroid
- Achieve Perigee

By setting up this sequence and simulating it, the required thruster vector and burn time to achieve the perigee at a certain moment in time can be calculated.

6.1.2. Piazzi in GMAT
For the simulation of the Piazzi mission in GMAT, the resources used such as force models, propagators, solvers and hardware & burns are explained throughout the preceding section. The details of the used mission sequence and spacecraft will be elaborated upon below.

Outbound trajectory
The second stage of the launch, which will put the Piazzi spacecraft into a transfer orbit towards the asteroid, is simulated in GMAT as follows.

The spacecraft will launch on the 18th of September 2025 on top of a Falcon 9. This launcher will also put the spacecraft into a transfer orbit. From there, it takes 441 days to the first manoeuvre to be performed by the spacecraft at 5,000 $[km]$ distance from the asteroid. The required C3-energy for this is 15.8 $[km^2/s^2]$ which the launcher can provide as explained in section 6.3.

After the 441-day journey towards the asteroid, the bipropellant engine will perform a burn of 526 $[s]$ to ensure a very close encounter 140 days later. This manoeuvre has a ΔV range of 0.7 to 0.9 $[km/s]$. In the GMAT software, simulating the approach from 5,000 $[km]$ from 140 days provides varying results due to inaccuracies close to the asteroid. Based on this inaccuracy, an additional amount of 5% of bipropellant is added as will also be explained in section 8.3. This is something to look into during the post DSE phase, when this project will get support from a space agency. However, this approach strategy is favourable as it allows the spacecraft to observe any irregularities in the data on the asteroid as is known today to adjust the mission time line accordingly. The manoeuvre puts the trajectory of the spacecraft at an inclination of 92 [°] at a orbital height of 600 meters on 29 April 2027.

The bipropellant engine will insert the spacecraft into an orbit around the asteroid with a burn time of 181 $[s]$, which starts at an altitude of 42 $[km]$ and puts the spacecraft into a circular orbit with a semi major axis of 4.8 $[km]$. This manoeuvre has a total ΔV of 0.41 $[km/s]$.

From here, the RCS-thrusters on the orbiter are used due to the high precision required near the asteroid to change the orbit. The high precision is a consequence of the low gravity field near the asteroid. With an 8.7 $[s]$ burn with 2 RCS-thrusters, the perigee of the orbit is set to 600 $[m]$ after which the RCS-thrusters will also circularise the orbit with a burn time of 12.6 $[s]$ to finish the outbound trajectory of the Piazzi spacecraft. The target orbit of Piazzi is polar and therefore having an inclination

of 90 degrees. If required, the Piazzi can change the inclination upon arrival, in worst case from 0 to 90 degrees performing a manoeuvre of ~0.56 $[m/s]$.

Inbound trajectory

The simulation of the return of the two landers in GMAT has been performed as follows. Departing on the 1st and the 2nd of June 2029 (both spacecraft return separated by one full day), they will both perform a burn using their monopropellant thruster to put them into a transfer orbit to Earth. For the lander, ACSAL, the burn time is 251 seconds and for SASH the burn time is 272 seconds. This burn will put them onto a transfer orbit back to Earth and after 454 days they will intersect with Earth. The manoeuvre to return has a total ΔV of 0.8 $[km/s]$. Two days before reentry, they will perform a so-called Final Target Burn with a burn time of 1.2 seconds to put the spacecraft over the middle of Australia at an altitude of 100 $[km]$ with a reentry velocity of ~13.0 $[km/s]$. As GMAT is unable to provide sufficient accuracy closer to Earth for the reentry, the atmospheric model is left out here in the propagator and continues up to an altitude of 100 $[km]$. Here, the SRC reenters with an angle of approximately 5.7 [°]. As elaborated upon in section 6.4, this angle is sufficient to ensure a safe reentry in Earth's atmosphere. First, the lander, ACSAL, will reenter on 30 August, 2030 followed by the hoverer, SASH, on 31 August, 2030. In Figure 6.2, one can see the spacecraft trajectory ending in the GMAT simulation at 100 $[km]$ altitude with the date and time beneath.

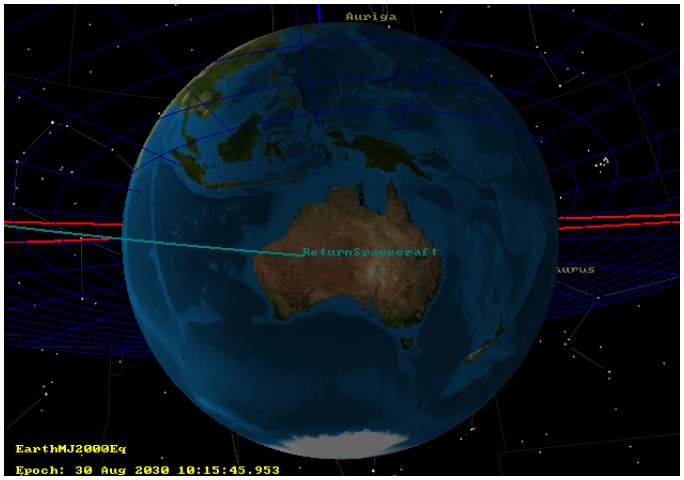

Figure 6.2: Trajectory of the Lander Before Reentry

The Piazzi spacecraft

To put the spacecraft into the GMAT the values shown in Table 6.1 are used. The propellant masses are found using the method described in section 8.3.

The asteroid 1989 UQ

To put the asteroid 1989 UQ into GMAT, a SPICE file is used which is made publicly available by NASA[2]. This allows user to put an arbitrary asteroid into GMAT and simulate missions to it. Other values used in for 1989 UQ in GMAT are shown in Table 6.2. The determination of the gravitational parameter is shown in section 6.2.

6.1.3. Verification & validation

To verify and validate the GMAT software used to simulate the Piazzi mission, multiple other tools were used. During the midterm phase of the design (Angyal et al. [2018]), the NASA Trajectory Browser has been verified by means of a Hohmann transfer. In GMAT, the most efficient mission sequence found from the trajectory browser for asteroid 1989 UQ has been simulated with the same orbital parameters having a outbound C3 energy of 15.8 $[km^2/s^2]$ and a total ΔV to match the asteroid of 1.17 $[km/s]$. This ΔV to get to the asteroid differs by 0.07 $[km/s]$, which is caused by the varying approach to observe the asteroid for 140 days from a distance of 5,000 km. For the return to Earth a ΔV-budget of 0.76 $[km/s]$ is given. In GMAT, the ΔV required to return over Australia with an angle of 5.8 degrees in total is equal to 0.82 $[km/s]$. This difference of 0.06 $[km/s]$ again shows that GMAT can be used as a reliable tool for interplanetary space mission planning.

Next, to determine the reliability of GMAT in simulating the gravitational environment surrounding the asteroid, the orbital period in GMAT is compared to the value found during the midterm phase. The orbital periods once orbiting the asteroid at

[1] http://www.dtic.mil/dtic/tr/fulltext/u2/b024727.pdf Accessed June 19, 2018
[2] `https://ssd.jpl.nasa.gov/x/spk.html` Accessed June 7, 2018

Table 6.1: Parameters used in GMAT

Spacecraft	Parameter	Value	Unit
Piazzi	Dry Mass	1,076	$[kg]$
	Drag Area	4.1	$[m^2]$
	Thrust	2,492 (4x 623)	$[N]$
	Specific Impulse	333	$[s]$
	Hydrazine Tank	224	$[kg]$
	MON3 Tank	204	$[kg]$
	Hydrazine Density	1,020 [1]	$[kg/m^3]$
	MON3 Density	1,440	$[kg/m^3]$
ACSAL	Dry Mass	125	$[kg]$
	Drag Area	0.66	$[m^2]$
	Thrust	445	$[N]$
	Specific Impulse	234	$[s]$
	Monoprop Tank	52	$[kg]$
	Monoprop Density	1,149	$[kg/m^3]$
SASH	Dry Mass	135	$[kg]$
	Drag Area	0.8	$[m^2]$
	Monoprop Tank	56	$[kg]$

Table 6.2: GMAT parameters of 1989 UQ

Parameter	Value	Unit
Radius	459	$[m]$
Gravitational parameter	$8.11 \cdot 10^{-8}$	$[km^3/s^2]$
Rotational Period	7.793	[hrs]

an altitude of 600 $[m]$ are compared. GMAT provides us with an orbital period of 6.6787 $[hr]$, whereas it was previously determined during the midterm phase (Angyal et al. [2018]) that the orbital period will be 6.6789 $[hr]$. This comes down to a difference of 0.0002 $[hr]$, equal to 0.72 $[s]$. Therefore, it can be concluded that GMAT is able to accurately model the gravitational environment surrounding the asteroid. The model used in the midterm to calculate the orbital parameters, is also used in section 6.2.

6.2. Asteroid mission phase

Upon approach of the asteroid the satellites will fulfil the tasks they were initially designed for. Mapping the asteroid, obtain scientific data through various measurements and land on or hover above the surface to finally obtain an asteroid sample to realise the goal of the mission. In this section the approach phase of the asteroid, the orbital manoeuvres of the spacecraft, the observation strategy and the stay at 1989 UQ are discussed. When all these steps are performed with success, the sample acquiring phase will be started which is also treated in this section.

6.2.1. Asteroid approach

When the spacecraft arrive close to 1989 UQ, at a distance of 5,000 $[km]$, the asteroid mission phase is initiated, which was discussed in detail in section 6.1. At this point the scientific instruments will be prepared for their respective objectives. The camera of the orbiter will thus start mapping the asteroid with the goal to obtain an estimate on the shape of the asteroid and the rotational axis as well as to confirm the rotational period and the diameter, which are currently based on coarse ground observations. While mapping, the asteroid will continue its journey to get closer to and eventually orbit 1989 UQ. The time needed to get from 5,000 $[km]$ into observation orbit is 140 days. This is enough to predict the shape, diameter and large abnormalities in shape and relay these data back to Earth, where this will be analysed to plan the further mission. When the measurements done during the approach will not raise problems for the optimal orbit altitude, green light will be given to enter the optimal mapping orbit, which corresponds to a polar orbit with an altitude of 600 $[m]$, justified in subsection 6.2.3.

6.2.2. Orbiting 1989 UQ

Once in the mapping orbit at 600 $[m]$ altitude the main goal of the spacecraft has changed from travelling to to observing of the asteroid and gather as much information as possible. The difficulty of the mission phase is the large amount of uncertainties on the asteroid. However, to still be able to execute the mission succesfully, procedures are set up for a wide range of scenarios. During the asteroid approach phase those unknowns can be estimated to a more detailed extent, resulting in a more accurate and definite mission phase design. Unfortunately, this data is not available yet, so the wide ranges are taken into account for the remainder of the report.

Asteroid uncertainties

To account for the large amount of uncertainties, a software program was written to calculate all margins where the final mission design should be based upon.

First of all, the largest and foremost uncertainties are the shape and size of 1989 UQ. Since from Earth only the rough shape and size could be defined with a low level of accuracy, not mentioning large abnormalities in this shape. Therefore the asteroid is assumed to be fully spherical. This assumption is needed in order to estimate the mass distribution and thus the gravitational forces and size of the Hill's sphere for 1989 UQ. Note however, that the shape is almost certainly not spherical and thus the mass (and dependent values) can not be estimated in an accurate manner. Next to that, the range of the possible radii equals 309 to 609 $[m]$ as explained in more detail in Angyal et al. [2018]. Based on that the orbital period at 600 $[m]$ altitude varies between 5.3 and 9.7 $[hr]$. Using the half cone width method, the eclipse time is estimated to be between 0.8 and 1.0 $[hr]$. The maximum Hill's sphere radii vary from 54 to 134 $[km]$, depending on both the asteroid's radius and the distance from the sun (Angyal et al. [2018]).

Orbital maintenance

Following from GMAT the orbital maintenance burns needed to stay in the mapping orbit are to be executed once every two months. Since they have a duration of 2.0 to 2.5 $[s]$ using a ΔV of 0.02 $[m/s]$, a ΔV-budget of 0.25 $[m/s]$ is brought for the orbit duration of 2 years and 1 month. The full approach of the asteroid including 2 months of orbiting can be seen in Figure 6.3. It is also observed that the orbit is slightly changing in the direction of the sun, before correction burns are applied.

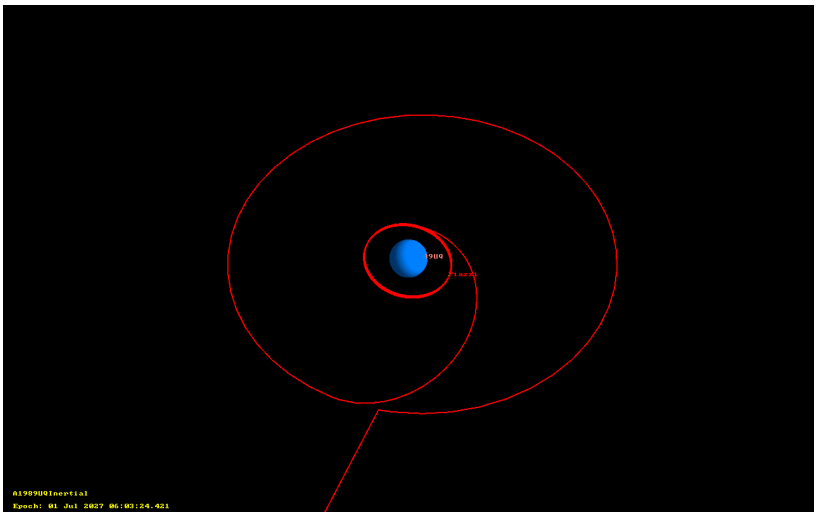

Figure 6.3: Asteroid Mission Phase

6.2.3. Observation procedure

Mapping of the asteroid starts at a distance of 5,000 $[km]$. Here the spacecraft will start decelerating and reach the observation orbit within 140 days. The time for all in orbit operations is 2 years and 1 month (764 days). Since this duration is rather long, the observation procedure could be stretched over a longer period of time. However, the data needed to observe potential landing site locations comes from the camera. Therefore the spacecraft will first start mapping and, since it is possible, at the same time observe and store all data obtained. As the camera is the instrument with the critical resolution, the observation altitude will be based on the camera. For determining the altitude of the mapping orbit the following considerations were made. The area pictured by the camera, is set to be 150 by 150 $[m]$, in order to efficiently map the asteroid. With a 10% overlap, the effective area pictured equals to be 135 by 135 $[m]$. This leads to a maximum ground track separation of 25 degrees for an asteroid radius of 309 $[m]$, and 13 $[°]$ for an asteroid radius of 609 $[m]$. Using GMAT, the orbit and ground track of Piazzi around the asteroid could be modelled, which lead to an ideal altitude of 581 $[m]$ for the lowest asteroid radius, and an altitude of 586 $[m]$ for the highest asteroid radius. Adding a few meters to account for irregularities in the simulation, the orbital altitude for detailed mapping was determined to be 600 $[m]$. Considering the 600 $[m]$ altitude and an unique ground track for each image, equal to 135 $[m]$, the amount of images per spacecraft orbital period ranges from 13 to 26. For this the length of the total ground track was calculated based on the circumference of the asteroid using the spherical assumption and radii given earlier. This was divided by the unique ground track of an image. However it was advised by Dr Daphne Stam (TU Delft) to image the asteroid from multiple angles to obtain more insight about the roughness of the surface and thus be able to determine a better sample site. Therefore once every 75 $[m]$ a picture is taken, so that the ground track is mapped from two different perspectives while

orbiting it only once. The amount of pictures per spacecraft orbital period thus equals 26 to 51. Also, the duration between two pictures could be calculated. For this, the amount of pictures was divided by the resultant speed vector, coming from the horizontal speed (rotation of the asteroid) and vertical speed (coming from the spacecraft orbit speed). It is evaluated that the pictures are obtained once every 5 to 13 minutes. The largest estimated asteroid can be covered in ten groundtracks, since the maximum radius is equal to 609 $[m]$ and image size is 135 by 135 $[m]$. Considering the maximum orbital period, it will take a little less than four days. Note however that during eclipse time, no images are taken, resulting are gaps in the asteroid mapping. To account for those, another 16 days and a 0.01 $[m/s]$ of ΔV are added for mapping previously in eclipse areas so that the probability of missing an area out on several orbits is reduced. Finally, after all data is sent back to Earth within approximately 18 days, this full procedure is repeated three to four times, so that the asteroid is fully mapped from eight different angles.

After the 80 mapping days and the transmission of the TT&C subsystem, taking up 152 days, the next phase can be initiated. Those of detailed observations. After the images have been analysed, the ground station will initiate further observation of the four potential landing/sampling sites chosen: two for SASH and two for ACSAL. Two landing sites are observed in order to be able to shift to another site, if one might turn out to be infeasible. The reserved time for this landing site observation phase is four months. A large margin is taken for this, so that other interesting measurements which are based on observations in the first mapping phase can be performed within the mission planning. Two months are again reserved for TT&C procedures.

At this point there are 485 days left before the lander and hoverer return to Earth. 60 days are reserved for unforeseen circumstances and 30 for additional measurements. Another 185 days are reserved for landing test runs, as described in the sample acquiring subsection below. 210 days before return, the lander will start the descent phase and land on the asteroid. SASH will stay attached to the orbiter so that no additional ΔV needs to be brought to perform orbital maintenance burns. Finally, eight days before return, the hoverer will obtain its sample. This will not take a full day, but a margin of seven days is taken, might additional attempts be needed.

6.2.4. Sample acquiring

Once the observation procedure is successfully executed and the majority of the data are sent back to Earth, the potential sample acquiring sites are identified. Following on the locating of these sites manoeuvres are programmed and sent from Earth to obtain the samples. For both landers two sample sites will be determined and investigated to a more detailed extent. From them, one is chosen as final sampling site. Between the final landing site determination and actual landing, six months are reserved for landing test runs. How ACSAL and SASH obtain their sample is described below.

SASH

SASH, dedicated to hover above the asteroid and then take a sample using a robotic arm, will perform its descent and material acquiring procedure fully autonomous, as further described in Figure 8.18. Since this process is fully autonomous and thus uncontrollable from Earth, the procedure will be tested in parts up to the final step. First SASH will descent and hover above the asteroid at a 100 $[m]$ altitude and return to orbit. Following, SASH will hover above the designated location at an altitude of 10 $[m]$ and return to orbit. If these movements are successful the hover-height is further reduced and the sample collection will be carried out.

ACSAL

ACSAL is the only spacecraft designed to stay on 1989 UQ for a longer period of time. When a landing site is chosen and confirmed by the ground station, ACSAL will descend and land on the asteroid. The claws in the landing legs in combination with the harpoons will secure the position on the surface so the sample drill can obtain a core sample. Once a sample is acquired successfully, ACSAL will take off, leaving the landing system on the asteroid.

6.3. Launcher

For the Piazzi mission, the ULA Atlas V had initially been chosen as the launcher based on the preliminary wet mass of the orbiter in combination with the required C3 energy to escape Earth's SOI. However, during the iterative process of the final preliminary design phase, the wet mass of the orbiter has been reduced to 1,506 $[kg]$ allowing the Piazzi mission to use a more cost-effective launcher. The Falcon 9 Full Thrust will be used of which the C3 energy required to escape Earth's SOI is shown with the amount of payload that the launcher can carry in Figure 6.4. In Figure 6.4, the C3-energy required for the Piazzi mission being 15.8 $[km^2/s^2]$ along with the payload it can carry is shown with green lines. It has to be noted though that the C3-graph shown displays the performance of the Falcon 9 Block 2, whereas the current version of the Falcon 9 is the Block 5. Unfortunately, no information on performance is available from this version of the Falcon 9. The Falcon 9 Block 5 did improve on performance compared to the previous versions though, which ensures that this launcher can be used for the Piazzi mission [3]. Next to that, the Falcon 9 has performed 57 launches over the last 8 years of which 55 were successful [4]. This shows us that

[3] http://spacenews.com/musk-details-block-5-improvements-to-falcon-9/ Accessed June 26, 2018

[4] https://spacexnow.com/stats.php Accessed June 26, 2018

the Falcon 9 meets user requirement ASRM-USR-NO10 having a launch succes rate of 90% or higher.

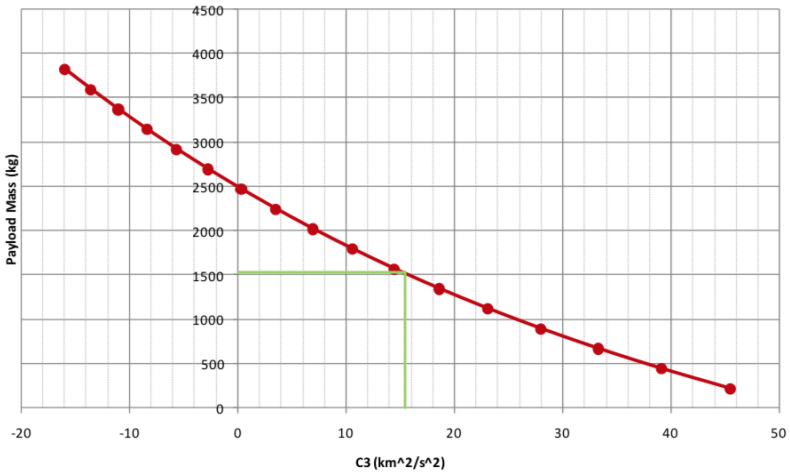

Figure 6.4: Falcon 9 C3-energy vs. Payload (Space Exploration Technologies Corporation [2009])

6.4. Reentry

Upon return to Earth, both landers will detach the reentry capsules, while giving them a spin, initiating the Earth reentry phase. During this phase the reentry capsule will be exposed to harsh atmospheric conditions resulting in intense heat generation and structural loads. To ensure the quality of the samples when arriving on Earth, reentry capsules and their trajectory are designed. In this section the design of both reentry capsules is discussed, followed by an outline of their predicted reentry flight trajectory to be able to determine the landing site of the capsules.

6.4.1. Reentry capsule design

Contrary, to what was concluded in the trade-off procedure described in the midterm phase (Angyal et al. [2018]), the sample return capsules used in the Piazzi mission will resemble the one used on the Hayabusa mission. The reason for this change is the size of the Hayabusa capsule compared to the one used in the Stardust mission: since this smaller capsule would result in a smaller and therefore lighter and more economical spacecraft, while still fulfilling the design requirements, the Hayabusa capsule was preferred. The Hayabusa capsule has proven to be successful in a space mission complying with the TRL requirement which is set for the Piazzi mission. Furthermore, it is small, lightweight, reliable and has a high level of autonomy. The layout and dimensions of the used capsule can be seen in Figure 6.5.

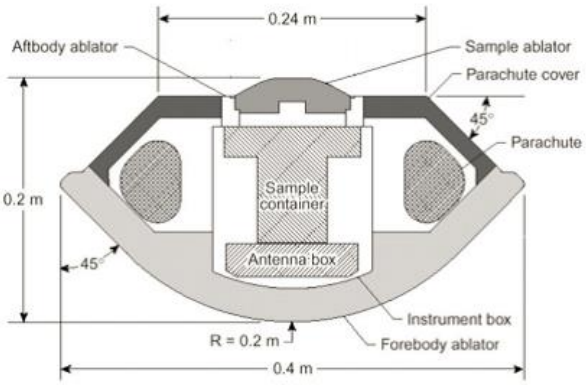

Figure 6.5: Hayabusa Reentry Capsule (Grinstead et al. [2011])

6.4.2. Reentry Trajectory

The trajectory followed by the reentry capsules was simulated to visualise where the capsules will land on the ground, in order for the search area for retrieval to be narrowed down. The reentry phase of the mission is the final phase, following up on the

return trajectory from the asteroid to the Earth. When reaching the earth at a distance of 120 $[km]$ the reentry phase of the mission is started, the capsules and spacecraft will leave outer space, while making an entry into the earth's atmosphere. To model the trajectory followed by the capsules, certain assumptions were made:

- The earth is assumed to be spherical;
- The earth is assumed to be non-rotating;
- The capsules are assumed to not have an initial acceleration;
- The drag constant of the capsule, C_D stays constant during reentry;
- The molecular weight of the atmosphere is assumed to be constant with altitude;
- The mass distribution of Earth is assumed to be radially symmetric;
- The effects of wind are neglected.

Furthermore, at an altitude of 8 $[km]$ the parachutes are deployed, bringing the capsule into vertical descent. Therefore, when modelling the horizontal travelled distance, this last part of the descent can be neglected.

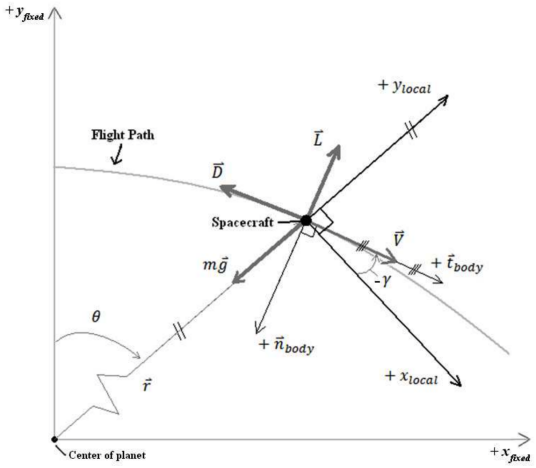

$$\dot{x} = V\ cos(\gamma) \tag{6.1}$$

$$\dot{V} = -\frac{\rho V^2}{2B} - g\ sin(\gamma) \tag{6.2}$$

$$\dot{h} = V\ sin(\gamma) \tag{6.3}$$

$$\dot{\gamma} = \frac{\rho V}{2B}\frac{C_L}{C_D} - \frac{g\ cos(\gamma)}{V} + \frac{V\ cos(\gamma)}{R_e + h} \tag{6.4}$$

$$\rho = \rho_0 \cdot e^{-\frac{h}{H}} \tag{6.5}$$

$$g = g_0\left(\frac{R_e}{R_e + h}\right)^2 \tag{6.6}$$

Figure 6.6: Free body diagram of Earth reentry (Tetzman [2010])

Implementing the assumptions stated above, from the free body diagram in Figure 6.6 the following equations of motion can be set up (Equation 6.1 to Equation 6.4).

The density and gravitational acceleration vary with altitude, as can be seen in Equation 6.5 and Equation 6.6 respectively.

These equations were simulated, giving the results depicted in Figure 6.7 and Figure 6.8. The starting values are γ_0 = 5.7 [°] and V_0 = 13 $[km/s]$, and the simulation starts at an altitude of 120 $[km]$. From these results it can be determined that the horizontal distance travelled by the capsule during its reentry is approximately 930 $[km]$. This shows that the return angle and speed determined by GMAT are valid and can be used for this mission.

6.4.3. Verification and validation

To verify the program used to simulate the reentry, a few tasks were executed. First of all, a unit test was performed, to make sure that the code works as expected. The code in the loop was reproduced by hand, and the program was let to run one loop, so that the results could be compared. As was expected, both the program and the manual calculations arrived at the same results. Furthermore, a sanity check was performed, verifying that the capsule indeed slows down, travelled in positive x-direction, and that the height decreases. All of these verified the program.

To validate the program the results were compared to reentry simulations done for meteors, which gives the results given in Figure 6.9 and Figure 6.10. From this it can be seen that comparable results are achieved using a different model. This validates the reentry model created for this mission.

6.5. Sensitivity analysis

Time is a big constraint for every design of aerospace vehicles: deadlines have to be met and everything needs to be time efficient. The consequence of a delay during building of the spacecraft for whatever reason would result in missing of the

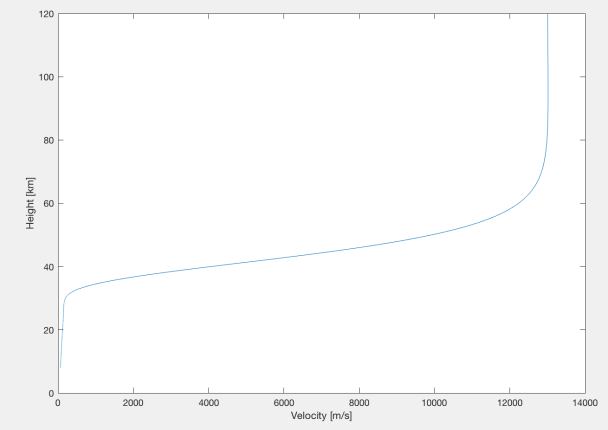

Figure 6.7: Velocity vs height for the reentry of the capsule

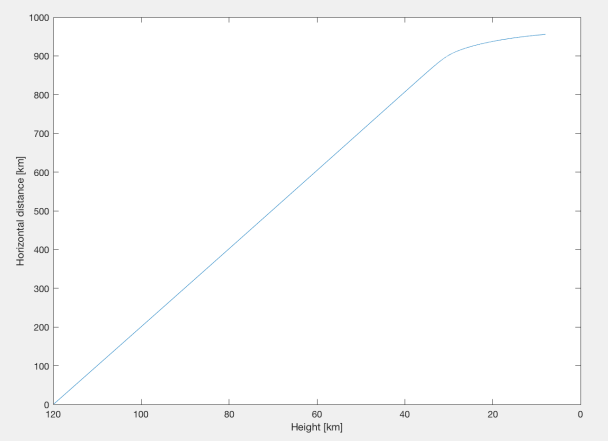

Figure 6.8: Height vs horizontal distance for the reentry capsule

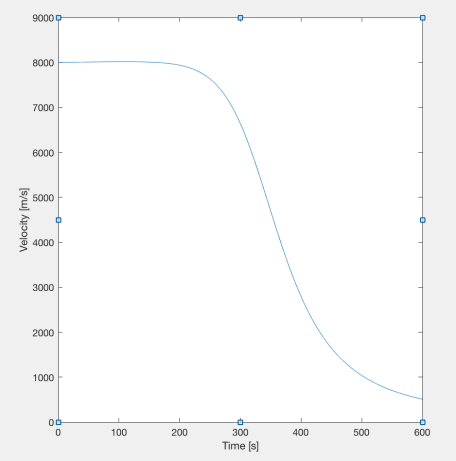

Figure 6.9: Velocity vs time for the model developed for this mission ($\gamma_0 = 1.42[°], V_0 = 8[km/s]$)

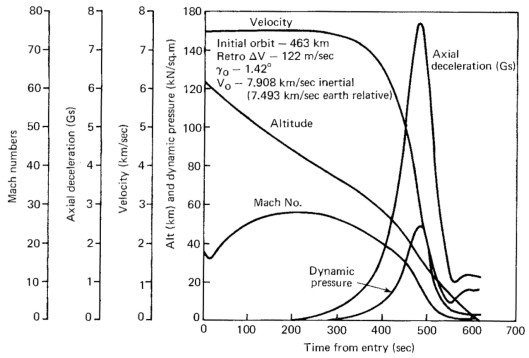

Figure 6.10: Velocity vs time (among other trends) for the validation model (Griffin and French [2004]).

launch window. This can be considered as a risk but a sensitivity analysis is still carried out in order to assess what would be the repercussion of such change in the mission time line and so on the performance of the whole spacecraft.

Two options arise if the launch date is missed, one is to postpone the launch and wait for the next beneficial launch window and obtain a comparable amount of ΔV as initially designed for, while the other option is to choose another asteroid. For the first option, it is computed that the next opportunity to have the same ΔV to reach 1989 UQ is possible in September 2031. This choice has no impact on the design of all spacecraft but have a major impact on the logistics and the cost. The spacecraft will have to be stored in a cleanroom for around seven years in order to keep the spacecraft from being contaminated. Also it is very expensive to keep a spacecraft on Earth when it is supposed to be in space as so the budget cost of 1000 million euros would definitely be exceeded. Additionally, degradation of components will result in affected performance or replacement of systems, driving the cost even further. While for the other option, that is to choose a different asteroid, as a first approach two would be favourable in terms of scientific value, which are 2001US16 and 2018EV5. For the former a launch date would be possible in May 2026; this asteroid could be reached with a little less ΔV which makes it a feasible alternative for the Piazzi mission design. For the 2018EV5 asteroid, a first estimation of the launch date was not found for the restricted ΔV that the Piazzi design can implement. As it can be concluded, there is a possibility to reach an asteroid and sample it after the original launch window is passed. This is not the case for the departure window from the asteroid towards Earth. This can not be missed since SASH and ACSAL may not survive for the long period in space due to radiation and degradation of critical components.

In order to assess the sensitivity of each spacecraft's criterion that was designed for, inputs are being altered. The analysis is focusing on the orbiter, lander, and hoverer separately and the sensitivity analysis is described in section 7.1, section 7.2 and section 7.3, respectively. First, the main design changes are explained and further specified in the corresponding sections.

The **density** of the asteroid is uncertain. The design assumes a density of 3,000 $[kg/m^3]$, but a large deviation is possible. A

higher density will result in a more stable orbit, hence requiring less cold gas to counteract disturbances. Manoeuvres on the other hand, will be more expensive. However, very few manoeuvres are planned for the mission, which would lead to an overall decrease in already small required cold gas fuel mass. If the density is lower, the contrary holds. The **rotational period** is currently estimated at 7.7 $[hr]$. A longer period does not have much effect on the mission phase, besides the fact that it might be necessary to wait for some areas to come out of eclipse to complete the mapping. A shorter period however poses more problems. Small asteroids (with radii between 0.3 $[km]$ and 10 $[km]$) have a so called spin barrier which is a lower limit on the rotational period. With an even shorter period and hence faster spinning, the centrifugal forces outweigh the gravitational forces and asteroids cannot exist (Carbognani [2017]). This is clearly not the case, so for 1989 UQ the rotational period must be higher than the spin barrier, which is 1.9 $[hr]$ (for ρ = 3,000 $[kg/m^3]$). Additionally, considering that the gravitational force must be higher than the centrifugal force, it can be assumed that there will be some regolith present on the asteroid. The **irregular shape** of the asteroid is taken into account. An irregular shape of the asteroid or a surface covered in craters would require more passes over the area to completely cover the surface. The asteroid shape might also result in large orbit perturbations, which would compromise the current mapping scheme and has a has a complicating effect on potential landing sites or manoeuvres. The same consequences hold for the case where the asteroid would have two rotational axes. Another factor is **solar pressure**. A higher radiation pressure would give a higher perturbation, which leads to more frequent correction burns. Additionally, attitude would suffer from a higher radiation pressure, so reaction wheels will need more frequent momentum dumping. During a solar maximum, the solar pressure increases with approximately 7%, and since the disturbance torque varies linearly with the pressure, this will also approximately equal the increase in cold gas required. This falls withing the 20% margin that was used in calculations. Naturally, lower radiation pressure would have the inverse effect.

Given the fact that there are approximately two and a half years between arrival near the asteroid and the return window, and the mapping operation in ideal conditions not including transmission of the data is estimated to takes significantly less time, the shape, surface or rotational axes of the asteroid will have little to no effect on mission feasibility or scientific yield. It could increase the mission risk, as an irregular shape or small asteroid complicates the landing and sampling procedure.

7
Spacecraft

In this chapter a detailed overview of the design for the orbiter (Piazzi), the hoverer (SASH, Sample Acquiring Surface Hover) and the lander (ACSAL, Asteroid Core Sample Acquiring Lander) will be given.

7.1. Orbiter - Piazzi

In this section the detailed design of the orbiter will be given. It will orbit the asteroid during the first part of the mission phase near the asteroid and observe it with multiple scientific instruments, both for landing and scientific purposes. First the requirements for the orbiter in general will be derived for which it will be designed. Next, the final architecture, mission time line, technical resource budgets, and block diagram of all the components are shown. The subsystems are designed based on requirements given in the section of that subsystem in chapter 8.

7.1.1. Requirements

`ASRM-ORB-001` The orbiter shall be able to perform an orbit insertion manoeuvre upon rendezvous with the asteroid. [A]
`ASRM-ORB-002` The orbiter shall be able to study the asteroid. [D]
`ASRM-ORB-003` The orbiter shall communicate with the landers and Earth. [D]
`ASRM-ORB-004` The orbiter shall contain a decoupling mechanism. [D]
`ASRM-ORB-005` The orbiter shall be able to correct its attitude. [A]
`ASRM-ORB-006` The orbiter shall control its temperature. [A]

7.1.2. The architecture of the orbiter

In this section, an overview is given of all the instruments that will be brought on the orbiter. In this overview all sources, except for the observational instruments, are given where applicable to find dimensions, mass, and power use, among specific characteristics.

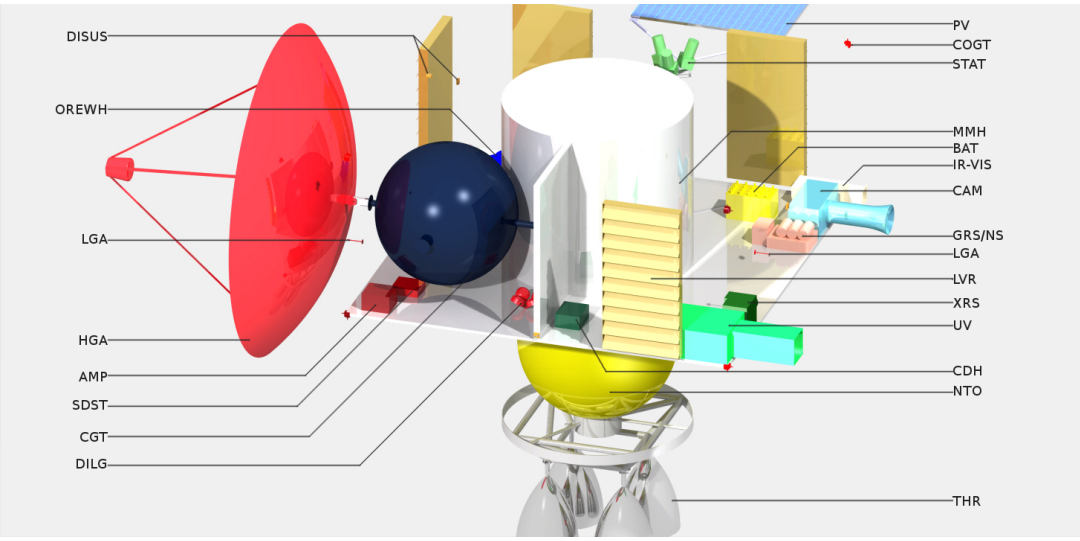

Figure 7.1: Orbiter Architecture (The outer skin has been left out for clarity.)

In Figure 7.1 the architecture of the orbiter is shown. In this figure one can clearly see the different position the instruments are attached to. The instruments are given in abbreviations for which the full names are given in Table 7.1 with a short description

of their function.

Table 7.1: Overview of Instruments on the Orbiter

Instrument	Abbreviation	Function
Star tracker sensor	STAT	Determines the attitude of the orbiter by tracking the stars.
Digital laser gyroscope	DILG	Determines the attitude of the orbiter in its inertial reference frame.
Digital sun sensor	DISUS	Determines the attitude of the orbiter by tracking the sun.
Cold gas thruster	COGT	Changes the attitude of the orbiter by the use of thrust.
Cold gas tank	CGT	Stores cold gas for pressurising the propulsion system and attitude control.
Low gain antenna	LGA	Reliable means to transmit housekeeping data.
High gain antenna	HGA	Transmit the science data back to Earth.
Transponder	TRA	The main communication computer on the orbiter.
Amplifier	AMP	Amplifies the communication signal.
Orbiter reaction wheel [7]	OREWH	Changes the attitude of the orbiter.
Peltier component	PLT	Cooling CCD-component of observational instruments.
Louver system	LVR	Regulates the amount of energy a radiator can radiate.
Radiator	RAD	Removes excess energy from the satellite.
Gammy-ray/neutron spectrometer	GRS/NS	Measures the gamma-ray/neutron spectrum of the asteroid.
UV spectrometer	UVS	Measures the UV spectrum of the asteroid.
X-Ray spectrometer	XRS	Measures the X-Ray spectrum of the asteroid.
Infrared-visual spectrometer	IR-VIS	Measures the IR and visual spectrum of the asteroid.
Magnetometer	MAG	Measures the magnetic field surrounding the orbiter.
Bipropellant thruster valve	BITV	Regulates the propellant for the thruster.
Bipropellant thruster [10]	AMBR	Decelerate the spacecraft near the asteroid.
MMH propellant tank	MMH	Contains the fuel for the AMBR
NTO Propellant Tank	NTO	Contains the oxidiser for the AMBR

7.1.3. The Mission Time line of the Orbiter

Figure 7.3 provides an overview of the mission time line for the orbiter. Starting point is the moment when it detaches from the launcher until its EOL.

The block diagram in Figure 7.5 shows the fashion software and the hardware are working together on board of the SASH lander. The orbiter is tasked with both studying the asteroid, as well as transporting the two smaller spacecraft, decoupling them, and operating as a relay station for their data. To be able to perform these tasks, adequate control over the spacecraft is required. The interfaces between software and hardware function as the regulatory system that allows for proper functioning according to the mission specifications.

[1] https://www.vectronic-aerospace.com/space-applications/star-sensor/ Accessed June 14, 2018

[2] https://aerospace.honeywell.com/en/~/media/aerospace/files/brochures/gg1320andigitallasergyro-bro.pdfAccessed June 15, 2018

[3] https://www.isispace.nl/brochures/NSS_Fine_Sun_Sensor_Datasheet_2c-.pdf Accessed: June 14th, 2018

[4] http://www.moog.com/content/dam/moog/literature/Space_Defense/Spacecraft/Propulsion/ColdGasThrusters_0717.pdf Accessed June 17, 2018

[5] https://gdmissionsystems.com/products/communications/spaceborne-communications/tracking-telemetry-and-control/small-deep-space-transponder Accessed June 18, 2018

[6] https://gdmissionsystems.com/-/media/General-Dynamics/Space-and-Intelligence-Systems/PDF/spaceborne-x-band-sspa-datasheet.ashx Accessed June 18, 2018

[7] http://bluecanyontech.com/wp-content/uploads/2018/01/DataSheet_RW_07_F.pdf Accessed June 14, 2018

[8] https://www.cui.com/product/resource/cp08-m.pdf Accessed June 21, 2018

[9] https://ntrs.nasa.gov/archive/nasa/casi.ntrs.nasa.gov/19940027766.pdf Accessed June 21, 2018

[10] http://www.rocket.com/files/aerojet/documents/Capabilities/PDFs/Bipropellant%20Data%20Sheets.pdf Accessed June 20, 2018

Table 7.2: Overview of the Orbiter

Subsystem	Part	Amount	Mass $[kg]$	Power $[W]$	Dimensions
Structure			**230**		
	Primary structure	1	92	-	1.194⌀ x 2.20 ↕ $[m]$
	Secondary structure and mechanisms	1	138	-	-
EPS			**33**		
	PV array	1	7	-	2.6 $[m^2]$
	Li-ion battery	8	2	-	0.0074 $[m^3]$
	PCDU	1	6	-	TBD
TT&C			**52**		
	LGA	2	0.4	-	100 $[mm]$
	HGA	1	24	-	2000 ⌀ $[mm]$
	DIP	3	0.2	-	TBD
	AMP [6]	2	1	395	174 x 134 x 47 $[mm]$
	TRA [5]	2	4	15.8	181.10 x 166.37 x 114.30 $[mm]$
	Cabling	1	18	-	-
ADCS			**50**		
	STAT [1]	3	0.3	2.5	80 x 100 x 180 $[mm]$
	DISUS [3]	6	0.04	0.0375	-
	DILG [2]	4	0.5	1.6	-
	COGT [4]	24	0.02	30	6.6 ⌀x 25.4 $[mm]$
	REWH	4	1	8	170 x 170 x 70 $[mm]$
	CGT	1	43	-	0.375 $[m^3]$
Propulsion			**472**		
	AMBR	4	5	-	400 x 701 $[mm]$
	Propellant tank	1	445	-	(section 8.3)
	Pressurant gas	1	5	-	-
C&DHS			**1**		
	CPU	1	0.5	5	96 x 81 x 92 $[mm]$
	Cabling	1	0.1	-	-
Thermal			**82**		
	Primary coating	1	61	-	28 $[m^2]$
	Radiator coating	1	6	-	3 $[m^2]$
	Radiator [9]	5	1	-	0.3 $[m^2]$
	Louver	5	2	-	0.31 $[m^2]$
	PLT [8]	8	-	7	-
Observation instruments			**61**		
	Camera	1	13	18.7	60 x 40 x 40
	Magnetometer	2	0.05	0.8	2.5 x 2.5 x 2.5 $[mm]$
	XRS	1	7	12.4	37 x 20 x 14 $[mm]$
	GRS/NS	1	11	9	26 x 18 x 20 $[mm]$
	UVS	1	5	4.4	20 x 41 x 12 $[mm]$
	IRVS	1	18	13.5	90 x 36 x 20 $[mm]$
	Cabling	1	9	-	-
Spacecraft			**473**		
	ACSAL	1	191	-	0.94 ⌀ 1.0 $[m]$
	SASH	1	203	-	0.94 ⌀ x 0.6 $[m]$
	Decouplers	2	~ 40	-	0.94 ⌀ $[m]$
Dry mass margin			**52**	-	-
Total	-		**1506**		

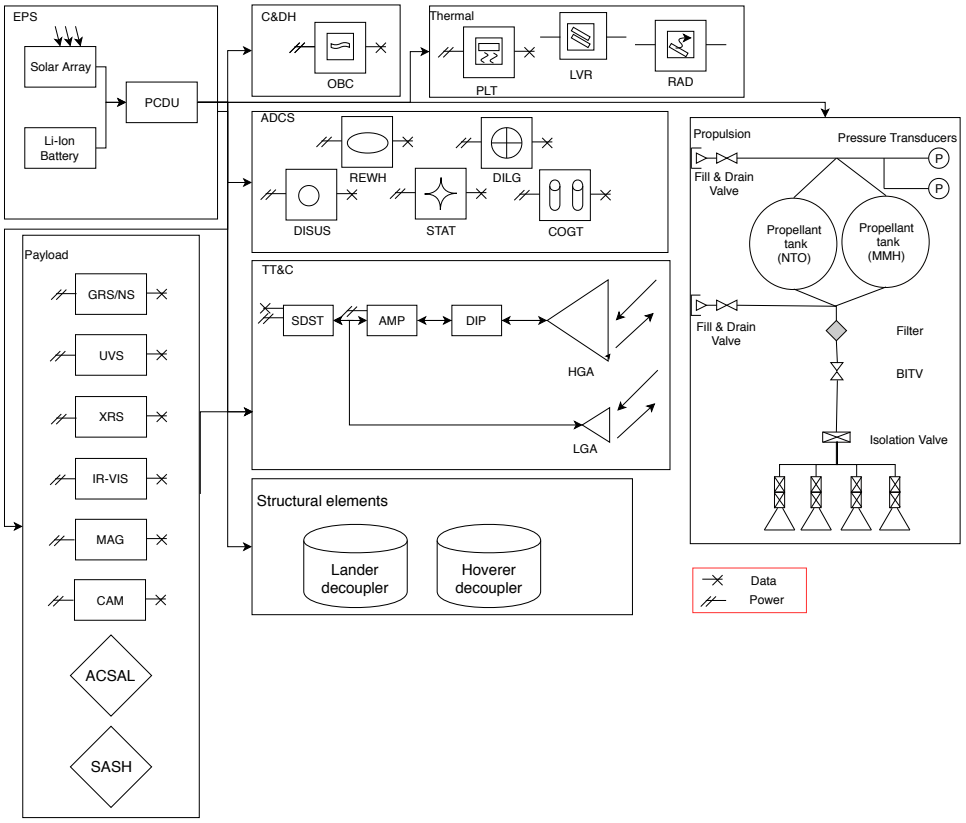

Figure 7.2: The Architecture Block Diagram of the Orbiter

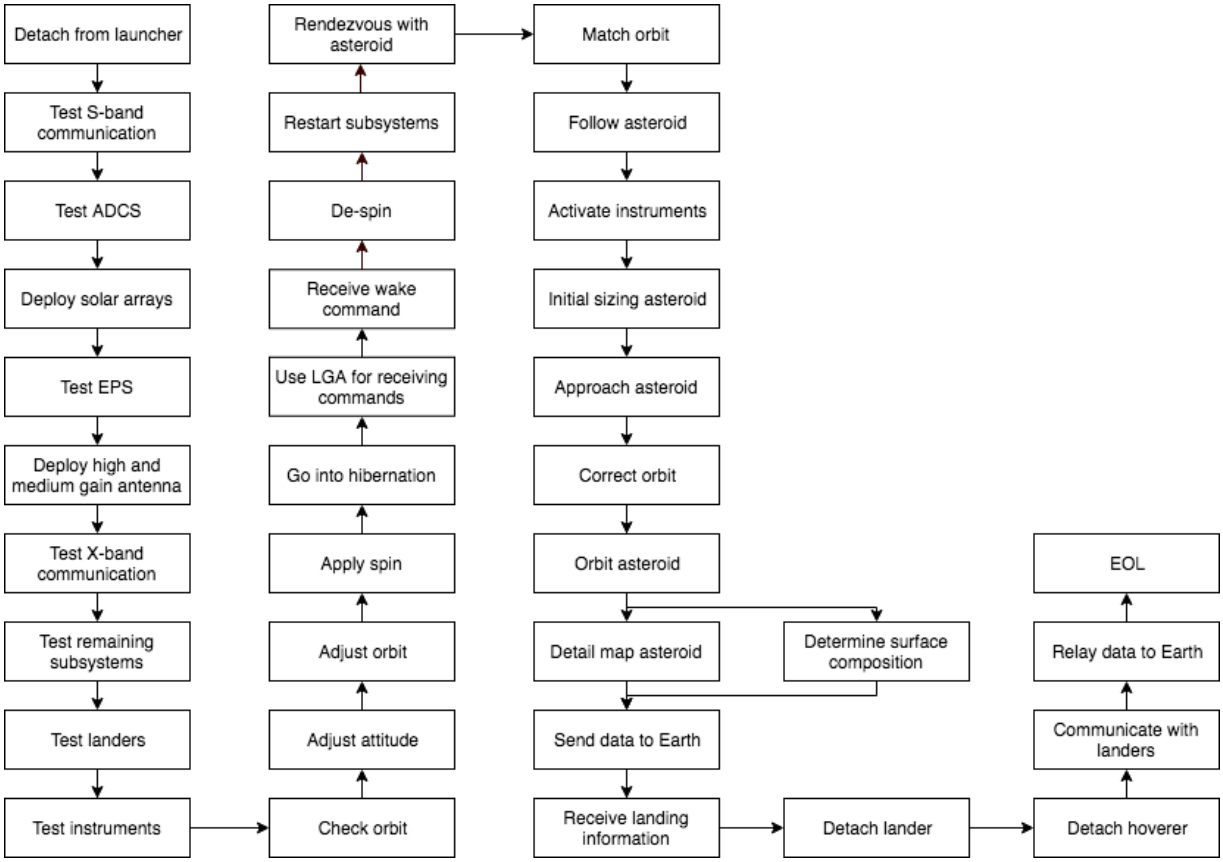

Figure 7.3: The Mission Time line of the Orbiter

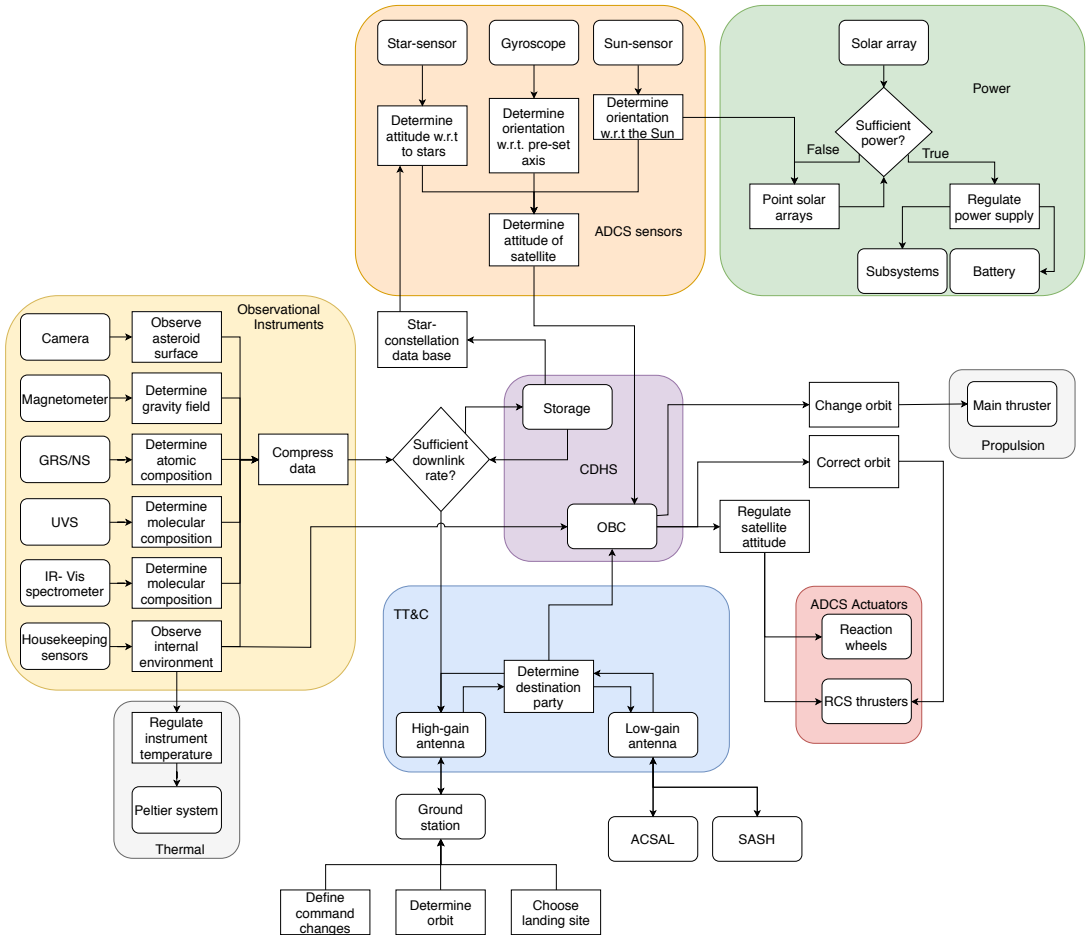

Figure 7.4: Software-hardware collaboration on board of the orbiter.

7.1.4. Observation Instruments

In this section the observation payload brought along the Piazzi mission is sized. The section starts with giving an overview of the background and the requirements. Following this, the mapping strategy is explained, and the choice of specific instruments is detailed. After this the performance parameters of the instruments, in terms of mass, power, dimensions, operating temperature, and data rate is estimated, as well as cost. Finally a sensitivity analysis is performed.

Background and requirements

The Piazzi mission has multiple scientific goals, that are explained in detail in Angyal et al. [2018]. These goals are summarised in the following requirements. Some requirements have been modified or specified in more detail.

`ASRM-SPL-001` The payload shall determine the age of the 1989 UQ. [T]
`ASRM-SPL-002` The payload shall determine the density of 1989 UQ. [A]
`ASRM-SPL-003` The payload shall determine atomic composition of 1989 UQ's surface. [T]
`ASRM-SPL-004` The payload shall determine molecular composition of 1989 UQ's surface. [T]
`ASRM-SPL-005` The payload shall aid in determining the landing site of the landers. [A]
`ASRM-SPL-006` The payload shall determine the shape of 1989 UQ. [I]
`ASRM-SPL-007` The payload shall detect the presence or former presence of a magnetic field on 1989 UQ. [A]
`ASRM-SPL-008` The camera shall map the surface of the asteroid with a resolution of at least 0.075 $[m/px]$. [D]
`ASRM-SPL-008` The camera shall be able to view 1989 UQ with a minimum resolution of four pixels from a minimum distance of 10,000 $[km]$. [D]
`ASRM-SPL-010` The camera shall be able to view the entire asteroid in one picture from a minimum distance of 8.5 $[km]$. [A]
`ASRM-SPL-011` The payload shall estimate the atomic composition of 1989 UQ's surface to a depth of one $[m]$. [A]
`ASRM-SPL-012` The payload shall determine the atomic composition of the potential sample area with a resolution of six $[m]$. [D]

From these requirements the mapping strategy was determined as was described in section 6.2, and instruments were chosen and sized.

To meet the requirements explained above, several instruments have to be brought as payload. These instruments and their usage will be explained in this section. Their selection is based on the requirements. Reference instruments that closely match the requirements were used to obtain an estimate for the performance parameters of each instrument, however, for this mission the instruments will be altered to better suit the requirements.

Camera

The first instrument to consider is a camera, which needs to be able to give sufficient detail of the surface of the asteroid, in order to determine a suitable landing site. The selection of the camera depends on the mapping orbit described. From this mapping orbit the required instantaneous field of view (IFOV) to achieve the required spatial resolution can be determined (ASRM-SPL-009), using equation Equation 7.1. This can then be converted to a field of view (FOV) using equation Equation 7.2. In these equations, both the IFOV and FOV are expressed in degrees. d is the ground resolution in $[m]$, h is the altitude in $[m]$, and n is the number of pixels. It should be noted that for cameras with an asymmetrical detector the horizontal and vertical IFOV, and thus ground resolution, are different.

$$IFOV = 2\tan^{-1}\left(\frac{d}{2h}\right) \tag{7.1}$$

$$FOV = IFOV \cdot n \tag{7.2}$$

By using the equations above, it was calculated that the required IFOV is 0.0072 degrees, for a ground resolution of 0.075 $[m]$ (with an altitude of 600 $[m]$). However, in order to view the asteroid from the required distance of 5,000 $[km]$ (with at least 4 by 4 pixels for the asteroid), an IFOV of 0.0014 degrees is needed. Finally, in order to achieve a ground area per picture of 150 by 150 $[m^2]$, a CCD with a size of 2,000 by 2,000 pixels is needed, and an optic system in order to increase the FOV when close to the asteroid. Using these numbers a reference camera could be selected, from a range of cameras used on previous missions. The cameras considered were the ones used on Rosetta (Keller et al. [2007]), OSIRIS-REx (Rizk et al. [2018]), and Dawn (Sierks et al. [2011]). Of these, the narrow-angle camera used on Rosetta was considered to be the closest to the specifications set above. Using it as reference, the specifications of the camera on Piazzi were determined to be as follows. It will have an IFOV of 0.0011 degrees. With the requirement of a CCD with 2,048 x 2,048 pixels, the image size will be 12 MB, using a 24 bit per pixel encoding, giving it full colour pictures. The shutter time of a typical image is ca. 100 $[ms]$. The camera's other performance parameters are given in Table 7.3.

Magnetometer

Since the choice of magnetometer has almost no impact on the mass and power performance of the payload, it was chosen to use the magnetometer that was taken on Rosetta (Carr et al. [2007]), since this instrument was specifically designed to measure the magnetic field of a small body. In order to limit the influence off the spacecraft on the measurements, the magnetometer will be placed on the end of one of the solar panels, and a second magnetometer will be taken, placed closer to the spacecraft. In this way the magnetic field of the spacecraft can be taken into account. The combined performance parameters for the two instruments can be found in Table 7.3. The magnetometers have a maximum sampling rate of 20 $[Hz]$.

Atomic Composition

For determining the atomic composition of the asteroid two instruments will be taken, as explained by Angyal et al. [2018]. One of these is a X-ray spectrometer (XRS), the other a combined gamma- and neutron ray spectrometer (GRS/NS). The XRS will be able to give an indication of atomic composition with a high spatial resolution (ASRM-SPL-012), but cannot penetrate the ground further than a few milimeters. To get data of up to a depth of one metre (ASRM-SPL-011) a GRS/NS is taken.

For the XRS, the compared instruments were REXIS (Masterson et al. [2018]), the XRS considered for a ESA Near Asteroid Sample Return concept mission (Agnolon [2007]), and the XRS on board of Messenger (Schlemm II et al. [2007]). The XSR considered for the ESA concept was discarded, because it has not the required TRL. Of the two left over, REXIS was chosen as the reference instrument for the XRS on Piazzi. Its spatial resolution is approximately 5 $[m]$ from the mapping orbit and uses a two by two array of CCDs, that each have 1,024 x 1,024 pixels. However, to limit the area in the image the FOV is limited, such that only an array of 64 x 64 pixels is actively used for imaging. The left over pixels are used for noise reduction.

Considering the GRS/NS, instruments compared were Dawn's GRaND (Russell and Raymond [2012]), and the instruments of both Messenger (Goldsten et al. [2007]) and Mars Oddysey (Boynton et al. [2004]). Of these three instruments, Dawn's GRaND has the best performance and it is therefore chosen as the basis in this design. It has a spatial resolution of something more than a kilometre from the mapping altitude. For both the XRS and this instrument the performance parameters can be found in table Table 7.3.

Table 7.3: Observation instruments to be used on board of the Piazzi spacecraft

Instrument	**Mass** $[kg]$	**Power** $[W]$	**Dimensions** $[cm^3]$	$\mathbf{T_{op}}$ $[^oC]$
Camera	13	19	60x40x20	No specification
Magnetometers	0.09	0.8	2.5x2.5x2.5 (2x)	- 85 ± 40
XRS	7	12	37x20x14	< -60
GRS/NS	11	9	26x18x20	20 ± 5
UVS	5	4	20x41x12	20
IR-Vis spectrometer	18	14	90x36x20	-168
Total instruments	**52**	**59**	**-**	**-**
Cabling	add 10 %	-	-	-
Total payload	**58**	**59**	**-**	**-**

Molecular Composition

To determine the molecular composition (ASRM-SPL-004) the electromagnetic spectrum with wavelengths around those of visible light is analysed (Angyal et al. [2018]). In order to determine the composition as complete as possible, both a UV spectrometer, to detect organic molecules, and an IR-VIS spectrometer are taken on the mission. The later will be used to detect minerals, and will be equipped with a polarimeter, which is used to detect the size of the grains.

The IR-VIS spectrometer will be based on the OVIRS instrument (Reuter et al. [2018]), used on board of OSIRIS-REx. It has a better performance than the other instruments considered, which were the ones taken on Galileo (Carlson et al. [1992]), Dawn (De Sanctis et al. [1992]), and Rosetta (Coradine et al. [1998]). The spectrometer taken on Piazzi will have a 4 $[mrad]$ circular FOV, which will give it a ground resolution of 20 metres. Additionaly, a polarimeter will be added to the instrument. This will not increase the data rate, or power usage, and the mass will barely raise, but it will give additional data that can be used in order to select the landing site. The combined mass of the IR-VIS spectrometer and the polarimeter can be found in Table 7.3.

For the UV spectrometer the instruments considered for reference were the ones taken on New Horizons (Stern et al. [2008]), Galileo (Hord et al. [1992]), Juno (Gladstone et al. [2017]), and Maven (McClintock et al. [2015]). From these, the instrument from New Horizons (ALICE) was chosen as a basis for the UV spectrometer taken on Piazzi. The instrument will have a 2 x 2 degrees FOV, which gives it a ground resolution of 6.3 metres. Its other performance parameters can be found in Table 7.3.

7.1.5. Performance analysis

In this section the performance of the observation instruments is analysed. It starts with giving estimates for the mass, power usage, dimensions, operating temperature, and image size. This information is based on the selected reference instruments and taken from their respective sources. An overview of these values can be found in Table 7.3. An estimation for the data rate of each of the instruments is given in Table 7.4.

Data rate

To estimate the data rate of the payload for each instrument the amount of measurements or pictures needed has to be estimated. Considering the fact that the spacecraft can orbit the asteroid for a long time, due to the long stay time, the data rate can be reduced by separating measurements optimising the data rate. For example, when the camera is taking photos, the remaining instruments of the scientific payload could be switched off. This way the data generated is reduced allowing for a lower bandwidth. On the other hand, using compression and data storage, the spacecraft could measure a large amount of data. This data is first stored and compressed on board of the spacecraft to be send to Earth later during dedicated communication windows. This way, mapping orbits can be carried out without interruption and all the gathered data could still be shared with the ground station as described in section section 6.2. Starting with the camera, of which the picture size equals 2,048 by 2,048 pixels and using 24 bits per pixel the resolution of an image is equal to 96 Mbit. For the remainder of the instruments the data rate is mainly given by literature (Stern et al. [2008], Reuter et al. [2018], Agnolon [2007], Coradine et al. [1998], Carr et al. [2007], Masterson et al. [2018], Russell and Raymond [2012]). The final data rate can be found in Table 7.4.

Table 7.4: Observation instrument data rate.

Instrument	**Data rate** $[kB/s]$
Camera	9.3
Magnetometer	0.02
XRS	0.9
GRS/NS	0.4
IR-VIS	0.40
UV	0.01
Total	**11**

7.2. Lander - ACSAL

In this section the detailed design of the lander, ACSAL (Asteroid Core Sample Acquiring Lander), will be given. ACSAL will land on the asteroid and acquire a subsurface sample which it then will return safely to Earth for further analysis. First, the requirements for the lander in general will be derived for which it will be designed. Next, the final architecture, mission time line, technical resource budgets and block diagram of all the components are shown. After this an explanation on the sample acquiring mechanism and landing mechanism is provided. The subsystems are designed based on requirements given in the section of the specific subsystem in chapter 8.

7.2.1. Requirements on ACSAL

To perform the individual mission, that is the acquisition of a core sample, the lander will be required to perform multiple, task-specific operations. These tasks should be performed at a certain event, continuously, or at a certain phase of the mission. Below, the requirements of the ACSAL are listed.

ASRM-ACSAL-001	ACSAL shall be able to touch down on the asteroid. [D]
ASRM-ACSAL-002	ACSAL shall be supported by landing legs. [D]
ASRM-ACSAL-003	ACSAL shall be able to attach harpoons to the asteroid surface. [D]
ASRM-ACSAL-004	ACSAL shall be able to pre-drill a 0.15 [m] deep hole below the solid surface of the asteroid in basalt-like material. [D]
ASRM-ACSAL-005	ACSAL shall be able to change the drill head of the drill mechanism. [D]
ASRM-ACSAL-006	ACSAL shall be able to acquire a core sample from a depth of 0.20 [m]. [D]
ASRM-ACSAL-007	ACSAL shall be able to attempt a backup sample acquisition at a depth of 0.25 [m]. [D]
ASRM-ACSAL-008	ACSAL shall be able to seal the acquired sample. [D]
ASRM-ACSAL-009	ACSAL shall be able to place the sealed sample capsule in the reentry capsule. [D]

7.2.2. Architecture of ACSAL

An overview of the architecture of ACSAL is provided in Figure 7.5 showing where the different subsystems and components are positioned, followed by a table explaining the different abbreviations used for the instruments attached to the lander in Table 7.5. Next to this, in Table 7.10 an analysis of the different subsystems connected to the lander is given with their specific mass per component, power consumption and dimensions. Finally in Figure 7.6 a block diagram is presented.

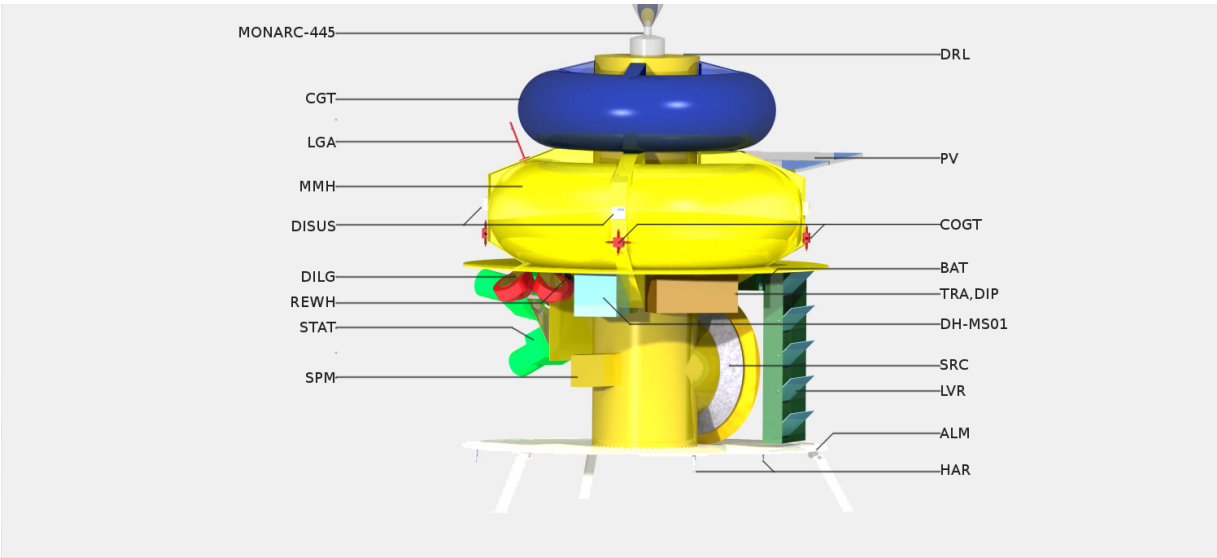

Figure 7.5: Lander architecture, the protective skin has been left out for clarity.

Table 7.5: Overview of the Instruments on the Lander

Instrument	Abbreviation	Function
Star tracker sensor	STAT	Determines the attitude of the lander by tracking the stars.
Digital laser gyroscope	DILG	Determines the attitude of the lander in its inertial reference frame.
Digital sun sensor	DISUS	Determines the attitude of the lander by tracking the sun.
Cold gas thruster	COGT	Changes the attitude of the lander by the use of thrust.
Low gain antenna	LGA	Reliable means to transmit housekeeping data.
Transponder	TRA	The main communication computer of the lander
Diplexer	DIP	Separates the incoming and outgoing signal.
Reaction wheel	REWH	Changes the attitude of the lander very precise.
Descent camera	DECAM	Ensures that the lander descends towards the chosen landing site.
Monomethylhydrazine	MMH	Monopropellant used for the propulsion system.
Monopropellant thruster	MONARC-445	Provides thrust on ACSAL to return to Earth.
Cold gas tank	CGT	Stores cold gas for pressurising the propulsion system and attitude control.
Monopropellant thruster valve	MOTV	Regulates the propellant for the thruster.
Computing unit	DH-MS01	The main computer of the hover.
Accelerometer	ACC	Determines the acceleration towards the asteroid during descent.
Peltier component	PLT	Cools the drill actuators.
Louver system	LVR	Louver system that regulates the amount of energy a radiator can radiate.
Radiator	RAD	Removes excess energy from the satellite.
Sample assurance laser	LAS	Ensures that a sample is acquired in the collector.
Asteroid landing mechanism	ALM	Ensure successful landing on the asteroid.
Sample drill	DRL	Acquire a subsurface sample of the asteroid.
Drill bit carousel	CAR	Rotating device to switch between drill bits.
Sample pushing mechanism	SPM	Mechanism to push the acquired sample into the SRC.
Sample return capsule	SRC	Capsule to ensure safe reentry through the earth's atmosphere.
Harpoon mechanism	HAR	Harpoon mechanism used to fasten lander to the asteroid.

Table 7.6: Overview of ACSAL's subsystem characteristics.

Subsystem	**Part**	**Amount**	**Mass** $[kg]$	**Power** $[W]$	**Dimensions**
Structure	Bus	1	~ 30		TBD
EPS			**16**	-	
	PV array	1	2	-	0.6 $[m^2]$
	Li-ion battery	4	2	-	TBD
	PCDU	1	3	-	TBD
TT&C			**11**		
	LGA	2	0.4	-	100 $[mm]$
	DIP	2	0.3	-	TBD
	TRA	2	4	5	181 x 166 x 114 $[mm]$
	Cabling	1	3	-	TBD
ADCS			**13**		
	COGT [21]	24	0.02	30	6.6 ⌀) 25 ↔ $[mm]$
	CGT	1	6	-	0.061 $[m^3]$
	STAT [11]	3	1	3	80 x 100 x 180 $[mm]$
	DILG [12]	4	0.5	2	88 ⌀45 ↕ $[mm]$
	DISUS [13]	6	0.2	0.2	34 x 32 x 21 $[mm]$
	REWH [14]	4	0.4	1	70 x 70 x 25 $[mm]$
	ACC [19]	2	0.01	0.08	20 ⌀1 ↕ $[mm]$
Propulsion			**59**		
	MONARC-445 [16]	1	2	-	148 ⌀ 410 ↕ $[mm]$
	MOTV [17]	1	1	58	TBD
	MMH	1	56	-	135 (inner ⌀) 404 (outer ⌀) 269 ↕ $[mm]$
	Pressurant gas	1	0.3	-	
C&DHS			**1**		
	CPU [18]	1	1	5	96 x 81 x 92 $[mm]$
	Wiring	1	0.1	-	TBD
Thermal			**9**		
	Primary coating	1	6	-	2.5 $[m^2]$
	Radiator coating	1	1	-	0.3 $[m^2]$
	Radiator	3	0.3	-	0.1 $[m^2]$
	Louver	3	0.5	-	0.1 $[m^2]$
	PLT [20]	2	-	7.04	-
Sample Mechanism			**40**		
	DECAM [15]	1	0.6	10	115 x 77 x 96 $[mm]$
	LAS	1	0.1	0.1	-
	ALM	3	1	-	-
	DRL	1	17	40.0	15 ⌀700 ↕ $[mm]$
	CAR	1	0.4	30	90 ⌀60 ↕ $[mm]$
	SPM	1	1	33.6	450 x 42 x 82 $[mm]$
	SRC	1	17	-	400 ⌀200 ↕ $[mm]$
	HAR	3	0.006	5	5 ⌀40 ↕ $[mm]$
Dry mass margin			**12**	-	-
Total			**191**		

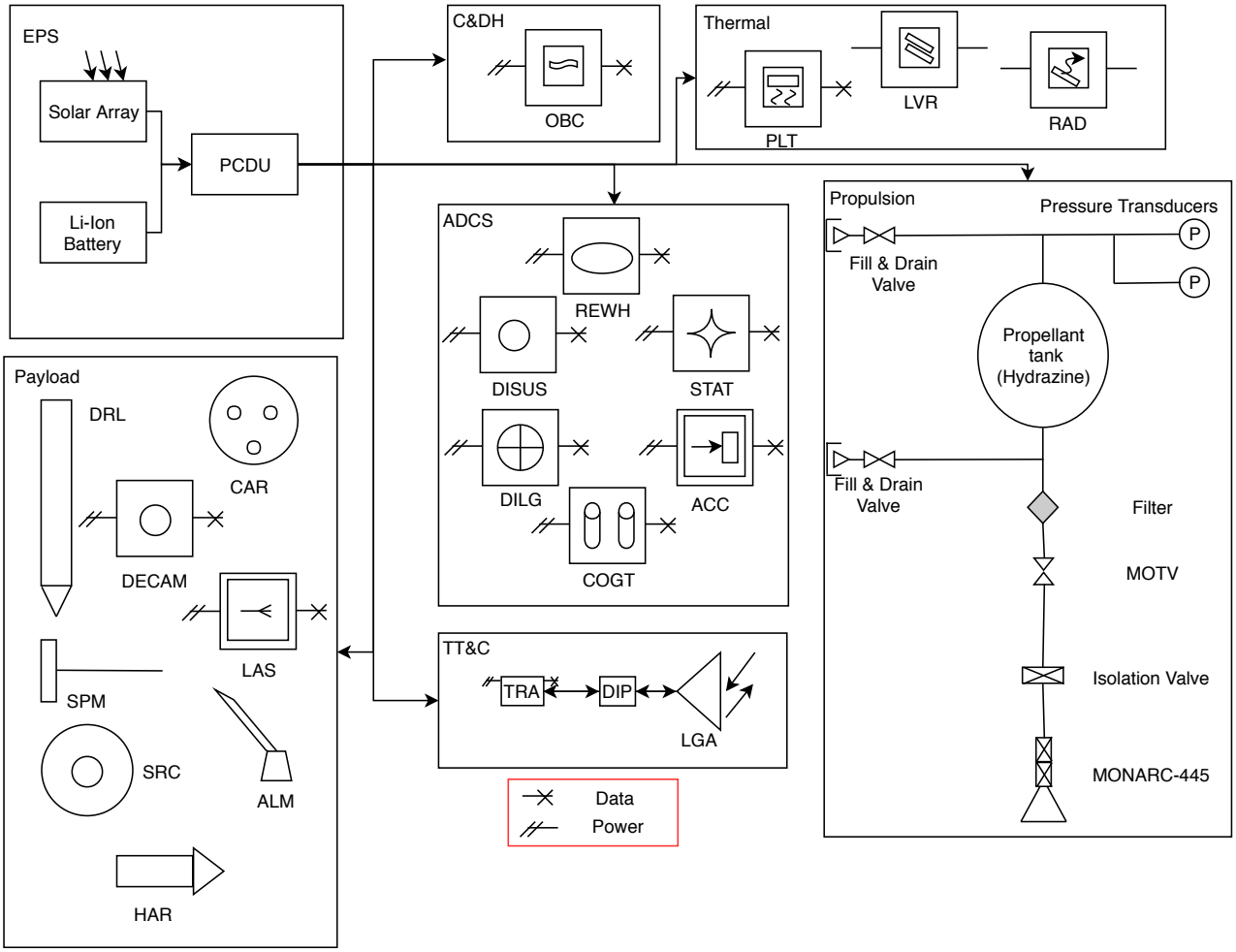

Figure 7.6: Block Diagram of the Lander

The graph represented above shows the connection between the software and the hardware on board of ACSAL. This collaboration is necessary to enable proper control of the satellite, as well as successful performance of the mission goal. The connections between these two disciplines ensure that all tasks throughout the mission profile are performed in a correct manner.

7.2.3. Mission timeline & sample acquisition (DRL)

In the following section the different steps the lander takes during it's journey from detaching from the orbiter until burning up in Earth's atmosphere are given, followed by a more detailed sequence of drilling into the asteroid, acquiring a sample and storing that in the reentry capsule, as summarised in Figure 7.7. Now a short description of the drill system will be given.

[11] https://www.vectronic-aerospace.com/space-applications/star-sensor/ Accessed June 14, 2018

[12] https://aerospace.honeywell.com/en/~/media/aerospace/files/brochures/gg1320andigitallasergyro-bro.pdf Accessed June 14, 2018

[13] https://www.isispace.nl/brochures/NSS_Fine_Sun_Sensor_Datasheet_2c-.pdf Accessed June 14, 2018

[14] http://bluecanyontech.com/rwp100/ Accessed June 18, 2018

[15] https://elib.dlr.de/86562/1/A_Camera_for_the_MASCOT_lander_on-board_Hayabusa_2.pdf Accessed June 15, 2018

[16] http://www.moog.com/content/dam/moog/literature/Space_Defense/Spacecraft/Monopropellant_Thrusters_Rev_0613.pdf Accessed June 14, 2018

[17] http://www.moog.com/content/dam/moog/literature/Space_Defense/spaceliterature/propulsion/MonopropellantThrusterValves_0418.pdf Accessed June 14, 2018

[18] http://aacmicrotec.com/sirius-cdh/ Accessed June 15, 2018

[19] https://aerospace.honeywell.com/en/~/media/aerospace/files/brochures/accelerometers/accelerexrba500accelerometer_bro.pdf Accessed June 16, 2018

[20] https://www.cui.com/product/resource/cp08-m.pdf Accessed June 21, 2018

[21] http://www.moog.com/content/dam/moog/literature/Space_Defense/Spacecraft/Propulsion/ColdGasThrusters_0717.pdf Accessed June 17, 2018

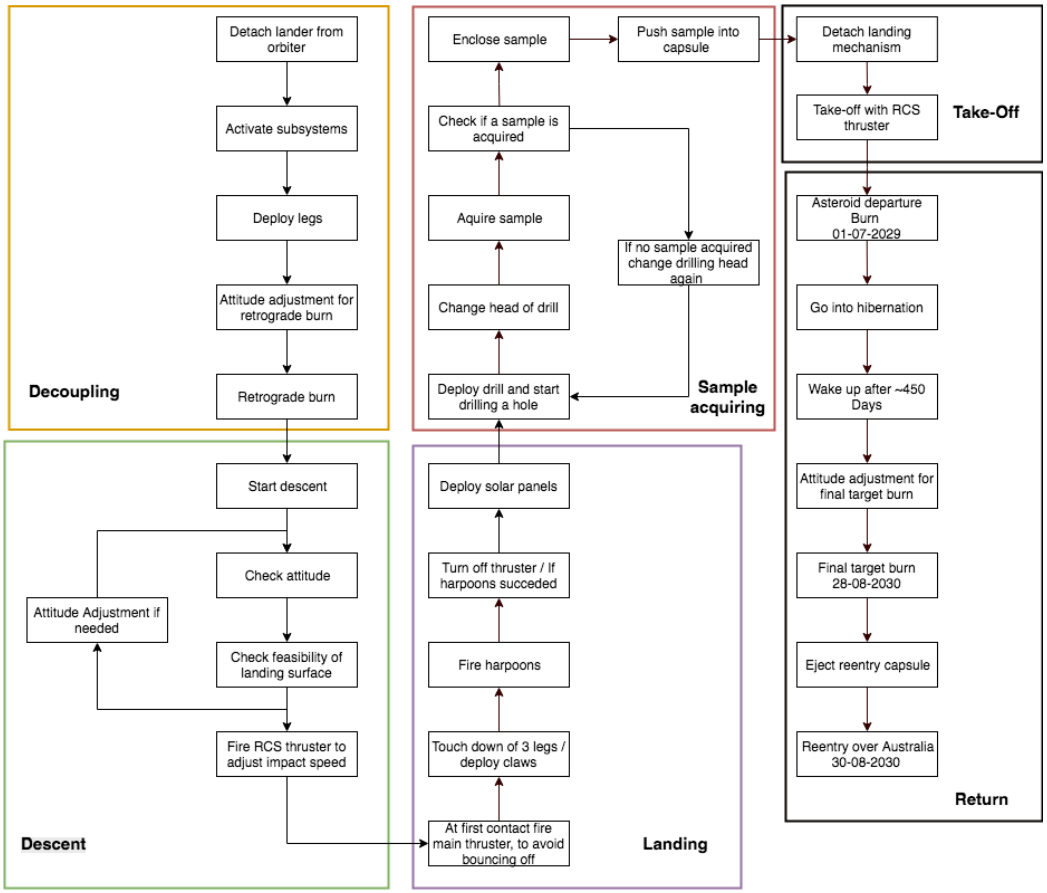

Figure 7.7: Mission profile of the lander

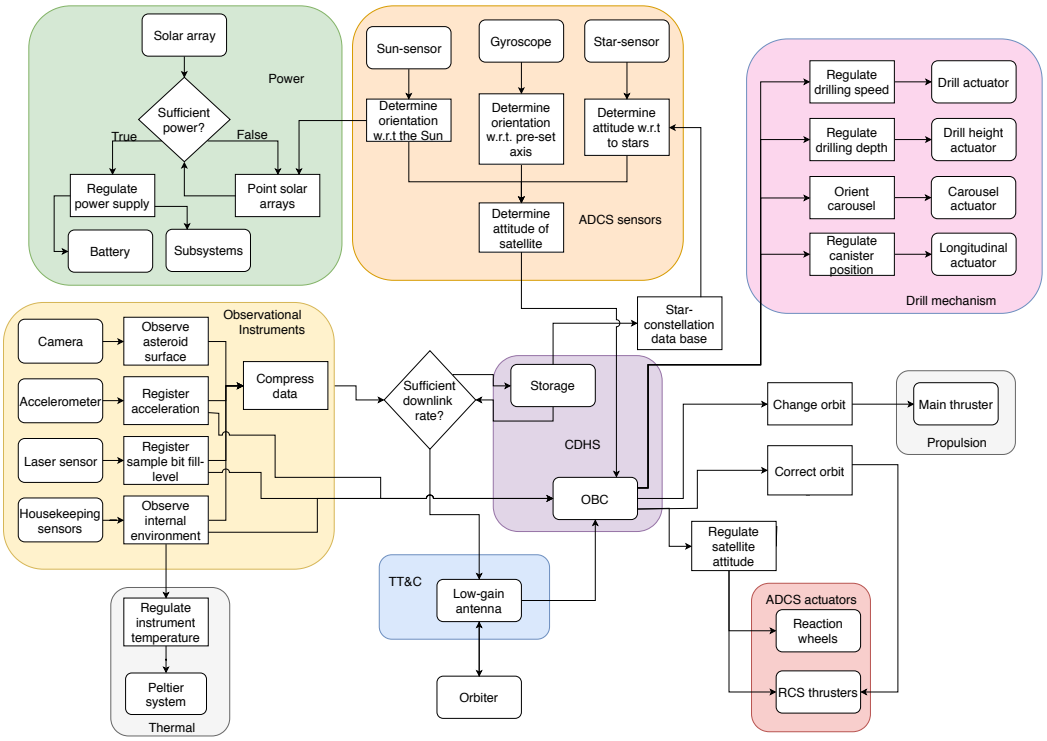

Figure 7.8: Software-hardware collaboration on board of ACSAL.

The mechanism features a drill with two different heads: a drill head and a special sampling head for the drill which are both stored on a carousel. Additionally, it includes a canister to seal the sample head, and a mechanism to store the canister with the sample head and the sample in the reentry capsule. Before specifics can be be discussed, requirements need to be set for the drilling mechanism. These will be used for computations concerning the system.

ASRM-ACSAL-DRM-001	The drill mechanism shall be able to lift the drill head above the carousel. [D]
ASRM-ACSAL-DRM-002	The drill mechanism shall be able to unscrew the drill head. [D]
ASRM-ACSAL-DRM-003	The drill mechanism shall be able to screw on the sample acquisition head. [D]
ASRM-ACSAL-DRM-004	The drill mechanism shall be able to place the sealing head below the drill arm. [D]
ASRM-ACSAL-DRM-005	The drill mechanism shall be able to screw the sample drill bit into the sealing head. [D]
ASRM-ACSAL-DRM-006	The drill mechanism shall be able to fasten the sealed sample capsule in the reentry capsule. [D]

The sequence of acquiring the core sample consists of multiple steps. The drill is initially equipped with the pre-drilling bit. The drill is deployed and lowered, where it will commence drilling. When it has a reached a depth of 150 $[mm]$, the drill fully retracts, lifting the drill bit above the carousel, where it places the pre-drill head in the carousel. The carousel then aligns the sampling head with the drill to allow the drill to equip itself with it. These drilling bits come with a screw thread, allowing the drill to fasten them on its tip. Next, the drill descends into the pre-drilled hole. As the sample head will have a smaller diameter than the drill head, it will allow it to reach the bottom without any friction. The drilling continues at 150 $[mm]$, and drills the sampling head 50 $[mm]$ further into the asteroid. The sampling head is hollow to house the attained sample and has teeth on the inside to both crush and hold the sample, filling up with asteroid core material the further it drills. The pressure exerted by the drill compresses the sample and in combination with the teeth inside, the sampling head prevents the sample from falling out.

Once a possible sample has been collected, the drill will be lifted up above the carousel. The carousel which will include a laser on the top side will rotate this laser accurately underneath the sample head. With this laser it is possible to examine if the sample head is filled with material and thus actually acquired a sample. If this is not the case, it is possible to drill another time into the asteroid's surface for another 50 $[mm]$, meaning the drill mechanism has a total of two tries to achieve an acquisition of a sample. After the second attempt it will be tested once again for a sample. If there should still be no sample it would imply that the lander's mission has come to a premature end.

However if a sample has successfully been collected, the drill retracts to store the sample in a canister. This canister is positioned one level above the carousel. The drill retracts far enough to allow an actuator to push the canister onto the sample head. The canister is equipped with a thread to enable the drill to hermetically seal the sample. The drill screws the sample head into the canister, hereby assuring the sample will remain sealed until opened on Earth.

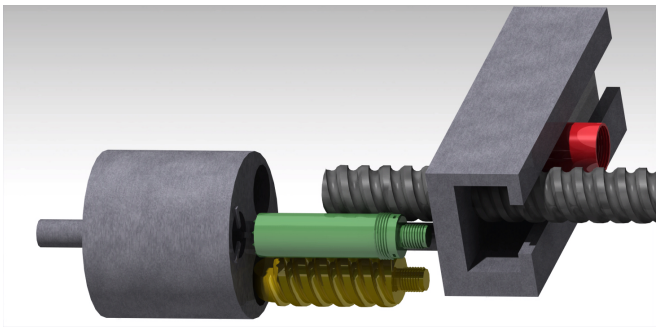

Figure 7.9: Drill mechanism

The screw thread of the drill head, sample head, as well as the thread of the canister rotate in the same direction, to prevent the drill heads from unscrewing themselves. Afterwards, when the canister is screwed on the sample head, in order to make sure that the drill head with the sample will unscrew from the main drill a small ball lock mechanism will be used between the canister and the sample head. This will provide enough counter force to unscrew the sample bit from the drill-arm, leaving the sample bit in the canister.

The canister is fixed onto the actuator by means of three pins. This actuator holds the canister in place while the sample head is screwed into it. When the sample head is secured, the actuator translates the canister into the reentry capsule, where it is fixed into a holder. Two of the three pins of the actuator retract, releasing the canister from the actuator, leaving the canister in the reentry capsule which then is ready to be deployed when necessary.

7.2.4. Drill

Once the lander has successfully landed on the asteroid and anchored itself onto its surface, the sample acquiring phase will start. To start this phase, a drill stored in the inside of the lander will extend and start drilling into the surface of the asteroid.

Table 7.7: Properties of the drills

	Diameter $[mm]$	**Thrust Force** $[N]$	**Torque** $[Nm]$	$\mathbf{P}_{req}$ $[W]$	**Mass**$[g]$
Drill head	15	703	4.0	43.5	63.7
Sample head	11	477	2.1	22.3	25.7

For this procedure, several aspects have to be taken into account. The strength of the surface has to be determined as well as the amount of regolith on it, in order to determine the properties of the drill manoeuvre.

To ensure that the collected sample can deliver a certain scientific value and still fit into the reentry capsule, it has been decided that the core sample shall have a diameter of 7 $[mm]$ and a height of 50 $[mm]$. Therefore, a diameter of 11 $[mm]$ has been given to the sample head. Moreover, to avoid friction between the sample head and the pre-drilled hole, a margin of 2 $[mm]$ on each side has been chosen, resulting in a diameter of 15 $[mm]$ for the main drill. Once the dimensions of the drills have been constrained, the thrust force and torque required to drill about 15 $[cm]$ into the asteroid have been calculated. From IL J. Furness [1992] Equation 7.3 and Equation 7.4 have been retrieved to calculate the thrust force and torque required for a certain diameter and feed. These calculations have been programmed in a computer program, which has been verified by means of using the values used in Bruzzi et al. [March 2013]. The resultant graphs ended up being the same as the one coming out our tool, therefore the forces and torques have been validated.

$$P_x = 0.195 \cdot HB \cdot S^{0.8} \cdot d^{0.8} + 0.0022 \cdot HB \cdot d^2 \tag{7.3}$$

In Equation 7.3, HB represents Brinell hardness in $[kg/mm^2]$. However, the results are usually reported with no units. S is the feed given in $[m/rev]$ and d is the diameter of the drill in $[m]$.

$$P_z = C \cdot d^2 \cdot S^{0.8} \cdot HB^{0.7} \tag{7.4}$$

In Equation 7.4, C is a constant given to be $2 \cdot 10^6$ retrieved from Bruzzi et al. [March 2013].

Since the drill has to be able to penetrate any surface material on the asteroid, ranging from organic matter to iron, basalt-like material was assumed to be the toughest material the drill could encounter, and thus the drill was designed to be able to operate in these conditions. A value of 600 of Brinell hardness has been used to avoid a failure of the drilling mechanism (Mills et al. [2004]). Next there were two properties of the drill still left to design for, the feed and the rotational speed. However, from Bruzzi et al. [March 2013], it is defined that according to several static models, speed has no effect on the drilling force and torque. Therefore, this will be decided on in a later stage, in order to increase or decrease the drilling time should this be required. In addition, this could be designed to meet the thermal requirements set by the drill-bit. A higher feed rate results in a higher thrust force needed, which is undesirable because this will push the spacecraft off the asteroid and stronger clamps and harpoons will be needed. After several iterations, a feed rate of 0.01 $[mm/rev]$ has been chosen to minimise the thrust force, while at the same time not resulting in an unacceptable slow rotational speed and drilling time.

Once the dimensions, forces and torques needed have been determined, the total power required by the drill had to be examined. This could be done by using Equation 7.5 which provides the power in watt .

$$P = \mu \cdot F \cdot R \cdot RPM \cdot \frac{2\pi}{60} \tag{7.5}$$

In Equation 7.5 and Equation 7.6 P is the power required in $[W]$, μ is the friction coefficient, F is the vertical load in $[N]$, R is bit radius in $[m]$, RPM is rotational speed and T stands for the torque in $[Nm]$. All of these variables are known except for the friction coefficient which can be determined with Equation 7.6.

$$\mu = \frac{T}{F \cdot R} \tag{7.6}$$

In order to be able to transport the material into which the drill penetrates and to avoid too high thermal stresses on the drill due to high speeds a rotational speed of 100 RPM has been chosen. Table 7.7 sums up the values resulting from these calculations. In these calculations the sample head is assumed to have a 11 mm diameter head, even though it is a hollow drill. This implies that this drill is most probably overdesigned and therefore does not need a safety margin. However for the main drill head a 5% safety margin has been added.

For the material of the drill, titanium and High Speed Steel (HSS) have been considered, which are superior to the older high-carbon steel tools due to the fact that formerly mentioned tooling materials are harder and much more heat resistant. They can be used to drill into a variety of materials which is desirable, because during the drilling into the asteroid several different types

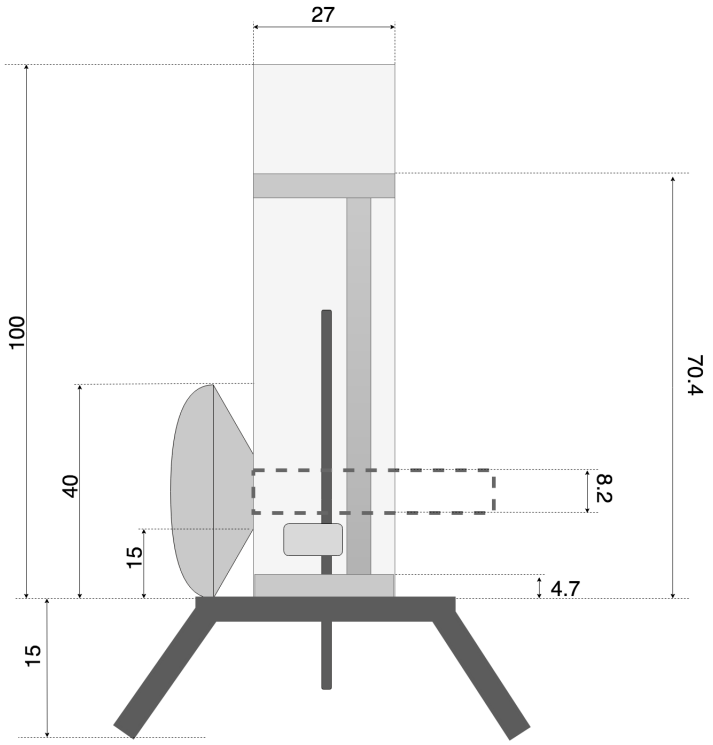

Figure 7.10: Drill tower dimensions in $[cm]$. The dotted line represents the sampling pushing mechanism.

of materials can be expected. Titanium is the final chosen material for the drill, because a 601 $[mm]$ long drill out of steel would have a considerably higher mass. However due to the high value of basalt's Brinell hardness, the drill bit of both heads will include diamonds. Diamond drill bits get their extra cutting power from little pieces of diamond powder embedded in them. A density of 4.51 $[g/cm^3]$ has been used for the drill, with which the masses of the different drill heads could be determined. These are given in Table 7.7, adding 480 $[g]$ for the main drill arm a total of 570 $[g]$ will be considered for the drill.

In order to be able to push the drill autonomous up and down while rotating, the SLS Rodless Screw Drive Actuator from Tolamatic Inc. [2018] has been chosen. With a feed of 0.1 $[mm/rev]$ and 100 $[rpm]$, this actuator can provide a maximal thrust force of 800 $[N]$ which is enough for the drilling manoeuvre required during this mission. Besides, the model MLS10 has a maximum stroke length of 1626 $[mm]$. The required stroke length is built up of multiple sections. The drill has to be able to move 150 $[mm]$ down to bridge the clearance between the lander and the asteroid surface. A 47 $[mm]$ clearance is required for the slide actuator. Furthermore, it has to drill a total of 250 $[mm]$ into the surface, as well as be able to lift the drill bit up by 162 $[mm]$ in order to seal the sample head and push it into the reentry capsule. On top of this, a rotational actuator is required to enable the torque needed. For this, the AX4009 with a weight of 5.5 $[kg]$ is chosen. When adding all of this together, a total stroke length of 610 $[mm]$ is required for the drill, hence this does not pose any problems, since it is in the range of the stroke length achievable by the SLS Rodless Screw Drive Actuator. The dimension of this Rodless Screw Drive Actuator are 108 $[mm]$ width and 704 $[mm]$ height, when adding the clearance on top and on the bottom to the stroke length. The mass of this actuator with the given dimensions is given to be 9.1 $[kg]$. One should note that the power required for this drill is lower than for usual drills, which is due to the fact that a low RPM will be used. Additionally the low feed rate results in a very low torque and hence a low required power. The peak power of the sampling acquiring mechanism is 50 $[W]$, when both the rotational and linear slide actuator are being used simultaneously. Figure 7.10 shows the dimension of the drill tower in $[cm]$ with its different components included.
It deserves mentioning that on the sample acquiring mechanism a brush is installed on the bottom part of the drill tower. The reasoning behind the brush is to make sure that no regolith or dust attached to the drill will be brought back into the lander, as this could harm other subsystems. Even more, if leftover material would be attached to the drill, it could get stuck in the carousel or the sealing capsule could fail to close the sample head properly, compromising the integrity of the sample acquisition.

The mass of the carousel made out of aluminium is estimated to be about 400 $[g]$ with the same actuator as the drill uses, the AX4009, hence 5.9 $[kg]$. The protective enclosure with a diameter of 120 $[mm]$ and a length of 704 $[mm]$ is made out of aluminium with 3$[mm]$ thickness. This tower is estimated to have a total mass of 0.95$[kg]$. The total mass of this drill mechanism has been determined, by adding the weight of the main drill with the different heads, the carousel, the linear drive

actuator and the protective en closer. When summing all of a total mass of 16.55 [kg] is given for this mechanism.

Figure 7.9 shows the carousel with the two different drill heads, in yellow is the main drill head, the green one is the sample head and the grey is the main drill which moves up and down and can attach to the drill heads. Below this carousel one can see the push mechanism with in red the sealing capsule, which will seal the sample head hermetically. After this is done the pusher will push the hermetically sealed sample head into the reentry capsule.

The drilling shall be performed in multiple sessions. The batteries of the lander were sized to allow 900 seconds of drilling, allowing a maximum drill depth of 15 centimetres per session. This enables the lander to pre-drill a hole to just above the required 15 centimetres, so that during the second session, the last bit can be drilled away. This keeps the sample sealed until the lander has enough energy to acquire the sample in one session, while not overdesigning the batteries. This tactic enables the lander to perform the sample acquisition in two sessions, with the possibility to drill once more to perform a second attempt. The entire sample acquisition can be performed within one phase of being on the sun-lit side of the asteroid.

7.2.5. Asteroid landing mechanism (ALM)

In this subsection, the design of the landing leg mechanism is discussed. This consists of three legs attached to a surface below the main module of the lander.

As the landing mechanism needs to ensure the most vital functionality of the lander, which is successfully landing on the asteroid, strict requirements need to be set to ensure that the mission is feasible. The following requirements were set.

`ASRM-ACSAL-ALM-001`	The landing legs shall unfold when released by pin-puller actuators. [T]
`ASRM-ACSAL-ALM-002`	The landing legs shall lock into place at an angle of 60 [°] with respect to the asteroid surface. [D]
`ASRM-ACSAL-ALM-003`	The landing legs shall carry the impact load that results from a 0.4 [m/s] impact speed. [A]
`ASRM-ACSAL-ALM-004`	The landing legs shall carry the thrust load of 445 [N] provided by the thruster during fastening of the satellite to the asteroid. [A]
`ASRM-ACSAL-ALM-005`	The landing legs shall be able to host the claw mechanism. [D]
`ASRM-ACSAL-ALM-006`	The landing legs shall provide a nominal ground clearance of 0.15 [m]. [I]
`ASRM-ACSAL-ALM-007`	The landing legs shall be able to carry the combined load of at least 703 [N] under unfolded orientation. [A]
`ASRM-ACSAL-ALM-008`	The platform shall be able to carry the combined load of at least 703 [N]. [A]
`ASRM-ACSAL-ALM-009`	The platform shall house three harpoon mechanisms. [D]
`ASRM-ACSAL-ALM-010`	The platform shall release the main satellite module during take-off. [A]

As can be concluded from the requirements, the Asteroid landing mechanism (ALM) consists of two elements: the platform the main module of the satellite rests upon, and three legs mounted below the platform. Together they support the loads the main module experiences, and provide adequate ground clearance stated in requirement `ASRM-ACSAL-ALM-006`.

As stated in `ASRM-ACSAL-ALM-001`, the landing legs shall unfold when released. This is done by two small mechanisms. The legs are stowed below the platform during orbit towards the asteroid. When the lander is decoupled from the main orbiter, the legs are unfolded once adequate clearance is determined between the orbiter and lander. This is done to allow immediate calibration for a leg-open configuration in the environment around the asteroid. The unfolding happens by activating a pin-pull mechanism. Once released, a torsional spring located in the attachment joint to the platform of each leg rotates the leg out until the final orientation of 30 [°] outward from vertical is reached. Here, the legs lock into place, and shall remain in this orientation for the rest of the mission.

During touchdown, the legs provide damping to the main module. They absorb the landing impact force. This helps to ensure that the spacecraft will not bounce off the surface of the asteroid in the low-gravity environment. The legs will also carry the loads the lander experiences while it fires the main engine to counteract the forces of the firing of the harpoons.

Sizing the landing legs requires the identification of the highest load that will occur. There are several load cases that have to be considered, including the impact at touchdown, the load when drilling and when not drilling.

The drilling force equals 703 [N], which is counteracted by the harpoons; the resultant force on the legs is then very small. In the period the drill is not operating, the harpoons will still exert a force of 703 [N], which has to be countered by the legs. The impact force can be calculated using equation Equation 7.7.

$$F_{impact} = 2 \cdot \frac{E_{impact}}{s} \qquad E_{impact} = \frac{1}{2} \cdot m \cdot v^2 \tag{7.7}$$

where F is the force in [N], E is the impact energy in [J], s is the damper height in [m], m is the lander mass in [kg] and v is the impact velocity in [m/s].

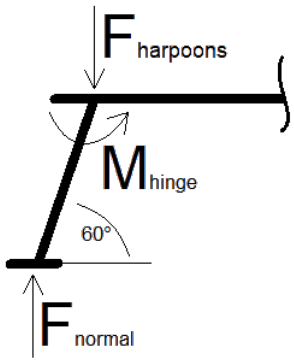

Figure 7.11: Free body diagram of a landing leg.

With an estimated mass of 200 $[kg]$ for the lander, and impact speed of 0.4 $[m/s]$ and a damper height of 5 $[cm]$, the impact force equals 640 $[N]$. That makes the case where the drill is not operating the critical load case. With three legs, each leg has to withstand a force of 234 $[N]$. This normal force generates a hinge moment of 20 $[Nm]$.

Considering the internal stresses, the leg is modelled as a cantilever beam with a normal and shear force acting at its end. Taking a circular cross section for the leg the normal (σ_z) and shear (τ) stresses can be calculated. Buckling is neglected as a failure mode due to the small height of the leg.Based on this, a mean radius of 21 $[mm]$ and thickness of 2 $[mm]$ is chosen.

Aluminium is used, and the dimensions take into account manufacturing constraints. The damping system in the legs will be a honeycomb structure that will be crushed by the impact force and absorb the energy.

The legs also provide torsional support. This is done by literally clawing into the asteroid. As the asteroid is porous, its surface is rough and contains many cavities. The nail-like pins on the feet fix the legs at a certain point and keep it there during drilling. By using multiple claws, the torsional forces are distributed over a large area, ensuring no claws will deform, or that the surface of the asteroid will not be chipped of which would result in (partial) release of the asteroid.

The platform is the second element involved in the ALM. The platform provides a mounting surface on which the main satellite module can rest and attach to. The platform has an opening in the middle. This allows the sample acquiring mechanism to be placed in the centre of the main satellite module, preferable for equilibrium. The platform also houses the harpoons. These are oriented vertically downwards. By placing the harpoon mechanisms on the platform, no special attention needs to be paid to their detachment during take-off. During take-off, the attachments of the main satellite module are pyrotechnically decoupled, allowing the satellite to thrust off of the asteroid using RCS-thrusters, before reorienting and leaving the asteroid. The landing legs will remain on the asteroid, fastened by the harpoons and the claw mechanism.

Since the platform has a relatively complicated load case, it will not be designed in detail. Instead, a honeycomb panel will be selected with a high safety factor, the Honeylite 15 from Honeylite [22].

.

As a first mass estimate for the landing mechanism calculations involving the volume of components were made possible, and if not a conservative estimate was given on the component mass. The dimensions from Table 7.8 were used to obtain the displayed masses. The length of the legs is the sum of the length needed for adequate ground clearance, the damping system length and 1 $[cm]$ of extra overlap. As densities, 2,700 $[kg/m^3]$ was used for aluminium, and 6.9 $[kg/m^2]$ for the honeycomb of the platform.

7.2.6. Harpoon (HAR)

As mentioned in subsection 7.2.4, a vertical force of 703 $[N]$ is pushing the satellite away from the asteroid. To counteract this force in a mass-efficient way, harpoons will be used on the satellite. These will perforate the asteroid where they will latch on to the surrounding material, hereby creating a counter force.

To ensure that the harpoon system is able to perform its task of fastening the satellite to the asteroid, requirements were set, which are presented below.

`ASRM-ACSAL-HAR-001` The lander shall be able to fire the harpoons towards the asteroid surface. [A]
`ASRM-ACSAL-HAR-002` The lander shall be able to tighten the rope attached to the harpoons. [A]

[22] `http://www.universalmetaltek.com/pdf/Aluminum-Honeycomb-Panel.pdf` Accessed June 25, 2018

Table 7.8: Mass count of the landing mechanism

Part	**Dimension** $[mm]$	**Unit Mass** $[kg]$	**Amount**	**Total Mass** $[kg]$
Leg	r=21, t=2, h= 243	0.2	3	0.5
Foot	r= 30, t= 2	0.02	3	0.05
Pin	r= 0.5, h= 50	$1/cdot10^{-4}$	60	$6/cdot10^{-4}$
Platform	r_{in}= 135, r_{out}= 400	3	1	3
Torsional Spring	TBD	0.05	3	0.15
Hinge	TBD	0.05	3	0.15
Damper	TBD	0.1	3	0.3
Total	**-**	**-**	**-**	**4**

To fasten the lander safely to the asteroid in a stable manner, three harpoons will be used. These harpoons are placed between the landing legs, pointed directly downwards to counteract the vertical forces occurring during drilling. Each harpoon system will consist of a projectile, a firing mechanism, and a winch to tighten the rope attached to the projectile. The harpoons will be used to counteract the drilling force of 703 $[N]$. This force is distributed over each harpoon, meaning each harpoon should be able to take on a force of 234 $[N]$. This configuration is also preferable for take-off, as the harpoons are attached on the landing platform which will be left behind.

The harpoons will go through two stages, firing and winching. When the lander lands, the accelerometer will identify the sudden deceleration, triggering the harpoons to fire. The harpoons will then penetrate the surface. Next, actuators located in the firing system will start to retract the wire attached to the projectile, hereby creating a combined tensile force in the wire equal to the maximum drilling force, and anchoring the lander to the surface.

The harpoon should be able to penetrate the asteroid deep enough for it to fasten itself and pull on the asteroid without pulling the material around the harpoon loose. To calculate this depth, Newton's estimation of impact depth (Equation 7.8) is used. This estimation is based on the law of momentum and work. The D represents the penetration depth $[m]$, L stands for the length of the projectile $[m]$, and ρ_{Harp} and ρ_{Ast} the density of the harpoon material and the asteroid $[kg/m^3]$ respectively.

$$D = L \cdot \frac{\rho_{Harp}}{\rho_{Ast}} \tag{7.8}$$

To calculate the force required to drive the harpoon into the ground, the equilibrium of work and kinetic energy was used. The kinetic energy provided to the harpoon will translate into work over the depth length (Equation 7.9). m stands for the mass of the harpoon $[kg]$, F for the required driving force $[N]$, and d the depth of penetration. The V in this equation is the velocity $[m/s]$ with which the harpoon strikes the surface. The harpoon is accelerated instantaneously (assumed at 0.001 $[s]$) by the force of pyrotechnics. Pyrotechnics are utilised to minimise the amount of regolith disturbed during firing.

$$\frac{1}{2} \cdot m \cdot V^2 = F \cdot d \tag{7.9}$$

These two equations are closely interrelated. A computer code was used to compute the best possible size and material of the harpoon. The force required to fire all three harpoons during landing should not exceed the force of the thruster on the lander as to not push the lander away from the asteroid. Furthermore, the penetration depth should be maximised in order to ensure secure fastening into the asteroid material. Finally, the found density should be achievable by common materials that can also be shaped into the computed geometry. Through these computations, the geometry of the harpoon was found to be a length of 5 centimetres with a radius of 4 millimetres, a density between 1,370 and 1,550 $[kg/m^3]$ resulting in a maximum projectile mass of 2 grams, and the pyrotechnics of the firing module should provide a force of 148 Newtons. The harpoons will have claw-like features that will prevent the harpoon from being pulled out. The penetration depth will be around 2.2 centimetres. It should be noted that the calculations were performed for an asteroid made of solid basalt. In reality, the chosen asteroid will most probably consist of softer, less dense materials improving the anchoring effect of the harpoons.

7.2.7. Sample return capsule

In this section the requirements set for the sample return capsule attached to the lander are provided.

`ASRM-ACSAL-SRC-009` The reentry capsule shall be able to return the sample to Earth. [A]
`ASRM-ACSAL-SRC-009-a` The error for the entry flightpath angle shall be less than 0.08 [°]. [A]
`ASRM-ACSAL-SRC-009-b` The entry attitude shall be less than 10 [°]. [A]
`ASRM-ACSAL-SRC-009-c` The maximum heat rate shall be less than 1,200 $[W/cm^2]$. [A]

ASRM-ACSAL-SRC-009-d The attitude at the max heat rate shall be less then 10 [°]. [A]
ASRM-ACSAL-SRC-009-e The maximum heat load shall be less than 32 [kJ/cm^2]. [A]

7.2.8. Sensitivity analysis

This section will elaborate on the consequences of changes in the main design parameters of the mission. The steps that were undertaken to account for uncertainties in these parameters will be explained.

Asteroid mass

The mass of the asteroid can change due to the density or the radius. Both variables have an impact on the lander craft.

The drilling mechanism has been designed for an upper limit of asteroid density of 3,000 [kg/m^3]. Lower densities will simplify the drilling, requiring less force and/or less time to drill. A higher density would, however, make it even more challenging to obtain a core sample. The drill time could increase drastically, but since the lander will stay on the asteroid until shortly before the return to Earth, there is enough time to drill at a slower pace.

Additionally, if that is the case, more cold gas would be necessary for the descent and lift off manoeuvres. For lift off and insertion into a 600 [m] circular orbit, the ΔV varies with the square root of the gravitational acceleration. The expelled mass is an exponential function of the required ΔV. The gravitational acceleration and hence the density is allowed to increase with a factor of 1.44 before the expelled mass would increase with 20%, the added safety factor. The density for the same size would be 4,340 [kg/m^3], the radius of the asteroid with a 3,000 [kg/m^3] density would be 519 [m]. The initial radius for these calculations was assumed to be 459 [m]. The calculation for the descent manoeuvre is less straightforward due to the multiple burns, but since the dynamics are very similar, it is expected the cold gas budget will vary in the same range.

Rotational period

The rotational period of the asteroid is currently estimated at 7.7 [hr]. While in orbit, the rotational period has little or no effect on the lander. However, during descent and the time on the asteroid surface, the rotational period can have a major impact. A decrease in period could alter the landing sequence, whereas an increase could have consequences on the thermal control and power generation of the lander.

Assuming an asteroid radius of 459 [m] with a density of 3,000 [kg/m^3], the circular velocity on the surface of the asteroid equals 0.42 [m/s], with an orbital period of 1.9 [hr]. Would the asteroid's rotational period drop below this value, matching the surface velocity for landing will result in an orbit with an apoapsis higher than the surface, making it very difficult to touch down as the timing is crucial. On the other hand, there would be less regolith on the surface, which would be beneficial for attaching to the surface and the drill depth that can be obtained.

The electrical power subsystem is designed for certain eclipse intervals and duration. Once the lander has touched down, the eclipse would approximately equal half the rotational period. If this would diverge too much from the design eclipse times, the battery might die and then the mission will be over. It is estimated that the maximum eclipse time would be about 7 hours. For the thermal subsystem, this does not pose a problem. The lander is passively cooled when in sunlight, hence it will not have the risk of cooling down too much when in eclipse.

Shape, surface, and rotational axis

An irregular shape of the asteroid or mountainous surface would alter the landing sequence of the lander. A faster and more vertical descent would be desired, with a minimal ground track to minimise influence from the gravity field and keep clear of more elevated areas. Some asteroid have two rotational axes, which would require more careful planning of the descent manoeuvre.

Solar pressure, flux, and radiation

The sun is expected to be in a solar maximum at the time of asteroid arrival. Solar maxima bring uncertainties with them in terms of pressure, flux and radiation that need to be accounted for. The spacecraft needs to be actively cooled, and for these calculations the maximum solar radiation was used. The electrical power system has been sized based on a worst-case scenario, meaning the lowest solar radiation that is encountered during the mission at the furthest distance from the sun. Hence, the lander is not sensitive to variations in solar radiation or flux.

A solar maximum also affects the ADCS system, since it results in higher disturbance torques on the spacecraft. However, the period of time in which the lander needs active control is limited, and has been very conservatively estimated in calculations. Hence, the solar pressure will not affect the ADCS budget.

7.3. Hoverer - SASH

In this section the detailed design of the hoverer, SASH (Sample Acquiring Surface Hover), will be given. SASH will hover above the asteroid surface and acquire a surface sample after which it will return to Earth. First the requirements for the hoverer

in general will be derived for which it will be designed. Next, the final architecture, mission time line, technical resource budgets and block diagram of the architecture of all the components are shown. The subsystems are designed based on requirements given in the section of that subsystem in chapter 8.

7.3.1. Requirements on SASH

In order to fulfil the user requirements, some requirements are set for SASH that enable the design team to make decisions with regards to the selection of components and mission elements.

ASRM-SASH-001	SASH shall be able to perform a hovering sample acquiring manoeuvre [A].
ASRM-SASH-002	SASH shall be able to perform two practice runs and one actual sample acquiring run. [A]
ASRM-SASH-003	SASH shall be able to move to a different sample acquiring location. [A]
ASRM-SASH-004	SASH shall be able to deflect the thrust required for the descent to prevent contamination of the sample. [A]
ASRM-SASH-005	SASH shall be able to locate the landing site selected by the orbiter from 100 metres above the surface. [T]
ASRM-SASH-006	SASH shall be able to track the surface during descent and ascent. [I]
ASRM-SASH-007	SASH shall be able to eject the SRC at the attitude and spin rate required for a safe reentry. [A]
ASRM-SASH-008	SASH shall be able to determine its altitude above the surface of the asteroid. [T]
ASRM-SASH-009	SASH shall provide protection for the critical components of the SRC. [I]

7.3.2. Architecture of SASH

The structure of the spacecraft is built with a 937mm diameter aluminium cylinder, which serves as the basis of all the subsystems and which diameter is determined by the decoupler between the orbiter and the hoverer. In Figure 7.12 it can be seen that inside this cylinder there are two decks with subsystems, with the lower deck containing the propellant tank with the monopropellant needed for the main thruster (MONARC-445), as well as a laser altimeter (CLA), and a descent camera (DECAM) which provide the system with data on the descent trajectory. Furthermore, the top deck contains the transponder (TRA) and diplexer (DIP) for the TT&C subsystem, along with the reaction wheels (REWH) and gyroscope (DILG) for the ADCS. At the centre of the structure the cold gas tank (CGT) is located, which provides the RCS-thrusters (COGT) with propellant. On the outside of SASH there are 4 louvers (LVR) to dissipate the excess heat of the spacecraft. Finally on the 'bottom' of the spacecraft the sample acquiring mechanism (SAM) and sample return capsule (SRC) are located.

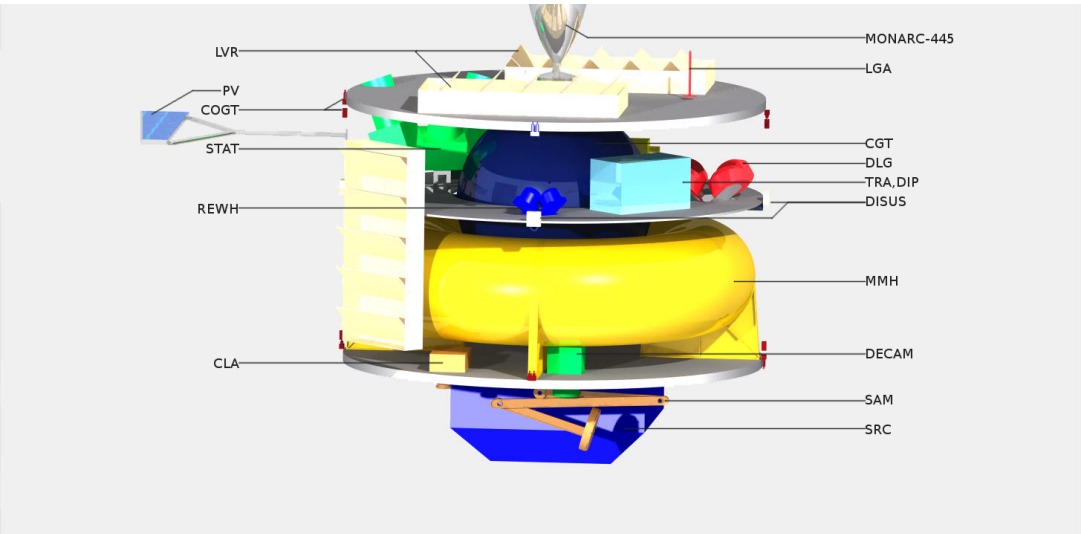

Figure 7.12: SASH's architecture, the outer skin has been left out for clarity.

In this section an overview of the final design of SASH is given based on the requirements of the previous section. In Table 7.9, all the instruments that are on SASH are given including the source from which the mass, power, operating temperatures, dimensions etc. are taken from. The abbreviations shown in Table 7.9 are used throughout this report.

Table 7.9: Overview of the Instruments on SASH

Instrument	Abbreviation	Function
Star tracker sensor	STAT	Determines the attitude of SASH by tracking the stars.
Digital laser gyroscope	DILG	Determines the attitude of SASH in its inertial reference frame.
Digital sun sensor	DISUS	Determines the attitude of SASH by tracking the sun.
Cold gas thrusters	COGT	Changes the attitude of SASH by the use of thrust.
Low gain antenna	LGA	Provides a reliable mean to transmit housekeeping data.
Reaction wheels	REWH	Changes the attitude of SASH very precisely.
Transponder	TRA	The main communication computer of SASH.
Diplexer	DIP	Separates the incoming and outgoing signal.
Compact laser altimeter	CLA	Determines the height above the surface by means of laser.
Computing Unit	CPU	The main computer of SASH.
Monomethylhydrazine	MMH	Monopropellant used for the propulsion system.
Monopropellant thruster	MONARC-445	Provides the thrust on SASH to return to Earth.
Cold gas tank	CGT	Stores cold gas for pressurising the propulsion system and attitude control.
Monopropellant thruster valve	MOTV	Regulates the propellant for the thruster.
Peltier element	PLT	Heats actuators outside satellite.
Louver system	LVR	Regulates the amount of energy a radiator can radiate.
Radiator	RAD	Removes excess energy from the satellite.
Descent camera	DECAM	Ensures that the hoverer descends towards the chosen landing site.
Sample arm mechanism	SAM	Collects a sample during the hovering manoeuvre.
Sample assurance laser	LAS	Ensures that a sample is acquired in the collector.
Sample return capsule	SRC	Ensure safe reentry through the earth's atmosphere.

7.3.3. Mission time line

The mission time line of SASH starts when it is separated from the orbiter and activates its subsystems. As soon as all systems have been checked, SASH will start its descent by performing several burns using the RCS-thrusters with the thrust deflector shields deployed. Several practice attempts are made in order to reduce risk caused by unforeseen hazards and to ensure successful completion of the mission. The sample will eventually be captured using the SAM, where it will be secured and placed inside the SRC. SASH will then take off and insert itself in orbit around the asteroid and wait for the return window. The return trajectory will be initiated after extensive checks, ensuring SASH will return to Earth with minimal adjustment. During the interplanetary coast phase, the system will go into a low-power mode, ensuring system health and power levels in the period until Earth reentry. When SASH arrives at Earth and has established contact with the ground station, a final attitude adjustment and target burn will be performed to ensure the right reentry angle for the SRC, while subsequently being released with the correct spin velocity and reenter above Australia.

Figure 7.15 The block diagram in Figure 7.15 above illustrates the way software and the hardware are interconnected on

[23] https://www.vectronic-aerospace.com/space-applications/star-sensor/ Accessed June 14, 2018

[24] https://aerospace.honeywell.com/en/~/media/aerospace/files/brochures/gg1320andigitallasergyro-bro.pdf Accessed June 15, 2018

[25] https://www.isispace.nl/brochures/NSS_Fine_Sun_Sensor_Datasheet_2c-.pdf Accessed June 14, 2018

[26] http://www.moog.com/content/dam/moog/literature/Space_Defense/Spacecraft/Propulsion/ColdGasThrusters_0717.pdf Accessed June 17, 2018

[27] http://bluecanyontech.com/rwp100/ Accessed June 18, 2018

[28] http://www.moog.com/content/dam/moog/literature/Space_Defense/Spacecraft/Monopropellant_Thrusters_Rev_0613.pdf Accessed June 14, 2018

[29] http://www.moog.com/content/dam/moog/literature/Space_Defense/spaceliterature/propulsion/MonopropellantThrusterValves_0418.pdf Accessed June 14, 2018

[30] http://aacmicrotec.com/sirius-cdh/ Accessed June 15, 2018

[31] https://elib.dlr.de/86562/1/A_Camera_for_the_MASCOT_lander_on-board_Hayabusa_2.pdf Accessed June 15, 2018

[32] https://www.cui.com/product/resource/cp08-m.pdf Accessed June 21, 2018

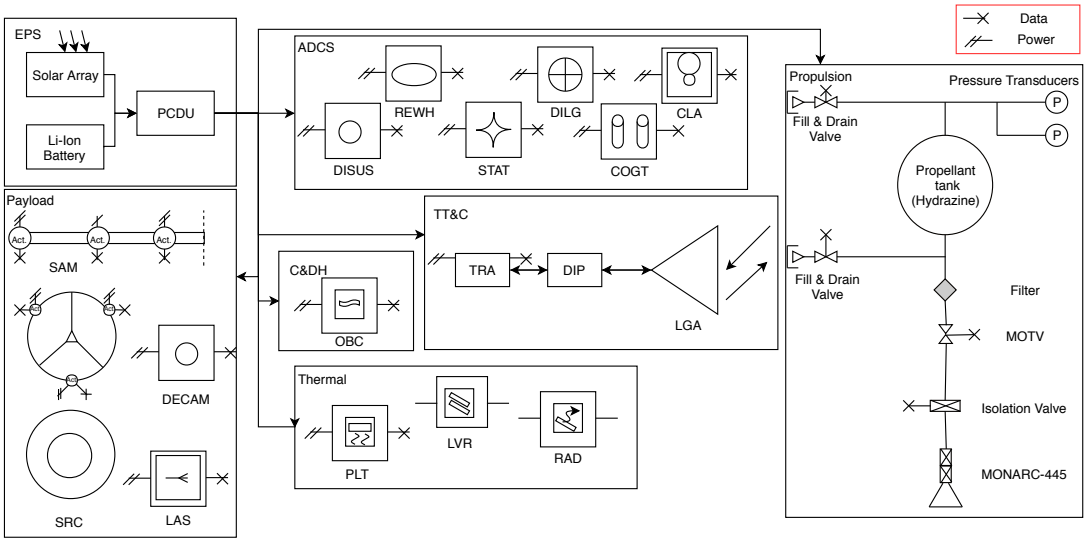

Figure 7.13: Block diagram of SASH

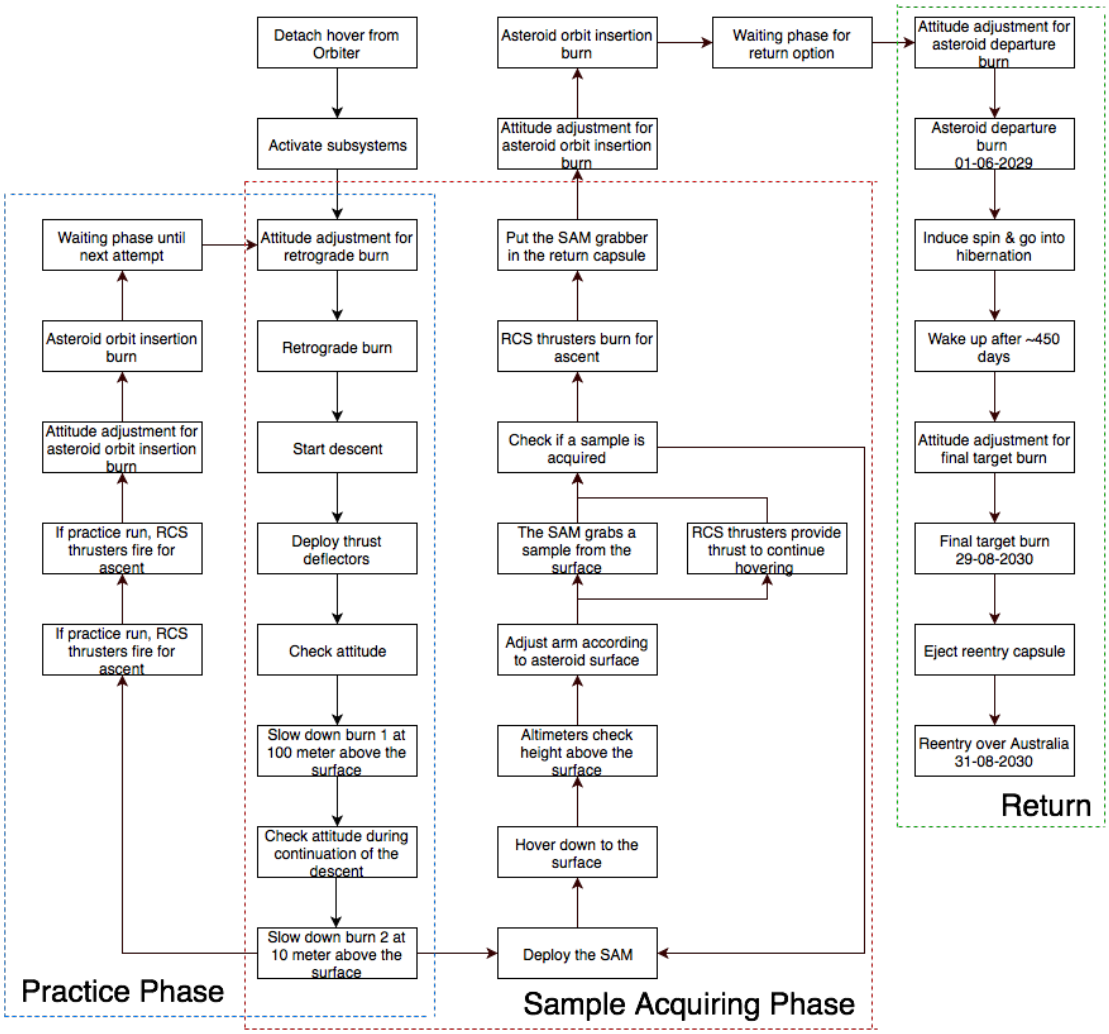

Figure 7.14: Mission time line of SASH

Table 7.10: Overview of SASH

Subsystem	**Part**	**Amount**	**Mass** $[kg]$	**Power** $[W]$	**Dimensions**
Structural	Bus	1	**~40**	-	-
EPS			**16**		
	PV array	1	2	-	0.8 $[m^2]$
	Li-ion battery	4	2	-	173 x 82 x 58 $[mm]$
	PCDU	1	3	-	TBD
TT&C			**11**		
	LGA	2	0.4	-	100 $[mm]$
	TRA	2	4	18	181 x 166 x 114 $[mm]$
	DIP	2	0.2	-	TBD
	Cabling	1	3	-	TBD
ADCS			**23**		
	COGT	24	0.02	30	6.6 $\varnothing$25 $\leftrightarrow$ $[mm]$
	CGT [26]	1	7	-	435 $\varnothing[mm]$
	STAT [23]	3	0.8	2.5	80 x 100 x 180 $[mm]$
	DILG [24]	4	0.5	1.6	88 $\varnothing$45 $\updownarrow$ $[mm]$
	DISUS [25]	6	0.04	0.21	34 x 32 x 21 $[mm]$
	CLA (Bruzzi et al. [2012])	2	5	12	121 x 137 x 100 $[mm]$
	REWH [27]	4	0.35	1	70 x 70 x 25 $[mm]$
Propulsion			**62**		
	MONARC-445 [28]	1	1.6	-	148 $\varnothing$410 $\updownarrow$ $[mm]$
	MOTV [29]	1	1.0	58	incl. in MONARC-445
	MMH	1	60	-	(inner radius) 450 (outer radius) 240 $\updownarrow$ $[mm]$
	Pressurant gas	1	0.3	-	
C&DHS			**1**		
	CPU [30]	1	0.5	5	96 x 81 x 92 $[mm]$
	Wiring	1	0.1	-	TBD
Thermal			**10**		
	Primary coating	1	7	-	3 $[m^2]$
	Radiator coating	1	1	-	0.2 $[m^2]$
	Radiator	4	0.2	-	0.1 $[m^2]$
	Louver	4	0.3	-	0.1 $[m^2]$
	PLT [32]	2	-	7	-
Sample mechanism			**26.24**		
	Arm	1	7	12	30 $\varnothing$830 $\updownarrow$ $[mm]$
	SRC	1	17	3	400 $\varnothing$200 $\updownarrow$ $[mm]$
	Container	1	1.7 (container) 0.04 - 0.06 (sample)	10	100 $\varnothing$130 $\updownarrow$ $[mm]$
	DECAM [31]	1	0.6	10	115 x 77 x 96 $[mm]$
	LAS	1	0.1	0.1	TBD
Dry mass margin			**13**	-	-
Total			**203**		

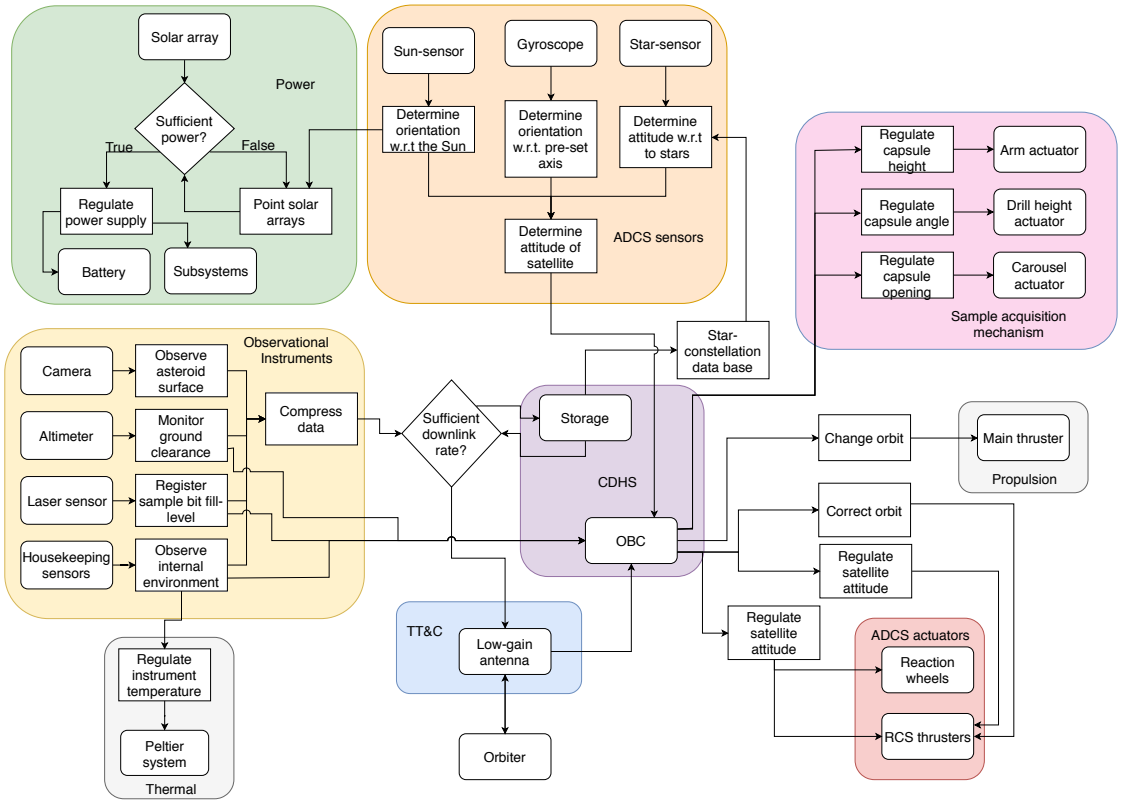

Figure 7.15: Software-hardware collaboration on board of SASH.

board of SASH. It is vital for SASH that proper control is attained over the spacecraft, as it will encounter mission phases where precise control is vital for both acquiring a sample as well as keeping the satellite safe. The collaboration between these two elements ensure that all tasks throughout the mission are performed in a correct manner.

7.3.4. Sample collection mechanism

In this section the SAM, sample collection mechanism, will be elaborated upon. All the details of the mechanism along with a functional analysis are shown.

`ASRM-SASH-SAM-001` The SAM on SASH shall be able to determine whether a sample is acquired. [T]
`ASRM-SASH-SAM-002` The SAM on SASH shall be able to collect more than 25 grams of surface sample from 1989 UQ. [T]
`ASRM-SASH-SAM-003` The SAM on SASH shall be able to put the collector into the SRC. [D]
`ASRM-SASH-SAM-004` The SAM on SASH shall be able to close the collected sample off hermetically. [T]
`ASRM-SASH-SAM-004` The SAM on SASH shall not damage the SRC. [I]
`ASRM-SASH-SAM-005` The SAM on SASH shall be able to retract and be stored outside of the spacecraft. [T]

Performance analysis

Throughout this subsection, the full performance analysis is carried out. This analysis was made using a CAD model in order to obtain the proper length for the several members. A closer look at the deployment, sampling and the final procedure which consist of placing the container inside the reentry capsule is then presented. A dynamic model was made in order to obtain the angular velocity and acceleration of the different members to correctly choose the most suited actuators. Finally a visual representation of the whole system will be presented through the representation of the kinematics section from the DSC Catia software.

In order to design such a mechanism, close attention has to be paid on the positioning of the reentry capsule. Since the sample, once collected, has to be secured carefully in the reentry capsule, the position of the latest was first determined. Earlier it has already been decided to have the SRC on the bottom of the spacecraft in order to ease the movements of the arm that collects the sample. It needs to be pointed out that the capsule mechanism is surrounded by a camera and other vital components to ensure the success of the mission. It is then decided to place the first member at 15 $[cm]$ after the edge of the container which holds the capsule in place. This leaves a certain clearance length to avoid damaging the camera that sits in between the sample mechanism and the reentry capsule. It can be seen that the box that is used as protection of the capsule, as described in the later

Table 7.11: Length of mechanism member

Part number	**Length** $[mm]$
Member 1	220
Member 2	410
Member 3	200

subsection 7.3.5, is 20 $[cm]$ high. This was a driving criteria as well as the height of the camera. A computational model is made that iterated the set of members in order to obtain the most accurate positioning of the system. It yields the length of each rod and the numbers of them. The program is set to optimise the most critical instant for the members of the mechanism. This turned out to be the exact moment when the third member is releasing the collection compartment in the reentry capsule. This is deemed critical since the mechanism is supposed to carry the sample inside the protection box for 15 $[cm]$ in a straight manner before releasing it. It is made possible through a movement of all members which means the space needed for this movement needs to be clear of any instrument present on the bottom of the spacecraft. This then yielded the dimension as seen in the Table 7.11.

Once the dimensions of the members were determined, a dynamic model of the mechanism was made in order to check whether the dimension are feasible, but most importantly to assess the different angular motions in order to determine what the actuators that will be fitted in the mechanism should provide in terms of force and rotation. This model allowed the accurate assessment of the operational modes of the whole system. In order to visualise it at the same time, the three main movements are shown in the next three sections, but first a visualisation of the five actuators is presented in Figure 7.16.

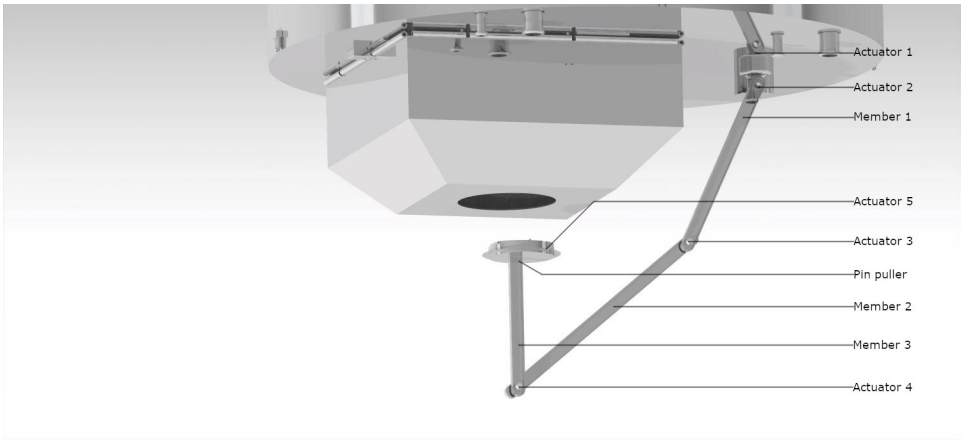

Figure 7.16: Actuators of the sample acquiring mechanism

The model is based on a dynamics of a three members mechanism. It describes the angular acceleration and most importantly the angular velocity of the members. As such it is possible to relate all members through the following equation.

$$a_2 = \boldsymbol{\alpha}_{12} \times \mathbf{R}_2 - \omega_{12}^2 \mathbf{R}_2 \tag{7.10}$$

Equation 7.10 describes the acceleration of the first member, in relation with the second member. The a_2 is the linear acceleration of the second member $[m/s^2]$, α is the vector form of the angular acceleration $[rad/s^2]$ while $\mathbf{R}_2$ is the vector position of the first member $[m]$. Furthermore, ω is the angular velocity $[m/s]$ that is the most relevant in this case.

Deployment

The deployment phase is rather simple, as the main criteria is to not hit any component that is on the bottom of the spacecraft. The folding position of the mechanism is set perpendicular to the reentry capsule in order to be able to fit all components under the spacecraft. This means that actuator 1 is only present to rotate the full system over 90 [°] once it is fully deploys. Former actuator is used to align the members with the reentry capsule opening. The position is as such: member 1 is making an angle with member 2 of exactly 5 [°] while member 2 is making an angle of 18 [°] with the last member. This can be seen in Figure 7.17. The first movement that initiates the mechanism is through actuator number 4 that rotates 162 [°] over the left as seen on Figure 7.18. It needs to be noted that almost all movements are made independently of the others.

The choice of actuators for all these movement was made depending on the most critical phase which needs high accuracy

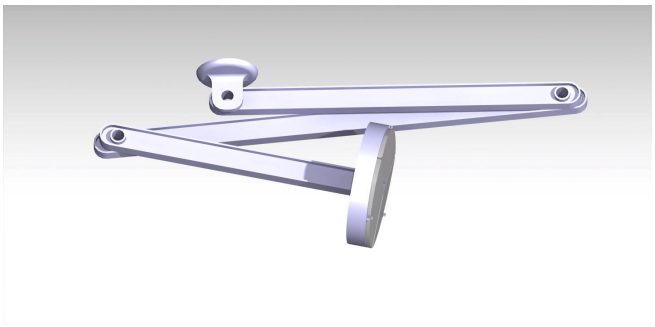

Figure 7.17: Retracted mechanism of the SAM.

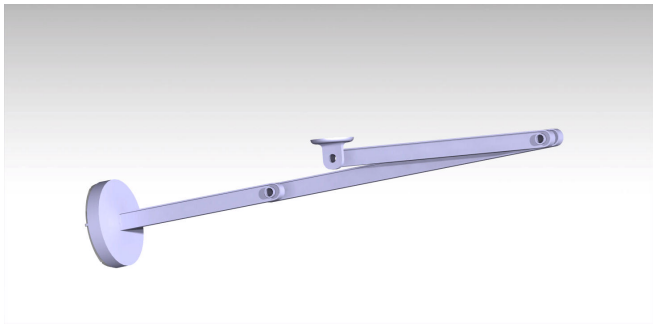

Figure 7.18: First procedure of initial positioning of the sample arm.

in its movement. As so, the actuator chosen for all the members with the actual sample compartment is a micro 3 Rotary Incremental Actuator developed by MOOG [33].

.

This is capable of a rotational speed of 1.8 $[deg/s]$ and has a power consumption of 3 $[W]$. This means that the first movement will take 90 $[s]$ total.

This is then followed by a rotation of member 1 by actuator 3 by an angle of 175 [°] at the same rate as the previous movement. The final position after this can be seen in Figure 7.19, which is then followed by a rotation around the actuator 2 as seen in Figure 7.20 of 90 [°] and finally a rotation of the whole mechanism over 90 [°]. This to align the mechanism with the reentry capsule. This whole procedure lasts a total of 147 $[s]$. Once the deployment of the mechanism is made, the sampling collection c an initiate.

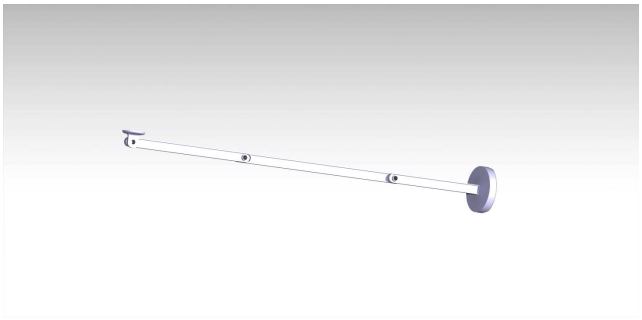

Figure 7.19: Second procedure of initial positioning of the sample arm.

Figure 7.20: Third procedure of initial positioning of the sample arm.

Sampling regolith

In order to sample regolith, the container first needs to open. It is made using three actuators with a high possible velocity since the sampling has to be done as fast as possible. The sample container is built up of three scoop-like compartments folding into a triangularly-shaped middle part. A laser is placed in this triangular part in order to assess properly if regolith was captured in the collectors or if a second sampling attempt is needed. The spacecraft is designed to a maximum of three sampling attempts in order to prevent the return of a empty capsule. The capsule container has a 10 $[cm]$ diameter and the three compartments that enable a maximum sample mass ranging from 40 $[g]$ to 60 $[g]$. This mass was computed using the computed volume of the container and the density of the material expected on the asteroid. The container opens as presented in the two following illustrations, Figure 7.21 and Figure 7.22. The opened compartment has the scoops at an angle of 80[°].

Once the container is opened, the sampling can begin. This process is rather short, less than 1 $[s]$, for several reasons. The first one is that the hoverer should not get stuck in the ground. This means it is designed that the three scoops enter the regolith until half of its width, which is exactly 2.2 $[cm]$. Once the scoops are deep enough, this is sensed by the altimeter and that fires the RCS-thrusters with a vertical force of 3.6 $[N]$, but it also initiates the three actuators connected to the scoops which will close at the same time. The RCS-thrusters then induce an acceleration of 0.02 $[m/s^2]$. This means that over the 2.2 $[cm]$ the time spent is 0.8 $[s]$ and the scoops must approach their initial position, that is they need to be closed. So it is deemed acceptable to have an actuator that closes the capsule in one second maximum.

[33] `http://www.moog.com/content/dam/moog/literature/Space_Defense/Spacecraft/Spacecraft_Mechanisms/500-613_Micro3.pdf` Accessed June 26, 2018

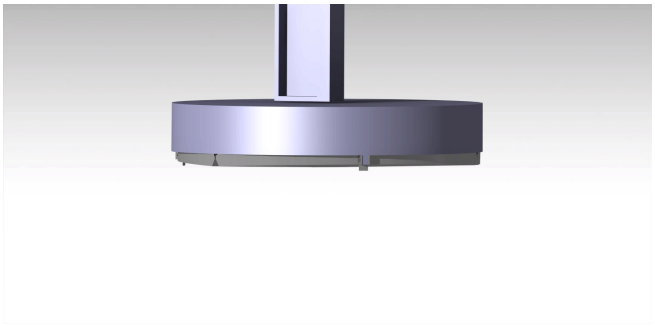

Figure 7.21: Closed SAM container.

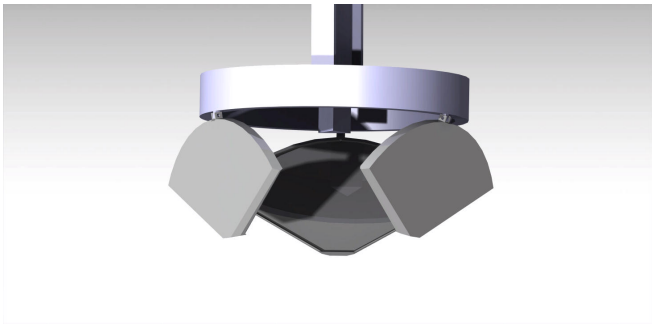

Figure 7.22: Opened SAM container.

Another reason for this fast manoeuvre is that it is set such that a maximum amount of regolith can be collected. Due to the barely present gravity on the asteroid, any disturbance induces an acceleration of the regolith and would cause it to drift away. By increasing the speed of the sampling, a higher chance of catching regolith is made but it also induces a lower chance of crashing on the asteroid since less time is spent near it. Once the material is inside the container, the procedure to place it in the reentry capsule can begin.

Placement it in the capsule

This is a critical phase of the mechanism design since the capsule is the vehicle that will bring the sample back to Earth. To do so, the movement of the actuators have to be precise in order to not damage the heat shield or other components of the capsule. The procedure is as follows: once the spacecraft has lifted off the asteroid and has reached a certain clearance altitude that is dependent on the highest hill present on the asteroid. If the sensor inside the sample container indicates that enough material is present, it initiates the procedure.

First, actuator 2 effectuates a rotation of 20 [°] in order to place all members in the right position. Then, the actuator 3 helps the second member to rotate for 17 [°]. The two steps are shown in the following illustration, Figure 7.23 and Figure 7.24. The time duration of this procedure is computed to be 20.5 $[s]$.

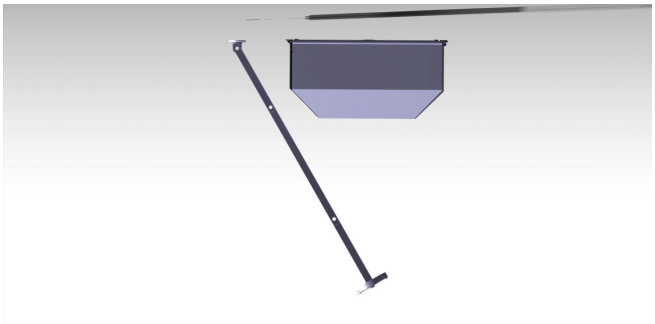

Figure 7.23: First rotation for placing the sample container in the SRC.

Figure 7.24: Second rotation for placing the sample container in the SRC.

Once the previous step is done, actuator 4 can rotate member 3 with an angle of 138 [°] in order to place the container right in front of the capsule. Now it is known that the sample needs to be placed 15 $[cm]$ inside the capsule in a straight manner. Therefore, a dynamic system was created in order to assess what angular velocity each member should move at. It is found that the motion is possible by using actuator 2, actuator 3 and actuator 4 at the same time but with different velocities. That is, member 1 should rotate clockwise with a angular velocity of 0.5 $[deg/s]$ while member 2 should rotate at 1.6 $[deg/s]$ counterclockwise and finally the last member that delivers the sample to safety in the capsule is rotating in a clockwise direction with a 1.8 $[deg/s]$ as angular velocity. This process is illustrated in the next two figures. The whole process takes exactly 120 $[s]$.

Securing the container

Securing the container inside the capsule can be a difficult process since it needs to be secured tightly. This is due to the potential forces of large magnitude that the capsule will encounter during reentry. Therefore, the capsule is designed in such a way that as the container and member 3 enter it over 15 $[cm]$ as stated earlier. Once the container is approaching the bottom of the container, the extra material that is present around it will create enough friction to be held in place. This extra material is seen

Figure 7.25: Container about to enter the SRC

Figure 7.26: Final position of SAM with respect to the SRC

as crushing ring on Figure 7.27. A small deformation of the extra material occurs in a controlled way. This is made possible thanks to the yield strength of the material (Aluminium 1100-O) and the force that the actuator can apply. They can develop a torque of 14 $[Nm]$ and have a resistant torque of 20 $[Nm]$. The force needed to deform the disk is retrieved as follows using Equation 7.11.

$$F = \sigma \times Area \tag{7.11}$$

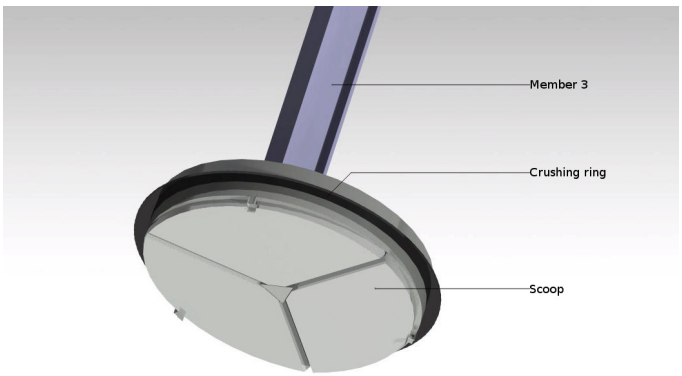

Figure 7.27: Crushing disk of SAM

In this case, σ_y is the yield strength of the material in $[Pa]$, which is chosen to be a low yield strength aluminium with a high elongation. That is the aluminium 1100-O alloy with a yield strength of 34 $[MPa]$ and a maximum elongation of 40% [34].
.

Here the area is computed through $2\pi Rt$ where t is the thickness $[m]$, and R is the radius of the disk $[m]$. Iterations were made with goal to obtain a force less than 20 $[N]$ since it was deemed acceptable for the actuators in the first place. It does yield that with a thickness of of 1 $[mm]$, a force of 10.7 $[N]$ would initiate a deformation in the aluminium part which is easily done by the three actuators. The releasing of the container is simply done by a pinpuller, placed at the root of member 3, as can be seen in Figure 7.16. Once the container is secured in the capsule, the arm simply retracts into its original position. In order to summarise the whole process, an overview of the technical aspects of the sample mechanism is presented. It encompasses the main information about the sampling mechanism.

V&V

The model that was made in order to obtain the dynamics of the system and the dimension of the members was first verified by hand in order to accurately visualise the input and output of the system. It was then implemented in DSC CATIA in order to verify that the length of the members are correctly estimated. A kinematic simulation was then created in order to visualise the possibilities that such combination of member lengths could give. If the visualisation of the system was not correct, iterations

[34] `http://www.matweb.com/search/datasheet.aspx?matguid=db0307742df14c8f817bd8d62207368e&ckck=1` Accessed June 22, 2018

Table 7.12: Main information about the sample mechanism

Parameters	Value
Length member 1	22 $[cm]$
Length member 2	41 $[cm]$
Length member 3	20 $[cm]$
Peak power	36 $[W]$
Max. weight sample	60 $[g]$
Min. weight sample	40 $[g]$
Time of full procedure	378 $[s]$
Mass sample mechanism	26 $[kg]$

were performed and the model was verified once again. A unit test of the program was carried out as well by changing some parameters to, for example, 10^6 times their initial value in order to assess the differences in the several outputs. The model shows a normal behaviour to this changes, thereby passing the unit test.

7.3.5. Sample return capsule

The return capsule box is a important aspect of this hoverer's mission since it protects the heat shield of the reentry capsule from any debris or small objects that may be harmful to it. The requirements of this capsule are presented here under qnd the protecting box zqs designed qround those.

`ASRM-SASH-SRC-001` The SRC on SASH shall be able to ensure a safe reentry through Earth's atmosphere. [A]
`ASRM-SASH-SRC-002` The SRC on SASH shall be able to carry at most 100 grams of sample acquiring by the SAM. [A]
`ASRM-SASH-SRC-003` The SRC on SASH shall not be damaged during operations until landing on Earth's surface. [T]
`ASRM-SASH-SRC-004` The SRC on SASH shall be able to open for the SAM to put in the sample. [D]

The setup of the reentry capsule on SASH is slightly different for conventional sample return spacecraft. Due to the fact that the Piazzi mission is using the Hayabusa reentry capsule, the only way to put a sample in is through the back of the capsule. Two solutions arose: either place the capsule by the side of the aircraft or at the bottom, next to the sample mechanism. The latter would then lead to having the heat shield facing inward the spacecraft. In order to ease the members' complexity, the second option was chosen. A box had then to be designed such that the capsule would be protected at all time during operations. This box is 20 $[cm]$ high and encloses the 40 $[cm]$ diameter capsule. It can be visualised in Figure 7.28 with the capsule facing up and the side panels of the box open (one is hidden for visibility). So as the box is positioned around the capsule, the sampling mechanism was designed as not to touch or damage this box. This avoided complications for the risk of damaging the capsule.

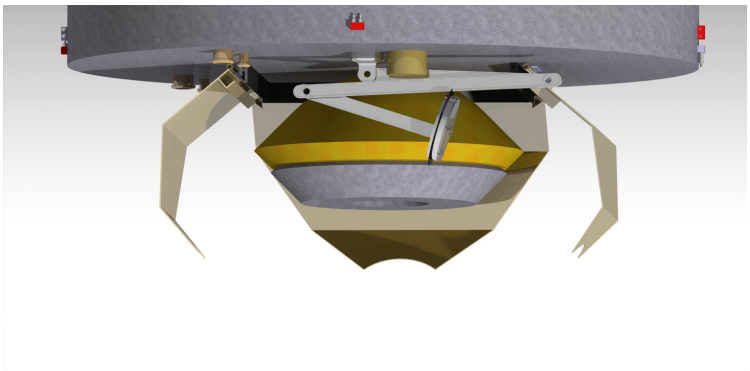

Figure 7.28: Render of the SRC with the SAM in front. The SRC box is opened, as upon Earth return. One panel is hidden for visibility.

When arriving at Earth, this capsule needs to be released at the right angle in order to land at the proper location. In order to have a successful reentry, the capsule needs to be released with the heat shield pointing towards Earth. Usually this is not a problem because the capsule can just be ejected forwards and the heat shield will be in the right direction. It is different for the hoverer of the Piazzi mission. Since the heat shield is facing the inside of the spacecraft, the capsule has to be ejected backwards. The box that protects the reentry vehicle has the ability to open up in order to leave enough space for the capsule to be ejected. Because the spacecraft is travelling towards Earth, once the altitude is optimal for release, the box opens up and

the capsule is ejected in the opposite direction, while the heat shield is still pointed towards Earth. It has to be noted that for the stability of the capsule it needs to be spun. This is achieved through a spring system that gives a rotational motion to the capsule as it is ejected from the spacecraft.

7.3.6. Sensitivity analysis

The main parameters that would influence a change in the whole design of SASH is explained below.

The first thing to consider is the density of the asteroid. As the asteroid density has been estimated from Earth, changes may occur in it as the spacecraft arrive. This has an influence on SASH as a higher density induces a stronger gravity. As so, the descent procedure of the hoverER would be faster and the RCS-thrusters would need more fuel to achieve this descent. As the hover reduces its descent velocity to zero $[m/s]$, it is highly dependant on the propulsion system. In order to calculate how this increase influences the propulsion, it is assumed that the gravity is increased by a factor two. From this it can be calculated that the fuel used by the RCS system for the descent is increased by 0.03 $[kg]$. This is rendered insignificant since the tank for the RCS-thrusters are designed to hold more than the needed fuel as a margin.

Another aspect that may affect the hoverer is the irregularity in the shape of the asteroid. During the whole design of the several spacecraft, the shape of the asteroid was assumed to be spherical. If, as the spacecraft arrives near the asteroid, it is found the shape of it is highly irregular, a different strategy for the hover spacecraft would be needed. Firstly, the orbiter may need a much longer mapping time and this could delay the descent of the hover spacecraft to a certain extent, that it may miss the return window to go back to Earth. Anyhow, the time that the spacecraft is around the asteroid is more than 114 weeks, that is more than what is needed for the mapping. As so it is assumed time-wise adequate to have minor changes in the whole hover mission. It must also be pointed out that a irregular shapes may yield a more difficult landing. Although the mapping strategy is key to choose the landing site, extra RCS fuel may be needed due to those shapes or possible hills. These changes in RCS fuel usage are rather small and assumed to be insignificant for the hover design as a whole.

An important aspect that needs to be taken into account is the rotational speed of the asteroid. First a rotational speed that is too high would induce a harder hovering and sample retrieving. Even if one would try to orbit the asteroid while matching its rotational speed, the attraction of the body will not be big enough to be able to orbit correctly making the descent really hard. But more importantly a very high rotational speed would mean that no regolith may be present on the surface of the asteroid. This is less of a challenge for the Lander spacecraft since it uses a drill in order to obtain a core sample but the Hover spacecraft only collects the regolith that lies on the surface of the body. As so if any regolith is present, a termination of the mission would occur.

The asteroid may also have two rotational axes which was not considered during the design. So if the number of rotational axis is changed from one to two, it would induces a more complicated landing procedure which would certainly induce a more frequent use of the RCS-thrusters. The two rotational axis asteroid was not modelled and analysed since it is a rather rare phenomenon and the chance of occurrence here is quite low.

Even if it was briefly touched up earlier in this section, the repercussion of missing the return window for the hoverer has to be analysed. So this induces a longer mission time meaning that the spacecraft has to survive longer in the harsh environment that space is. Even though, if the mission time is extended by ten years, calculations yield that the degradation of the solar panel would be around 29 % which can still provide enough energy for the spacecraft's functionality. Therefore, the EPS system would still be running but some other components such as the reaction wheels, due to the mechanical nature are at a higher failure risk and may not be able to survive until the next departure window. Energy can also be saved by turning instruments off as they should not be needed once the sample is collected. In other words, it is undetermined if the spacecraft can survive until the next departure window, but the odds of missing that are rather small.

A closer look can now be drawn onto the solar activity during the mission. The spacecraft are travelling during a solar maximum, which means that the amount of solar radiation that hits the hoverer is higher and not beneficial for the instruments but especially harmful for more vital electronics in the spacecraft. Assuming that the solar radiation is doubled, the health state of the hoverer electronics may be at risk. Fortunately, electronics are always overdesigned with respect to the incoming solar radiation. For example, a processor with nowadays technology is capable of sustaining over 300 $[krad]$ [35] which is overdesigned since it is a processor. Therefore not much change would be needed in the design of the spacecraft.

Doubling solar pressure would induce a change in the ADCS system since the force acting on SASH would be larger and more fuel would be needed to counteract it. Although, it is deemed negligible and assumed tolerable with the present design. As the solar flux is the source of energy of the spacecraft changing it to half its intensity would have major changes in the design of the spacecraft. Especially when it comes to the solar panel. That is, if the solar flux is halved, the solar panel needs to be doubled. This changes from the 0.8 $[m^2]$ to a 1.6 $[m^2]$. Since the mass of the solar panels have a linear relation with the size, it will be doubled as well. The solar arrays do not weight much but a doubling in size may be disadvantageous for the deployment and structural integration. This change will not affect the launch since the fairing has extra space by the side of spacecraft.

[35] https://www.voragotech.com/products/va10820-radiation-hardened-arm%C2%AE-cortex%C2%AE-m0-mcu Accessed June 21, 2018

8

The Spacecraft Subsystems

In this chapter the design and architecture of all the subsystems of the three spacecraft are addressed. Per subsystem, a general method to determine the required components or size is given, after which per spacecraft the specific requirements for each subsystem are given. Out of these requirements a design for the specific spacecraft comes out using the general method explained at the start of each section.

The chapter start with an analysis of the structures required for the spacecraft, after which the EPS, propulsion, ADCS, thermal control, TT&C and C&DH system are addressed.

8.1. Structural Design

This section will elaborate upon the backbone of the spacecraft that not only supports all the different subsystems, but above all ensures the satellite can be taken into space intactly. On all this there are some requirements, such as that the spacecraft should fit inside the launcher fairing and the structure's characteristics should fall inside the launcher's payload envelope. First a general explanation of the structure will be given, followed by the primary load carrying structure, after which the deployment of various systems will be discussed.

8.1.1. General structure

The overall structure of the spacecraft is mainly dependent on the mission it has to fulfil. The orbiter then is for a large part composed of fuel tanks, required for orbit injection around the asteroid and a flat side for accompanying the payload. The hoverer is made as small as possible, with the center of gravity as close as possible to the centreline, there this simplifies attitude control by the ADCS, required for the hovering over the surface. Due to its complexity, a definite mass estimate cannot be made for the complete structure, therefore it will be assumed to be 20% from the dry mass (Wertz et al. [2011]).

The lander's main function, on the other hand, is to drill into the surface, for which a large cylindrical structure (the drill tower) is required. The following subsections will elaborate on the overall structure of all mentioned spacecraft.

Orbiter

A first design of the layout of the orbiter was based on the dimensions of the fuel tanks, since these both were significantly in volume during the first iterations (both approximately 500L). It was decided, with structural efficiency, accessibility after assembly and volume taken into account, to mount the propellant tanks in the centre of a cylindrical frame; other forms of enhancing the backbone will be discussed in subsection 8.1.2. The cylinder would then be divided in sections, such that the lower tank with the heavier fluid (the fuel) could still be accessed after integration of the spacecraft. Another advantage of this decision is that the buckling load increases by a factor four, due to the effective length halving. The propellant tanks will be polar mounted with the mounts attached to the cylindrical section interface to minimise weight and to minimise stress concentrations on the thrust structure, therefore eliminating required stiffening material and thus additional weight.

Continuing with the electronics bay, which is composed of both the bus and the payload, it is placed around the top cylindrical section. Enclosed and mounted hereon are all electronic subsystem components, such as EPS (batteries, PV elements etc.), TTC (amplifiers, high gain and low gain antennae), and the payload, composed of several sensors in different bands of the electromagnetic spectrum, that thus need a clear view of the asteroid. The latter had major influence in the sizing of the width of the electronics bay, since it would be beneficial for all instruments to have a view of the asteroid simultaneously, in order to reduce the number of actuations by the ADCS system if instruments were mounted on different sides. The height of the electronics bay was for a first estimate taken equal to the cylindrical section height, not only to allow for mounting of cold gas tanks and payload, but also since this would reduce the weight if the section interface could also be used for transferring the loads of the electronics bay to the thrust structure.

The floor and ceiling of the bay will be made of aluminium honeycomb panels, as these are a weight-efficient way to resist bending loads, caused by loads during launch by systems mounted on the floor and ceiling and onto the side panels. These side panels will be aluminium plates, used not only for transferring the loads experienced by the bottom and top floor, but also to

allow for mounting of sun sensors, RCS-thrusters, antennae, thermal louvers and PV elements. For calculating the thickness it should be taken into account that stress concentrations as caused by cut-outs for e.g. instruments do not result in shear-out or buckling during launch; local reinforcements can also be applied. Additionally, the shear loads will be transferred to the thrust structure by the use of shear plates, perpendicular to the floor and the cylindrical structure. These will be manufactured of aluminium plates as well and rigidly attached to all sides to ensure efficient load transfer. The shear plates also create a rigid mounting point for the high gain parabolic dish and the solar panels, in this way reducing the required thickness of the side plates and thus the weight. Fastening of the surface panels to each other can either be performed by welding, bonding or bolting, the latter being preferred with respect to accessibility. Welding is structurally more efficient than bolting, but eliminates the possibility of replacing components inside the spacecraft. The same applies for bonding, where in addition special adhesives need to be used that do not suffer from outgassing. Another disadvantage of bonding is the high accuracy needed for aligning the bonding lines, which results in high expenses.

SASH
The hover is built around a standard 937 $[mm]$ cylinder, which houses all subsystems internally, except for the payload, the antenna and the PV panels. The payload is mounted on the top of the spacecraft, composed of SAM and the SRC, which is encapsulated to ensure integrity of the heat shield during the mission. The louvers are mounted on the surface of the cylinder, to expose them to the environment, while being away from the solar panels to allow full view of the sun for heating and shadow when cooling is needed.

ACSAL
For the lander the structure had to comply with several constraints, among others the base with the landing legs and harpoons and the drill tower. Since the latter was already composed of a cylindrical section, it was decided to use this cylinder with a 270 $[mm]$ diameter to transfer the loads to all other components. To still host the fuel and gas tanks, it was decided to make use of toroidal tanks, which can be mounted around the cylinder. The mounts of the fuel tank will also be used to mount a loading floor for ADCS components, batteries etc. Additionaly, the louvers required for thermal control need also mounting on the payload floor. The solar panels will be attached to the tank mounts, which will be structurally enhanced in order to carry the required loads. The sample return capsule will be mounted on the drill tower, since this is necessary for the drill to move the sample herein.

8.1.2. Primary structure

Due to the highly complex loading scenarios of the spacecraft, the focus of this preliminary structural design is mainly focused on the primary structure of the space system, also known as thrust structure, since this cylindrical structure is responsible for carrying the loads as experienced during the launch. For simplified analysis of this structure, all elements (e.g. orbiter, lander and hover) are assumed to be cylindrical with uniformly distributed mass. The diameters of the cylinders have, where possible, been taken to be equal to the EELV standards (Kendall [2000]) [1]. This was done to not only limit the scope of the analysis, but also to ensure compatibility with off-the-shelf payload adaptors (PLA) so as to reduce cost. The diameter of the orbiter's thrust structure was decided to be 1194 $[mm]$, as this enables placing the propellant tanks inside the structure.

`ASRM-ST-001` The structural design of every spacecraft shall be able to withstand the launch loads. [A]

`ASRM-ST-002` The structural design of every spacecraft shall enable the mounting of subsystems. [I]

Four loading conditions are analysed for the structure, which will be elaborated upon in the following sections.

- Vibrations. The structure should ensure that the lowest vibrational mode of the satellite lies above the specified natural frequency of the launcher, which could else lead to resonance with possibly fatal consequences.
- Bending loads caused by lateral vibrations of the launcher result in both compressive and tensile loads. The structure should not yield under the given bending loads.
- Compressive loads as caused by axial loading during the launch, both continuous and momentous.
- Column buckling due to a compressive load in combination with small cross-sectional area leads to catastrophic failure of the structure.

The considered materials for the structure are aluminium, steel, magnesium, titanium and beryllium, materials common in the space industry; composites were not considered due to the complexity in designing and manufacturing of composite structures, although being more efficient with respect to weight. The densities, yield stresses and elasticity moduli used in the calculation can be found in Table 8.1, also the normalised yield strengths and elasticity moduli can be found there. Each of

[1] I.e. 2800, 2624, 1666, 1194, 937, 610, 432 and 381mm, where the first two are as of now not flight proven on the selected launcher, and thus not taken into account.

Table 8.1: Material properties used in the calculations on the structure, while the normalised yield strength and elasticity by density are displayed for easy comparison for structural effectiveness.

Material	**Density** $[kg/m^3]$	**Yield Strength** $[MPa]$	**Normalised Yield Strength** $[MPam^3/kg]$	**Elasticity Modulus** $[GPa]$	**Normalised Elasticity Modulus** $[MPam^3/kg]$
Aluminium	2700	300	0.11	70	25.9
Steel	7900	700	0.0886	200	25.3
Magnesium	1770	200	0.11	45	25.4
Titanium	4430	800	0.18	110	24.8
Beryllium	1800	200	0.11	290	16.1

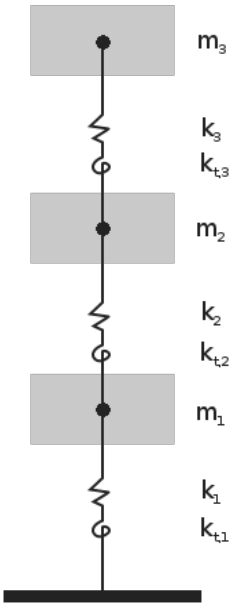

Figure 8.1: Simplified three-element model for analysis of the primary structure.

these materials has their own strengths and weaknesses. Aluminium is easily machinable, allowing relatively cheap complex structures, whereas titanium is very difficult to machine due to its toughness and expensive.Beryllium on the other hand has a low density and a relatively high elasticity modulus; disadvantages of beryllium are its low yield strength, brittleness (which could lead to cracks during ground handling) and its relatively high cost, besides from the associated toxicity during manufacturing. It is therefore not a preferable material and use should be avoided. Steel is a very common material in construction, due to the highly tailorable strength and stiffness, while being relatively cheap; this all at the cost of a high density. Magnesium is a lightweight material, is easily machinable and because of its low density it is used where buckling loads are the prominent failure mode.

8.1.3. Load analysis

For the vibrational analysis the structure has been subdivided in the individual mission elements: the orbiter, the lander and the hoverer, of which the final masses were assumed to be as in tables Table 5.1, Table 7.2, Table 7.10 and Table 7.6, respectively, excluding the PLAs (which weight around 80 $[kg]$ [2], see subsection 8.1.4), that will each be accounted for 50% to both the parts it interfaces. As the launch vehicle's PLA is commonly excluded from the payload mass when this is a standard interface diameter, this will not be included in the vehicle mass. As a simplified analysis a three body lumped-mass model (see Figure 8.1) will be analysed, connected by torsional and axial springs. The model assumes a linear relation between the compression load and the strain experienced, where the stiffness constant k is assumed to be $\frac{EA}{l}$, where E is the elasticity modulus $[GPa]$, A the

[2]https://www.ruag.com/sites/default/files/2017-01/PLE-Brochure-Payload-Adapter-and-Separation-Systems.pdf Accessed June 5, 2018

cross-sectional area [m^2] and l the section length [m]. For the lateral loads, a torsional spring model is assumed with a stiffness K_t of $\frac{3EI}{l}$ where E and l have the same definition as before and I is the area moment of inertia [m^4]. The equations of motion for both angular and axial are then set up and the equations are converted to a state-space system and the eigenvalues of the resulting matrix are then evaluated. The lowest natural frequency should be higher than the specified launcher ground frequency, as divergence could result in constructive resonance which could ultimately lead to catastrophic failure. If the aforementioned condition is not met, material should be added in the form of additional thickness.

If compliance with the vibrational load is ensured, compliance with the bending loads must be ensured, i.e. these must not exceed the yield stress of the material. First the current bending stresses are evaluated using Equation 8.1, and if necessary the thickness needs to be increased. Then, the compressive axial stresses due to the launcher's acceleration are calculated and these are superimposed with the previously calculated bending stresses. These stresses are then compared with both the yield stress and the buckling stress (Equation 8.2). The final mass required for the different materials considered is then compared.

$$\sigma_Z = mg\left(LF_{ax} + LF_{lat} Z_{cg} \sqrt{2}\pi \frac{1}{R^2 t}\right) \tag{8.1}$$

$$\sigma_{crit} = \frac{\pi^2 EI}{4Al^2} \tag{8.2}$$

The final universal thickness of 4.1 mm across the structure with aluminium is the most efficient thickness, resulting in a mass of 92 [kg] for the orbiter, 23 [kg] for SASH and 9 [kg] for ACSAL. Masses can be significantly improved by applying a finite element method with combined loading scenarios. Unfortunately the model could not be verified with a simplified analytical model or a FEM model, the first one because the used system of equations is already the simplest form of viewing a three-radii system; the latter because time does not allow generation of such a model. The model can however be verified with unit testing: by increasing the launch loads or the mass, the thickness should increase as well and vice versa. It can also be tried for decreasing the elasticity moduli or the yield strengths, this should yield an increase in thickness as well. Applying these tests to the model does result in aforementioned changes and thus the model can be considered verified.

8.1.4. Subsystem deployment

Several items that are mounted on the spacecraft could not fit in the condition they need to be in, such as the solar panels and the high gain antenna. Therefore it is necessary that they are stowed in such a way that they can both survive the launch conditions and be deployed efficiently without influencing the operations. For solar panels, they can be mounted on the surface, but since this offers not sufficient area in this case, external PV panels are used. These need to be folded in order to fit inside the launcher fairing. The unfolding during the mission can be done both reversible and irreversible, where for this mission it is chosen to not use reversible folding elements, since this adds complexity and mass, while the advantage is low: the solar panels of ACSAL and SASH only will be unfolded after arriving at the asteroid, and are designed in such a manner that they will be able to withstand the loads associated with touching down, without colliding with the surface. Liftoff will be done with a small thrust, so as to not induce large loads. Return orbit injection will be the most severe launch case, where 445 [N] will be supplied to the structure, while the start-up of the thruster will be gradually to reduce shock loads. Detailed design is necessary to calculate the required stiffness for this condition. The high gain antenna of the orbiter will also need protection against the launch conditions. This can be done by for instance deploying the parabolic dish in an umbrella-like manner, as can be seen in Figure 8.2, while during launch being stowed against the surface of the orbiter to reduce bending loads.

Another mission critical deployment phase is the separating of the lander and hover from the orbiter after mapping of the asteroid. This will be done with off-the-shelf payload separating mechanisms, as generally used for spacecraft separation from launchers. Explosive bolts will first physically separate the lander from the adaptor, while simultaneously releasing springs in order to push it away from the rest of the system. Afterwards, the rest of the adaptor will be ejected from SASH, so as not to negatively influence its functioning. SASH itself will then finally be equivalently separated from the orbiter, while the adaptor will be stuck thereon, since this does not influence the mission objectives of the orbiter significantly. According to the launcher manual (Space Exploration Technologies Corporation [2009]), launcher adaptors vary in mass between 60 and 115 [kg]. Since our hover and lander weight significantly less than regular launcher payloads, it can be assumed that the used PLAs will be approximately 80 [kg], with a safety margin taken into account to allow for custom demands.

At the end of the mission, as both spacecraft approach Earth, the SRC needs to be ejected from both the encapsulation on the hover and the drill tower of the lander. The ejection will be performed in a similar manner as the detachment of both systems for the orbiter, with the springs in this situation positioned in such a way that the capsule is given a spin, so as to stabilise its reentry trajectory. For SASH, first the encapsulation will be folded away, before atmospheric entry ejection.

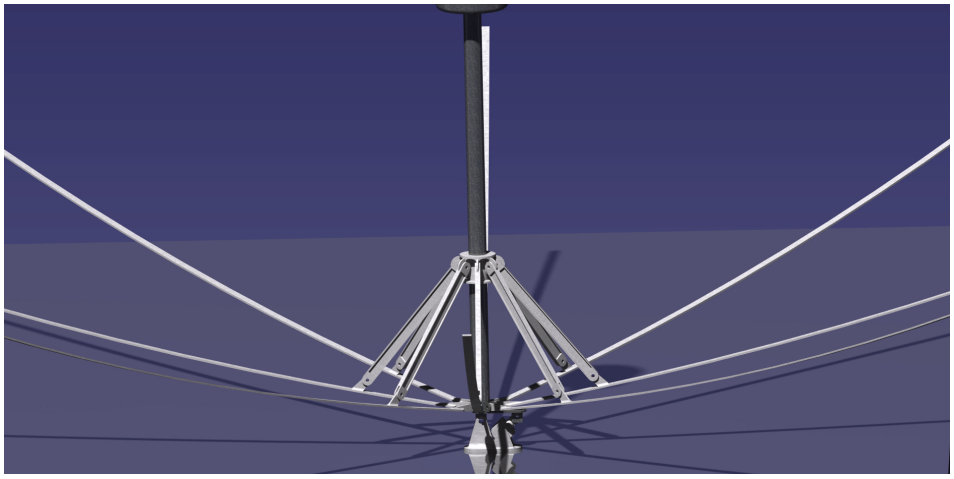

Figure 8.2: Impression of the high gain antenna unfolding mechanism

8.2. Electronic Power Subsystem

In this section, the electronic power subsystem will be explained. First, the requirements will be listed, after which the design method and the final architecture will be presented.

8.2.1. Mission & Design Requirements

A general architecture of an EPS consists of a power source, power storage, power regulation and power distribution units; these working together ensure the power supply of the spacecraft subsystems. A power source is important so that the satellite can operate long-term while constantly generating power. Storage of power is essential to specific phases of the mission when the power generator cannot be utilised (e.g. during detumble mode, emergency mode, eclipse phase). The EPS is responsible for regulating the supplied power to match the subsystem's needs. Furthermore, the EPS is required to function autonomously for longer periods of time. Besides these requirements, the EPS has many more requirements which are stated below.

ASRM-EPS-001	The EPS shall provide a continuous source of electrical power to the spacecraft loads during the mission life. [T]
ASRM-EPS-002	The EPS shall control and distribute power in the spacecraft. [T]
ASRM-EPS-003	The EPS shall provide command and telemetry capability for EPS health and status. [T]
ASRM-EPS-004	The EPS shall allow control by the ground station. [D]
ASRM-EPS-005	The EPS shall be able to function autonomously. [T]
ASRM-EPS-006	The EPS shall protect the spacecraft from failures within the EPS. [D]
ASRM-EPS-007	The EPS shall dissipate excess power. [T]
ASRM-EPS-008	The EPS shall protect the spacecraft payload against failures within the EPS. [A]
ASRM-EPS-009	The EPS shall support a safe mode. [D]
ASRM-EPS-010	The EPS shall support a low-power mode. [D]
ASRM-EPS-011	The EPS shall keep the angle of incidence of the sun rays below 1 [°]. [T]
ASRM-EPS-012	The spacecraft shall be able to operate in low-power mode on battery power for one week.

The driving mission parameters behind the sizing of the EPS are: demands for average and peak electrical power, the orbital profile, and mission lifetime (Wertz et al. [2011]). One of the key factors that also weighs in when designing for this critical part of the spacecraft bus, is the fact that the chosen concept consists of one orbiter and two landers. This means that three independently operating Electrical Power Subsystems have to be designed, manufactured, and tested. This poses a significant challenge, since the landers have an unconventional mission profile from the moment they are decoupled from the orbiter. Unconventional because in order to fulfil the mission objective they do not simply orbit the asteroid, causing them not to have the cyclical daytime-eclipse orbit. Rather than this determining the size of the battery and solar array, an analysis into the operational modes was made, determining what the peak energy demands for the landers are and deriving requirements for the system which ensures that the state of charge for the batteries return to acceptable levels within a realistic time frame.

Following from requirements ASRM-EPS-001 and ASRM-EPS-004, it is logical to derive the need for the obvious components of the EPS: a power source, power storage, and a power control & distribution unit (PCDU). All of these components will be elaborated upon in the following subsections, with more details on the chosen hardware and their performance characteristics.

Table 8.2: Values for EPS sizing

Variable	Description	Value	Source
$d_{sol,max}$	Maximum distance from Sun	1.157 [AU]	Orbital parameters[3]
S_{min}	Minimum solar flux	1017 $[W/m^2]$	$1361 \cdot \left(\frac{1}{1.16}\right)^2$
X_e	Path efficiency from the solar arrays through the batteries to the individual loads	65%	Wertz et al. [2011]
X_d	Path efficiency from the solar arrays directly to the individual loads	65%	Wertz et al. [2011]
η_{sc}	Solar cell efficiency BOL	29.8%	AzurSpace[4]
η_{deg}	Degradation factor	3.75% per year	Wertz et al. [2011]
η_{DA}	Design & Assembly efficiency	85%	Wertz et al. [2011]
η_T	Temperature efficiency	85%	Wertz et al. [2011]
$T_{asteroid}$	Asteroid rotational period	7.8 [hr]	
n	Transmission efficiency between the battery and the load	90%	Wertz et al. [2011]

Requirement ASRM-EPS-015 was determined by agreement within the design team that should any crisis arise with any of the spacecraft, enough time was permitted for the ground support team to solve the issue at large.

8.2.2. Method

As determined in the midterm phase of the design, the EPS setup of this spacecraft will be comprised of a photovoltaic power source, supported by a secondary battery based on lithium-ion technology (Angyal et al. [2018]). This setup will be used in the orbiter, SASH, and ACSAL, albeit in customised sizes for each stage of the spacecraft.

Although specific values for components could be found after the system has roughly been sized in order to further the accuracy of the design, at this stage a more detailed performance calculation of the EPS compared to the midterm phase is done using values such as those given in Table 8.2. These values are deemed accurate and are therefore used in the sizing of the EPS for all stages of the spacecraft.

The first step in sizing the power system as it is now defined is using the following formula (Equation 8.3) to determine the power the solar panel array has to deliver (Wertz et al. [2011]).

$$P_{sa} = \frac{\frac{P_d T_d}{X_d} + \frac{P_e T_e}{X_e}}{T_d} \tag{8.3}$$

Where $P_s a$ is the power that the solar array has to deliver, P_d and P_e are the average powers for day- and eclipse time respectively, T_d and T_e are the duration of day- and eclipse time, and the path efficiency X_d and X_e to account for losses caused by the power distribution.

This equation can be applied to determine the performance requirement of the solar array of all stages. The determination of the average power and day and eclipse times has proven to be more of a challenge as this required intermittent updates on the details of the mission time line and the power requirements of the different phases in the mission. However as the design progressed into more detail this was made possible, and the results of this per stage are elaborated upon in the subsections below.

The next step in designing the EPS for all the stages of the spacecraft was sizing the battery capacity. For the electrical energy storage unit batteries will be used. As multiple types of batteries exist, three best-fit options will be considered: Ni-Cd batteries, Ni-H_2 batteries, and Li-ion batteries. A weak point analysis has been performed in the midterm phase by Angyal et al. [2018] and it was found that Li-ion has far more benefits than either Ni-Cd and Ni-H_2. Especially energy density (125 $[Wh/kg]$ for Li-Ion, 30 and 60 $[Wh/kg]$ for Ni-Cd and Ni-H_2, respectively and energy efficiency (98% for Li-ion, 72% and 70% for Ni-Cd and Ni-H_2, respectively (Wertz et al. [2011])) make Li-Ion technology the right choice for Piazzi as this results in lower battery mass and less power lost.

[3] https://ssd.jpl.nasa.gov/sbdb.cgi?sstr=65679;orb=1 Accessed June 22, 2018

[4] http://www.azurspace.com/images/0003429-01-01_DB_3G30C-Advanced.pdf Accessed June 23, 2018

There are many proven commercial options available when it comes to the selection of a Li-ion battery. Companies such as AzurSpace[3] sell Li-Ion batteries that have demonstrated their capabilities in previous missions, which is necessary for the design in order to meet the TRL 6 requirement.

The sizing of the battery capacity was done using the Equation 8.4.

$$C_{bat} = \frac{P_e T_e}{DoD \cdot n} \tag{8.4}$$

The depth of discharge (DoD) is of great importance and has direct consequences on the lifetime of the battery when combined with the amount of cycles it must run through during the mission. For the orbiter, since many cycles are required by the mission geometry, a DoD of 40% was chosen as a design factor. For both SASH and ACSAL, since the amount of cycles is much lower than the orbiter, a DoD of 60% was chosen. There are several specific design requirements with regards to the batteries for all stages of the system which will be elaborated upon later in this section.

The general architecture of the EPS, characterised by the chosen PCDU is largely determined by the fluctuation in power throughout the mission and the difference in voltage requirements of the various components of the spacecraft.

Most important to the battery sizing is the amount of time the system has to be able to survive should there be a loss of power or any other issue which requires reasonable time to solve. Since this mission has high stakes (1,000 M€ budget), this is critical to mission success. In order to give the ground operations team enough time to respond to any crisis that would arise during the mission, a week was chosen as a reasonable time.

A tool was built that incorporated all the performance aspects of the EPS and calculated those values that were needed for the design.

8.2.3. Orbiter

Requirements

The orbiter does not have any specific requirements outside of the general EPS requirements as it does not have unique mission elements in the sense that SASH and ACSAL have. The sizing of the system is determined by the geometry of the mapping orbit as that determines the day and eclipse times.

Sizing

As mentioned before, the most important performance characteristic that needs to be determined is the average power of, in this case, the orbiter. This is calculated by finding the power demands of all subsystems, and then estimating the duty cycle of these components. The power subsystem will experience the largest loads during its asteroid mission phase and is therefore sized accordingly. The post-launch phases and interplanetary coast phase use less power as the payload is not used and low-power modes can be used.

The duty cycles are a preliminary estimation of the components activity during an orbit. The transmitter is generally turned on to transmit the data after the mapping phase of the mission, however it is not activated for the entire orbit as there are times when the asteroid eclipses the line of sight between the earth and orbiter, as well as moments where the attitude of the orbiter is in such a way that the HGA is not pointed towards Earth (for example when establishing connection with either SASH or ACSAL). The communication system, which has to output a transmitting power of 3 $[W]$ (HGA) and 1 $[W]$ (LGA) has a 28% conversion rate (see section 8.6), and thus uses 54 $[W]$.

The duty cycle for the observation instruments is largely determined by the fact that they do not operate continuously (as this would be akin to filming the asteroid) and demand their power for short, but many, bursts throughout the orbit. The RCS-thrusters are expected to operate in the same way the observation instruments do, which is through small bursts. The power requirements of the RCS-thrusters is derived from the relatively high power the valves need to operate.

The power required when an emergency arises has been determined to be 11 $[W]$, which has direct consequences on the sizing of the battery.

In Table 8.3 below are the results for the power overview for the orbiter.

[3] http://www.azurspace.com/index.php/en/products/products-space Accessed June 11, 2018

[6] https://www.vectronic-aerospace.com/space-applications/star-sensor/ Accessed June 22, 2018

[7] https://www.isispace.nl/brochures/NSS_Fine_Sun_Sensor_Datasheet_2c-.pdf Accessed June 18, 2018

[8] https://aerospace.honeywell.com/en/~/media/aerospace/files/brochures/gg1320andigitallasergyro-bro.pdf Accessed June 19, 2018

[9] http://www.moog.com/content/dam/moog/literature/Space_Defense/Spacecraft/Propulsion/ColdGasThrusters_0717.pdf Accessed June 21, 2018

[10] http://bluecanyontech.com/wp-content/uploads/2018/01/DataSheet_RW_07_F.pdf Accessed June 24, 2018

[11] http://www.rocket.com/files/aerojet/documents/Capabilities/PDFs/Bipropellant%20Data%20Sheets.pdf Accessed June 22, 2018

[12] https://www.eaglepicher.com/sites/default/files/EP%20SLC%2021060%20DATA%20SHEET.pdf Accessed June 23, 2018

[13] http://aacmicrotec.com/mini-pcdu/ Accessed June 23, 2018

Table 8.3: Overview of the power demand per component for the orbiter

Subsystem	Part	Amount	Power [W]	Duty Cycle [%]
EPS	PV array	1	-	
	Li-ion battery	1	-	
	PCDU	1	-	
TT&C	LGA	2	-	
	HGA	1	-	
	DIP	1	-	
	Transmitter	1	54	100
	Cabling	1	-	
ADCS	STAT	3	2.5[6]	100
	DISUS	6	0.04[7]	100
	DILG	4	1.6[8]	100
	COGT	24	30[9]	5
	OREWH	4	8[10]	100
	CGT	1	-	
Propulsion	AMBR	1	70[11]	0
	MMH	1	-	
	NTO	1	-	
CDHS	CPU	1	5	100
	Wiring	1	-	
Observation instruments	CAM	1	19	5
	MAG	2	0.8	5
	XRS	1	12	5
	GRS/NS	1	9	5
	UVS	1	4	5
	IR-VIS	1	13.5	5
	Cabling	1	-	
Thermal	PLT	8	7	100

From these values the average and peak power were derived to be 200 [W] and 456 [W], respectively. The average power is important to the sizing of the solar panel array and the battery, whereas the peak power is the upper limit the PCDU has to be able to handle.

Because the orbiter continues operations in the same way during eclipse as it does during day time, the average power for both periods is the same. Knowing these values and the system inherent values for efficiency and degradation, the outcome of the sizing of the EPS of the orbiter is as given in Table 8.4.

8.2.4. Hover

Requirements

SASH has its own mission specific system level requirements from which several more requirements for the EPS can be found which drive the sizing of the EPS components.

`ASRM-SASH-EPS-3` The EPS shall be capable of recharging the energy storage after sample acquisition% within 3 [hr]. [T]

`ASRM-SASH-EPS-4` The EPS shall be capable of delivering 425 [W] for 900 [s] at any point during the mission. [T]

These requirements have been derived from the mission time line and the actions performed to fulfil the mission from the perspective of the hovering stage. As SASH descends towards the asteroid, it has to be able to handle the period it might spend in eclipse. This naturally is dependent on the geometry of the asteroid and future decisions made on how the approach will look like, forcing the design to have margins in order to account for all outcomes. The system will be designed in such a way that the required solar array size is minimized, reducing the risk of it causing issues during the phase near the asteroid. The timeframe of 3 [hr] for `ASRM-SASH-EPS-3` is derived from the rotational period of the asteroid at 7.8 hours, and therefore sizing the PV array in such a way that it can recharge once per revolution of the asteroid. The DoD at 60% is relatively high, however since the amount of cycles (with this DoD) the battery has to withstand is in the order of 100 times, and therefore would not pose a problem to the battery life. `ASRM-SASH-EPS-4` is a requirement for the EPS of SASH as it this is the peak power during the

Table 8.4: Sizing results for EPS components of the orbiter

Name	Value	Source
P_{avg}	200 $[W]$	Using Table 8.3 and Equation 8.3
P_{peak}	456 $[W]$	Table 8.3
$P_{emergency}$	11 $[W]$	Table 8.3
Solar Array area	2.6 $[m^2]$	Using Table 8.3 and Equation 8.3
Solar Array mass	7 $[kg]$	2.8 $[kg/m^2]$ (Wertz et al. [2011])
Depth of Discharge (DoD)	40 %	-
Battery Capacity	2042 $[Wh]$	Using Table 8.3 and Equation 8.4; Emergency mode was driving
Number of batteries	8	-
Battery pack mass $[kg]$	16 $[kg]$	Using 125 $[Wh/kg]$ (Wertz et al. [2011])
Battery dimensions	172 x 81 x 58 $[mm]$	EP SLC 21060 for reference [12]
PCDU mass	6 $[kg]$	AAC Microtec MS02 [13]

sample collection. The duration of this action is not defined into detail at this phase as it is something that will be determined as the sample collection phase is determined after the asteroid has been mapped, therefore 900 $[s]$ (or 15 minutes) have been taken in order to make sure this manoeuvre succeeds.

Sizing

Determining the average power for SASH is a more difficult endeavour as it does not have a mission profile with a regular power cycle such as the orbiter. Its mission is to separate from the orbiter, descend, rehearse and execute the sample collection, and finally return to Earth. It does not have a mapping orbit or any orbit around the asteroid, making it difficult to estimate duty cycles. Therefore the power demands of SASH with different mission phases have been put next to the length of these phases to estimate the average power required. Just like the orbiter, only the actual asteroid mission phase has been considered in the sizing as this is the most power demanding period of the mission.

The duration of the manoeuvres for SASH is explained in section 7.3, which, combined with the power demands of the components of the spacecraft, allow for the calculation of the average power.

Table 8.5: Sizing results for EPS components of SASH.

Name	Value	Source
P_{avg}	23 $[W]$	Using Figure 8.3
P_{peak}	425 $[W]$	Figure 8.3
$P_{emergency}$	5 $[W]$	Table 8.3
Solar Array area	0.8 $[m^2]$	Using Table 8.2, P_{avg}, and Equation 8.3
Solar Array mass	2 $[kg]$	2.8 $[kg/m^2]$ (Wertz et al. [2011])
DoD	60 %	-
Battery Capacity	1111 $[Wh]$	Using Figure 8.3 and Equation 8.4
Battery mass	9 $[kg]$	125 $[Wh/kg]$ (Wertz et al. [2011])
PCDU mass	3 $[kg]$	-

From these values it is determined that when considering the dimensions of SASH that the sizing of the EPS fits within the system. The PCDU mass is more of an estimation as no existing products could be found, however this estimate is based on the fact that the PCDU for the orbiter has a mass of 6 $[kg]$ and that a PCDU for low-powered spacecraft such as cubesats at most weigh 1 $[kg]$. This component eventually will be custom-made for the mission and therefore the details at this point are not known.

8.2.5. ACSAL

Requirements

ACSAL is unique in the sense that it is going to land on the asteroid and perform a sample collection manoeuvre. This puts specific requirements on the EPS for ACSAL.

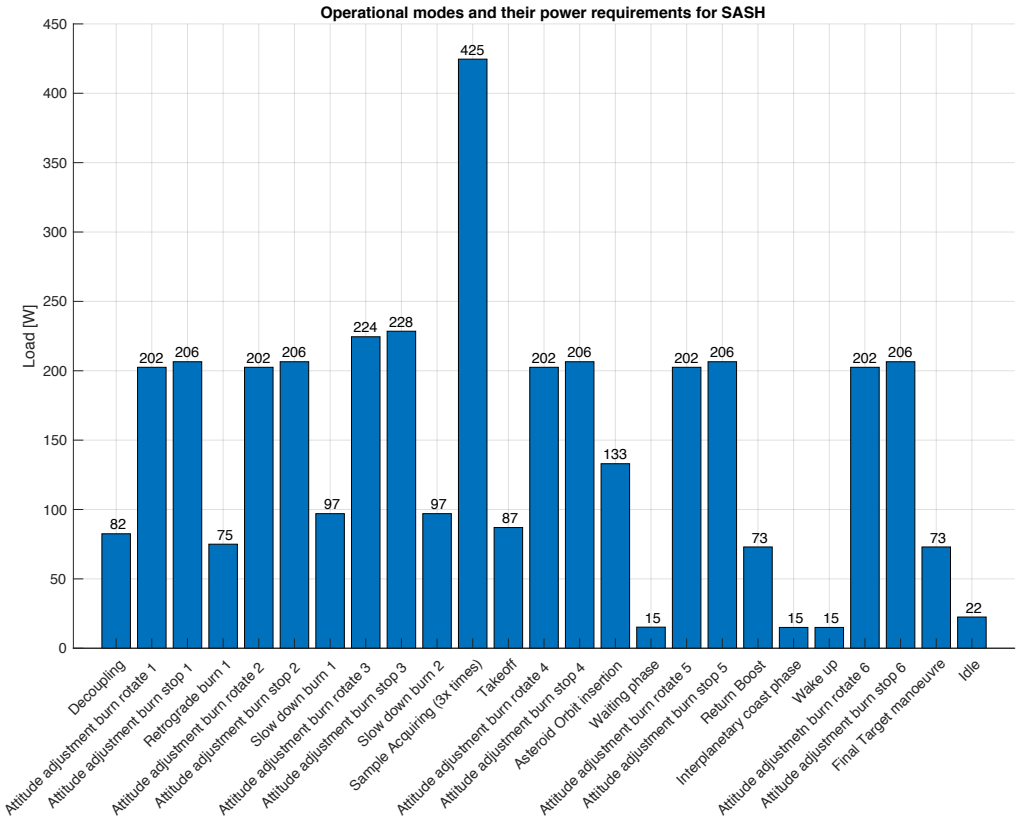

Figure 8.3: Power requirements for the operational modes of SASH.

`ASRM-ASCAL-EPS-3` The EPS shall be capable of recharging the energy storage after sample acquisition at a depth of discharge of 60 % within 3 [hr]. [T]

`ASRM-ASCAL-EPS-4` The EPS shall be capable of delivering 141 [W] for 900 [s] [T]

The actions that ACSAL has to perform throughout the mission time line resulted in these specific requirements. `ASRM-ASCAL-EPS-3` is derived from the fact that since the rotational period of the asteroid is 7.8 [hr], which means that for half that time ACSAL can recharge its batteries as there will be a line of sight with the sun. These quantities will be taken into account when sizing the EPS components. `ASRM-ASCAL-EPS-4` is required since this is the power required during the sample collection phase, of which the duration can at this phase only be estimated. 900 seconds was considered enough to perform one drill, as this only happens once per 'day' on the asteroid. ACSAL shall be able to fulfil this requirement regardless of the fact whether it is in eclipse or not.

Sizing

To assess the average power that is demanded by ACSAL's components, an operational mode analysis has been made, similar to the one made for SASH. The most important manoeuvre among them is the sample collection by use of a drill. The energy storage of ACSAL will be sized according to the mission demands for the sample collection as described in section 7.2. The findings of the operational mode analysis are listed in Figure 8.4. Again the average power will be determined.

Just as with SASH, the EPS system of ACSAL will fit within the spacecraft, based on these values. The PCDU mass is estimated in the same way and will in the end most probably be custom made as in this stage, no compatible devices were found.

8.2.6. Architecture

Essentially the system will have three electrical power subsystems which have the capability to operate independently, therefore needing all essential components albeit in different sizes.

The architecture of the system is the final design option for the EPS to be considered as the power source and power storage have now been chosen and sized.

A weak point in the unregulated direct energy transfer method is that there is no power regulation, and since the solar flux changes throughout the eccentric orbit of the asteroid, where most of the mission will be spent, it is not a feasible option.

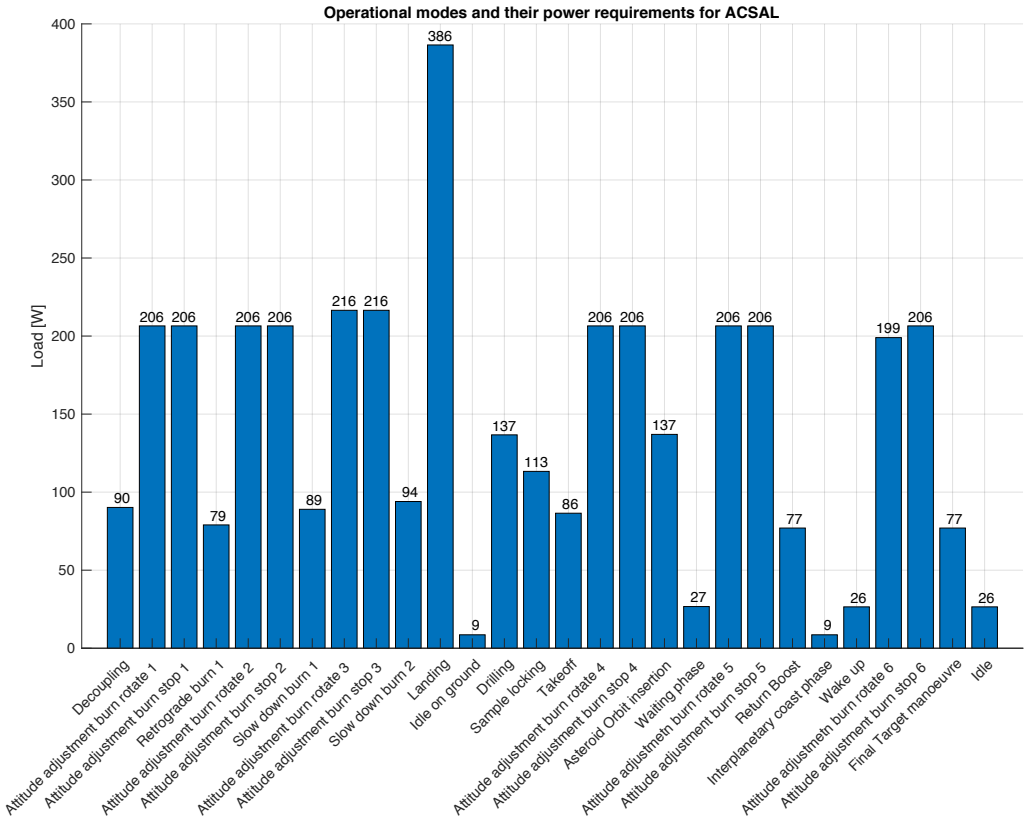

Figure 8.4: Power requirements for the operational modes of ACSAL.

Table 8.6: Sizing results for EPS components of ACSAL.

Name	**Value**	**Source**
P_{avg}	50 $[W]$	Using Figure 8.4
P_{peak}	401 $[W]$	Figure 8.4
$P_{emergency}$	5.4 $[W]$	Table 8.3
Solar Array area	0.7 $[m^2]$	Using Table 8.2, P_{avg}, and Equation 8.3
Solar Array mass	2.0 $[kg]$	2.8 $[kg/m^2]$ (Wertz et al. [2011])
DoD	60 %	-
Battery Capacity	65 $[Wh]$	Using Figure 8.4 and Equation 8.4
Battery mass	0.5 $[kg]$	125 $[Wh/kg]$ Wertz et al. [2011]
PCDU mass	3.0 $[kg]$	

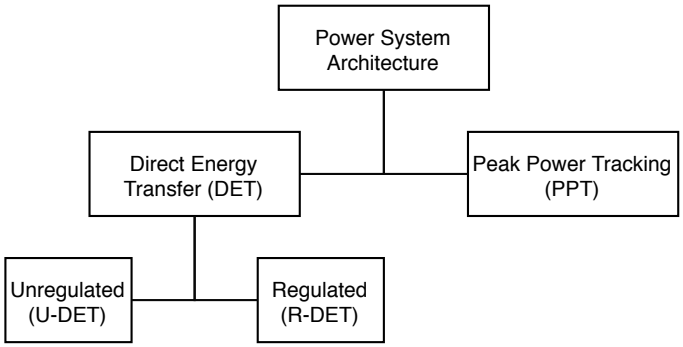

Figure 8.5: Electrical Power System Design Options

Moving on to the final two options, it is known that Peak Power Tracking is less efficient and therefore a less favourable option than the former, meaning that the right choice lands on the Regulated Direct Energy Transfer.

8.2.7. Electrical block diagrams

The electrical block diagrams of the orbiter, lander and hoverer are shown in Figure 8.6, Figure 8.7 and Figure 8.8 respectively. These diagrams shows the connection between the EPS system of all spacecraft and their components.

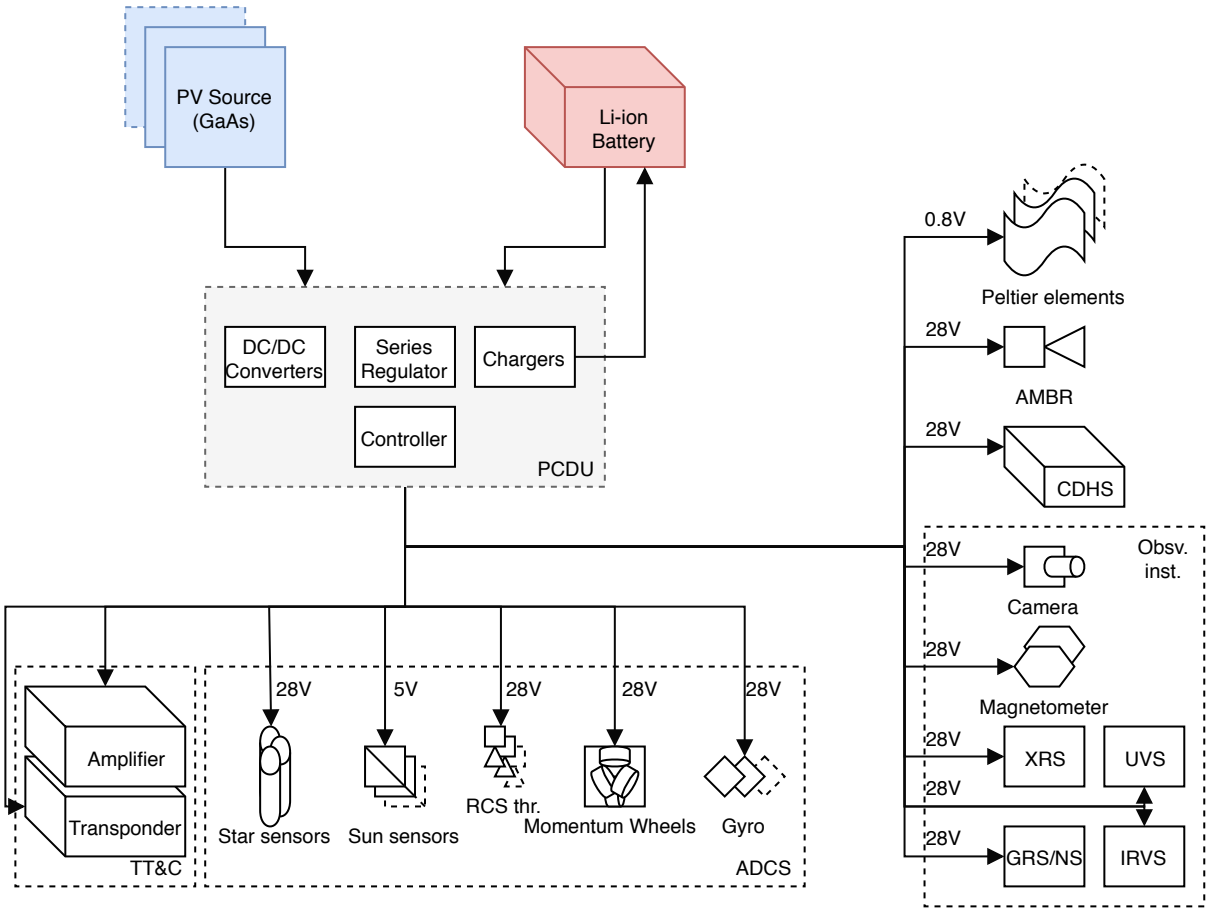

Figure 8.6: Electrical block diagram for the orbiter

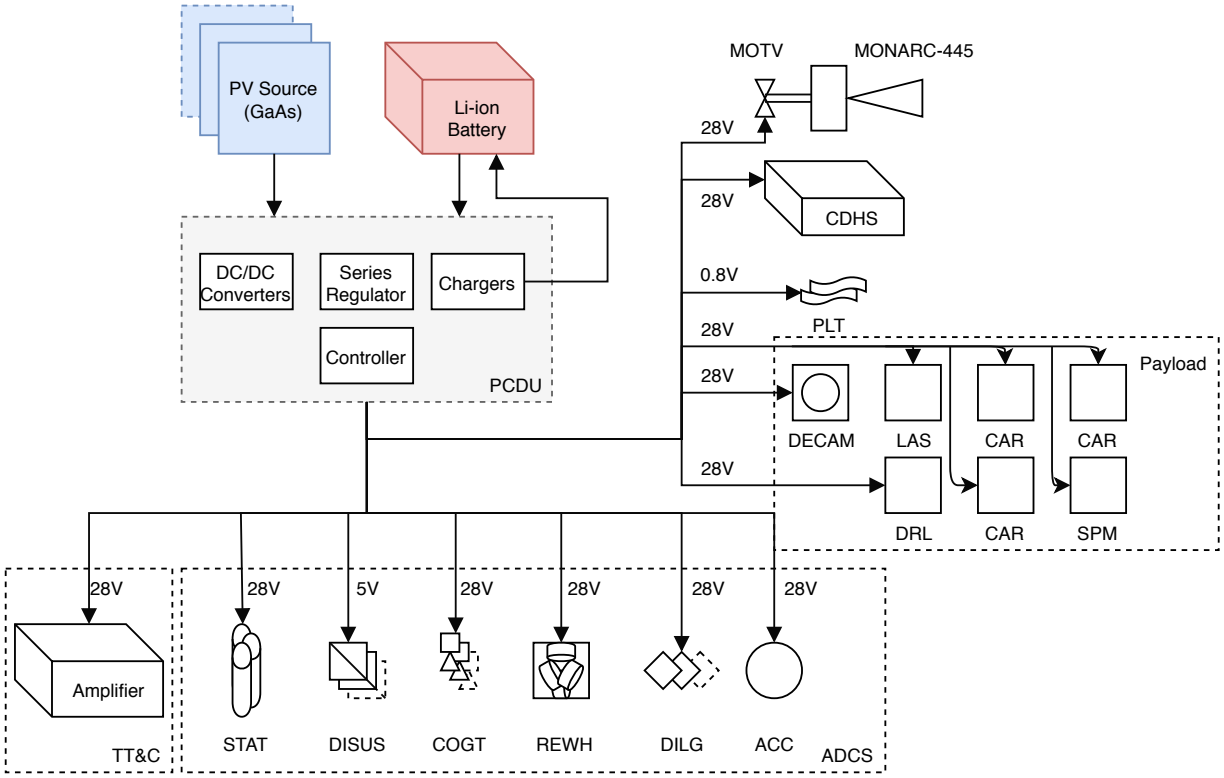

Figure 8.7: Electrical block diagram for ACSAL

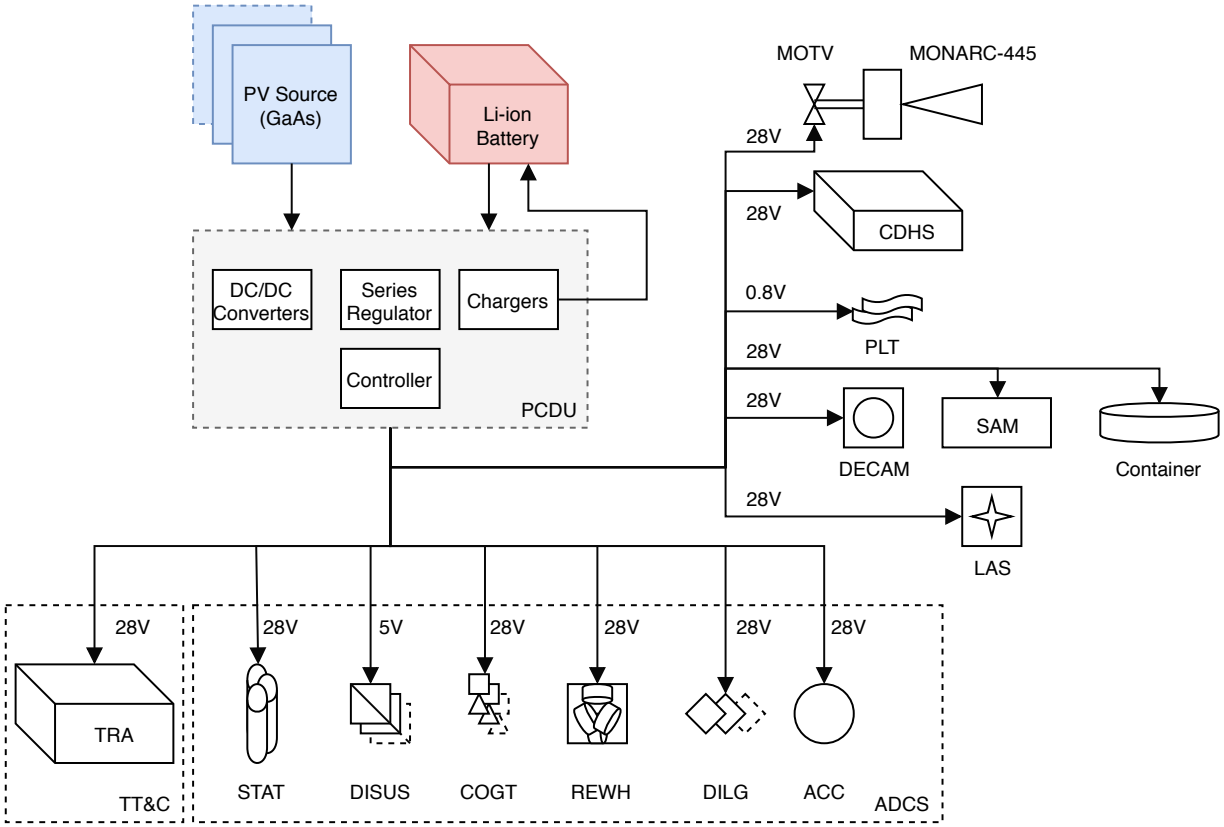

Figure 8.8: Electrical block diagram for SASH

8.3. Propulsion

In this section the propulsion system of the spacecraft will be detailed.

8.3.1. Requirements

The requirements for the propulsion system, as discussed in the midterm report, and updated where required, are given below. Requirement ASRM-PRP-003 excludes solid fuel rockets, as they do not allow for multiple burns.

ASRM-PRP-001 The propulsion system shall provide the 1.1 $[km/s]$ ΔV required for orbit matching. [D]
ASRM-PRP-002 The propulsion system shall provide the 0.8 $[km/s]$ ΔV required for returning to Earth. [D]
ASRM-PRP-003 The propulsion system shall allow for multiple actuation cycles. [T]
ASRM-PRP-004 The propulsion system shall have a reliability above 90 [%]. [A]

8.3.2. Method

In order to design the propulsion system, an iterative process is required as some characteristics of the system can not be estimated before selecting a specific thruster, whereas other characteristics are what the thruster is selected on.

First, a rough estimate is made for the class of thruster required. One should take into account the amount of ΔV required and the I_{sp}, which are found in section 6.1. Then, a thruster is selected. Using Equation 8.5 and when assuming a final mass, a begin mass and thus a mass difference (which is equal to the propellant mass) is found.

$$\Delta V = I_{sp} \cdot g_0 \cdot ln\left(\frac{m_0}{m_1}\right) \tag{8.5}$$

In the equation above, ΔV is the measure of the impulse that is needed to perform a manoeuvre, where $v_e q = I_{sp} g_0$ is the effective exhaust velocity and where m_i and m_f reflect initial and final mass, respectively.

When the propellant mass is found, the burn time for a manoeuvre should be calculated by Equation 8.6 and Equation 8.7. In those equations, F denotes the thrust, whereas I_{sp} and g_0 denote the specific impulse and the standard gravitational acceleration. m_i, m_f and $\dot{m}$ denote the begin mass, end mass and mass flow, whereas t_b denotes the burn time. The burn time should be checked for sanity: if manoeuvres take several hours to perform, a more powerful thruster may be considered.

$$\dot{m} = \frac{F}{I_{sp} \cdot g_0} \tag{8.6}$$

$$t = \frac{m_i - m_f}{\dot{m}} \tag{8.7}$$

The process described above should be iterated until a thruster is found that fulfils thrust requirements and the burn time is considered reasonable.

8.3.3. Orbiter

ASRM-ORB-PRP-001 The propulsion system of the orbiter shall be able to provide enough thrust for a ΔV manoeuvre of 1.1 $[km/s]$ [A]

As explained in section 6.1, the launch vehicle is able to directly place the orbiter and landers into the transfer orbit to the asteroid. Therefore, the orbiter does not need to propel itself anymore. Upon arrival, the spacecraft will need to slow down in order to match the target velocity, for which a ΔV of 1.1 $[km/s]$ is required.

For the propulsion four engines are used. This number is chosen so that when one fails, (almost) symmetrical thrust can still be provided if one other is shut down, whereas using two or three engines would make this difficult. The selected engine, after following the procedure described above, is the AMBR by Aerojet Rocketdyne [14], which has a thrust of 623 $[N]$ and an I_{sp} of 333 $[s]$. This engine is fuelled by hydrazine while it uses nitrogentetraoxide as oxidiser.

The total mass during the manoeuvre is the sum of the wet masses of the two landers combined with the dry mass of the orbiter itself. This adds up to a total mass of 1,060 $[kg]$. The ΔV manoeuvre of 1.1 $[km/s]$ will then require a propellant mass of 425 $[kg]$.

The thruster, being a bipropellant engine, will need two tanks: a fuel tank and an oxidiser tank. The oxidiser/fuel ratio is given to be 1:1.1 by the manufacturer. The tanks will be cylindrical with spherical end caps, to reduce stress concentrations and minimise required volume. Due to an uncertainty in the approach phase, a margin of 5% will be pursued, as stated in section 6.1. This means that the mission requires 233 $[kg]$ of fuel and 212 $[kg]$ of oxidiser. As the inlet pressure is given to be 12.1 to 22.4 $[bar]$, it is chosen to store the propellants at 20 $[bar]$ at 20 $[°C]$, to allow for expansion in case the tank heats up during for

[14] http://www.rocket.com/files/aerojet/documents/Capabilities/PDFs/Bipropellant%20Data%20Sheets.pdf Accessed June 20, 2018

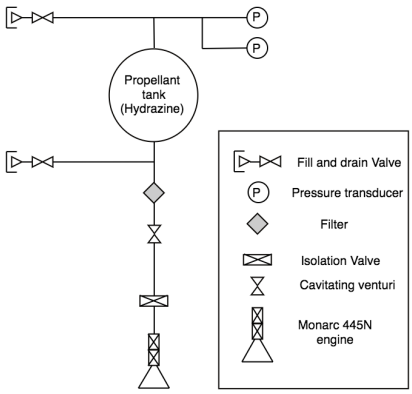

Figure 8.9: Architecture of main propulsion system

Table 8.7: Dimensions of the inside tank

	SASH	**ACSAL**
R $[mm]$	145	127
r $[mm]$	135	135

example launch. Using densities of 1,020 $[kg/m^3]$ and 1,440 $[kg/m^3]$ for the fuel and oxidiser, respetively, it is found that the tanks require to be 0.22 $[m^3]$ and 0.14 $[m^3]$.

The tank needs to be pressurised in order to ensure fuel being forced out at all times. The tanks, being at 12.1 bars minimum will therefore, using the ideal gas law, require 5.1 $[kg]$ of nitrogen that needs to be injected in the tank's ullage to ensure pressurisation of at least 12.1 bars.

8.3.4. SASH and ACSAL

As will be discussed, the hoverer and lander will have the same architecture in order to minimise cost and development. Only the sizing has some minor differences, in order to not overdesign and bring extra mass where it is not required. For those similarities, their designs will be combined in this section.

`ASRM-SASH-PRP-001` The propulsion system of SASH shall provide 0.8 $[km/s]$ of ΔV to return back to Earth. [A]

`ASRM-ACSAL-PRP-001` The propulsion system of ACSAL shall fire as soon as the lander makes contact with the asteroid. $[m/s]$ [A]

`ASRM-ACSAL-PRP-002` The propulsion system of ACSAL shall provide 0.8 $[km/s]$ of ΔV to return back to Earth. [A]

The landers will be equipped with a single monopropellant engine, as has been decided in the midterm phase (Angyal et al. [2018]). A monopropellant engine has the ability to fire multiple times, so that multiple manoeuvres can be made. In this final design phase it has been decided that the Monarc-445 from MOOG Space and Defense Group [2018] will be used. This thruster will be able to provide 445 $[N]$ of thrust which is enough to keep the lander pushed against the asteroid at landing until the harpoons are attached. Furthermore it provides enough ΔV to transfer the lander into transfer orbit towards Earth, as will be discussed. This thruster with a length of 41 $[cm]$ and a nozzle exit diameter of 15 $[cm]$ will be placed on top of the drilling tower, hence on top of the lander.

For the hoverer, using the method above and a dry mass of 135 $[kg]$, a propellant mass of 60 $[kg]$ is found. For the lander, which has an estimated dry mass of 143 $[kg]$, a propellant mass of 56 $[kg]$ is found.

Figure 8.9 shows the architecture of the main propulsion system of the lander. The valves, filters and the thruster have all been chosen from existing models. Due to the lander's special shape with the drill tower in the centre, a spherical fuel tank has been discarded, due to its weight distribution not being symmetric with respect to the centre of the lander. Therefore, a toroidal shaped fuel tank as shown in Figure 8.10 was opted for. The same tank shape has been adopted in the hoverer, in order to minimise development cost and complexity.

The inner radius of this fuel tank has been constrained to be the same as the radius of the drill tower, resulting in 13.5 $[cm]$. In order to determine the other dimensions of this fuel tank, the total volume needed for the fuel is needed. This results from

the propellant mass needed for the lander, which has been determined with Equation 8.5. Multiplying this by the density of Hydrazine (1,020 $[kg/m^3]$) and adding a safety margin of 5% to allow for expansion of the propellant during the mission, the tanks for the hoverer and lander require to be 58 $[L]$ and 55 $[L]$, respectively.

The tank needs to be pressurised in order to ensure fuel being pumped out at all times. The Monarc-445 engine requires a feed pressure of at least 4.7 $[bar]$ and therefore, using the ideal gas law, for the lander and hoverer 0.3 $[kg]$ of nitrogen is required to ensure pressurisation of at least 4.7 $[bar]$.

$$V_{torus} = 2 \cdot \pi^2 \cdot R \cdot r^2 \tag{8.8}$$

With Equation 8.8 the final dimensions of the toroidal fuel tank have been determined. The final dimensions of this fuel tank are given in Table 8.7.

The toroidal tank system has been used before in space, namely on the Pioneer mission.[15] Care should be taken in production in order to make sure that the tank stays operational throughout the mission. A careful analysis of stress concentrations needs to take place and where required, reinforcements should be applied. The production could take place in two parts: the top and bottom can be produced separately and welded on top of each other, where again, reinforcements should be placed if required.

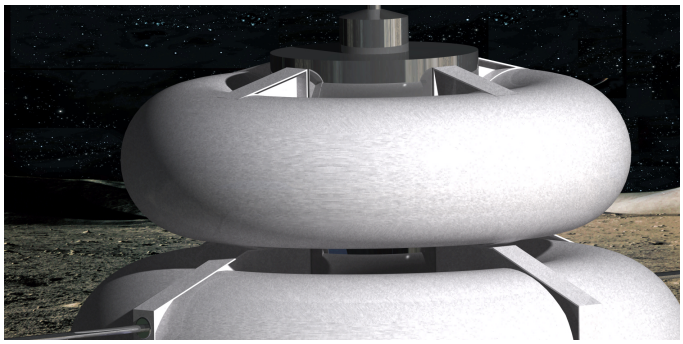

Figure 8.10: Fuel tank dimensions

8.4. Attitude determination and control system

In this section, the design of the Attitude Determination and Control Systems (ADCS) will be discussed for the orbiter, ACSAL and SASH. First, in subsection 8.4.1 requirements will be listed, both general and spacecraft-specific, after which the architecture will be discussed in more detail for every spacecraft in the following sections. Lastly, orbital maintenance shall be discussed.

8.4.1. Requirements

`ASRM-ADC-001` The ADCS shall provide a pointing accuracy of 1.6 [°]. [T]
`ASRM-ADC-002` The ADCS shall be able to determine the attitude of the spacecraft for rotation rates smaller than 5 $[°/s]$. [D]
`ASRM-ADC-003` The ADCS shall eliminate jitter sufficiently to avoid blurring of sensor data. [D]
`ASRM-ADC-004` The ADCS shall limit spacecraft drift to less than 1 $[°/hour]$. [T]
`ASRM-ADC-005` The ADCS shall be able to provide a rotation rate of at least 20 $[°/s]$ around any axis. [D]
`ASRM-ADC-006` The ADCS shall be able to control the spacecraft's attitude during main engine burns. [D]
`ASRM-ADC-007` The ADCS shall be able to rotate the spacecraft over 180 [°] within 90 $[s]$. [D]
`ASRM-ADC-008` The ADCS sensors shall have a clear field of view. [A]
`ASRM-ADC-009` The ADCS actuators exhaust shall not cause damage to other systems. [T]

8.4.2. Method

The design of the ADCS will be a standard, off-the-shelf solution. Star sensors will be used for attitude determination in the external reference frame, and gyroscopes in an inertial reference unit (IRU) for additional relative attitude measurements. Coarse sun sensors will provide backup attitude information when the system goes in safe mode. Attitude control will be taken care of by reaction wheels and cold gas thrusters. Reaction wheels are to counter disturbance torques, while the thrusters take care of manoeuvring and momentum dumping of the reaction wheels. The following sections will elaborate on the sizing of the

[15] `https://ntrs.nasa.gov/search.jsp?R=19780033972` Accessed June 28, 2018

system actuators. Sensors have to be selected from existing components that meet the requirements, which will be done in a later section.

Thrusters
Thrusters are required for fast manoeuvres and corrections, having a higher accuracy than the main thruster. In the mission, the main manoeuvre to be performed by the ADCS is the turning requirement that was set and the descent slowdown. These are therefore the main influences on thruster sizing.

Wheels
The reaction or momentum wheels serve for more precise pointing and for disturbances. The wheels will therefore be sized after disturbances, as there is no minimum pointing information available for the wheels. It is assumed that the wheels can be controlled with enough precision to provide the pointing accuracy required.

A consideration has to be made whether wheels are necessary on all spacecraft: not all spacecraft require a high pointing accuracy. Therefore, bringing wheels may be redundant and only adding weight to the spacecraft.

8.4.3. Orbiter

`ASRM-ORB-ADCS-001` The ADCS shall provide enough accuracy to point the telecommunication system. [A]
`ASRM-ORB-ADCS-002` The ADCS shall be able to provide a 180 [°] turn in 90 seconds. [A]
`ASRM-ORB-ADCS-003` The ADCS shall be able to correct the orbit when required. [A]
`ASRM-ORB-ADCS-004` The ADCS shall be able to counteract any disturbances. [A]
`ASRM-ORB-ADCS-005` The ADCS shall be able to point the instrumentation towards the asteroid. [A]

Judging on these requirements, for the orbiter, a combination of thrusters and wheels will be required, as high accuracy is required by the instruments and by the telecommunication subsystem, while simultaneously manoeuvres need to be performed.

The requirement for the orbiter is to make a 180 degree turn in 90 seconds. This results in a average angular velocity of 2 $[deg/s]$. The fastest way to turn is to accelerate in the first half of the turn and decelerate in the second half, leading to a peak angular velocity of 4 $[deg/s]$ and thus an angular acceleration of 0.04 $[rad/s^2]$, using a very rough estimate of 2,000 $[kgm^2]$ for the mass moment of inertia. Using Equation 8.10, one can find a required thrust of 0.3 $[N]$. Using 3.6 $[N]$ thrusters developed by MOOG [16] will therefore fulfil the requirement by a large margin. One could opt for a smaller cold gas thruster, however, as will be shown later, this will require a lot of cold gas as the thrusters will also be used for orbital corrections.

8.4.4. Lander

`ASRM-ACSAL-ADCS-001` The ADCS shall be able to put the lander in the descent orbit. [A]
`ASRM-ACSAL-ADCS-002` The ADCS shall be able to point the landing gear towards the asteroid. [A]
`ASRM-ACSAL-ADCS-003` The ADCS shall limit the impact velocity to a maximum of 0.4 $[m/s]$. [A]

Thrusters, as mentioned before, will be used for manoeuvring near the asteroid, especially for the descent manoeuvre.

As the descent manoeuvre is quite a costly manoeuvre, relatively large cold gas thrusters are applied. Using the same thrusters as the orbiter, a model was developed that calculated the burn time of the thrusters to ensure that upon touchdown, the velocity tangential to the surface matched the surface velocity as close as possible. The type of thruster was found during the testing of the model, which found that in order to not have very long burn times which could cause inaccuracies, a force in the range of several Newtons was necessary.

From the model, an ideal burn time of 8.5 $[s]$ was found. This burn time was optimised in order to match the surface velocity as close as possible and minimise the forces that a high tangential velocity might pose. This puts the lander in an elliptical orbit that crosses the surface after about an hour. After this initial burn, the spacecraft will start accelerating again due to gravity. This acceleration will result in a relatively high speed of impact, perpendicular to the surface. Upon impact, a perpendicular velocity of 0.5 $[m/s]$ is present.

For the lander, the impact speed is limited to 0.4 $[m/s]$. This means that in the surface-outward direction, a velocity decrease in velocity of 0.1 $[m/s]$ is required. Using the momentum equation, a burn time for this manoeuvre can be found, assuming the change in mass is negligible and the force is perfectly directed.

$$mv_i + \int_{t_b} \sum F dt = mv_f \tag{8.9}$$

[16] `http://www.moog.com/content/dam/moog/literature/Space_Defense/Spacecraft/Propulsion/ColdGasThrusters_0717.pdf` Accessed May 31, 2018

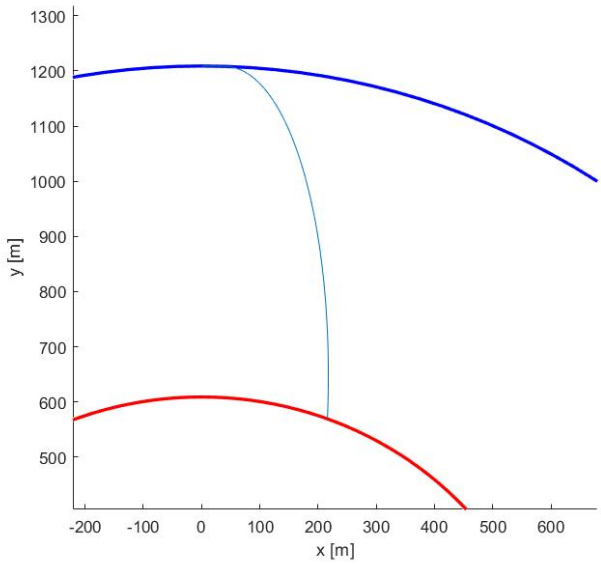

Figure 8.11: Graphic representation of the descent trajectory.

Using conservation of momentum, it is found that a 3.7 second burn is required for slowing down sufficiently. This way, a total burn time of 12.2 $[s]$ is required for this manoeuvre. Considering the fact that always two thrusters have to be activated to minimise the resultant torque, while having a mass flow of 6 $[g/s]$, this requires 0.1 $[kg]$ of cold gas. A graphic representation of the descent trajectory is displayed in Figure 8.11.

8.4.5. Hover

`ASRM-SASH-ADCS-001` The ADCS shall be able to put the lander in the descent orbit. [A]
`ASRM-SASH-ADCS-002` The ADCS shall be able to point the sample collection mechanism towards the asteroid. [A]
`ASRM-SASH-ADCS-003` The ADCS shall thrust the craft away from the asteroid when collection is completed. [A]
`ASRM-SASH-ADCS-004` The ADCS shall limit the impact velocity to a maximum of 0.05 $[m/s]$. [A]

The hoverer, as will be discussed later, shall bring altimeters that require high pointing accuracy in order for the sample collection to function properly. Therefore, in this descending spacecraft, reaction wheels will be brought, so that high accuracy can be guaranteed.

For the hovering spacecraft, the impact velocities needs to be limited further than was the case for the lander. As SASH uses a mechanical arm which can not withstand a lot of force, a very slow descent is required. Therefore, a series of burns will be necessary to ensure the velocity is as low as possible while simultaneously disturbing the surface as less as possible, in order to make sure sampling is still possible. Every burn will set the velocity normal to the surface to zero to minimise the terminal velocity. If the last burn takes place at two meters altitude, where the thrust vector will be deflected in order to not disturb the regolith directly under the spacecraft, the impact velocity is estimated to 4.2 $[cm/s]$, which fulfils the requirement. Important to note is that this assumes a point mass, which especially near the surface is not an accurate assumption. Therefore, the real impact velocity will be lower, which will be even more favourable.

Using a total of three burns, at 30, 10 and 2 meters, a total velocity increment of 0.7 $[m/s]$ is required. Bearing in mind that the last burn is deflected and thus rendering part of the thrust in horizontal direction, a total burn time for slowing down of 23 $[s]$ is found using the momentum equation, making the total burn time equal to 32 $[s]$, resulting in 0.4 $[kg]$ of cold gas.

Lastly, the hoverer will need to ascend again. Upon touchdown, a sample will be collected immediately. Then, an impulse will be given, normal to the surface, to get the spacecraft back to a 600 meter near-circular orbit. Upon reaching 600 meters, the velocity normal to the surface approaches zero, when another impulse will be given in tangential direction, to give the spacecraft a near-circular orbit again. The total velocity increments add up to 48 $[s]$ of burns, resulting in 0.3 $[kg]$ of cold gas.

A graphic representation of the last part of the descent trajectory is displayed in Figure 8.12.

The manoeuvres displayed above will be performed autonomously. Upon studying the asteroid in detail, more detailed data on gravity and rotation will be known. These calculations should then be redone and uploaded to the spacecraft, so that the

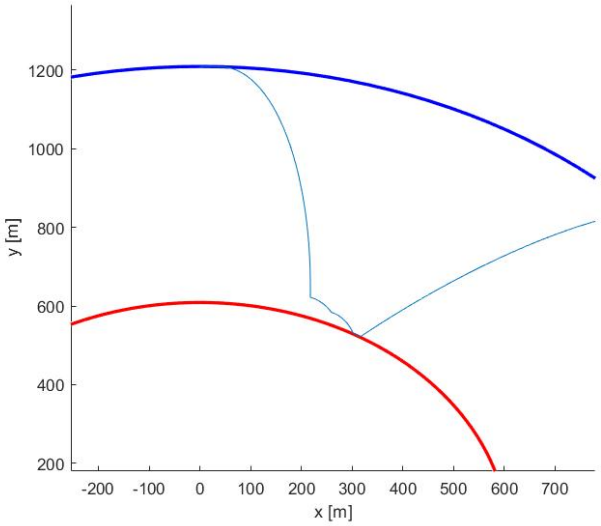

Figure 8.12: Graphic representation of detail of last part of descent trajectory.

manoeuvre will be optimal. Right now, a worst-case scenario is made, in order to make sure enough cold gas is brought for manoeuvring.

$$I\alpha = \sum Fr \tag{8.10}$$

8.4.6. Reaction wheels

The reaction wheels are used for more precise movements and for counteracting disturbance torques. However, these are mostly about minimal changes: the precision is in the end dependent on how slow something can change and not necessarily on how fast for example the spacecraft can be rotated. Therefore, a sizing is made based on a rough estimate of what size is required: for the orbiter, relatively large wheels are used whereas for the landers, smaller wheels are used. In later design stages, these can be refined easily, as they are off-the-shelf wheels and their setup is determined already.

As discussed in the midterm, four reaction wheels will have a pyramid setup, so that redundancy is assured. For the orbiter, 4 $[kg]$ wheels (RW4 by MOOG[17]) are used which can deliver a torque of 0.3 $[Nm]$. For the lander and hoverer, 0.35 $[kg]$ wheels (RWP100 by MOOG[17]) are used, capable of delivering a torque of 7 $[mNm]$. These wheels are believed to provide a balance between accuracy while simultaneously providing enough angular velocity, might this be required.

8.4.7. Sensors

Sensors are the same for all the spacecraft, with a few minor exceptions. As discussed in the midterm, the sensors for attitude determination will be as follows:

- **Three star trackers**
  A single star tracker can track multiple stars, thereby defining the 3-axis attitude of the spacecraft. A second and third star tracker pointing in different directions are added for redundancy in case one fails or is unable to take measurements due to bright objects in view.
- **Six coarse sun sensors**
  They will be positioned on each positive and negative axis end, to allow acquisition of attitude and stabilisation in case of a critical event. Redundancy is not strictly required, as the probability of failure is very low.
- **A three-axes fully redundant Inertial Reference Unit**
  This IRU is to provide relative attitude information in between the star trackers' measurements. The latter have a frequency in the order of 1 $[Hz]$, so intermediate references are required. The IRU shall consist of gyroscopes.

Next to that, two magnetometers will be brought on board as well. This is to measure the possible magnetic field around the asteroid, which, if present, could cause a non-negligible disturbance torque. Also, the hoverer requires very exact altitude measurements. Therefore, two altimeters will be brought on board.

[17] `http://bluecanyontech.com/wp-content/uploads/2018/01/DataSheet_RW_07_F.pdf` Accessed May 31, 2018

Table 8.8: Overview of sensors

Sensor	Choice
Star tracker	VST-41M by Vectronic Aerospace[4]
Laser gyroscope (IRU)	GG1320AN Digital Ring Laser Gyroscope by Honeywell Aerospace [5]
Sun sensor	Fine Sun Sensor by NSS[6]
Magnetometer	Magnetometer by MEISEI [7]
Altimeter	Compact Laser Altimeter by APLBruzzi et al. [2012]

8.4.8. Orbit determination and control

Accurate trajectory and orbit determination is needed in order to plan the manoeuvres, reach the right orbit, and return to Earth. In this section the tracking (to determine the orbit), the possible disturbances in the orbit, and the maintenance during transfer from Earth to the asteroid, and back, is explained. Orbit determination and control (ODC) has the following requirements:

ASRM-ODCS-001 The orbit of the spacecraft of the Piazzi mission shall be able to be determined during cruise with an accuracy of 300 [m]. [A]

Tracking

Tracking of the spacecraft will be done by analysing the S-band communication with the Earth. Based on the time the signals take to be transmitted to and fro the asteroid the distance of the spacecraft from the ground station can be determined, and through the Doppler shift the radial velocity along the light of sight can be calculated. From these two parameters a highly precise orbital path can be determined, using Lambert's method (Jordan [1964]).
When using the DSA network for communication, a 250 [m] accuracy can be achieved at a distance of 2 [AU]. Finally, for determining the orbit around the asteroid a higher accuracy is needed than during cruise. This can be achieved by combining the methods above with landmark observation of the asteroid, which can be done both by humans or Earth, or autonomously by the spacecraft, and statistical modelling of the orbit (Godard et al. [2015]).

Orbital disturbances

In an ideal situation a spacecraft would be put into an orbit and stay in that same orbit indefinitely. However, in the real world, both internal and external disturbances will change the orbit of a spacecraft. For the Piazzi mission the main disturbances are the solar pressure, the variation in density within the sun, and the gravitational pull of the planets, with Jupiter as the main factor. Even though these disturbances are small (Wertz et al. [2011]), they have to be corrected for.

Orbital maintenance

The strategy for orbital maintenance is to let the disturbances accumulate for a period of time, after which a so called trajectory correction manoeuvre (TCM) will be performed (Wertz et al. [2011]). These manoeuvres require small amounts of ΔV (1-10 [m/s]), and will be performed by the RCS-thrusters on board of the orbiter. For both the inbound and outbound trajectory, two to three of these TCMs will be performed. At least one will be done before entering hibernation, to make sure the trajectory is as precise as possible. An additional one or two manoeuvres are necessary when leaving hibernation, to be able to rendezvous with the asteroid at the specified moment, and to start the preliminary mapping phase before orbiting the asteroid. For the worst case scenario this will lead to a required ΔV of 30 [m/s], for each of the individual spacecraft.

The amount of cold gas required for these manoeuvres should be taken into account. However, as the ΔV is dependent on a mass ratio, the mass needs to be estimated. For the orbiter, the assumption is made that no propellant has yet been used (assumed mass at moment of determination is 750 [kg]), whereas for the ACSAL and SASH, the assumption is made that all propellant has been used (assumed mass is $\pm$ 100 [kg]). Then, using Equation 8.5 with an exhaust velocity of 638 [m/s], a mass fraction of 1.048 is found. In that case, the orbiter requires 36 [kg] of cold gas and the two landers will require 4.8 [kg] of cold gas. For the orbiter, the 0.3 [kg] for orbit maintenance on site at the asteroid that was found in section 6.2 shall also be included.

Finally, the total amount of cold gas can be found per subsystem. A margin shall be included, as in this design stage, there is not yet an indication how often certain manoeuvres will have to be performed. This margin is set to 20%, so that the total cold gas masses add up to the values presented in Table 8.9. Also presented in the table is the tank volume required, given a pressure of 100 [bar].

8.4.9. Verification and validation of model

Verification of the descent model is performed in several ways during design, to check individual components. First, the general physics were programmed. The spacecraft was 'put' in a position and given a tangential velocity of the orbit velocity for a

Table 8.9: Cold gas masses and volumes required.

Spacecraft	**Cold gas mass** $[kg]$	**Tank volume** $[m^3]$
Orbiter	44	0.38
Hoverer	7	0.06
Lander	6	0.05

circular orbit. By observing the trajectory that was then generated, it was verified that the gravitational model was correct, as the orbit was observed to be circular.

Next, forces were applied on the lander. It was then important to check whether the model was valid for orbits that were elliptical. If the model still held after the impulse, the orbit should be stable and follow the same path every period. This too worked, verifying another part of the program.

Lastly, it was important to verify whether the output perpendicular and tangential velocity were correct. A range of values was used and it was found that for example, when a visual inspection of impact angle was found to be about 45 [°], the tangential and perpendicular velocity were almost equal, which they should be. This concludes the main verification. The program has been run several times, checking for sanity in several applications in order to find irregularities, which were not found.

Also, the model needs validation. The model iterates through several impulse times in order to find one that matches the surface velocity as close as possible, which is what was required, in order to find propellant mass.

8.5. Thermal control

The satellite includes multiple precision instruments that require a specific range of temperatures to operate in to ensure their accuracy of measurements. The thermal control system described in this chapter will be tasked to control the thermal environment of each subsystem. In subsection 8.5.1, the requirements are stated, as well as the operational ranges of the subsystems placed on board of the spacecraft. Next, in subsection 8.5.2, the sources and sinks of thermal energy are discussed, when they affect the satellite, and how they do this. Finally, subsection 8.5.3 describes the system used on board of each spacecraft.

8.5.1. Requirements

The integrity and stability of the thermal environment within a satellite is vital to its functioning. Crucial equipment such as the batteries or camera require a specific range of temperatures to allow proper functioning. To be able to provide the subsystems with proper thermal control, requirements have to be set for this system. These are listed below:

`ASRM-THERM-001` The thermal control system shall place each subsystem within its operational temperature range. [A]
`ASRM-THERM-002` The thermal control system shall account for eclipse phases during orbit. [A]
`ASRM-THERM-003` The thermal control system shall ensure a constant temperature throughout hibernation mode. [A]
`ASRM-THERM-004` The thermal control system shall account for different power consumption rates. [A]
`ASRM-THERM-005` The thermal control system shall account for changes in solar radiance. [A]

These requirements are set in place to ensure proper operation of the control system. Furthermore, each element in the spacecraft sets a requirement on the thermal control system in the form of operational temperature ranges; see the list of subsystems in Table 8.10.

Table 8.10 lists the outer boundaries of the operational temperature ranges of each component. Using these ranges, the standard temperature of the satellites can be determined; this will be the temperature the inner environment of the satellite will tend towards. Analysing the temperature ranges, a few conclusions can be made. By taking all components into account, our temperature range would be set between 10 [$°C$] and 30 [$°C$]. This allows only 20 [$°C$] of fluctuation, which would set a stringent requirement on the thermal control system. By granting the batteries their own controlled environment, the range for the other components expands to between 4.4 and 45 [$°C$], a range of 40 [$°C$] and an expansion with a factor two. By applying the same methodology, MOTV, MMH, DRL, and CAR can be removed from the equation to expand the range to allow 70 [$°C$] fluctuation between -20 and 50 [$°C$]. The system design shall incorporate these changes in temperature ranges in its sizing, as it is beneficial for the entire satellite to have the same temperature, multiple goals will be set for the thermal control system:

1. The primary goal of the thermal control system is to provide a general temperature range the system's temperature will fluctuate in.

2. The preferable outcome of the thermal control system is to provide a temperature range in which most systems can operate in, meaning some systems shall require their separate thermal control system.

Table 8.10: Operational temperature ranges of the lander and hoverer.

Subsystem	**Part**	**Lower limit operational temperature** [$°C$]	**Upper limit operational temperature** [$°C$]
Structure	Bus	TBD	TBD
EPS	PV array	TBD	TBD
	BAT	10	30
	PCDU	-30	60
TT&C	HGA	TBD	TBD
	LGA	TBD	TBD
	TRA	-9	32
	DIP	0	50
	Cabling	-	-
ADCS	COGT	-40	60
	CGT	-	-
	STAT	-20	65
	DILG	-54	85
	DISUS	-25	50
	REWH	-	-
	ACC	-55	105
	CLA	TBD	TBD
Propulsion	MONARC-445	-	-
	MOTV	4.4	149
	MMH	2	113.5
C&DHS	CPU	-30	60
	Wiring	-	-
Sample mechanism	DECAM	-55	80
	LAS	-	-
	ALM	-65	75
	DRL	0	45
	CAR	0	45
	SPM	-26	66
	SRC	-	-
	HAR	-	-
	SAM	-45	85
General range		10	30

3. The best outcome of the thermal control system is a system capable of sustaining a temperature range that enables all systems to operate within that range.

In the case of the Piazzi mission, the best outcome involves sizing a thermal control system that is capable of controlling the thermal environment within the satellite in a range between 10 and 30 [$°C$]. This will be the primary goal of the sizing, should this not be attainable, the preferable outcome shall be opted for, meaning some components such as the battery will be excluded from the temperature range and shall be sized for separately. Finally, the primary goal is the least preferable, as this will involve multiple control systems having to function individually.

This enables the general thermal control system to be as passive as possible, only having to tackle a more general range. The separation of components from the general system will be evaluated during the sizing of the thermal control system. Generally speaking, the more constant the temperature environment, the better for the components.

Two frequent terms that will be discussed in this section are irradiance and radiance. Knowing the difference between the two is vital for the understanding of the methodology. Irradiance refers to the density of energy per square meter. Radiance on the other hand is the total energy striking a surface, and is therefore the integral of irradiance over the area affected.

Table 8.11: Comparable asteroid characteristics

Asteroid	a $[AU]$	e [-]	H	Diameter $[km]$	Period $[hr]$	Bond albedo [-]	Gamma $[\frac{J}{m^2}\sqrt{s}K]$
1989 UQ	0.91	0.26	19.3	0.73	7.73	-	-
Ra-Shalom (2100)	0.83	0.44	16.1	2.24	19.8	162	0.05
Hathor (2340)	0.84	0.45	19.9	0.3	-	-	0.24
1992 BF	0.91	0.27	19.6	0.51	-	-	0.02
Icarus (1566)	1.08	0.83	16.7	1.3	2.27	76	0.04
1999 RQ36	1.13	0.2	20.6	0.49	4.29	175	0.01
Toro (1685)	1.37	0.44	14.3	3	10.2	144	0.05
Eros (433)	1.46	0.22	10.8	23.3	5.27	89	0.1
Apollo (1862)	1.47	0.56	16	1.4	3.06	162	0.12
1950 DA	1.7	0.51	17	1.4	2.12	-	0.08
Betulia (1580)	2.19	0.49	14.3	4.57	6.13	117	0.03
Golevka	2.52	0.6	19.1	0.27	6.03	137	0.23
Toutatis (4179)	2.53	0.63	15.1	2.8	176	-	0.05

8.5.2. Thermal pathways

To be able to design a thermal control system for a satellite in a specific scenario, the environment it is in has to be modelled. For this model of the environment, each aspect has to be assessed separately. For an environment at a near-Earth asteroid, there are five aspects which need to be dealt with: solar radiance, albedo effect of the asteroid, infrared radiance of the asteroid, internally generated heat, and the emission of heat. In this subsection, these aspects will be dealt with individually, and summed up to form a basis for the thermal environment model near the target asteroid.

Solar radiance

The most obvious, and most substantial pathway of energy is the radiance the sun emits. This radiance will contribute the most to the heating of all three satellites. It is also utilised for power generation, but more on that in section 8.2.

The solar irradiance received at a certain point is mainly influenced by the distance between the sun and the spacecraft. As the sun can be assumed a point-emitter, with its emitted energy spreading spherically, the following holds for the irradiance at a specific position.

$$SI = \frac{P}{4\pi r^2} \tag{8.11}$$

For Equation 8.11, SI represents the solar irradiance $[W/m^2]$ at the specific distance away from the sun, P the total power emitted by the sun ($3.830 \cdot 10^{26}$ $[W]$), and r the distance from the sun $[m]$. Using this equation to compute the irradiance at a specific point, then multiplying it with the surface area being radiated ($A_{radiated}$ $[m^2]$), the radiance (SR, [W]) incident on the body can be computed.

$$SR = SI \cdot A_{radiated} \tag{8.12}$$

Albedo effect

In space there are also other bodies besides the satellites at hand, and these are also radiated by the sun. Depending on their proximity to the sun, they will experience an amount of solar irradiance. Would the objects in space be perfect black bodies, they would absorb all irradiance on their surface. As this is never the case, the bodies also reflect a certain amount of irradiance.

The level of reflection depends on multiple characteristics of the body: surface smoothness or roughness, surface colour, surface geometry, and surface material are some general factors. Each has an effect on the amount of irradiance reflected by the body. There are multiple factors that describe the level of reflectance of the body. These factors are called albedo factors. The one of most importance for this analysis is the Bond albedo. This albedo factor describes the reflectance over all wavelengths and over all phase angles. It describes to what extent the body reflects the total energy it is radiated with, be it inside or outside the visual spectrum of light. As this factor takes every phase angle around the planet into account, it cannot be determined by observing it from just one point, as well as it cannot be determined from a distance, as the energy levels might be too low and could disperse. As the target asteroid, 1989 UQ, has not been approached in the past, the Bond albedo is unknown. To be able to still give an estimate, statistical estimations are used. For this specific asteroid, the Bond albedo was estimated at 0.02 following the data-set of asteroid presented in Table 8.11.

Using the determined Bond albedo, the amount of energy reflected off a body, in the case of this analysis the energy reflected off of the target asteroid, can be estimated. This energy will also contribute to the energy equilibrium that will exist on

the satellite. The irradiance as a result of the albedo effect can be computed using Equation 8.13.

$$J_{Alb} = \alpha_{Bond} \cdot J_{SI} \cdot F_{view} \tag{8.13}$$

In this equation, J_{Alb} represents the albedo irradiance $[W/m^2]$, α_{Bond} the Bond albedo factor, and F_{view} the visibility factor of the satellite with respect to the radiated face of the asteroid. The view factor can be simplified to Equation 8.14, where r_{body} is the radius of the respective body $[m]$, whereas r_{orbit} is the orbit height $[m]$.

$$F_{view} \left\{ \begin{array}{cc} \left(\frac{r_{body}}{r_{orbit}}\right)^2 & \text{Sun-lit half} \\ 0 & \text{Eclipse side} \end{array} \right\} \tag{8.14}$$

Using Equation 8.14 in Equation 8.13, the irradiance can be computed at the surface of the asteroid. This will have to be to be divided once again by the spherical dispersion factor in the same manner as in Equation 8.11. This way, the albedo irradiance of a body on a satellite around it can be computed. The influence of this on the satellite will depend on the distance of the body to the sun, the Bond albedo of the body, the distance of the satellite to the body, and the satellite's position with respect to the sun and main body. Again, the product of irradiance and the radiated surface results in the radiance on the satellite.

Planetary IR emission

The third source of incoming radiance on the satellite in this situation is the infrared emittance of the asteroid. This can be interpreted as the heat of the asteroid being radiated. This factor is also greatly influenced by the distance of the asteroid to the sun. It is also dependant on multiple other factors required to compute the temperature of the asteroid. This can be done using the Near Earth Asteroid Thermal modelling tool developed by Mueller [2012]. Using the knowledge provided herein, and the NEATM parameter acquired from ([18]), the temperature of the asteroid can be computed using the following:

$$T_{SS} = \frac{(1-A)S}{r^2} \frac{1}{\epsilon \cdot \sigma \cdot \eta} \tag{8.15}$$

In this equation, multiple factors are used. A in this case is the Bond albedo of the asteroid, determined at 0.02. S represents the standard solar radiance $1362[W/m^2]$, r represents the distance to the sun $[m]$, ϵ the emittance of the asteroid, σ is the Stefan-Boltzman constant $[W/m^2K^4]$, and η is the NEATM-model parameter which is 2.401 ± 0.048 ([18]). T_{SS} is the subsolar temperature $[K]$. To transform this subsolar temperature to the asteroid temperature, the following equation is used [18]:

$$T(\theta\phi) = \left\{ \begin{array}{cc} T_{SS} \cdot \cos^{1/4}\theta \cdot \cos^{1/4}\phi & \cos\theta \cdot \cos\phi \geq 0 \\ 0 & \text{Otherwise} \end{array} \right\} \tag{8.16}$$

This temperature is radiated into space, therefore the temperature radiation equation (Equation 8.17) holds.

$$J_{emit} = A_{total} \cdot \epsilon \cdot \sigma T^4 \tag{8.17}$$

Here, A_{total} is the surface area of the asteroid $[m^2]$, ϵ the emittance of the asteroid, σ the Stefan-Boltzman constant, and T the temperature of the asteroid $[K]$. This radiation is then to be spread out over the sphere space using Equation 8.11. This is the radiation the spacecraft will receive due to the temperature of the asteroid.

Internal heat

As the external pathways of heat have been addressed, the source of heat within the satellite also has to be taken into account. Inside the satellites, multiple electrical instruments operate. Most systems do not perform substantial amount of work, leading to the assumption that they lose most of their power to heat. An exception to this assumption is the TT&C module where a considerable amount of energy is cast away in the form of radio signal to Earth. For these subsystems, the effective power that leaves the satellite is not used in terms of internal heat generation. This heat, the one generated by the instruments, adds to the energy the satellite holds, meaning its temperature will rise. This effect also needs to be addressed by the thermal control system.

Emission

Losing energy is complicated in a vacuum environment. Out of the three ways of heat transportation (convection, conduction, and radiation), only the radiation is possible. This involves radiating the energy the object holds in the form of infrared waves; the same way the asteroid emits its heat. For a satellite, the same concept holds. The satellite will emit its energy over its surface. The rate of emission is influenced by multiple factors: the coating the satellite receives, its temperature, and the area

[18] `https://sbn.psi.edu/pds/asteroid/EAR_A_COMPIL_5_NEOWISEDIAM_V1_0/data/neowise_neos.tab` Accessed June 7, 2018

it emits over. As the emission rate of the coating is increased, the more it emits, the more energy the satellite loses, and the lower the base temperature of the satellite will lay. The higher the system temperature, the more energy it holds compared to its surroundings, meaning it will tend to lose that energy to find equilibrium with its surroundings, and the area it emits over influences the availability to emit. These relations are represented in Equation 8.18.

$$J_{emit} = A_{total} \cdot \epsilon \cdot \sigma T^4 \tag{8.18}$$

Here, J_{emit} represents the radiated energy $[W]$, A_{total} the total area $[m^2]$ the satellite can emit energy over, σ is the Stefan-Boltzman constant, and T the system temperature $[K]$.

8.5.3. Sizing of the system

The previously mentioned factors all play a major role in the housekeeping and control of the system temperature. Each aspect contributes to the energy in- or outflow which has major impacts on the temperature level as well as the methods and sizing of thermal control. As stated before, the best outcome of the sizing process of the thermal control system is that a system is achieved that is able to sustain a temperature range over the entire duration of the mission within 10 and 30 $[^\circ C]$. In order to size the control system, a model was created that models the factors mentioned previously, depending on the phase of the mission the satellite finds itself. Using this model, the energy flows shall be evaluated, and the best solution shall be identified to manipulate the temperature of the system.

As the first three pathways of energy depend on the location of the asteroid with respect to the sun, and the position of the satellite with respect to the asteroid, these will be addressed first. To compute the position of the asteroid and distance to the sun, the Bessel function of the first kind was implemented to compute the phase angle of the asteroid at an instance. This equation computes the phase angle as a function of the mean motion, which parametrises the position of the body over its orbit as a function of time. The mean motion ranges from 0 to 2π as one entire orbit of the asteroid will be modelled. Furthermore, the function is also dependant on the eccentricity and the number of samples per orbit. The function written out as a function is as shown in Equation 8.19.

$$\alpha(M) = M + \sum_{k=n}^{\infty} \frac{2}{k} \cdot J_k(ke) \sin kM \tag{8.19}$$

Here, α is the eccentric anomaly $[rad]$, M the mean motion $[rad]$, e the eccentricity of the orbit, k represents the k^{th} Bessel's differential equation, with J_k being a Bessel's first function of the first kind for the k^{th} iteration. These are differential equations. By choosing a high value for k, the differential equation converges, providing a factor relating the eccentric anomaly with the mean motion.

The mean motion has to be translated to the true anomaly (θ) which can then be used to acquire the distance between the body and the midpoint (in the case of the asteroid, the midpoint is the sun). The translations mentioned are done using the following equations (Equation 8.20 and Equation 8.21).

$$\tan\left(\frac{\theta}{2}\right) = \sqrt{\frac{1-e}{1+e}} \tan\left(\frac{\alpha}{2}\right) \tag{8.20}$$

$$r_{ast} = \alpha \frac{1-e^2}{1+e \cdot \cos(\theta)} \tag{8.21}$$

In Equation 8.20 and Equation 8.21, θ is the true anomaly $[rad]$, e is the eccentricity [-], α the mean anomaly $[rad]$, and r_{ast} the distance between the asteroid and the sun $[m]$.

Next, the orbital height is added to this distance, but this is also phased to model the satellite orbiting or landed on the surface of the asteroid. This is done using Equation 8.22.

$$r_{sat} = r_{ast} + (R_{ast} + h_{orbit}) \cos\zeta \tag{8.22}$$

For this equation, r_{sat} is the distance between the satellite and the sun $[m]$, R_{ast} is the asteroid radius $[m]$, h_{orbit} is the orbital height of the satellite around the asteroid $[m]$, and ζ the angular position of the satellite over its orbit around the asteroid $[rad]$, where 0 corresponds to being behind the asteroid, perfectly on the sun-asteroid line.

Using this distance, the solar radiance, the albedo effect and the IR radiation from the asteroid can be computed. The internal generated heat is known from the EPS subsystem, therefore the only remaining factor to be calculated is the emission. To compute the rate of emission, the system temperature needs to be known, for which the absorbance factor of the coating is key, as the satellite only absorbs a fraction of the energy it is radiated with. The energy absorbed by the satellite adds to the already contained energy. On the other hand, the already contained energy results in a system temperature, which will be emitted through emission following Equation 8.18. The change in energy results in an change in temperature as a function of

the specific heat capacity C $[J/mK]$ and the mass of the satellite m $[kg]$. This way, the system temperature of the system can be iterated for each instance of orbit.

$$\Delta T = \frac{Q}{m \cdot C} \tag{8.23}$$

Q represents the total flow of energy $[J]$ involving the satellite. The heat flow consists of the incoming minus the out flowing energy (represented in Equation 8.24)[19].

$$Q = J_{in} - J_{out} = J_{SR} + J_{Alb} + J_{IR} - J_{emit} \tag{8.24}$$

The thermal flow presented is what the thermal control system aims to influence. The first way of influencing the thermal flow is by changing the coating on the satellite. By lowering the absorbance of the coating, the effectively received radiation is also lowered, whereas increasing the emission factor increases the outflow of energy resulting in a lowered system temperature. By picking the correct coating, the range of system temperatures can be limited, meaning the need for application of active thermal control is lowered. Using the table provided by Kauder [2005] as well as by Wertz et al. [2011], multiple coating characteristics can be implemented to find the best fit.

As the distance between the sun and the asteroid vary drastically (0.67-1.15 AU), so does the environment the satellite is in. Studying the coatings available, not one will be able to reduce the external factors to keep the system temperature steady. To aid this, another thermal control system needs to be implemented. From the two types of thermal control systems, active and passive, the latter are preferred as they do not require power, and are more reliable as they are directly influenced by the satellite, minimising the number of points of failure. To address the changes in environment, this system also needs to be dynamic. A radiator with a louver system does exactly this: a blind-system opens and closes, hereby changing the rate the radiator radiates excess energy. Once it closes, less energy will be radiated, therefore system temperature will rise, and vice versa. The coating of the radiator has to be chosen carefully, to prevent heating of the satellite by the radiation striking the radiator unit.

These two systems were considered first, due to their simplicity and their reliability. They need to be balanced out to prevent over-cooling or overheating the system. The system was set to keep the system temperature at 293 $[K]$ without using any active heating or cooling. As radiators can only radiate energy, the coating needs to heat up the system. This immediately implies that the system has to be sized for solar maximum so that the system can handle that kind of environment. When the solar maximum decreases, the cooling required will drop meaning the system has less to do. By examining multiple combinations of body and radiator coating, a minimal area of radiators was achieved. This optimisation was conducted for each satellite separately, as each will have to endure different environments, either due to different mission profiles, or due to different satellite characteristics. As the ACSAL and SASH have about the same system characteristics, and a mission profile that resembles the other, they have the same thermal control system. The results of the optimisation are as follows:

- The lander shall have a coating consisting of silver vaporised on glass (absorbance factor = 0.04, emission factor = 0.02) with a 0.26 $[m^2]$ radiator-louver system where the radiator shall have a barium sulfate with polyvinyl alcohol coating (absorbance factor=0.06, emission factor=0.88). Total weight: 8.8 $[kg]$
- The hoverer shall have a coating consisting of silver vaporised on glass (absorbance factor=0.04, emission factor=0.02) with a 0.23 $[m^2]$ radiator-louver system where the radiator shall have a barium sulfate with polyvinyl alcohol coating (absorbance factor = 0.06, emission factor=0.88). Total weight: 10 $[kg]$
- The orbiter shall have a coating consisting of silver vaporised on glass (absorbance factor = 0.04, emission factor = 0.02) with a 1.65 $[m^2]$ radiator-louver system where the radiator shall have a barium sulfate with polyvinyl alcohol coating (absorbance factor=0.06, emission factor=0.88). Total weight: 82 $[kg]$

All three of these systems are capable of attaining the desired 293 $[K]$ (25 $[°C]$) and maintaining it throughout the entire orbit of the asteroid. As the louvers make the system dynamic, there is no need to use active thermal control to manipulate the overall system temperature.

8.5.4. Verification of model

Verification of the thermal environment model and thermal control model was performed in several steps. The two programs were initially one code, but were split to ease verification and to lower computation times.

The thermal environment model consists of multiple elements. The environment model starts with the modelling of the asteroid orbit. This computation was verified by comparing it to the known orbit. Next, the solar radiance was modelled and verified using sanity checks as well as unit testing. The further the asteroid got, the lower the solar irradiance. The albedo effect was highly dependent on this, but also on the view factor. The view factor was unit tested on its own to verify its correctness.

[19] https://ocw.mit.edu/courses/aeronautics-and-astronautics/16-851-satellite-engineering-fall-2003/lecture-notes/l23thermalcontro.pdf Accessed June 8, 2018

The planetary IR emission was tested using available data on planetary emission. As each factor was verified individually, and because there is no exceptional relation between these radiance levels, the total radiation level at the asteroid was also verified.

The thermal control model used the output values to compute the thermal level of the satellite. This was done using relations from trustworthy sources. Each relationship was unit tested by altering the inputs and performing sanity checks on the outcomes. The characteristics of the satellites (total surface area, radiated area, mass) were verified using CAD drawings as well as using values that were computed by other subsystems. As the control system is sized by means of iterations, this was verified by manually altering the control system properties and verifying the outcome through sanity checks.

Finally, the model needs validation. The main aim of this model is to allow the sizing of the thermal control surface area. By performing an iterative process with a changeable step size, the level of accuracy of the model can be altered. By setting it at a level that is deemed acceptable, the model assures that the accuracy required is met.

8.5.5. Exceptional thermal cooling

Although the overall temperature of the satellite system is maintained passively at 293 [K], there are specialised equipment on board of the satellite that require special attention. On board of the orbiter there are multiple sensors. These equipment utilise sensitive sensors which need to be cooled well below the system temperature. As the sensor in each equipment is small, no large system is required to cool these. A Peltier cooling system shall be implemented due to their small volume, mass, and low power consumption. Using a CUI Inc Peltier component[20], the heat removed equals 3.7 [W], resulting in an approximate 68 [K] difference. Using the Table 7.3, three systems can be identified inside the orbiter that need to be cooled exceptionally: the camera, the XRS, and the IR-Vis spectrometer. As the magnetometer operates outside the satellite, it is assumed it is cooled adequately, while being warmed by conduction from the satellite. To cool the three observational instruments, eight Peltier coolers will be used, which will use 7 watt each. These will be placed directly on the observational instruments's sensor chips.

Although there are no observational instruments on board of the lander or the hoverer, there are important actuators that need to function. On top of ACSAL, the drill actuator is housed within the satellite. It creates excessive heat that needs to be countered. Although the satellite operates its drill in the eclipses when keeping warm is required, the drill can reach high levels of heat. To counter this, two Peltier coolers are used to make sure that the system does not overheat. On the other hand, SASH has multiple actuators outside the satellite that need to operate precisely to ensure the success of the mission. Two Peltiers heaters are used to keep those actuators at operating temperatures by combining their heat and the heat of the satellite through conduction in the arm. All of these heaters and coolers have been taken into account by the EPS system.

Another consideration for the thermal control system are the solar arrays. These arrays hold solar cells which operate best at low temperatures as the higher the energy level, the more energy they can harvest. The cells have an absorptivity of around 0.91. To counter this, the array structure should emit as much energy as possible. This is aided by the fact that the structure the cells are on is always pointed away from the sun. The array material is therefore chosen to have a high level of emissivity hereby fulfilling this requirement. This can also be aided by coatings. The decision of using Z93SC55 conductive coating was made as its emission (0.94) exceeds most types, whereas its absorptivity (0.14) is adequately low to not absorb any energy from other sources such as planets or the satellite itself.

An instrument that is majorly influenced by temperature is the antenna interface. The antenna needs to be cooled as low as possible to reduce the noise added by system temperature. To assure that the temperature of the antenna is low, a coating is used to enable passive control, and to keep the power required to the minimum. To keep the temperature as low as possible, the aim is to lose as much power as the system can. This can be ensured by a coating with a high emissivity rate, and a low absorptivity to counter the absorption of energy. It can be concluded that these requirements are the same as for the solar arrays. Therefore, the antenna will also be coated with a layer of Z93SC55 conductive coating (emissivity=0.94, absorptivity=0.14).

8.6. Telemetry, Tracking and Command

In this section, the Telemetry, Tracking and Command (TT&C) subsystem design will be elaborated.

8.6.1. TT&C Requirements

In order to keep the design within the bounds of the mission goal, several requirements were derived which guided the sizing of the components.

ASRM-ORB-TTC-001	The TT&C subsystem shall be able to send and receive data over a distance of 2.16 [AU]. [A]
ASRM-ORB-TTC-002	The TT&C subsystem shall be able to send commands to either SASH or ACSAL with a minimum data rate of 1.1 [$kbit/s$]. [T]
ASRM-ORB-TTC-004	The communications link with Earth shall have a maximum bit error rate of 10^{-5}. [A]
ASRM-ORB-TTC-005	The TT&C subsystem HGA of the orbiter shall use X-band for communication with Earth with a minimum data rate of 20 [$kbit/s$]. [T]

[20] `https://www.cui.com/product/resource/cp08-m.pdf` Accessed June 20, 2018

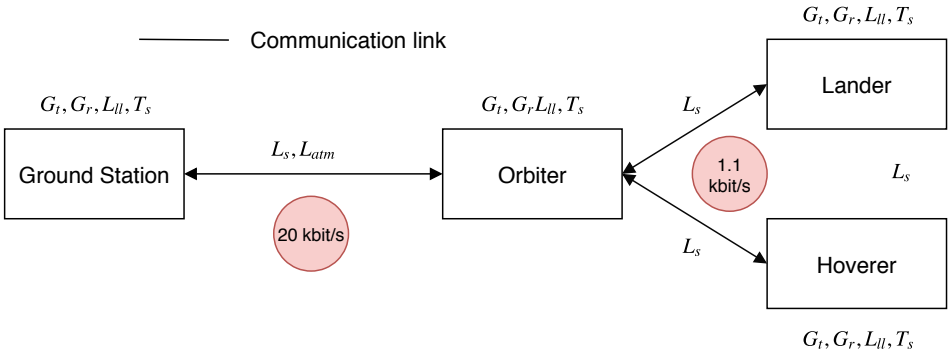

Figure 8.13: Communication diagram of the ground and space segment of Piazzi.

Since the orbiter serves as the main relay, it has more stringent requirements when compared to either ACSAL or SASH. The link distance is determined by the worst relative position of the asteroid with regards to the distance between the spacecraft and Earth, and is therefore a driving parameter for the sizing of the components. The 20 $[kbit/s]$ are derived from the fact that the scientific data has to be transferred within reasonable time.

ASRM-ACSAL-TTC-001	The TT&C subsystem of ACSAL shall have a minimum data rate for scientific and housekeeping data of 1.1 $[kbit/s]$. [T]
ASRM-ACSAL-TTC-002	The TT&C subsystem of ACSAL shall use S-band. [T]
ASRM-SASH-TTC-001	The TT&C subsystem of SASH shall have a minimum data rate for scientific and housekeeping data of 1.1 $[kbit/s]$. [T]
ASRM-SASH-TTC-002	The TT&C subsystem of SASH shall use S-band. [T]

Both ACSAL and SASH are sized for a much less demanding communications link since the link distance is in the order of several kilometres instead of 2.16 $[AU]$. This allows for less specialised and lower powered components, which is favourable when considering the size of these stages.

8.6.2. Architecture

The architecture of the TT&C subsystem is spread over all the separate spacecraft. To get a sense of the architecture, a communication diagram can be used. Such a diagram is shown in Figure 8.13.

From the diagram, one can see that the orbiter shall be able to communicate with Earth as well as with the two descending spacecraft. Here, the first architectural decisions are made. The orbiter shall communicate with Earth with a directional antenna, with as high gain as possible. As the lander and hover have non-fixed positions with respect to the orbiter and the orbiter also needs to point its main antenna to Earth, directional antennas could heavily constrain operations of the spacecraft. Therefore, as the distance from the orbiter to the lander or hoverer will most likely not exceed one kilometre, it is chosen to use non-directional antennas on those.

Besides the antennas itself, less visible components are required for operation. These include amplifiers, transponders and diplexers.

Amplifiers are installed in the orbiter to amplify the signal to the main antenna. Transponders are installed in all spacecraft. Transponders serve as the actual component communicating, converting a message to a signal to be sent through the antenna or vice versa. Diplexers serve to split the received and sent signal in a way that they are both able to use one communication channel.

8.6.3. Link budget

The most important performance characteristic of any communication link is the signal-to-noise ratio, which needs to be above 9.5 dB (Wertz et al. [2011]) in order to meet requirement ASRM-TTC-006 when using BPSK / QPSK coding. To check whether this ratio can be achieved, all gains and losses (in decibels) are added.

One of the driving factors for the sizing of the TT&C subsystem was the size of the data gathered from the observation instruments, which, combined with the telemetry of all the subsystems, needs to be communicated to Earth. The sizing of the components that constitute the TT&C subsystem is an iterative process, since the duration of the transfer of the scientific data gathered by the mapping process as well as the environmental factors and the chosen components have influence on the signal-to-noise ratio (SNR) of the link. The most important and also most sensitive link of the mission is the one between the orbiter to ground.

Table 8.12: Sizing parameters of the TT&C subsystem for the orbiter, SASH, and ACSAL.

Parameter	Ground station	Orbiter (HGA)	Orbiter (LGA)	SASH & ACSAL
Frequency $[GHz]$	X-band at 7.75	X-band at 8.4	S-band at 2.2	S-band at 2.2
Dimensions $[m]$	35 ⌀ parabolic	2.0 ⌀ parabolic	0.1 ↕ dipole	0.1 ↕ dipole
Power $[W]$	20,000[22]	13.4	1	1
Noise Temperature $[dBK]$ T_s	21.3	21.3	27.2	27.2
Minimum data rate up/-downlink B_R $[kbit/s]$	20/20	20/20	1.1/1.1	1.1/1.1
Line loss $[dB]$	1	2	2	2
Atmospheric loss $[dB]$	0.3	-	-	-
Gain $[dB]$	75 (X-Band), 74 (S-Band)[23]	43.4	2.2	2.2

A model was built using the existing formulae for the performance characteristics of a TT&C subsystem and known values of existing infrastructure on the ground provided by ESA. The chosen network, Estrack by ESA[21], provides the operations team with continuous coverage, except for the moment that the spacecraft is eclipsed by either the sun or the asteroid. The steps taken are described below.

The link budget is set up using the transmitting power P_t, the transmitter gain G_t, the receiver gain G_r, the line loss(es) L_{ll}, the atmospheric loss L_{atm}, space loss L_s, noise temperature T_s, and the bitrate B_R.

$$SNR[dB] = P_t + G_t + G_r - L_{ll} - L_{atm} - L_s - T_s + 228.6 - B_R \tag{8.25}$$

The gain of a parabolic antenna is calculated using Equation 8.26 (from Wertz et al. [2011]) and the gain for the LGA dipole antenna is determined to be 2.2 dB (Kraus [1997]).

$$G_{parabolic}[dB] = 20.4 + 20\log_{10}(f) + 20\log_{10}(D) + 10\log_{10}(\eta) \tag{8.26}$$

The half-power beamwidth is also calculated, which has consequences for the pointing accuracy of the TT&C subsystem, as it is generally taken to be 10% of $\theta_{1/2}$ (according to Wertz et al. [2011]).

$$\theta_{1/2}\ [deg] = \frac{21}{fD} \tag{8.27}$$

Obviously the largest loss in the link budget is caused by the immense distance the signal has to travel. Equation 8.28 quantifies this loss.

$$L_s[dB] = 92.45 + 20\log_{10}(d) + 20\log_{10}(f) \tag{8.28}$$

A first estimation was made for the size of the HGA on the orbiter by looking at other similar missions, like OSIRIS-REx, which has a parabolic dish with a 2.1 metre diameter. This was a starting point for the iteration of the sizing of our dish.

The following subsections show why these values ensure that all links work properly.

8.6.4. Link Characteristics

The multitude of links that exist within the system have been analysed in the computational tool and plotted against a range of distances in order to assess the TT&C subsystem performance during the mission.

Main communications link

The main downlink between the orbiter and the ground station is shown in Figure 8.14. Using the design requirement `ASRM-TTC-002` which demands a data rate of 20 $[kbit/s]$ at the maximum range between Earth and the spacecraft, the SNR was determined. In the same plot the maximum allowed data rate is calculated to illustrate the flexibility of the system's data rate performance throughout the mission.

Using a transmitting power of 13 [W] the link budget is closed with a data rate of 20 $[kbit/s]$ which means requirement `ASRM-TTC-002` has been met. Since the uplink (ground station to orbiter) in this case would have a larger transmitting power, it

[21] `https://download.esa.int/esoc/estrack/esa_estrack_brochure_2015_EN.pdf` Accessed June 24, 2018

[22] `https://ieeexplore.ieee.org/stamp/stamp.jsp?tp=&arnumber=931263` Accessed June 22, 2018

[23] `https://ieeexplore.ieee.org/stamp/stamp.jsp?tp=&arnumber=1367713` Accessed June 22, 2018

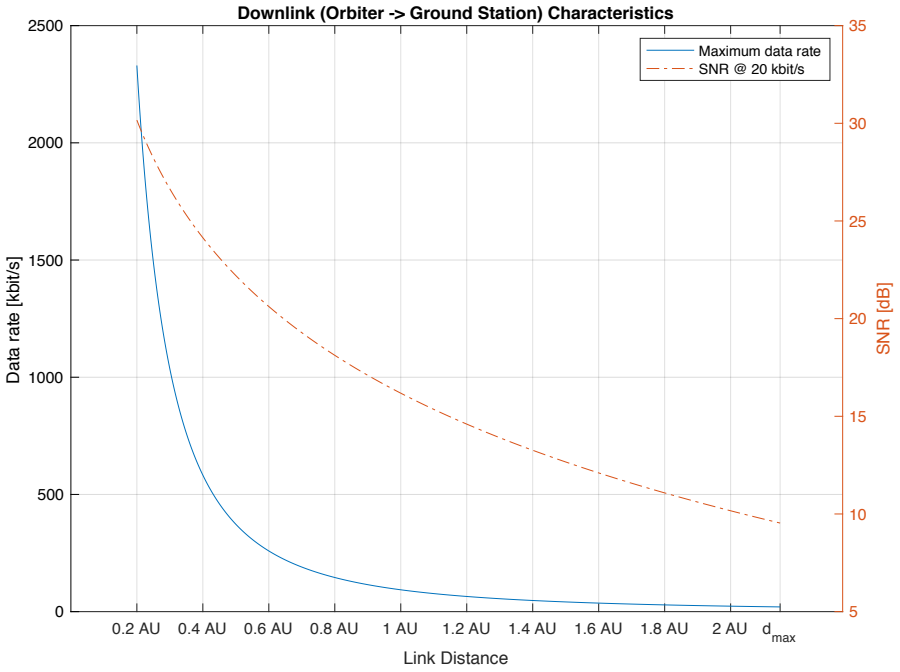

Figure 8.14: Data rate and SNR for the downlink between the orbiter and the ground station plotted against the link distance.

is obvious when examining Equation 8.25 that this link would provide a high enough data rate for commands as received power is higher.

The implications of the data rate of the main downlink is the amount of time it takes to send back the scientific data from the mapping phase, which affects the time line of the mission as this data is used to detail the subsequent parts of the mission.

The maximum allowable pointing error of the HGA is determined to be 0.13 [°] using Equation 8.27. This will be achieved in conjunction with the ADCS and a boom on which the HGA is mounted.

Interstage communications link

Since the orbiter acts as a relay between the ground station and SASH and ACSAL, the characteristics of the communications link has been assessed in the same manner as the main communications link. SASH and ACSAL transmit all their housekeeping and a comparably small amount of scientific data back to the ground station through the orbiter. Especially during the sample collection phases it is vital that the link between the stages is ensured and real-time.

Figure 8.15 shows that even if the distance between the orbiter and SASH/ACSAL would be more than 5 [km], the link between these stages is strong enough to ensure a much higher data rate than requirement `ASRM-SASH-TTC-002` prescribes. This might seem as if the system was oversized, however the same LGA on SASH/ACSAL is used to communicate with the ground station during its return trajectory.

SASH / ACSAL return

During the return orbit of both SASH and ACSAL, a link has to be established, although the purpose of this link is not for scientific purposes, but rather for performance monitoring of the spacecraft's subsystems and the orbital parameters. Doppler tracking can be used to accurately determine whether either SASH or ACSAL is performing nominally when considering their orbital parameters.

Figure 8.16 and Figure 8.17 show that even though the bit rate is not rather low, a working link can still be established that allows for the communication of telemetry and commands.

8.6.5. Software Tool Verification

Using the values given before, a unit test using Equation 8.25 is made to determine the accuracy of the computational tool used to evaluate the link between the orbiter and the ground station.

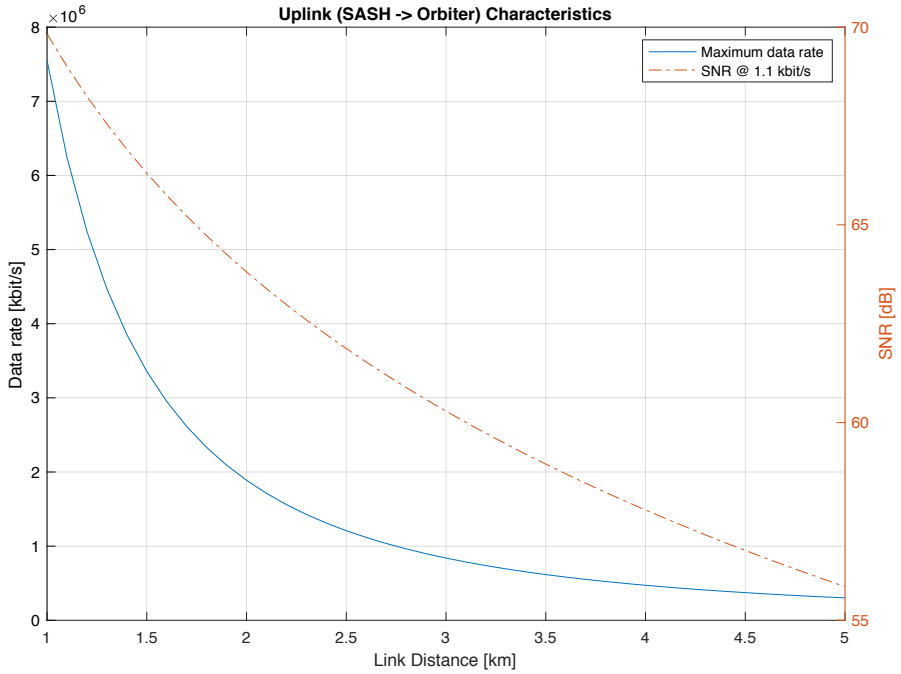

Figure 8.15: Data rate and Signal-to-Noise Ratio for the uplink between SASH and the orbiter plotted against the link distance.

$$G_t\ [dB] = 20.4 + 20\log_{10}(8.4) + 20\log_{10}(2.0) + 10\log_{10}(0.7)$$
$$= 43.4\ [dB]$$

$$L_s\ [dB] = 92.45 + 20\log_{10}(2.16 * 149597870.7) + 20\log_{10}(8.4)$$
$$= 281.1\ [dB]$$

$$9.5\ [dB] = 10\log_{10}(P) + 43.36 + 75 - (1+2) - 0.3 - 281.12 - 21.3 + 228.6 - 10\log_{10}(4500)$$
$$P = 13.4\ [W]$$

Now compared to the output of the software tool:

Software output: `The maximum data rate between the orbiter and the ground station is 20.16 kbit/s at dmax`

Which has been rounded to 1 decimal and is considered equal. The reason why this unit test verifies the tool is because it uses all the relevant variables that make plots such as Figure 8.14.

8.7. Command and data handling system

All three satellite modules are in effect self-regulating systems tasked with specific actions. For the satellites to be able to perform these tasks, they need to understand commands, perform calculations on their own, perform the actual process, then reflect and react on what they have done. Furthermore, they need to be able to handle the data coming from the payload section or from the ground section. To enable the spacecraft to do all mentioned, it needs a centralised brain. This is the task of the CDHS. In this section, this system will be discussed, requirements will be set, and specific components will be chosen to account for each element.

In subsection 8.7.1, the requirements set on the CDHS will be elaborated. Next, subsection 8.7.2 will present the methodology of sizing the components of the CDHS, and subsection 8.7.3 uses these sizing parameters to select CDHS components. Moreover, in subsection 8.7.4 the architecture of the CDHS system is outlined and finally in subsection 8.7.5 the level of autonomy of the Piazzi mission is covered for each of the satellites.

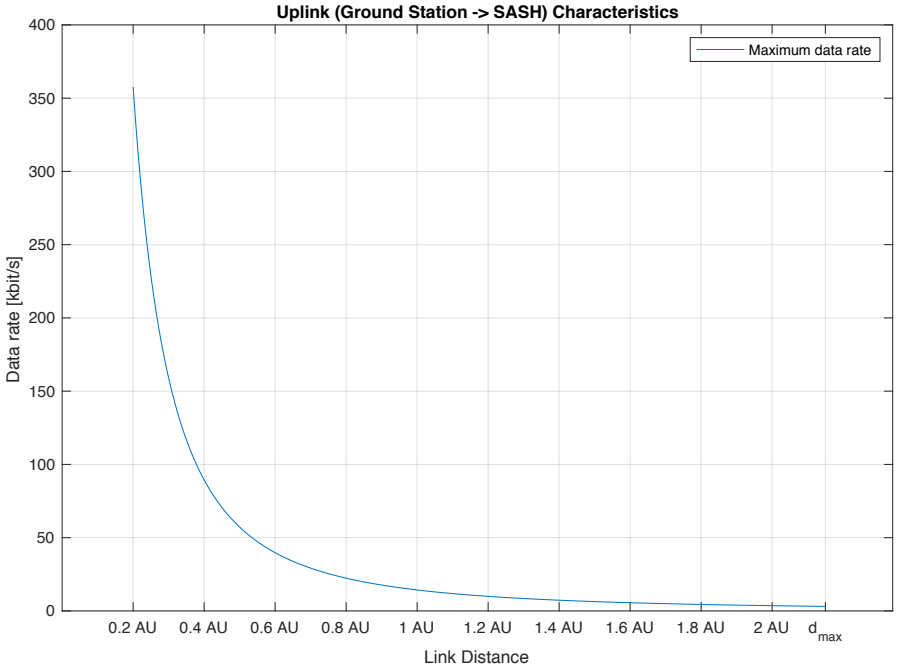

Figure 8.16: Data rate for the uplink between the ground station and SASH plotted against the link distance.

8.7.1. Requirements

The command and data handling system represents the core of the satellite. The CDHS is responsible for keeping the satellite safe, handle the payload data in a proper manner, process inputs and perform tasks. Without a correctly functioning CDHS, the satellite will underperform, either requiring more intervention from ground control, or even lead to termination of the mission. The requirements set for the CDHS module is therefore vital for the proper performance of the mission.

Below, the requirements for the CDHS are listed. Each requirement tackles a specific issue or task that is of importance for the mission. All three satellite modules should abide these requirements: each should be able to perform these tasks individually throughout the mission.

`ASRM-CDHS-001` The C&DH subsystem shall perform housekeeping tasks autonomously. [T]
`ASRM-CDHS-002` The C&DH subsystem shall be able to identify specific situations with effect on the mission. [T]
`ASRM-CDHS-003` The C&DH subsystem shall be able to initialise specific operational modes. [T]
`ASRM-CDHS-004` The C&DH subsystem shall be programmable through commands from the ground station. [T]
`ASRM-CDHS-005` The C&DH subsystem shall be commandable from the ground station. [T]
`ASRM-CDHS-006` The C&DH subsystem shall be able to prioritise commands. [T]
`ASRM-CDHS-007` The C&DH subsystem shall allocate storage space for the payload data. [T]
`ASRM-CDHS-008` The C&DH subsystem shall shall store payload data until it is downlinked to Earth. [T]
`ASRM-CDHS-009` The C&DH subsystem shall delete downlinked data. [T]
`ASRM-CDHS-010` The C&DH subsystem shall be in contact with all interfaces. [T]
`ASRM-CDHS-011` The C&DH subsystem shall be able to downlink data through the TT&C subsystem. [T]
`ASRM-CDHS-012` The C&DH subsystem shall have 3.6 [GB] of storage.

8.7.2. Sizing of CDHS modules

The CDHS consists of two main components: hardware and software. The hardware is composed of the onboard computer (OBC), remote terminal units (RTUs), the storage space and the wiring connecting them. The OBC is the element which is responsible for internal communications between the bus and other subsystems. The storage space is further split up into writable storage (RAM) and fixed storage (ROM). These two main hardware components will have to be sized for each specific mission, taking every element of the mission and satellite system into account. The software side of the CDHS includes the pre-programmed software that performs the housekeeping, operates the payload, and ensures the planned level of autonomy.

The OBC is the main element in the CDHS. It is assigned the task of handling data and performing specific computations or commands. The data to be handled is determined by the number of housekeeping sensors on board of the satellite, the type of

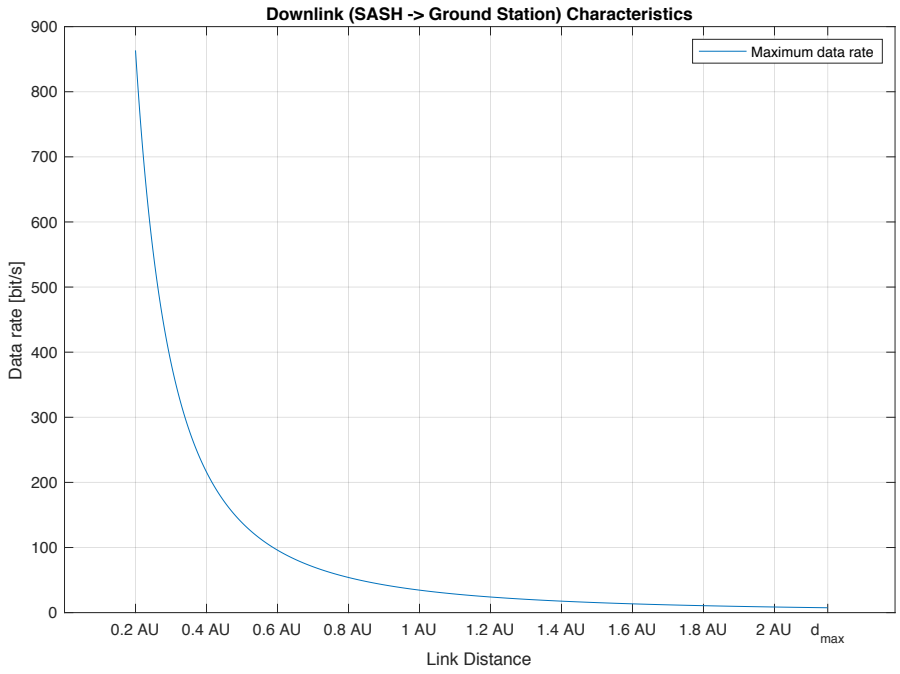

Figure 8.17: Data rate for the downlink between the SASH and ground station plotted against the link distance.

payload data, the amount of autonomy, and the operations to be performed. The housekeeping sensors provide data about the internal systems of the satellite with a number of sensors and a specific frequency. The payload also has a specific frequency with which it provides data, but it also has a resolution which influences the magnitude of the data provided per measurement. The amount of autonomy influences the amount of data and the frequency of received and downlinked commands from and to the ground station. Finally, the operations to be performed combine the data from sensors that determine the state of the task to which the CPU will have to react through commands.

The OBC will be sized for each satellite depending on its mission objectives. The orbiter will be placed into orbit around the asteroid where it will operate its observational instruments. These instruments will provide large amounts of data to be downlinked to the ground station. Furthermore, as the orbiter acts as a relay station for the hoverer and lander, it will have to handle the data received from the two satellites. These data rates will have to be handled together with housekeeping data and commands.

To minimise the size and mass of the storage unit, data compression will be applied to non-functional data (data not controlling anything, such as payload data or housekeeping that will be downlinked). Multiple types of compression methods exist, but only some are used in spacecraft. The issue that can occur with compression methods is the probability of radiation damage, meaning the compression method should account for this so that the data will not be completely useless should it be corrupted. As the storage size should be minimised, the compression method that compresses a 16-bit payload image most effectively is chosen. The method chosen is the ICER, developed by The Consultative Committee for Space Data Systems [2015] algorithm. This compression algorithm is capable of compressing multiple types of data at a compression rate of 16:10.86.

In section 6.2, the range of orbital times around the asteroid have been mentioned. These orbital periods depend on the orbital height at which the orbiter will be placed. To account for worst-case scenario, the longest periods were chosen and sized for. In the calculations below, the orbital period of 9.6 hours and an observational period of 8.8 hours per orbit are used, as well as the assumption that the orbiter can downlink during the orbital phase where the asteroid is not between Earth and the orbiter (8.8 hours per orbit).

The data rate produced by the observational instruments is estimated at 11 $[kB/s]$ Table 7.1.5. The housekeeping data rate of the orbiter has been estimated at 22.9 $[kB/s]$ The Consultative Committee for Space Data Systems [2015] and the housekeeping data of the lander and hoverer has been estimated at half of that of the orbiter (11.5 $[kB/s]$). Because it is not necessary to downlink the housekeeping data at every instance, it has been chosen to store one second of housekeeping data per 60 seconds which then will be downlinked, spread out over each minute. This holds for the orbiter. As SASH and ACSAL undergo more precise manoeuvres more housekeeping is sent back on earth. The rate was determined at one second every ten seconds (6 seconds per minute). This means the orbiter receives a data rate of 1.1 $[kB/s]$ from SASH as well as from ACSAL, adding up

to a total of 2.2 [kB/s].

To reduce the required data rate of the downlink, the observation data downlink will be spread out over multiple orbits, as TT&C allows 20.0 [kb/s] downstream in the worst-case scenario. Taking the data rate to downstream the housekeeping data into account, the orbiter is capable of downlinking 20.0 [kb/s] of payload data. This means that the entire payload data of one full mapping procedure of the orbiter will be downlinked within 18 days. To do so, the observational data shall be stored on board of the orbiter. This will require a storage buffer of 3.6 [GB]. An additional 30 [kB] of storage is required to store the housekeeping data in the period where the asteroid is between Earth and the satellite. This will ensure that when downlinking the observation data together with the housekeeping data, the data rate at worst-case scenario will not surpass the by the TT&C set 20.0 [kb/s]. The downlink rate of the observational data will be varied as the distance to Earth varies as well. During this constant transmission of observational data, camera-imaging data will have priority to aid quick determination of landing sites.

As stated before, the lander and hover do not have measurement payloads. They only produce housekeeping data at half the rate of the orbiter each, which equals 11.5 [kB/s]. They transmit 6 seconds worth of housekeeping data (11.5 [kB] per 60 seconds) each to the orbiter, which then will be relayed back by the orbiter to the ground station as payload data.

The storage accounted for the software commands are estimated using historical statistics (Bollendonk [2015]) and a linear trend line. This results in a prediction of 356,000 lines of code for the orbiter and the half is assumed for the other two satellites. As estimated in a TU Delft aerospace reader (Zandbergen [2012]), about 2 to 4 [KB] of storage is required for 1000 lines of code. This requires the system to allocate a maximum of 8.5 [MB] of storage for the command lines in the orbiter, and 4.3 [MB] for the lander/hover.

To sum up, the incoming data rate to be handled by the orbiter is 56 [kB/s] during observational phase, and 45.2 [kB/s] otherwise. After compression of the non-functional data, these data rates reduce to 52 [kB/s] and 44.5 [kB/s] respectively. The downlink during observational phase and non-observational period will be set at 20.0 [kb/s] to maximise utilisation of the TT&C module. The downlink rate of observational data will be 1.7 [bit/s] and that of the housekeeping data 18.3 [kb/s]. An overview of CDHS elements mentioned are presented in Table 8.13.

The storage of the CDHS is also an important component, as the data transmission is limited by the capability of the TT&C module. The required storage should be sized for the maximum amount of payload data that is to be stored together with the storage required for the commands. As stated before, 3.6 [GB] is required for the observational data, and around 8.5 [MB] for the commands in the orbiter and 4.3 [MB] in SASH/ACSAL. Therefore, including a 100% margin, resulting in a 7.2 [GB] hard drive.

The data that has to be handled by a computer is deterministic for its specifications. The computer needs to be sized for the most critical phase in the mission, for the orbiter this occurs during downlink to the ground station, as high amounts of data need to be moved. Using the assumption that 896 [kb/s] can be reached using one million instructions per second (MIPS). Using 1.7 [GB] for the amount of compressed non-functional data that is to be streamed by the orbiter and 0.33 [GB] for the hoverer and lander, the requirement for MIPS is set for the OBC. The orbiter will need an OBC capable of at least 15.1 [MHz] and that of the hoverer and lander needs to handle at least 2.94 [MHz].

8.7.3. Selection of components

Now it is known what is needed from the CDHS system to fulfil the requirements, the components fulfilling these requirements are selected. Based on the CPU requirements the Cube Computer [24] is chosen for all spacecraft. It has a CPU which could handle 48 [MHz] which is sufficient given the 35 [MHz] needed. Since the low power usage, cost and mass, two Cube Computers are added to the orbiter as well as to ACSAL and SASH. This is done for redundancy purposes, as a failure in the OBC would mean end of (a part of the) mission. The required storage is based on the amount of data generated by the scientific payload over a certain period of time and the compression rate managed by the OBC. As described in subsection 8.7.2, the internal storage of the orbiter should be at least 3.6 [GB]. However, since storage is crucial for the scientific value of the mission not only a 100% is used. Therefore the data storage equals 7.2 [GB]. To increase the redundancy even to a further extent. Two of these data storages are used, each linked to one of the Cube Computer in a completely separate circuit. This way the systems would not affect each other when short circuit is made or one system is affected by a computer virus. Finally, since only one of the Cube Computers is active at a all times, the power usage is equal to 200 [mW]. For the orbiter, RTUs are used in order to let the OBC use the CPU for the payload while still being able to perform automated tasks of the subsystems. The power of the RTUs is negligible [8]. The mass of the full computer system (CPU, RTU, wiring) including the radiation hardened storage solution equals 1 [kg].

[24] https://www.cubesatshop.com/product/cube-computer/ Accessed June 22, 2018

[8] `http://www.soletop.com/data/products/nanortu_low.pdf` Accessed June 22, 2018

Table 8.13: CDHS component requirements.

Module	Component	Specification
Lander	Housekeeping data rate	11.5 $[kB/s]$
	Stored housekeeping data rate	1.2 $[kb/s]$
	Total sent data rate	1.2$[kb/s]$
	Total handled data rate	13.4 $[kB/s]$
	Number of lines of code	178,000
	Storage	8.5 $[MB]$
Hoverer	Housekeeping data rate	11.5 $[kB/s]$
	Stored housekeeping data rate	1.2 $[kb/s]$
	Total sent data rate	1.2 $[kb/s]$
	Total handled data rate	13.4 $[kB/s]$
	Number of lines of code	178,000
	Storage	8.5 $[MB]$
Orbiter	Observational data rate	11.0 $[kB/s]$
	Housekeeping data rate	22.9 $[kB/s]$
	Sent housekeeping data rate	0.4 $[kB/s]$
	Housekeeping data received from lander	1.15 $[kB/s]$
	Housekeeping data received from hoverer	1.15 $[kB/s]$
	Compression rate	10.86/16
	Compressed observational data rate	7.5 $[kB/s]$
	Compressed housekeeping data rate from orbiter	0.3 $[kB/s]$
	Compressed housekeeping data rate from lander	0.8 $[kB/s]$
	Compressed housekeeping data rate from hoverer	0.8 $[kB/s]$
	Sent housekeeping data rate	1.8$[kb/s]$
	Sent observational data rate	18.2 $[kb/s]$
	Total sent data rate	20.0 $[kb/s]$
	Total handled data rate observation phase	56.2 $[kB/s]$
	Number of lines of code	356,000
	Storage	7.20 $[GB]$

8.7.4. CDHS Architecture

The architecture of the CDHS of the orbiter, SASH and ACSAL can be found in Figure 8.18. The Cube Computers are represented by the blue blocks stating OBC (onboard computer). Starting with the orbiter where the OBC is in direct contact with the payload in order to initiate mapping and measurement procedures. From the payload there is a high-speed link to the data storage and TT&C system of the orbiter. This is needed to store and transmit the scientific data. There is also a regular link present between the OBC, data storage and TT&C. This to execute data compression and give commands to the TT&C. Lastly the onboard computer communicates to the subsystems using RTUs, which contain microprocessors performing small tasks such as actuator control on behalf of the main computer. These remote terminal units help the system to perform more tasks autonomously.

Considering SASH and ACSAL, the CDHS system is rather similar. There is a Cube Computer on board representing the brain of the satellite, which is linked with the specific elements that need commands or generate data. Furthermore, there is data storage to stack the generated data and a TT&C system by means of a low gain antenna to communicate with the orbiter.

8.7.5. Level of autonomy

The level of autonomy is an important consideration during the design phase. Including autonomy could be of great value to a space mission, as it reduces the mission cost, allows for more efficient use of the communication window and gives the ability to perform tasks which were not able before, due to the long time between the command given and execution of the task. As the Piazzi mission makes use of multiple spacecraft, autonomy should be evaluated for each sub-spacecraft separately. There are several areas where autonomy could be of added value. First of all, making use of automated guidance, navigation and control. Next to that, the ability of the spacecraft to perform fault diagnosis, anomaly detection and fault recovery will greatly reduce the time to recover from these events. Finally, automating onboard science processes will not only save time, but also reduce the amount of data that needs to be communicated with Earth. Even though a high level of autonomy is desired, the spacecraft

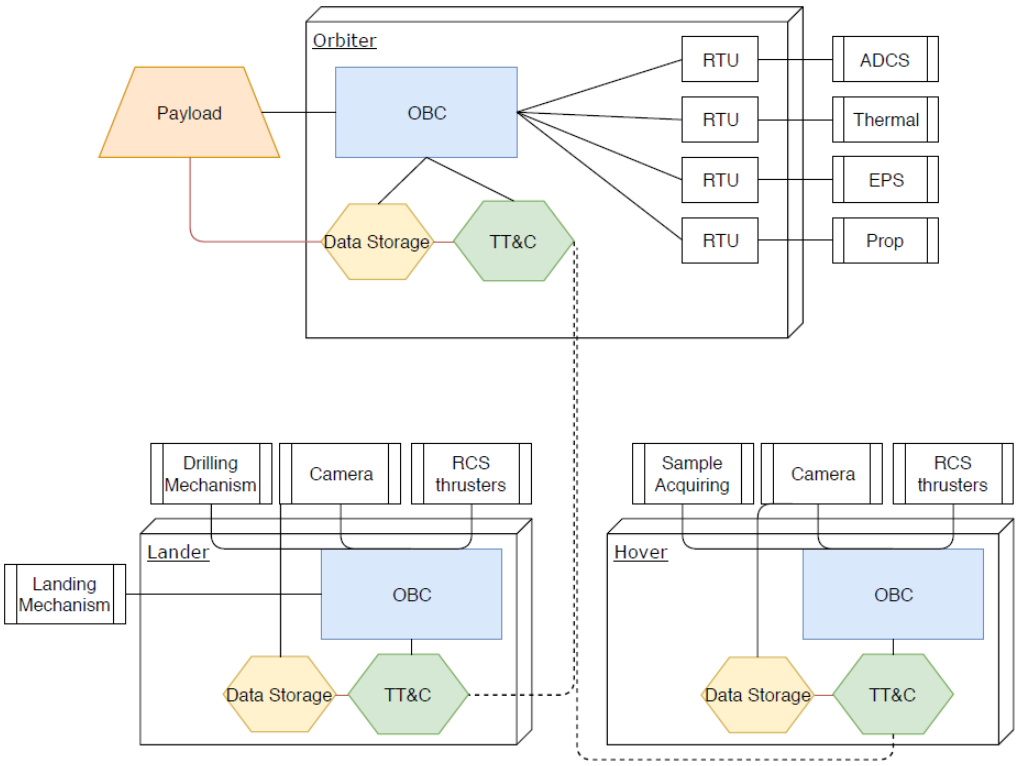

Figure 8.18: CDHS architecture of the space segment.

still needs to be able to be commanded from Earth, as unexpected scenarios can arise that only humans can deal with.

Orbiter
Starting with the orbiter, which will operate its ADCS subsystem fully autonomous ensuring attitude and orbit control. The orbiter is responsible for all communication with Earth. This means that also the communication of ACSAL and SASH are done via the orbiter. The data acquisition within the spacecraft is also fully automated. During each mission phase, the spacecraft will interchange data from the relevant spacecraft based on that mission phase.

ACSAL
ACSAL still requires feedback and commands from Earth. For example, before drilling, ground operations will check the sampling site before initiating the drilling procedure by a command from Earth. Automated processes are the landing procedure and communications to the orbiter. It thus has a certain level of autonomy, however a lot of processes are still checked and regulated by ground control.

SASH
SASH has the highest level of autonomy as it performs the hover trajectory and sample acquiring autonomously. It does, however only happen when in sight of the earth and the sun such that the process can be controlled. The spacecraft can only be controlled when back in orbit. There, if the first attempt fails, another try could be initiated by command from Earth. The data generated by SASH is returned to Earth via the orbiter.

9 Technical Risk Assessment

This chapter is a follow-up on the technical risk assessment of the previous design phase, where it has been noted that for space missions, especially deep space missions, the risk of failure of critical systems or subsystems has to be minimised by the means of risk mitigation. This due to the fact that reparations are not feasible in terms of additional cost and complexity.

The structure of this chapter is following the five processes needed for a risk management process. Starting with the planning, explaining how risk will be managed, followed by their identification and assessment, where they will be stated and quantified, including a risk register for each spacecraft. Finally a mitigation for the critical ones will be given with the final risk assessment matrix.

9.1. Risk planning

During the previous design phase the ECSS guidelines and the Failure mode, effects and criticality analysis (FMECA) approach (ECSS Secretariat [2009]) have been used to analyse the system for critical points considering failure and the consequences these failures will pose. The ranking of probability of occurrence associated with risk events is shown in Table 9.1; the ranking of severity of consequences is shown in Table 9.2. The quantification of the different risks has been done during several brainstorming session where each team member agreed upon the severity and probability of each risk.

Table 9.1: Probability levels, limits and numbers (ECSS Secretariat [2009])

Level	Probability number (PN)
Probable	4
Occasional	3
Remote	2
Extremely remote	1

Table 9.2: Severity of consequences (ECSS Secretariat [2009])

Severity category	Severity number (SN)
Catastrophic	4
Critical	3
Major	2
Minor or negligible	1

This risk register with the quantified risks, given in the next section will be used to generate the different risk maps shown in Table 9.3, Table 9.4 of all the risks combined to visualise the critical ones. At the end the risk factor is given, which is computed by multiplying the total P times the total S. After doing so three different risk assessment matrices can be set up to determine the fatal risks which have to be mitigated.

9.2. Risk identification & assessment

This section will be divided into four subsections, in order to identify all the risks for each spacecraft, being the orbiter, SASH and ACSAL. The fourth subsection will examine the general risks which are the same for all the spacecraft. To quantify these risks, P- and S-values are mentioned between brackets behind them. Some of the P- and S-values were already assigned to some of the risks during the previous phase of the project, but will be reevaluated for this phase. Each spacecraft's risk will be divided into three categories: technical risks, cost risks and schedule risks. Next to this, general risks for this mission are divided in the same categories but in addition there will be programmatic risks.

9.2.1. General

Technical risk

`GE.TE.1` Mistakes are made during the production process in terms of dimensions or reshaping of materials. (P = 2, S = 3)

`GE.TE.2` One of the thrusters fails during the launch of the spacecraft. (P = 1, S = 4)

`GE.TE.3` Structural failure of the space segment due to vibrations, during the launch.(P = 2, S = 4)

GE.TE.4 The numerical methods used to calculate orbital manoeuvres contain unidentified errors which can potentially result in missing the rendezvous point with asteroid 1989 UQ. (P = 1, S = 3)
GE.TE.5 Collision with space debris existing in Earth orbits affect multiple subsystems. (P = 2, S = 3)
GE.TE.6 Degradation of the spacecraft systems and subsystems, possibly inducing problems to the mission execution. (P = 2, S = 3)
GE.TE.7 The pressure gradient during launch damages components of the spacecraft should the protection for this fail. (P = 1, S = 2)
GE.TE.8 Space dust from 1989 UQ damages subsystems as on the Apollo missions to the Moon (Stubbs et al. [2007]). (P = 3, S = 3)
GE.TE.9 Solar weather disrupts the functionality of multiple subsystems during the mission. (P = 1, S = 3)
GE.TE.10 The valves of the propulsion system fail to open leading to absence of a populsive force. (P = 1, S = 4)
GE.TE.11 A switch in the EPS malfunctions due to degradation. (P = 2, S = 3)
GE.TE.12 Possible corrosion of the subsystems during pre-launch storage. (P = 1, S = 3)
GE.TE.13 The deployment mechanism of an antenna fails, which results in an unusable antenna (Galileo mission[1]). (P = 2, S = 3)
GE.TE.14 The data handling system contains hidden software bugs. (P = 2, S = 3)
GE.TE.15 Due to radiation exposure, bits in the program of the EPS change, possibly resulting in software errors. (P = 1, S = 3)
GE.TE.16 The detachment mechanism fails to detach one of the spacecraft. (P = 1, S = 4)
GE.TE.17 The detachment mechanism detaches one of the spacecraft with a too high ΔV (P = 1, S = 2)
GE.TE.18 The thermal system fails to protect system components during the thermal cycle of the mission. (P = 1, S = 3)
GE.TE.19 The ADCS-system is unable to effectively account for the disturbance torques experienced during lifetime. (P = 1, S = 3)
GE.TE.20 The centre of gravity of the spacecraft shifts during the mission resulting in required ADCS corrections. (P = 1, S = 3)
GE.TE.21 Timely correction of the orbit is prohibited by loss of communication (due to for instance the sun being between spacecraft and the earth). (P = 2, S = 4)

Cost risk

GE.CO.1 The cost of manufacturing complex parts for the system increases unexpectedly. (P = 3, S = 1)
GE.CO.2 The cost to receive certain permissions is higher than expected. (P = 2 , S = 2)

Schedule risk

GE.SC.1 The transportation of the produced parts is delayed. (P = 1, S = 2)
GE.SC.2 The manufacturing process is delayed due to insufficient planning or unforeseen situations. (P = 3, S = 2)
GE.SC.3 The launch of the space system is delayed due to bad weather conditions, affecting the planning of the entire mission as the orbital trajectory and manoeuvres are based on a certain launch date. (P = 2, S = 3)

Programmatic risk

GE.PR.1 Unexpected orbital perturbations change the transfer orbit to 1989 UQ and jeopardise the desired rendezvous. (P = 2, S = 2)
GE.PR.2 The authorisation to launch on a certain launch window is not permitted. (P = 1, S = 3)

Table 9.3: General mission risk assessment matrix

Severity (S)	Extremely remote [1]	Remote [2]	Occasional [3]	Probable [4]
Catastrophic [4]	*GE.TE.2*, *GE.TE.10*, *GE.TE.16*	*GE.TE.3*, *GE.TE.21*		
Critical [3]	*GE.TE.4* , *GE.TE.9*, *GE.TE.12* , *GE.TE.15*, *GE.TE.18* , *GE.TE.19*, *GE.TE.20* , *GE.PR.2*	*GE.TE.1* , *GE.TE.5*, *GE.TE.6* , *GE.TE.11*, *GE.TE.13*, *GE.TE.14*, *GE.SC.3*	*GE.TE.8*	
Major [2]	*GE.TE.7*, *GE.TE.17*, *GE.SC.1*	*GE.PR.1*, *GE.CO.2*	*GE.SC.2*	
Minor [1]			*GE.CO.1*	
	Likelihood (P)			

9.2.2. Orbiter

Technical risk

OR.TE.1 In the case that one thruster fails to ignite, it will have large consequences for burn time and torques generated on the spacecraft. (P = 1, S = 3)
OR.TE.2 The transfer orbit trajectory after insertion appears to result into collision with the asteroid. (P = 1, S = 4)
OR.TE.3 The spacecraft has a permanent dipole that will try to align with that of the asteroid should the asteroid 1989 UQ prove to be magnetic and in the case that the asteroid, causing an additional torque disturbance. (P = 2, S = 3)

[1] https://www.jpl.nasa.gov/news/news.php?feature=5661 Accessed May 18, 2018

OR.TE.4 The surface mapping instrument degrades too much before it performs its function. The consequence is that picking a suitable landing spot becomes more complex. (P = 2, S = 3)
OR.TE.5 The orbiter fails to enter 1989 UQ's Hill's sphere, hence to orbit around the asteroid. (P = 2, S = 4)

Cost risk

OR.CO.1 The final cost of the orbiter turns out to be above the expected cost, due to unforeseen changes in the design. (P = 3, S = 2)

Schedule risk

OR.SC.1 Manufacturing of the orbiter is not finished at the launch date. (P = 1, S = 4)

9.2.3. SASH

Technical risk

SASH.TE.1 The ADCS is unable to cope with the rotational rate of the asteroid which makes sample acquiring impossible. (P = 1, S = 3)
SASH.TE.2 The propulsive system that allows hovering fails and either crashes or makes it float away before completing the sample acquiring. (P = 1, S = 4)
SASH.TE.3 The reentry capsule experiences a higher temperature than expected and disintegrates during reentry. (P = 1, S = 4)
SASH.TE.4 Unexpected high loads on the reentry capsule leads to structural failure. (P = 1, S = 4)
SASH.TE.5 Return manoeuvres are performed inaccurately resulting in a too low reentry angle causing the return capsule to bounce off the atmosphere back into space. (P = 2, S = 4)
SASH.TE.6 The hoverer hovers above a part of the asteroid from which the composition is mostly uniform leading to lower scientific value. (P = 1, S = 3)
SASH.TE.7 There is less or no regolith on the asteroid's surface, hence no sample can be collected. (P = 1, S = 4)

Cost risk

SASH.CO.1 The final cost of SASH turns out to be above the expected cost, due to unforeseen changes in the design. (P = 3, S = 1)

Schedule risk

SASH.SC.1 SASH is not ready at launch date. (P = 1, S = 3)

9.2.4. ACSAL

Technical risk

ACSAL.TE.1 The ADCS is unable to cope with the rotational rate of the asteroid which makes landing impossible. (P = 1, S = 3)
ACSAL.TE.2 The lander fails to land correctly and crashes or tips over. (P = 3, S = 3)
ACSAL.TE.3 The reentry capsule experiences a higher temperature than expected and disintegrates during reentry. (P = 1, S = 4)
ACSAL.TE.4 Unexpected high loads on the reentry capsule leads to structural failure. (P = 1, S = 4)
ACSAL.TE.5 Return manoeuvres are performed inaccurately resulting in a too low reentry angle causing the return capsule to bounce off the atmosphere back into space.(P = 2, S = 4)
ACSAL.TE.6 The drill mechanism gets stuck in the carousel. (P = 2, S = 4)
ACSAL.TE.7 The harpoons fail to penetrate into the asteroids surface. (P = 3, S = 3)
ACSAL.TE.8 Leg claws do not attach into asteroid's surface. (P = 2, S = 2)
ACSAL.TE.9 Detachment of landing legs fails. (P = 1, S = 4)
ACSAL.TE.10 ACSAL lands above a part of the asteroid from which the composition is mostly uniform leading to lower scientific value. (P = 1, S = 2)
ACSAL.TE.11 There is more regolith on the asteroids surface then expected, hence the drill mechanism or landing manoeuvre could fail. (P = 1, S = 3)

Cost risk

ACSAL.CO.1 The final cost of ACSAL turns out to be above the expected cost, due to unforeseen changes in the design. (P = 3, S = 1)

Schedule risk

ACSAL.SC.1 ACSAL is not ready at the launch date. (P = 1, S = 3)

Table 9.3 and Table 9.4 sums up the general risks of this mission and of the three different spacecraft, given in 2 risk assessment matrix. This matrices simplify to determine the most critical risks.

9.3. Risk mitigation

Risk mitigation can be done in two ways, as risk is a function of two variables (likelihood and severity). By either decreasing the likelihood or the consequence of a risk, the risks in the risk map are translated from the upper right corner (high risk) towards

Table 9.4: Spacecraft specific risk assessment matrix

Severity (S)					
	Catastrophic [4]	*OR.TE*.2, *OR.SC*.1, *SASH.TE*.2, *SASH.TE*.3, *SASH.TE*.4, *ACSAL.TE*.3, *ACSAL.TE*.4, *ACSAL.TE*.9, *SASH.TE*.7	*SASH.TE*.5, *ACSAL.TE*.5 , *ACSAL.TE*.6, *OR.TE*.5		
	Critical [3]	*OR.TE*.1, *SASH.TE*.1, *SASH.TE*.6, *SASH.SC*.1, *ACSAL.TE*.1, *ACSAL.TE*.11, *ACSAL.SC*.1	*OR.TE*.3, *OR.TE*.4	*ACSAL.TE*.2, *ACSAL.TE*.7	
	Major [2]	*ACSAL.TE*.3	*ACSAL.TE*.8	*OR.CO*.1	
	Minor [1]			*SASH.CO*.1, *ACSAL.CO*.1	
		Extremely remote [1]	**Remote [2]**	**Occasional [3]**	**Probable [4]**
		Likelihood (P)			

the lower left corner (low risk). The risks that have a combined risk factor of at least 8 will be listed below, along with possible mitigation actions.

Mitigation can be performed in risk-specific manners, but the general groups are testing, simulation, active preventive mechanisms and research/planning/analysis. Testing involves performing the commands or operations in a controlled environment, simulation means that the computer is tested for its reactions to a scenario, active preventative mechanisms can be implemented on the satellite to allow autonomous risk prevention, and research/planning/analysis is a way of risk mitigation where more detail is placed in risky situations or observations.

GE.TE.3 The severity of this risk can not be decreased, however the probability of it happening can be. By strengthening the structural support of the space segment the probability can be mitigated from a 2 to a 1.

GE.TE.8 In order to mitigate this risk, one has to decrease the probability of occurrence. This can be done by adding certain protection on the different subsystems or hermetically sealing the subsystems with protectional blankets. This mitigates the probability of this risk from 3 to a 2.

GE.TE.21 During the final design phase, the orbital trajectory of the spacecraft will be known in more detail. Based on this, the instance during the mission can be determined at which the communication could be interrupted due to interference by the sun. If this is the case, an additional amount of ΔV could be accounted to correct for potential orbital disturbances during the time that communication is lost. This will mitigate the severity of consequence from 4 to 2.

OR.TE.5 Due to the fact that the Hill's sphere of the asteroid is dependent on its density, which is unknown, by adding a certain safety margin and designing for the worst-case scenario the probability of this risk can be decreased from a 2 to a 1.

SASH.TE.5 By performing a thorough analysis on the reentry phase of the mission and monitoring the spacecraft's orbital trajectory

ACSAL.TE.5 Upon encountering Earth, one can adjust the orbital parameters for successful reentry if necessary. This will reduce the likelihood from level 2 to 1.

ACSAL.TE.2 To avoid failure of the landing procedure, the harpoons and landing legs can be tested several times on Earth on a similar material (basalt). By doing so main issues on this design can be found and improved for the final design. This will decrease the probability from a 3 to a 2.

ACSAL.TE.6 Similar to risk *ACSAL.TE*.2 this can be tested on Earth to determine weak points and to improve the design. This will mitigate the probability of this risk from a 2 to a 1.

ACSAL.TE.7 As learned from the Rosetta mission performed by ESA (Ercoli Finzi et al. [2007]), several instruments (including scientific ones) on the spacecraft degraded over time and were not able to function properly after the rendezvous with the asteroid. Additionally, because the condition of the surface (fine powder, regolith-free and porous) is not know, the current design is based on a porous layer with a small regolith layer, while the ground is composed of basalt. By analysing the life cycle of the instruments used on the spacecraft, and designing the harpoons for the

worst-case scenario, the likelihood of occurrence can be mitigated from 3 to 2.

Table 9.5: General risk assessment matrix, with mitigation taken into account.

Severity (S)					
	Catastrophic [4]	*GE.TE.2*, *GE.TE.10*, *GE.TE.16*, *GE.TE.3*			
	Critical [3]	*GE.TE.4*, *GE.TE.9*, *GE.TE.12*, *GE.TE.15*, *GE.TE.18*, *GE.TE.19*, *GE.TE.20*, *GE.PR.2*	*GE.TE.1*, *GE.TE.5*, *GE.TE.6*, *GE.TE.11*, *GE.TE.13*, *GE.TE.14*, *GE.SC.3*, *GE.TE.8*		
	Major [2]	*GE.TE.7*, *GE.TE.17*, *GE.SC.1*	*GE.PR.1*, *GE.CO.2*, *GE.TE.21*	*GE.SC.2*	
	Minor [1]			*GE.CO.1*	
		Extremely remote [1]	**Remote [2]**	**Occasional [3]**	**Probable [4]**
		Likelihood (P)			

Table 9.6: Spacecraft specific risk assessment matrix, with mitigation taken into account.

Severity (S)					
	Catastrophic [4]	*OR.TE.2*, *OR.SC.1*, *SASH.TE.2*, *SASH.TE.3*, *SASH.TE.4*, *ACSAL.TE.3*, *ACSAL.TE.4*, *ACSAL.TE.9*, *SASH.TE.7*, *SASH.TE.5*, *ACSAL.TE.5*, *ACSAL.TE.6*, *OR.TE.5*			
	Critical [3]	*OR.TE.1*, *SASH.TE.1*, *SASH.TE.6*, *SASH.SC.1*, *ACSAL.TE.1*, *ACSAL.TE.11*, *ACSAL.SC.1*	*OR.TE.3*, *OR.TE.4*, *ACSAL.TE.2*, *ACSAL.TE.7*		
	Major [2]	*ACSAL.TE.3*	*ACSAL.TE.8*	*OR.CO.1*	
	Minor [1]			*SASH.CO.1*, *ACSAL.CO.1*	
		Extremely remote [1]	**Remote [2]**	**Occasional [3]**	**Probable [4]**
		Likelihood (P)			

Conclusions on Risk

Table 9.5 and Table 9.6 show that the risks can be mitigated from the upper right corner closer to the bottom left. The previously mentioned methods illustrate the possibility to reduce the risk of issues that would pose problems without mitigation. Risks that pose a smaller threat can also be mitigated, but these will not be elaborated upon at this stage of the design phase.

10
RAMS Analysis

In this chapter a RAMS (reliability, availability, maintainability and safety) analysis will be performed on the design of the Piazzi mission. In the first section, the reliability of the design will be assessed and tested to the set user requirements on reliability. Next, the other aspect of the RAMS analysis will be discussed and preventive design measures are discussed.

10.1. Reliability

Based on the three user requirements on reliability given at the start of the design phase, the Piazzi mission has been designed for reliability. These user requirements are shown below.

`ASRM-USR-NO10` The system shall survive the launch with a probability of at least 90%. [A]
`ASRM-USR-NO11` The system shall survive the transfer to asteroid 1989 UQ with a probability of at least 80%. [A]
`ASRM-USR-R004` The system shall return to Earth with a probability of at least 50%. [A]

To meet these requirements, a FMECA worksheet is created for the three spacecraft of the mission. Next, a FTA (fault tree analysis) for the three spacecraft is created to determine the structure of the reliability model. Finally, an overview of the model used to determine the reliability of the spacecraft and the verification of the requirements is shown.

By determining the failure distribution function F(t) using Equation 10.1, the reliability R(t) can be found for the given operational time (t) using Equation 10.2. In Equation 10.1 f(t) is the failure density function. The failure density function for all components is set to the exponential function shown in Equation 10.3 which represents random failures of the components (Hamann and Van Tooren [2006]). In this formula, θ is the mean life of a component. The mean life of the components on the orbiter and landers are determined from literature, but if not available assumed based on engineering judgement.

$$F(t) = \int_0^t f(t)dt \qquad (10.1) \qquad R(t) = 1 - F(t) \qquad (10.2) \qquad f(t) = \frac{1}{\theta} \cdot e^{\left(\frac{-t}{\theta}\right)} \qquad (10.3)$$

To determine the overall reliability of a spacecraft, a reliability model can be created. Depending on whether failure of components are correlated, the reliability of them either is set into series or parallel. If the reliability network is in series, Equation 10.4 is applicable. If the reliability network is in parallel, then Equation 10.5 is applicable. Determining the reliability of spacecraft, critical failure of subsystems by the failure of single or multiple components is considered by means of the value for β, which is the failure effect probability, which represents the probability of loss of function of the system or the entire mission (Hamann and Van Tooren [2006]). For lower values of β, the consequence of a failure to the entire system reduces. Therefore, only if the value for $\beta > 0.2$, the probabilities of the components are taken into account for the overall probability.

$$R = R_a \cdot R_b \qquad (10.4) \qquad R = 1 - (1 - R_a) \cdot (1 - R_b) \qquad (10.5)$$

10.1.1. Reliability of the Launcher

For the Piazzi mission the Falcon 9 launcher is used and this launcher has to comply with the user requirement `ASRM-USR-NO10`. Based on the data from launches performed by the Falcon 9 up to the June 26, 2018, the Falcon 9 has achieved 55 out of 57 successful launches [1]. This shows a reliability of $R_{launcher}$ is 97%. Therefore, the Falcon 9 fulfils user requirement `ASRM-USR-NO10`.

10.1.2. Reliability of Piazzi

To determine the reliability of the orbiter, Piazzi, up to the asteroid 1989 UQ an operational lifetime of 1.6 $[yr]$ is used. The outbound journey to the asteroid takes approximately 557 days, equal to 1.58 $[yr]$ is rounded up for alterations in the mission time line to 1.6 $[yr]$. This operational time is used to calculate the reliability of the different components using Equation 10.1, Equation 10.2, and Equation 10.3. For each component on the orbiter, the mean life, failure rate (excluding and including redundancy) and found reliability are shown in Table 10.1.

[1] `https://spacexnow.com/stats.php` Accessed June 26, 2018

Table 10.1: FMECA Worksheet of the orbiter.

Subsystem	**Component**	**Failure modes**	**Mean lifetime** [years]	**Redundancy have / need**	**Failure rate (FR)** [-]	**FR with redundancy** [-]	**Reliability** [-]
EPS-1	Li-ion battery	Anode, cathode, separator, terminal, casing	10	10/5	2.210^{-9}	1.110^{-9}	0.94
EPS-2	Solar array	Reduction power, degradation, by-pass diode, encapsulant	20	4/1	1.310^{-9}	3.310^{-10}	0.98
EPS-3	PCDU	Internal failure	50	3/2	5.910^{-10}	3.910^{-10}	0.98
EPS-4	Architecture	Internal damage	30	2/1	9.410^{-10}	4.710^{-10}	0.98
CDH-1	CPU	Internal failure	15	2/1	1.710^{-9}	8.310^{-10}	0.96
CDH-2	Storage	Memory alternation	15	2/1	1.710^{-9}	8.310^{-10}	0.96
CDH-3	Architecture	Internal failure	15	1/1	1.710^{-9}	1.710^{-9}	0.92
TTC-1	SDST	Electronic or structural failure	50	2/1	5.8910^{-10}	3.010^{-10}	0.99
TTC-2	AMP	Electronic failure	20	2/1	1.310^{-9}	6.610^{-10}	0.97
TTC-3	DIP	Electronic failure	20	3/1	1.310^{-9}	4.410^{-10}	0.98
TTC-4	HGA	Structural failure	50	1/1	5.910^{-10}	5.910^{-10}	0.97
TTC-5	LGA	Structural failure	50	1/1	5.910^{-10}	5.910^{-10}	0.97
TTC-6	Architecture	Internal failure	50	2/1	5.910^{-10}	3.010^{-10}	0.99
ADCS-1	DISUS	Internal / external failure	15	6/1	1.710^{-9}	2.810^{-10}	0.99
ADCS-2	LREWH	Internal / external failure	25	4/3	1.110^{-9}	8.210^{-10}	0.96
ADCS-3	STAT	Internal / external failure	15	3/1	1.710^{-9}	5.510^{-10}	0.97
ADCS-4	DILG	Internal / structural failure	50	4/3	5.910^{-10}	4.410^{-10}	0.98
ADCS-5	COGT	Internal / electronic failure	30	2/1	9.410^{-10}	4.710^{-10}	0.98
ADCS-6	Architecture	Internal failure	30	1/1	9.410^{-10}	4.710^{-10}	0.95
Prop-1	Fill & drain valve	Internal failure	30	1/1	9.410^{-10}	9.410^{-10}	0.95
Prop-2	NTO tank	Structural failure	100	1/1	3.110^{-10}	3.110^{-10}	0.98
Prop-3	MMH tank	Structural Failure	100	1/1	3.110^{-10}	3.110^{-10}	0.98
Prop-4	Pressure transducer	Internal failure	100	1/1	3.110^{-10}	3.110^{-10}	0.98
Prop-5	Filter	Internal failure	50	1/1	5.910^{-10}	5.910^{-10}	0.97
Prop-6	BITV	Internal failure	50	1/1	5.910^{-10}	5.910^{-10}	0.97
Prop-7	Isolation valve	Internal failure	50	1/1	5.910^{-10}	5.910^{-10}	0.97
Prop-8	AMBR	Internal failure	50	4/2	5.910^{-10}	3.010^{-10}	0.99
Ther-1	Louvres	Structural failure	15	1/1	3.110^{-10}	3.110^{-10}	0.98
Ther-2	Radiators	Structural / electronic failure	100	1/1	3.110^{-10}	3.110^{-10}	0.98
Ther-3	Peltier coolers	Electronic failure	50	1/1	5.910^{-10}	5.910^{-10}	0.97

By using Table 10.1, a FTA for the orbiter can be created and is shown in Figure 10.2. The symbols used in this FTA and their meaning are shown in Figure 10.1. These symbols contribute to the architecture of the reliability as the AND-function represents a parallel relation between components, whereas the OR-function represents a relation in series between components.

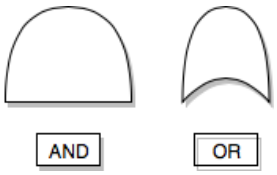

Figure 10.1: FTA symbols.

Using the FTA shown in Figure 10.2 in combinations with equations for the reliability model shown in Equation 10.4 and Equation 10.5, a value for the reliability of the orbiter can be determined. In Figure 10.2, the subsystem payload is shown having multiple failures with a $\beta > 0.2$, but these are not considered to determine the reliability of the orbiter during the outbound journey to the asteroid, as these components are not critical for this. The final equation to calculate the reliability of the orbiter is shown in Equation 10.6. The calculations on the reliabilities of the subystems are shown in Equation 10.7, Equation 10.8, Equation 10.9, Equation 10.10, Equation 10.11, and Equation 10.12. For these variables, $R_{orb_{EPS}}$ represents the reliability of the EPS system of the orbiter based on Table 10.1 and Figure 10.2.

$$R_{orbiter} = R_{orb_{EPS}} \cdot R_{orb_{CDHS}} \cdot R_{orb_{TT\&C}} \cdot R_{orb_{ADCS}} \cdot R_{orb_{PROP}} \cdot R_{orb_{THERMAL}} \tag{10.6}$$

$$R_{orb_{EPS}} = R_{pcdu} \cdot R_{batt} \cdot R_{pvarray} \tag{10.7}$$

$$R_{orb_{CDHS}} = 1 - (1 - R_{cpu}) \cdot (1 - R_{arc}) \tag{10.8}$$

$$R_{orb_{TT\&C}} = R_{dip} \cdot R_{amp} \cdot R_{sdst} \cdot R_{antennas} \cdot R_{arc} \tag{10.9}$$

$$R_{orb_{ADCS}} = R_{lrewh} \cdot (1 - (1 - R_{stat}) \cdot (1 - R_{dilg})) \tag{10.10}$$

$$R_{orb_{PROP}} = R_{mo3} \cdot R_{nto} \cdot R_{ambr} \cdot (1 - (1 - R_{fdval}) \cdot (1 - R_{presstd}) \cdot (1 - R_{filter}) \cdot (1 - R_{isovalve})) \tag{10.11}$$

$$R_{orb_{THERMAL}} = 1 - (1 - R_{radiator}) \cdot (1 - R_{peltier}) \tag{10.12}$$

Using the values on reliability per component shown in Table 10.1 for this model, a reliability for the orbiter of 80.5% can be found from the launch up to arrival at the asteroid after approximately 557 days. This verifies user requirement `ASRM-USR-NO11` having a reliability larger than 80%.

10.1.3. Reliability of ACSAL and SASH

To determine the reliability of the landers returning to Earth, ACSAL and SASH, an operational lifetime of 3.7 years (2/3 of the mission duration) is used, as the spacecraft will be in hibernation for more than 1/3 of the mission, approximately 2 out of the 5 years to be more precise, but to take into account a safety margin in case hibernation is not an option, 1/3 is used. This operational time is used to calculate the reliability using Equation 10.1, Equation 10.2, and Equation 10.3. For each component of the landers, the mean life, failure rate (excluding and including redundancy) and found reliability are shown in Table 10.2. However, for the payload elements considering the sample acquiring by both landers, an operational time of 10 days is used, as these devices will only be operational for a very short time during the mission.

By using Table 10.2, a FTA for both landers can be created and is shown in Figure 10.3 and Figure 10.4. As mentioned before, the symbols used in this FTA and their meaning are shown in Figure 10.1. Using the aforementioned FTAs in combinations with equations for the reliability model shown in Equation 10.4 and Equation 10.5, a value for the reliability of both landers can be determined. The final calculation of the reliability of ACSAL is done using Equation 10.17 and for the SASH, using Equation 10.18. The calculations on the reliabilities of the subsystems are shown in Equation 10.13, Equation 10.15, Equation 10.14, Equation 10.21, and Equation 10.16.

The difference in reliability between ACSAL and SASH comes from the ADCS and the payload, as for ACSAL this is determined using Equation 10.19 and Equation 10.22, while for SASH it is found using Equation 10.20 and Equation 10.23.

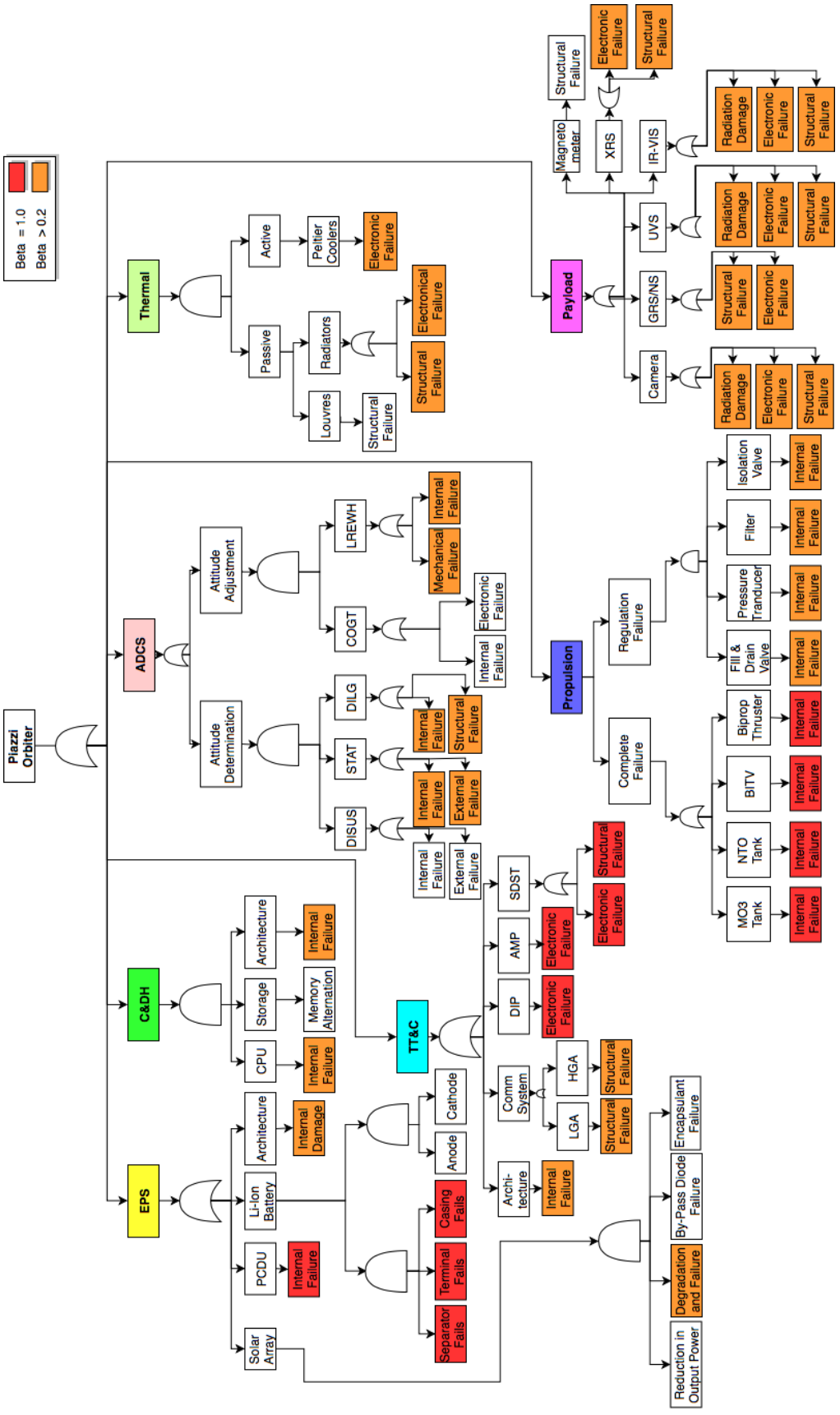

Figure 10.2: Fault tree analysis diagram of the orbiter

Table 10.2: FMECA sorksheet of the lander

Subsystem	Component	Failure modes	Mean life-ime [years]	Redun-dancy have / need	Failure rate (FR) [-]	FR with redundancy [-]	Reli-ability [-]
EPS-1	Li-ion battery	Anode, cathode separator, terminal casing	10	10/5	2.210^{-9}	1.110^{-9}	0.87
EPS-2	Solar array	Reduction power, degradation, by-pass diode, encapsulant	20	4/1	1.310^{-9}	3.310^{-10}	0.96
EPS-3	PCDU	Internal Failure	50	3/2	5.910^{-10}	3.910^{-10}	0.95
EPS-4	Architecture	Internal Damage	30	2/1	5.910^{-10}	3.010^{-10}	0.97
CDH-1	CPU	Internal Failure	15	2/1	1.710^{-9}	8.310^{-10}	0.90
CDH-2	Storage	Memory Alternation	15	2/1	1.710^{-9}	8.310^{-10}	0.90
CDH-3	Architecture	Internal Failure	15	1/1	1.710^{-9}	1.710^{-9}	0.81
TTC-1	TRA	Electronic / structural failure	50	2/1	5.910^{-10}	3.010^{-10}	0.97
TTC-2	AMP	Electronic failure	20	2/1	1.310^{-9}	6.610^{-10}	0.97
TTC-3	DIP	Electronic failure	20	2/1	1.310^{-9}	6.610^{-10}	0.92
TTC-4	LGA	Structural failure	50	2/1	5.910^{-10}	3.010^{-10}	0.97
TTC-5	Architecture	Internal failure	50	2/1	5.910^{-10}	3.010^{-10}	0.99
ADCS-1	DISUS	Internal / external failure	15	6/1	1.710^{-9}	2.810^{-10}	0.98
ADCS-2	REWH	In-/external failure	25	4/3	1.110^{-9}	8.210^{-10}	0.90
ADCS-3	STAT	In-/external failure	15	3/1	1.710^{-9}	5.510^{-10}	0.94
ADCS-4	DILG	Structural failure	50	4/3	5.910^{-10}	4.410^{-10}	0.95
ADCS-5	COGT	Electronic failure	30	2/1	9.410^{-10}	4.710^{-10}	0.95
ADCS-6	Architecture	Internal failure	30	1/1	9.410^{-10}	4.710^{-10}	0.89
ADCS-ACSAL-1	ACC	Electronic failure	30	2/1	9.410^{-10}	4.710^{-10}	0.95
ADCS-SASH-1	CLA	External failure	50	2/1	5.910^{-10}	3.010^{-10}	0.97
Prop-1	Fill & drain valve	Internal failure	30	1/1	9.410^{-10}	9.410^{-10}	0.89
Prop-2	MMH tank	Structural failure	100	1/1	3.110^{-10}	3.110^{-10}	0.96
Prop-3	Pressure transducer	Internal failure	100	1/1	3.110^{-10}	3.110^{-10}	0.96
Prop-4	Filter	Internal failure	50	1/1	5.910^{-10}	5.910^{-10}	0.96
Prop-5	MOTV	Internal failure	50	1/1	5.910^{-10}	5.910^{-10}	0.96
Prop-6	Isolation valve	Internal failure	50	1/1	5.910^{-10}	5.910^{-10}	0.96
Prop-7	MONARC-445	Internal failure	50	4/2	5.910^{-10}	5.910^{-10}	0.93
Ther-1	Louvres	Structural failure	15	1/1	3.110^{-10}	3.110^{-10}	0.96
Ther-2	Radiators	Structural /elec-tronic failure	100	1/1	3.0610^{-10}	3.0610^{-10}	0.96
Ther-3	Peltier coolers	Electronic failure	50	2/1	5.910^{-10}	3.010^{-10}	0.97
PL-ACSAL-1	DRL	In-/external failure	30	1/1	1.110^{-9}	1.110^{-9}	0.999
PL-ACSAL-2	CAR	In-/external failure	30	1/1	1.110^{-9}	1.110^{-9}	0.999
PL-ACSAL-3	SPM	In-/external failure	30	1/1	1.110^{-9}	1.110^{-9}	0.999
PL-ACSAL-4	ALM	In-/external failure	30	1/1	1.110^{-9}	1.110^{-9}	0.999
PL-ACSAL-5	HAR	In-/external failure	8	1/1	4.010^{-9}	4.010^{-9}	0.997
PL-SASH-1	SAM	In-/external failure	5	1/1	6.310^{-9}	6.310^{-9}	0.995
PL-SRC	SRC	In-/external failure	50	1/1	5.910^{-10}	5.810^{-10}	0.93
PL-DEC	DEC	In-/external failure	50	1/1	6.210^{-10}	6.210^{-10}	0.98
PL-DECAM	DECAM	In-/external failure	10	1/1	3.210^{-9}	3.210^{-9}	0.997
PL-LAS	LAS	External failure	10	1/1	3.210^{-9}	3.210^{-9}	0.997

$$R_{lnd_{eps}} = R_{pcdu} \cdot R_{batt} \cdot R_{solararray} \tag{10.13}$$

$$R_{lnd_{ttc}} = R_{dip} \cdot R_{amp} \cdot R_{sdst} \cdot R_{lga} \cdot R_{arc} \tag{10.14}$$

$$R_{lnd_{cdh}} = 1 - (1 - R_{cpu}) \cdot (1 - R_{arc}) \tag{10.15}$$

$$R_{lnd_{ther}} = 1 - (1 - R_{radiator}) \cdot (1 - R_{peltier}) \tag{10.16}$$

$$R_{ACSAL} = R_{lnd_{eps}} \cdot R_{lnd_{eps}} \cdot R_{lnd_{cdh}} \cdot R_{lnd_{ttc}} \cdot R_{lnd_{adcs}} \cdot R_{lnd_{prop}} \cdot R_{lnd_{ther}} \cdot R_{lnd_{payloadACSAL}} \tag{10.17}$$

$$R_{SASH} = R_{lnd_{eps}} \cdot R_{lnd_{eps}} \cdot R_{lnd_{cdh}} \cdot R_{lnd_{ttc}} \cdot R_{lnd_{adcs}} \cdot R_{lnd_{prop}} \cdot R_{lnd_{ther}} \cdot R_{lnd_{payloadSASH}} \tag{10.18}$$

$$R_{lnd_{adcsACSAL}} = R_{rewh} \cdot R_{acc} \cdot \left[1 - (1 - R_{stat}) \cdot \left(1 - R_{dilg}\right)\right] \tag{10.19}$$

$$R_{lnd_{adcsSASH}} = R_{rewh} \cdot R_{cla} \cdot \left[1 - (1 - R_{stat}) \cdot \left(1 - R_{dilg}\right)\right] \tag{10.20}$$

$$R_{lnd_{prop}} = R_{MO3} \cdot R_{MONARC-445} \cdot (1 - (1 - R_{fdval}) \cdot (1 - R_{presstd}) \cdot (1 - R_{filter}) \cdot (1 - R_{isovalve})) \tag{10.21}$$

$$R_{lnd_{payloadACSAL}} = R_{dec} \cdot R_{decam} \cdot R_{drl} \cdot R_{car} \cdot R_{spm} \cdot R_{las} \cdot R_{src} \cdot R_{alm} \cdot R_{har} \tag{10.22}$$

$$R_{lnd_{payloadSASH}} = R_{dec} \cdot R_{decam} \cdot R_{sam} \cdot R_{src} \cdot R_{las} \tag{10.23}$$

Using the values on reliability per component shown in Table 10.2 for this model, a reliability for ACSAL of 51.7% can be found and for SASH of 51.8%. Therefore, the overall reliability of bringing back a sample to Earth is 76.7%. Therefore, the reliabilities of both landers separately and combined verify user requirement `ASRM-USR-RO04` by having a larger reliability than 50%.

10.2. Availability, maintainability and safety

The other three aspects of the RAMS analysis are availability, maintainability, and safety. These aspects will be addressed in the continuation of this chapter.

10.2.1. Availability and maintainability

For the Piazzi mission, maintainability and availability also have to be taken into account to perform a complete RAMS analysis. However, maintainability is not applicable to the Piazzi mission design. Maintainability is defined as part of a design and can be quantified by the amount of maintenance required, the duration of the maintenance, the support in terms of logistics and the human factors involved (Hamann and Van Tooren [2006]). For space missions, especially interplanetary missions like the Piazzi mission, maintainability is impossible and should be designed for. In such a way, the maintainability is already taken into account when designing for reliability, as the spacecraft has to be able to be fully operational during its mission lifetime. Availability can be defined as the probability that a system, as a whole and component specific, will be completely available when required for use (Hamann and Van Tooren [2006]). Availability consists of a combination between maintainability and reliability, and as explained above, maintainability is designed for in such a way for an interplanetary space mission that the reliability of the system is sufficient to fulfil the mission lifetime. Therefore, the concept of availability is included in the approach on reliability and is not separately elaborated upon.

10.2.2. Safety

The final aspect of the RAMS analysis is safety, which the Piazzi mission concept has taken into account. The safety of the design is there to prevent the following along with the measures to do so.

- **Endangering human beings.**
  To prevent endangering human beings while manufacturing the system, preventative measures have been taken and will be elaborated upon in chapter 11. When operating the system, humans could potentially be at risk during launch and the reentry phase of the spacecraft. For the launch, which is planned to be executed from Cape Canaveral, Florida, the spacecraft will be directed over the Atlantic Ocean, such that if a system of the launcher fails, the launcher will not pose a threat to populated areas on which it could potentially crash. During reentry, which is planned to take place over the middle of Australia at the end of August 2030, uninhabited areas will be the target areas for the landing site of the capsule to prevent crashing onto populated areas. The spacecraft that release the two reentry capsules will be put under another reentry angle to ensure that it burns up in upon entering Earth's atmosphere.

- **Damaging the system that is designed.**
  As for preventing endangering human beings during the production process, measures are also taken to prevent damaging the actual system that is being manufactured. This will also be elaborated upon in chapter 11.
- **Damaging foreign systems while operating the system.**
  To prevent damaging other systems while operating the system, the phase near Earth is considered to be of high importance. In a later design stage, it should be taken into account that the spacecraft will cross several orbits of spacecraft orbiting Earth from the launch up to the transfer orbit. The probability and risk of colliding with an orbit-crossing spacecraft has to be evaluated as the mission comes closer to the launch date.
- **Damaging the environment in which the system operates.**
  To ensure that the Piazzi mission does not hurt the environment that it operates in, multiple design measures have to be taken. The environment on Earth will be affected by the propellants expelled during launch, but with the launcher technology as is known today, this can not be prevented. Taking into account possible contamination of Earth's environment with the sample brought back from 1989 UQ, design measures have been taken and elaborated upon in chapter 4.

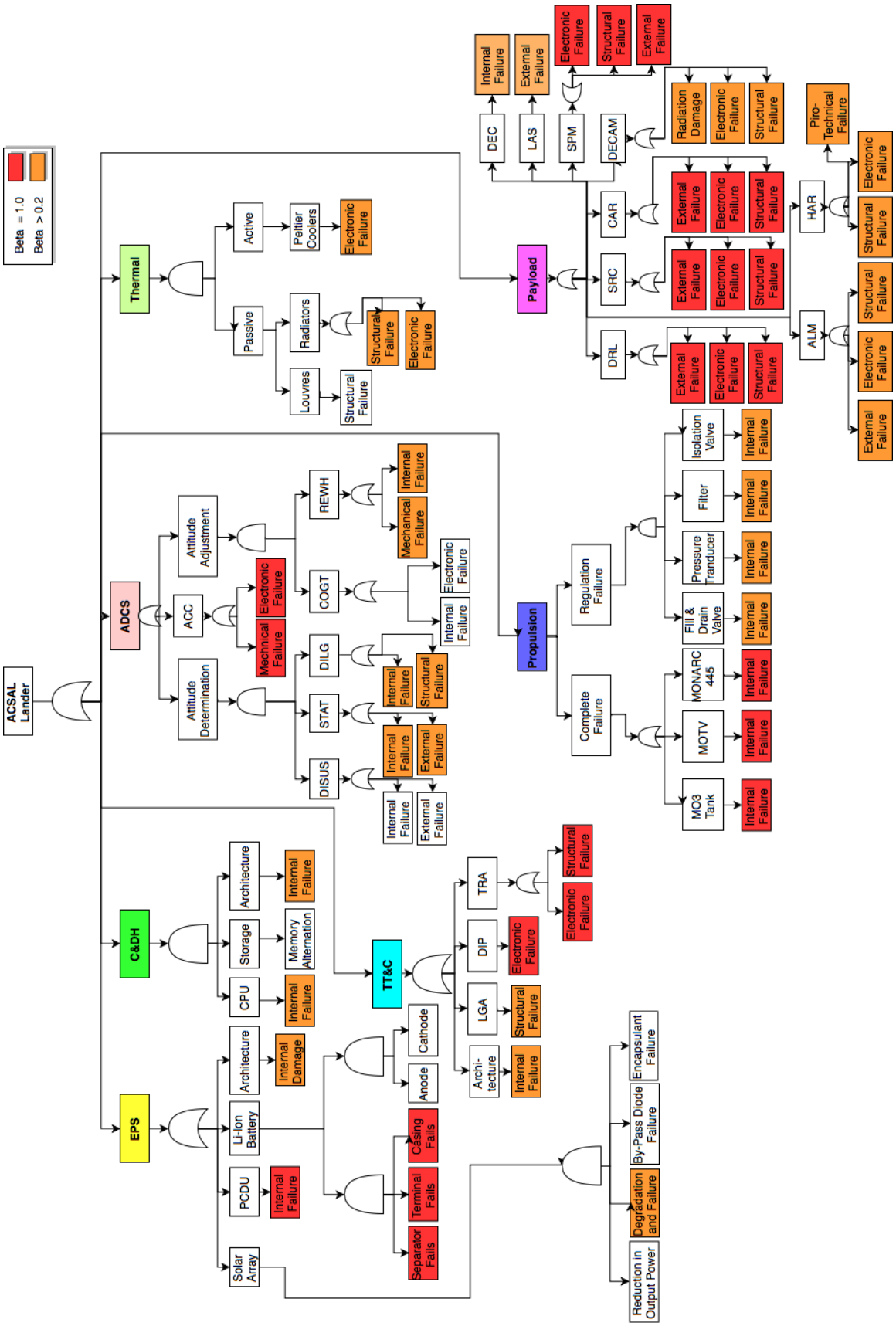

Figure 10.3: Fault tree analysis diagram of ACSAL.

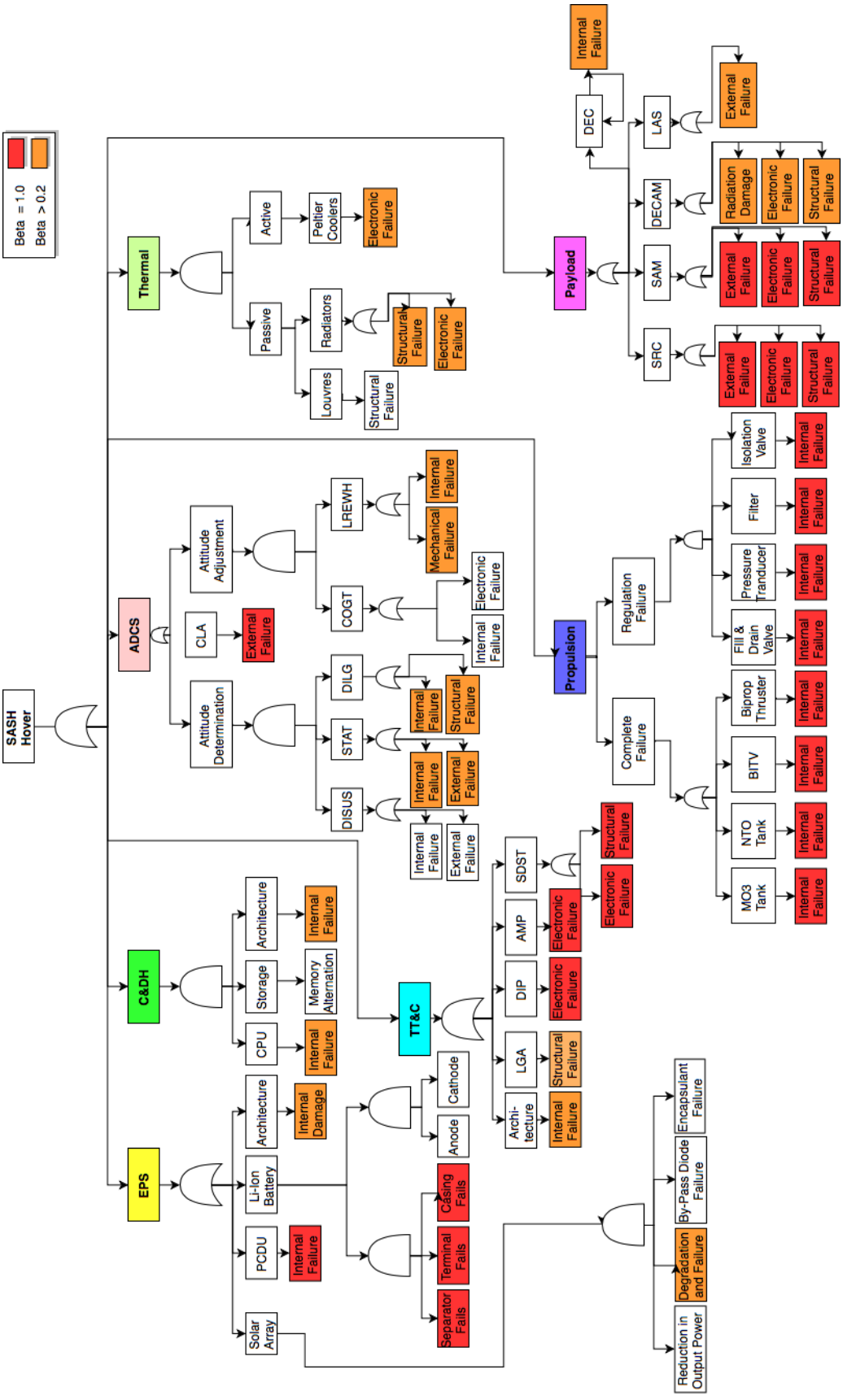

Figure 10.4: Fault tree analysis diagram of SASH.

11
Operations & Production

This chapter focuses on all the supporting elements that enable the Piazzi mission. The main focus of this report is on the design of the spacecraft systems and the logistics have not yet been considered. Here, the operation will be clearly explained without going into to the design again. A production plan will then be presented at the end of this section to visualise the several steps to obtain a proper final product.

11.1. Logistics

During any space mission the logistics have to be considered in order to obtain reliable product in a set time limit. Logistics influence all mission phases, starting from the manufacturing until the retrieval of the return capsule. Logistics support is rather important throughout the whole design of the spacecraft, it is one of the criteria that have a big influence on the design.

11.1.1. Manufacturing

Manufacturing is a critical phase of the design. A mistake made during manufacturing can delay the whole design for several months, or even years. It may induce a malfunctioning of a component and result in mission failure. As such, careful scheduling of manpower and machining is of the highest importance. The production has to be carefully planned in order to meet deadlines and to be able to launch the spacecraft on time. Manpower is also a big part of the manufacturing process. Enough personnel need to be allocated to the proper position to fulfil the desired job. The staff also need to be trained to perform precise work. This training for the personnel is part of the logistics support and is completed by the training facilities as described in a further subsection. Manufacturing time can be shortened through good planning as stated earlier, but also by using detailed technical documentation. This can be implemented in the manufacturing process, where either the documentation is already made and ready for use or the part needs a new manufacturing technique which has to be documented in order to ease the next part's processing. The spacecraft is made of many different materials resulting in different companies that are involved in the process. The deadline for the different part to be finalised is set to be at 2021 to 2022. This leaves 2 years to do all procedures, such as final assembly, transport to launch site, integration, and many more.

11.1.2. Testing

A procedure that should not be forgotten at all cost is the testing of the product. Every element produce should be tested in order to proof that it can fulfil its purpose. This is called the verification of a product and it is fundamental to accomplish the success of the mission. There should be different type of testing throughout the manufacturing and assembly phase. One test should always be conducted once the component is built to check whether it can work on its own, another when it is integrated in the subsystem in order to verify the whole in accordance to what is expected. The whole spacecraft is then tested thoroughly before performing its action. That is, the arm on SASH will be tested in space before it tries to grab regolith off the surface. The testing on Earth should be done by the manufacturer in the first case, then by the engineers that assemble the spacecraft.

11.1.3. Transportation

Transportation, the major contributor to logistics, ovvurs at any instant until launch. Some parts need to be manufactured in multiple factories and so need to be transported to be assembled to other assets. It is of utmost importance that the transport is safe and secure while keeping in mind that it has to be timely. The main reason so many parts need to be moved is because the subsystems of the spacecraft are made by different companies, spread throughout different nations. All parts then need to be transported to a central assembly area, where they are put together in a clean room. The attachment of the spacecraft onto the LVA is also considered as part of the logistics, since it has to be fitted on the launch vehicle, which itself has to be transported to the launch site. This whole process of the transportation has to be precisely monitored so it does not interfere with the success of the space mission.

11.1.4. Assembly and launch

Once the spacecraft subsystems are produced, they have to be assembled together, as stated earlier this has to be done in a clean room with extreme precision. A mistake at this stage yields a poor integrity of the whole spacecraft. As for every logistics aspect, time is a big constraint. The assembly has a set time limit that has to followed in order to not miss the launch window. Missing the launch date generates a delay of almost 6 years to reach the same asteroid or a 5 years delay for a different asteroid with similar ΔV. As such, the assembly can not take longer than the set time, this has needs to be supervised by dedicated personnel. Once the assembly is completed, the launch can be prepared. At the moment the spacecraft is fixed to the launcher and the launcher is ready to liftoff, many tasks are still to be performed, so as to ascertain the launch is prepared in a safe manner to reduce risk of failure. These includes, for example, the ground track of the launcher needs to be cleared of sea traffic, fuel needs to be loaded, the countdown needs to be initiated, a full systems check needs to be performed, the weather needs to be monitored continuously, tracking stations need to be ready to track the launcher on its ascent trajectory, and possible recovery teams need to be ready. Most of these tasks need to be planned well in advance, and this is to be taken into account.

11.1.5. Facilities

Many facilities need to be available for a full space mission, it starts from the facilities to train the personnel which are usually only needed before the launch. Other facilities such as communication ground segment are of the highest importance since they receive the information sent by the orbiter or the two landers and send back commands in order to sample correctly, or in a more general manner, commands to control the spacecraft. Since the ground segment is of such importance it has to be chosen at the beginning of the mission. The ground segment chosen in this case is the ESA Deep Space Antenna network which is a network of several antennas. These kind of antennas are quite demanded and need to be reserved in advance. So it is a necessity that the mission time line is defined in detail. For instance during the interplanetary coasting phase, the communication will not be as needed, in contrast to during the sampling procedures. Proper planning is then the key for this mission to be successful with respect to the ground segment. The most critical section of the mission has to be monitored constantly from the DSA facilities.

11.1.6. Retrieval

This mission is composed of three spacecraft, namely one orbiter, one lander and finally one hoverer. Knowing that if the mission is successful two reentry capsules will land on Earth at two different dates. The landing site after reentry is decided to be Australia. Agreements have to be made between the Australian authorities and the mission management of the Piazzi mission in order to obtain permission to land in a desert in central Australia. This will have to be overseen by a team of engineers that know how to handle the capsule once it has reentered the atmosphere. This team need to be composed of at least ten people, consisting of a helicopter pilot and co-pilot to obtain a first visual of the landed capsules. Since the capsules are equipped with a beacon, the helicopter will first fly towards it to see if it is safe to approach, which is followed by the retrieval of the capsule.

11.2. Production plan

This Piazzi mission is a spacecraft mission which means that its components are made of many different elements. Since it would be time consuming and unnecessary to analyse how each component is made, instead the main materials used will be listed in Table 11.1 accompanied with an analysis of the main production techniques.

Table 11.1: Several materials allocated component

Material	**Components**
Titanium	Sampling mechanisms
Aluminium	Spacecraft structure
Composite	Solar panels
Pyrotechnics	Separator mechanisms
Aluminium honeycomb	Loading floors

Titanium

Titanium is used for the sampling mechanism of SASH, the main reason for its use is its high strength-to-density ratio. It is used in order to reduce the chances of breaking the sampling mechanism.

In order to manufacture the scoop of the hoverer, milling is the best option. Nowadays technology shows that it is possible to mill titanium with precision without excess of heat that would damage the milling tooling. In order to increase the precision of the machinery, a computer numerically controlled machineres will be employed. The desired shape can be programmed into the machine computer and it will precisely create the part as it chips material away. This kind of production method has been widely used for a long time and can be very precise with the least damage to the piece as possible.

Aluminium

There are many ways to process aluminium; it is one of the most used materials in the aerospace industry due to its low weight and rather low cost. Five examples are given, the first modification of the billet is done through rolling. Rolling is a subclass of the forming processes. This yields usually sheets, plates or foil. It can be seen in Figure 11.1, it makes use of rollers that compress the material in a sheet form that will be used on the spacecraft.

Since many metal alloys such as aluminium are used on the spacecraft, metal forming will be used more often than just rolling. Another method is rubber forming which includes a male or female die against which the material is pressed using a rubber-covered hydraulic press. This method is widely used in industry due to its simplicity and accuracy while not damaging the product. It is used a lot for parts with edges and other structural features. Bending is the general process of rolling, it uses the principle that a sheet can be deformed smoothly while going in the middle of secured rollers, through bending stresses. Stretch forming is another variant of forming that is very efficient to produce sheet with a curvature in two directions. The material is attached on multiple side and stretched while a die come to deform it in the middle. This is seen as in Figure 11.2.

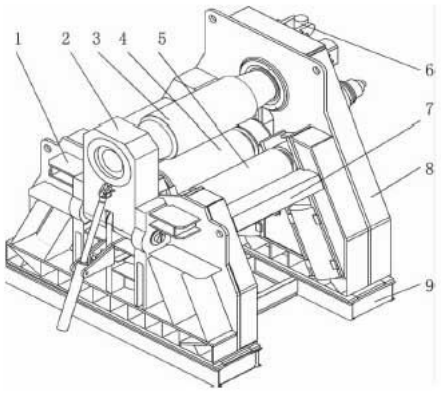

Figure 11.1: Rolling machine

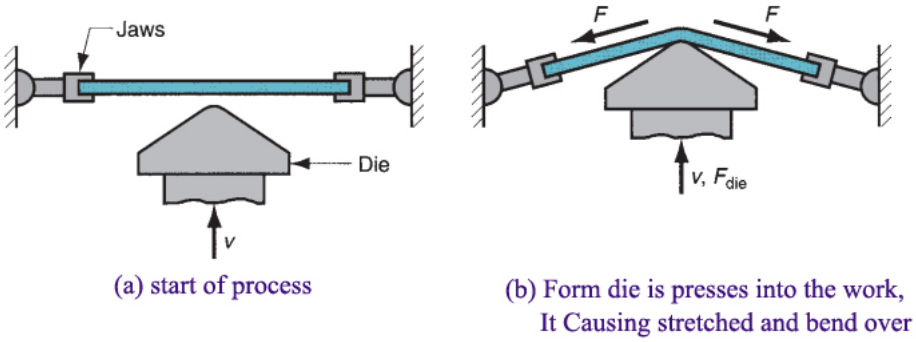

Figure 11.2: Stretch forming process illustration [1]

If the need of making parts with flanges and other fine features arise, deep drawing may be used. It consists of three elements: the punch, the drawing die and the blank holder. The three of the them working together in order to shape parts. To illustrate the process, Figure 11.3 is presented.

And finally there exist many more forming method such as superplastic forming but it was deemed unnecessary to explain them in detail since the others are more widely applicable.

Composites

The solar panel backing is made of composites, while the PV cells themselve are composed of Gallium-Arsenide semiconductor material. A composite is usually made in three ways, either with an open mould, a closed mould or cast polymer moulding. For the open moulding, the composite is set in a open mould and left in there until the resin has hardened. Closed moulding consist of having a vacuum or two-sided mould. Of course, the process is happening in a closed environment. Pulltrusion is also another way to produce composite material as well as pullwinding and continuous lamination.

Pyrotechnics

Pyrotechnics is the art of using materials that have the capacity of a controlled chemical reaction in order to achieve a distinct purpose. In this case it is mostly used in bolts to separate different stages of the spacecraft or deploy subsystems. The bolts that will be used are made of high strength steel and are manufactured in the same manner as explained in the aluminium section. The pressure cartridge that contains the pyrotechnics is made of stainless steel. The workings of this pyrotechnic bolt is that

[1] `http://techminy.com/stretch-forming-process/principle-of-stretch-forming` Accessed June 27, 2018

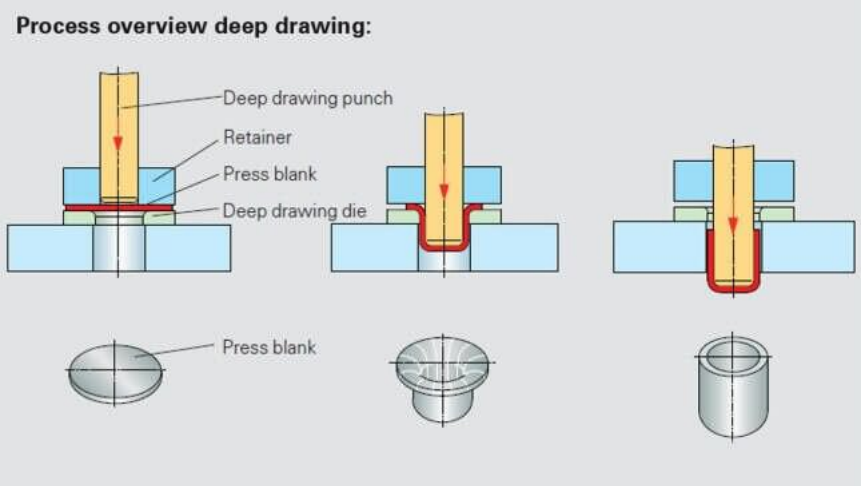

Figure 11.3: Deep drawing process overview.

there is a chamber from which a high pressure is created by reaction of the pyrotechnical components. The bolt also has a so-called weak point that is designed to rupture as the pressure inside is too high.

Honeycomb

Honeycomb structures are often used due to their low weight and high specific strength. There exist multiple ways to fabricate honeycomb structures. An extrusion die can be used to shape the material into a honeycomb-like structure. Also moulds can be used to obtain honeycomb structures. Sandwich panel may be a very attractive material for some parts of the spacecraft where the core, or honeycomb structure in this case, would act against the shear induced while the top and bottom panel are mainly carrying the compressive and tensile stresses. These panels will be used for the component floors.

11.3. Operations

Ground support of a spacecraft is a critical part of every space mission. It involves careful scheduling and cost considerations, as well as risk assessment and complexity analyses. Since these topics have already been touched upon in earlier chapters of this report, this section will mainly focus on the personnel preparing and operating the ground control centre, and the scheduling of tasks that have to be performed during the mission (Uhlig et al. [2015]).

11.3.1. Ground segment preparation

Staff

The organisational structure of the ground segment preparation crew involves multiple people in various roles. They all have specific tasks and responsibilities and a position in the project hierarchy.

The ground segment preparation team includes a management part, as well as a systems engineering and operations department. The overall organisation and management of the project is the responsibility of the project manager. When mission operations start, he/she might become mission director, who is responsible for the mission execution. The mission director is supported by the systems engineer and flight director, who in turn are the heads of the systems engineering and operations department, respectively. The systems engineer takes care of the ground system engineering and supervises the development and technical implementation of the ground segment. The flight director oversees the preparation of the of mission operations. In cooperation with the simulation offices, he/she defines the training effort for the flight operations team and supervises their activities. The flight director works closely together with the systems engineer. Next to that, a quality manager assures compliance to quality standards, both internal and external. Every subsystem of the spacecraft has a dedicated subsystem engineer whose task is to monitor the performance and ensure optimal functioning of their subsystem. To help monitor the project budget, a controller provides reports on the financial aspects of the mission in predefined intervals.

Tools

Designing and verifying a properly functioning ground segment involves a number of tools that have to be developed. This includes a set of test telemetry data or a spacecraft simulator, either a physical or software model or a combination of both. Additionally, command software needs to be implemented to send commands to the spacecraft. Procedures need to be developed

for nominal as well as contingency situations, and everything has to be documented in project documentation, a spacecraft user manual, operational documentation and a ground segment description.

11.3.2. Mission execution

Ground station operations

Once the spacecraft has been launched, inserted into its transfer orbit towards the asteroid and separated from the Falcon 9 upper stage, the mission's ground control will step in. It will be responsible for the spacecraft's operation over the whole span of the mission.

In the first phase, communication has to be established with the spacecraft and a first check of the performance of the systems has to be performed. It is then crucial for the spacecraft to gain attitude control to ensure communication and deploy its solar arrays to allow power generation. After these tasks have been completed, a more elaborate systems check is performed and the spacecraft can be tracked from ground. If necessary, manoeuvring commands can be uplinked to the spacecraft.

During its cruise towards the asteroid (or Earth), the spacecraft is in hibernation mode. It will assume an attitude allowing power generation and homogeneous heat distribution, while still being able to receive commands from Earth.

When the spacecraft is approaching the asteroid and comes out of hibernation, a checkout on subsystem level is performed, including redundant components. Problems arising during checkout are taken into account in risk assessment and future operation planning.

After a successful check of all subsystems, the science mission can start. This part of operation is coded as routine processes in the spacecraft's onboard computer. The ground station is responsible for mission planning as well as tracking its position and monitoring the spacecraft's telemetry. In this specific case, the ground station will also take care of science data analysis and select landing sites.

The reentry phase is a critical stage for the ground segment. After separation of the reentry capsule from the lander of hover spacecraft, no interaction with the sample capsule is possible. Nevertheless, the capsule needs to be tracked as accurately as possible, using its radio beacon and switching to optical tracking once it enters the ionosphere.

11.4. Sensitivity Analysis

Naturally, uncertainties are involved in the production process and logistics setup, as well as the preparation process for the operations segment.

Production is always prone to delays. Regardless of how much systems engineering and careful scheduling is applied, it is very hard to avoid any delays. Contingency measures are taken in terms of buffers in the schedule, but in case this would prove insufficient, there is still the possibility to delay the launch by one year to September 21 of 2026, with negligible decrease in ΔV budget. However, the departure window to leave the asteroid for Earth cannot be changed, hence the mission schedule would need to be compressed. Currently, very large margins are present in the mission planning, so this is not expected to pose a major problem or affect the feasibility to an unacceptable extent.

12
Project design & development

In this chapter the stages of the design and development of the Piazzi mission that will take place after this DSE project are outlined. It starts with giving the logic of the future work packages in a block diagram. After this, the work needed is scheduled. At the end of this chapter a Gantt chart is presented.

12.1. Project design & development logic

The logic of the design and development of the project can be found in Figure 12.1. It shows the activities that have to be undertaken in the phases of the project after this design phase. It is divided in nine work packages, which are grouped into three major phases, the detailed design, the development, and the post-development. These work packages are further worked out, and most work packages are ended with a milestone. It should be noted that some of the activities in the work packages have overlap, and are partly done in parallel. An overview of the scheduling can be found in the next section.

12.2. Gantt chart for post-DSE phases

In Figure 12.2 the phases and their work packages are scheduled, from the end of the DSE until September 2025. Most tasks are dependant on earlier tasks which is depicted using arrows. For most of these dependencies, the next task can start before the task before has ended.

Some comments can be made regarding the scheduling of the work packages. Firstly, acquiring funding will start early during the design phase, and this work package will be completed before the next. However, should there be a delay in acquiring funding, the whole schedule could be delayed. Secondly, from the point that the design is ready to be launched until the start of the launch phase there is a delay. The reason for this is to make sure that in case there is some delay in the schedule, the launch can still continue as planned. Finally, the post-DSE phase ends with the start of operations, on September 19, 2025. More information on this can be found earlier in the report, in chapter 11.

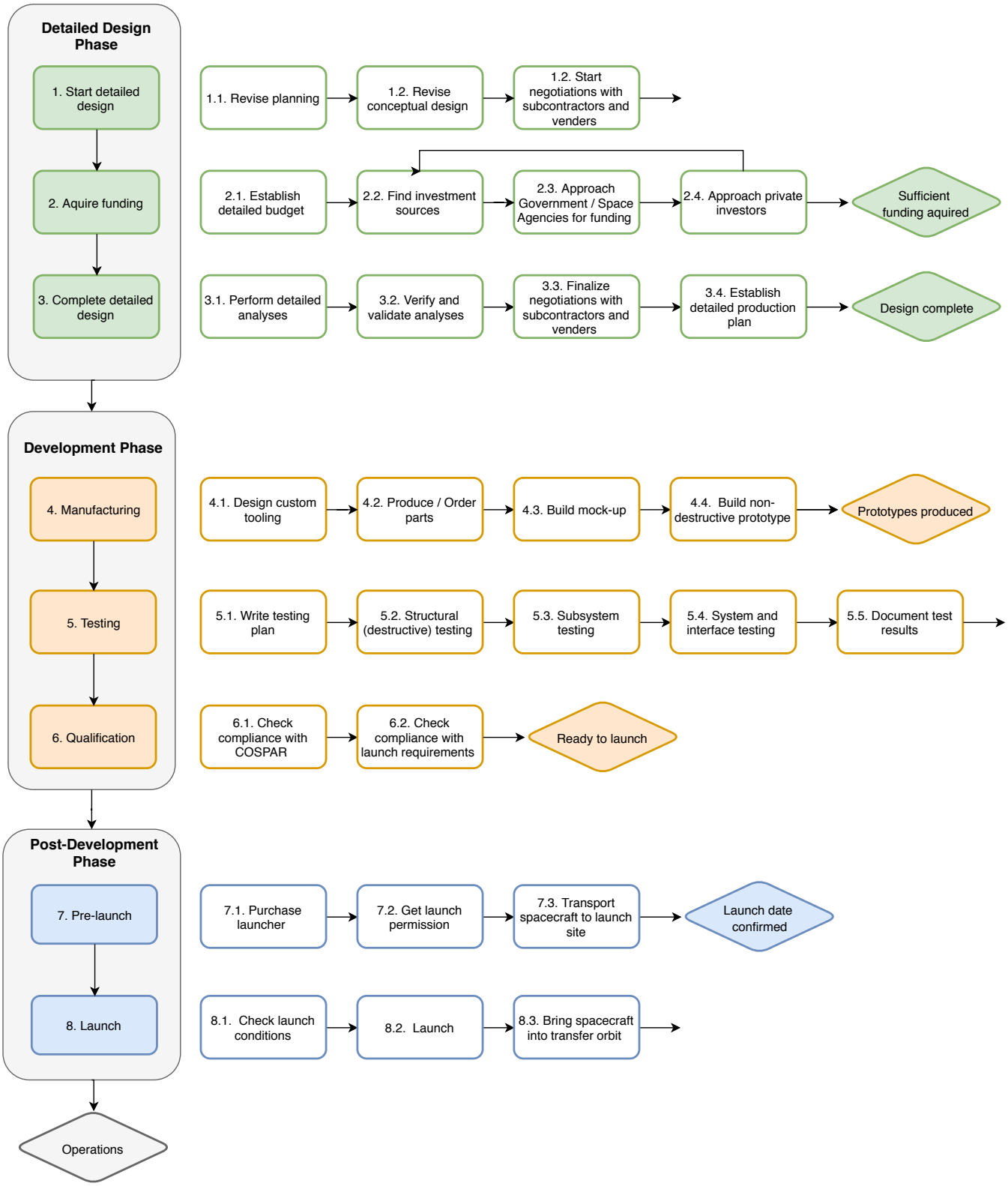

Figure 12.1: Block diagram of the project design & development logic

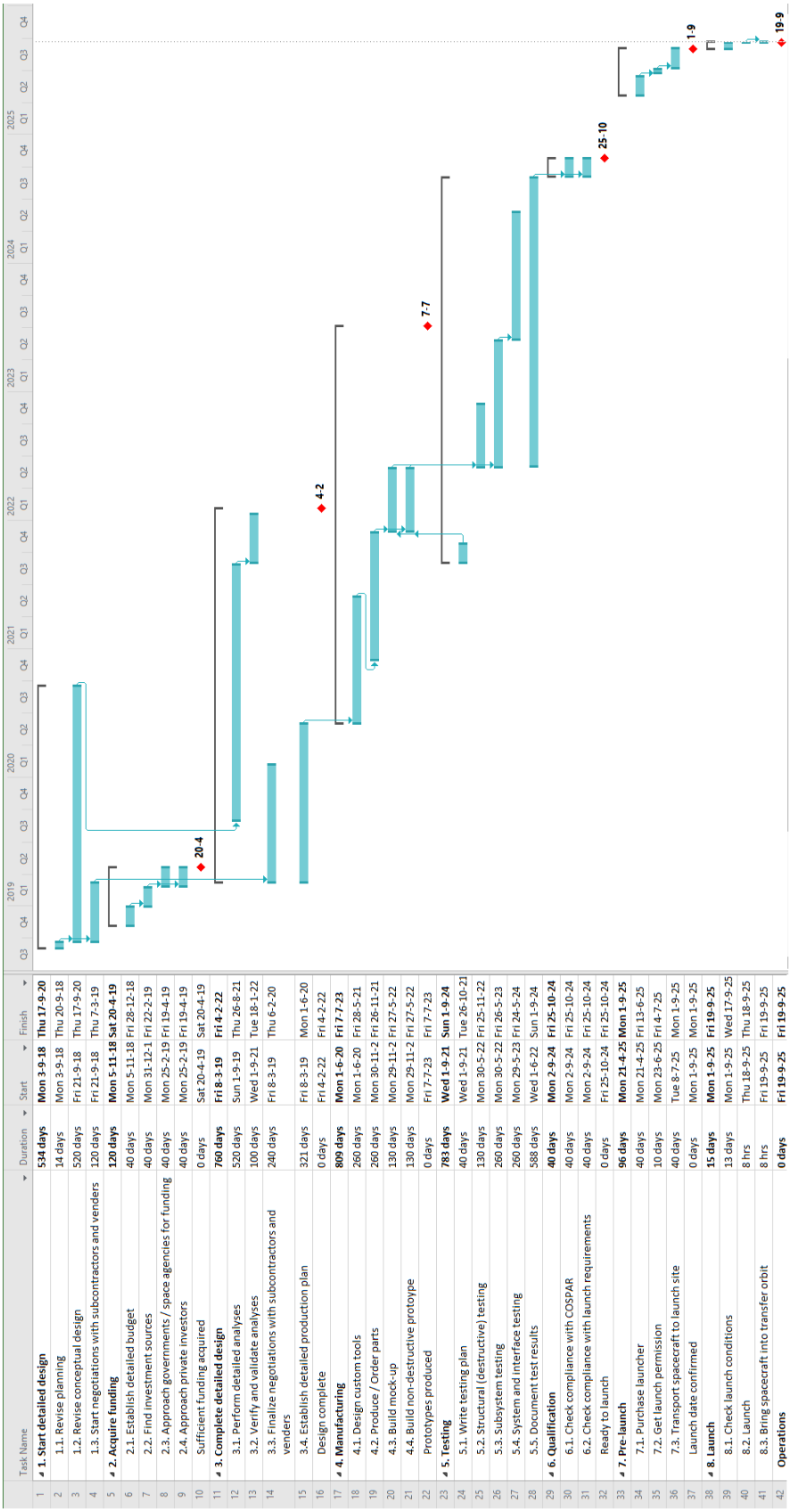

	Task Name	Duration	Start	Finish
1	**1. Start detailed design**	**534 days**	**Mon 3-9-18**	**Thu 17-9-20**
2	1.1. Revise planning	14 days	Mon 3-9-18	Thu 20-9-18
3	1.2. Revise conceptual design	520 days	Fri 21-9-18	Thu 17-9-20
4	1.3. Start negotiations with subcontractors and venders	120 days	Fri 21-9-18	Thu 7-3-19
5	**2. Acquire funding**	**120 days**	**Mon 5-11-18**	**Sat 20-4-19**
6	2.1. Establish detailed budget	40 days	Mon 5-11-18	Fri 28-12-18
7	2.2. Find investment sources	40 days	Mon 31-12-18	Fri 22-2-19
8	2.3. Approach governments / space agencies for funding	40 days	Mon 25-2-19	Fri 19-4-19
9	2.4. Approach private investors	40 days	Mon 25-2-19	Fri 19-4-19
10	Sufficient funding acquired	0 days	Sat 20-4-19	Sat 20-4-19
11	**3. Complete detailed design**	**760 days**	**Fri 8-3-19**	**Fri 4-2-22**
12	3.1. Perform detailed analyses	520 days	Sun 1-9-19	Thu 26-8-21
13	3.2. Verify and validate analyses	100 days	Wed 1-9-21	Tue 18-1-22
14	3.3. Finalize negotiations with subcontractors and venders	240 days	Fri 8-3-19	Thu 6-2-20
15	3.4. Establish detailed production plan	321 days	Fri 8-3-19	Mon 1-6-20
16	Design complete	0 days	Fri 4-2-22	Fri 4-2-22
17	**4. Manufacturing**	**809 days**	**Mon 1-6-20**	**Fri 7-7-23**
18	4.1. Design custom tools	260 days	Mon 1-6-20	Fri 28-5-21
19	4.2. Produce / Order parts	260 days	Mon 30-11-2	Fri 26-11-21
20	4.3. Build mock-up	130 days	Mon 29-11-2	Fri 27-5-22
21	4.4. Build non-destructive protoype	130 days	Mon 29-11-2	Fri 27-5-22
22	Prototypes produced	0 days	Fri 7-7-23	Fri 7-7-23
23	**5. Testing**	**783 days**	**Wed 1-9-21**	**Sun 1-9-24**
24	5.1. Write testing plan	40 days	Wed 1-9-21	Tue 26-10-21
25	5.2. Structural (destructive) testing	130 days	Mon 30-5-22	Fri 25-11-22
26	5.3. Subsystem testing	260 days	Mon 30-5-22	Fri 26-5-23
27	5.4. System and interface testing	260 days	Mon 29-5-23	Fri 24-5-24
28	5.5. Document test results	588 days	Wed 1-6-22	Sun 1-9-24
29	**6. Qualification**	**40 days**	**Mon 2-9-24**	**Fri 25-10-24**
30	6.1. Check compliance with COSPAR	40 days	Mon 2-9-24	Fri 25-10-24
31	6.2. Check compliance with launch requirements	40 days	Mon 2-9-24	Fri 25-10-24
32	Ready to launch	0 days	Fri 25-10-24	Fri 25-10-24
33	**7. Pre-launch**	**96 days**	**Mon 21-4-25**	**Mon 1-9-25**
34	7.1. Purchase launcher	40 days	Mon 21-4-25	Fri 13-6-25
35	7.2. Get launch permission	10 days	Mon 23-6-25	Fri 4-7-25
36	7.3. Transport spacecraft to launch site	40 days	Tue 8-7-25	Mon 1-9-25
37	Launch date confirmed	0 days	Mon 1-9-25	Mon 1-9-25
38	**8. Launch**	**15 days**	**Mon 1-9-25**	**Fri 19-9-25**
39	8.1. Check launch conditions	13 days	Mon 1-9-25	Wed 17-9-25
40	8.2. Launch	8 hrs	Thu 18-9-25	Thu 18-9-25
41	8.3. Bring spacecraft into transfer orbit	8 hrs	Fri 19-9-25	Fri 19-9-25
42	**Operations**	**0 days**	**Fri 19-9-25**	**Fri 19-9-25**

Figure 12.2: Gantt chart of the schedule of the post-DSE design and development.

13
Conclusion & recommendations

In 11 weeks, ten students managed to develop a preliminary design for a mission to an asteroid, where two samples will be collected and returned to Earth. The design takes into account all aspects of a mission and the most important parts of every subsystem are designed and in the end, a closing budget is found to fulfil the mission. Several models are set up and validated in order to get visual or time-dependent estimates, helping to sketch an image of the spacecraft.

Next to these technical aspects, several other aspects have been studied and discussed: risk, reliability, and cost. This was done in order to ensure the mission's feasibility.

Even though this project has reached its end, the design process certainly has not. There is a long design process still ahead. A more detailed design needs to be created before production can start: every part of the spacecraft needs to worked out in full detail. Next, some recommendations for the continuation of the project will be given. These recommendations are based on findings from the team during this phase.

First and foremost, more design iterations should be carried out. It is strongly recommended to automate this process as much as possible, so that communicative issues will not influence the design.

Secondly, the team should consider the order in which the subsystems will be designed and how these will be iterated. Implying a well-defined method for concurrent engineering may decrease iterations required for the design, decreasing design cost.

Thirdly, in order to provide more detailed estimates, more companies or institutions should be contacted in order to provide more accurate values for several components. Especially, for example, cost can be further detailed in this manner.

After designing, it is time for development and deployment. In these processes, further detailed in the report, custom tooling needs to be developed after which all the components need to be produced and assembled. After this, testing shall be required and the system shall undergo a qualification process to check all system's compliance. Lastly, the launch shall be prepared and executed, after which the spacecraft will be deployed.

Bibliography

4, I. W. G. "IADC Space Debris Mitigation Guidelines". Technical report, Inter-Agency Space Debris Coordination Committee, 2007.

Agnolon, D. "Study Overview of the Near Earth Sample Return". Technical Report SCI-PA/2007/004/DA, "ESTEC, ESA", Noordwijk, The Netherlands, May 2007.

Angyal, Z., Doppenberg, W., den Hertog, K., et al. "ASRM Midterm Report". Technical report, Delft University of Technology, Delft, The Netherlands, June 2018.

Bollendonk, G. "Planetary Spacecraft FSW Workshop on Spacecraft Flight Software". Lockheed Martin Space Systems Company, October 2015.

Boynton, W., Feldman, W., Mitrofanov, I., et al. The Mars Odessey Gamma-Ray Spectrometer Instrument Suite. *Space Science Reviews*, Vol. 110, 2004, pp. 37–83. doi:10.1023/B:SPAC.0000021007.76126.15.

Bruzzi, J. R., Strohbehn, K., Boone, B. G., et al. A Compact Laser Altimeter for Spacecraft Landing Applications. *Johns Hopkins Apl Technical Digest*, Vol. 30, No. 4, 2012, pp. 331–345.

Bruzzi, J. R., Strohbehn, K., Boone, B. G., et al. Prediction of Thrust Force and Torque In Drilling on Aluminium. *IJERT International Journal of Engineering Research and Technology*, Vol. 1, March 2013, pp. 6.

Carbognani, A. The spin-barrier ratio for S and C-type main asteroids belt. *Planetary and Space Science*, Vol. 147, 2017, pp. 1 – 5. doi:https://doi.org/10.1016/j.pss.2017.07.019.

Carlson, R., Weissman, P., Smythe, W., et al. Near-Infrared Mapping Spectrometer experiment on Galileo. *Space Science Reviews*, Vol. 60, No. 1-4, 1992, pp. 457–502. doi:10.1007/BF00216865.

Carr, C., Cupido, E., Lee, C., et al. RPC: The Rosetta Plasma Consortium. *Space Science Reviews*, Vol. 128, 2007, pp. 629–647. doi:10.1007/s11214-006-9136-4.

Clark, B. C. Survival of life on asteroids, comets and other small bodies. *Origins of Life and Evolution of Biospheres*, Vol. 29, 1999, pp. 521–545. doi:10.1023/A:1006589213075.

Coradine, A., Capaccioni, F., Drossart, P., et al. Virtis: an imaging spectrometer for the rosetta mission. *Planetary and Space Science*, Vol. 46, No. 9-10, 1998, pp. 1291–1304. doi:10.1016/S0032-0633(98)00025-7.

De Sanctis, M., Coradini, A., Ammannito, G., et al. The VIR Spectrometer. *Space Science Reviews*, Vol. 163, 1992, pp. 329–369. doi:10.1007/s11214-010-9668-5.

ECSS Secretariat. "Space product assurance: Failure modes, effects (and criticality) analysis (FMEA/FMECA)". Technical Report ECSS-Q-ST-30-02C, ESA-ESTEC, March 2009.

Elkins-Tanton, L. T., Asphaug, E., Bell, J., Bercovici, D., Bills, B. G., Binzel, R. P., Bottke, W. F., Jun, I., Marchi, S., Oh, D., Polanskey, C. A., Weiss, B. P., Wenkert, D., and Zuber, M. T. Journey to a Metal World: Concept for a Discovery Mission to Psyche. In *Lunar and Planetary Science Conference*, volume 45, pp. 1253, March 2014. doi:10.1109/AERO.2017.7943771.

Ercoli Finzi, A., Bernelli Zazzera, F., Dainese, C., et al. "SD2 - How To Sample A Comet". *Space Science Reviews*, Vol. 128, No. 1-4, 2007, pp. 281–299. doi:10.1007/s11214-006-9134-6.

Foster, C. and Frost, C. "NASA Ames Research Center Trajectory Browser". In *"NASA Ames Web-based Trajectory Generation Tool [online database]"*, 2018. URL: https://trajbrowser.arc.nasa.gov, [cited 15 May 2018].

Gill, E. Verification and Validation for the Attitude and Orbit Control System. In *AE3211-I: Systems Engineering and Aerospace Design*. Faculty of Aerospace Engineering, Delft University of Technology, Delft, 2018.

Gladstone, G., Persun, S., Eterno, J., et al. The Ultraviolet Spectrograph on NASA's Juno Mission. *Space Science Reviews*, Vol. 213, 2017, pp. 447–473. doi:10.1007/s11214-014-0040-z.

Godard, B., Budnik, F., Munoz, T., et al. "Orbit Determination of Rosetta around Comet 67P/Churyumov-Gerasimenko". In *ISSFD*, International Symposium on Space Flight Dynamic. Munich, Germany, 2015.

Goldsten, J., Rhodes, E., Boynton, W., et al. The MESSENGER Gamma-Ray and Neutron Spectrometer. *Space Science Reviews*, Vol. 131, 2007, pp. 339–391. doi:10.1007/s11214-007-9262-7.

Griffin, M. and French, J. *Space Vehicle Design*, 2 ed. American Institute of Aeronautics and Astronautics, Reston, Virginia, 2004.

Grinstead, J., Jenniskens, P., Cassel, A. M., et al. "Airborne Observation of the Hayabusa Sample Return Capsule Re-entry". In *42nd AIAA Thermophysics Conference*. *42nd AIAA Thermophysics Conference*, AIAA, Hawaii, HI, 2011. pp. 1-11.

Hahn, G. and Mottola, S. "The Near-Earth Asteroids Data Base". In *"Data Base of Physical and Dynamical Properties of Near Earth Asteroids (NEAs) [online database]"*. DLR, 2018. URL: http://earn.dlr.de/nea/, [cited 8 May 2018].

Hamann, R. J. and Van Tooren, M. "Systems Engineering and Technical Management Techniques - Part II". Technical report, "TU Delft, Aerospace Engineering", Delft, The Netherlands, January 2006.

Henderson, M. and Blume, W. Deep Impact – A Review of the World's Pioneering Hypervelocity Impact Mission. *Procedia Engineering*, Vol. 103, 2015, pp. 165 – 172. doi:https://doi.org/10.1016/j.proeng.2015.04.023.

Holdridge, M. E. NEAR Shoemaker Spacecraft Mission Operations. *Johns Hopkins APL technical digest*, Vol. 23, 2002, pp. 58–70.

Hord, C., McClintock, W., Stewart, A., et al. Galileo Ultraviolet Spectrometer Experiment. *Space Science Reviews*, Vol. 60, 1992, pp. 503–530. doi:10.1007/BF00216866.

IL J. Furness, C. L. W. DYNAMIC MODELING OF THE THRUST FORCE AND TORQUE FOR DRILLING. *1992 American Control Conference*, Vol. 1 and 2, 1992, pp. 7. doi:10.23919/ACC.1992.4792094.

Jordan, J. F. "The Application of Lambert's Theorem to the Solution of Interplanetary Transfer Problems". Technical Report 32-521, "Jet Propulsion Laboratory, California Institute of Technology", Pasadena, California, February 1964.

Kauder, L. "Spacecraft Thermal Control Coatings References". Technical Report NASA/TP–2005–212792, "NASA Center for AeroSpace Information ", Hanover, MD, December 2005.

Kawaguchi, J., Uesugi, K. T., Fujiwara, A., and Saitoh, H. The MUSES-C, mission description and its status. *Acta Astronautica*, Vol. 45, No. 4, 1999, pp. 397 – 405. doi:https://doi.org/10.1016/S0094-5765(99)00159-9.

Keller, H., Barbieri, C., Lamy, P., et al. OSIRIS - The Scientific Camera System Onboard Rosetta. *Space Science Reviews*, Vol. 128, No. 1-4, February 2007. doi:10.1007/s11214-006-9128-4.

Kendall, R. "Evolved Expendable Launch Vehicle Standard Interface Specification". Technical Report 6, "Evolved Expendable Launch Vehicle Program Office", September 2000.

Kraus, J. D. *Antennas*, 3^{rd} ed. McGraw-Hill Book Co., New York, NY., 1997.

Masterson, R., Chodas, M., Bayley, L., et al. Regolith X-Ray Imaging Spectrometer (REXIS) Aboard the OSIRIS-REx Asteroid Sample Return Mission. *Space Science Reviews*, Vol. 214, 2018, pp. 48. doi:10.1007/s11214-018-0483-8.

McClintock, W., Schneider, N., Holsclaw, G., et al. The Imaging Ultraviolet Spectrograph (IUVS) for the MAVEN Mission. *Space Science Reviews*, Vol. 195, No. 1-4, 2015, pp. 75–124. doi:10.1007/s11214-014-0098-7.

Mills, D., Jones, M. G., and Agarwal, V. *Handbook of Pneumatic Conveying Engineering*, 1^{st} ed. Marcel Dekker, Inc., New York, Basel, 2004.

MOOG Space and Defense Group. Monopropellant Thrusters, 2018. URL `http://www.moog.com/content/dam/moog/literature/Space_Defense/Spacecraft/Monopropellant_Thrusters_Rev_0613.pdf`.

Mosher, T., Lao, N., and Davalos, E. A comparison of NEAR actual spacecraft costs with three parametric cost models. *Acta Astronautica*, Vol. 45, No. 4-9, 1999, pp. 457–464. doi:10.1016/S0094-5765(99)00165-4.

Mueller, M. Surface Properties of Asteroids from Mid-Infrared Observations and Thermophysical Modelling. *ArXiv e-prints*, August 2012. doi:10.1111/j.1945-5100.2002.tb01174.x.

National Research Council. *Evaluating the Biological Potential of Samples Returned from Planetary Satellites and Small Solar System Bodies: Framework for Decision Making*. The National Academies Press, Washington, DC, 1998. doi:10.17226/6281.

Nicholson, W. L., Schuerger, A. C., and Setlow, P. The solar UV environment and bacterial spore UV resistance: considerations for Earth-to-Mars transport by natural processes and human spaceflight. *Mutation Research/Fundamental and Molecular Mechanisms of Mutagenesis*, Vol. 571, No. 1, 2005, pp. 249 – 264. ISSN 0027-5107. doi:https://doi.org/10.1016/j.mrfmmm.2004.10.012.

Picone, J., Hedin, A., and Drop, D. NRLMSISE-00 empirical model of the atmosphere:Statistical comparisons and scientific issues. *Journal of Geophysical Research Atmosphere*, Vol. 107, No. A12, December 2002. doi:10.1029/2002JA009430.

Reuter, D., Simon, A., Hair, J., et al. The OSIRIS-REx Visible and InfraRed Spectrometer (OVIRS): Spectral Maps of the Asteroid Bennu. *Space Science Reviews*, Vol. 214, 2018, pp. 54. doi:10.1007/s11214-018-0482-9.

Rizk, B., Drouet d'Aubigny, C., Golish, D., et al. OCAMS: The OSIRIS-REx Camera Suite. *Space Science Reviews*, Vol. 214, No. 1, February 2018. doi:10.1007/s11214-017-0460-7.

Rummel, J. D. "Planetary protection overview: the role of COSPAR in international missions". In *COSPAR*, COSPAR Panel on Planetary Protection, East Carolina University. Greenville, NC, USA, 2011. doi:10.1002/9780470015902.a0004034.pub2.

Russell, C. and Raymond, C. (ed.). *The Dawn Mission to Minor Planets 4 Vesta and 1 Ceres*. Springer Science+Business Media, New York, NY, 2012.

Schlemm II, C., Starr, R., Ho, G., et al. The X-Ray Spectrometer on the MESSENGER Spacecraft. *Space Science Reviews*, Vol. 131, 2007, pp. 393–415. doi:10.1007/s11214-007-9248-5.

Sierks, H., Keller, H., Jaumann, R., et al. The Dawn Framing Camera. *Space Science Reviews*, Vol. 163, No. 1-4, December 2011, pp. 457–464. doi:10.1007/s11214-011-9745-4.

Space Exploration Technologies Corporation. "Falcon 9 Launch Vehicle Payload User's Guide". Technical report, "SpaceX", Hawthorne, California, 2009.

Stern, S. A., Slater, D. C., Scherrer, J., et al. ALICE: The Ultraviolet Imaging Spectrograph Aboard the New Horizons Pluto–Kuiper Belt Mission. *Space Science Reviews*, Vol. 140, No. 1-4, August 2008, pp. 155–187. doi:10.1007/s11214-008-9407-3.

Stubbs, T., Vondrak, R., and Farrell, W. Impact of Dust on Lunar Exploration. Technical report, Solar System Exploration Division, NASA Goddard Space Flight Center, Greenbelt, Maryland, January 2007.

Tapley, B., Ries, J., Watkins, M., and Marshall, J. The Joint Gravity Model 3. *Journal of Geophysical Research Atmosphere*, Vol. 1012, No. B12, December 1996, pp. 28029–28050. doi:10.1029/96JB01645.

Tetzman, D. G. "Simulation and Optimization of Spacecraft Re-entry Trajectories". Technical report, "University of Minnesota", May 2010.

The Consultative Committee for Space Data Systems. "Report Concerning Space Data System Standards: Image Data Compression", February 2015.

Tolamatic Inc. "SLS RODLESS SCREW DRIVE ACTUATOR - Part Sheet", 2018.

Uhlig, T. et al. *Spacecraft Operations*. Springer-Verlag, Vienna, 2015. doi:10.1007/978-3-7091-1803-0_2.

Van den Abbeele, B., Angyal, Z., Doppenberg, W., et al. "ASRM Baseline Report". Technical report, Delft University of Technology, Delft, The Netherlands, May 2018a.

Van den Abbeele, B., Angyal, Z., Doppenberg, W., et al. "ASRM Project Plan". Technical report, Delft University of Technology, Delft, The Netherlands, May 2018b.

Wertz, J., Everett, D., and Puschell, J. (ed.). *Space Mission Engineering: The New SMAD*. Microcosm Press, Hawthorne, CA, 2011.

Zandbergen, B. T. C. Part: Spacecraft (bus) design and sizing. In *AE1222-II: Aerospace Design & Systems Engineering Elements I*. Faculty of Aerospace Engineering, Delft University of Technology, Delft, 2012. pp. 175-192.

A

Functional flow diagrams and functional breakdown diagrams

The functional flow diagrams and the functional breakdown diagrams are given in this appendix. The functional flow diagram has to be separated over two pages in order to fit. The first level is omitted for clarity, being 'perform mission'. The broken down functions are listed in a single column, after which their function flows to the right again. The functional breakdown diagrams are structured as AND-trees. Every function is the sum of the function below that.

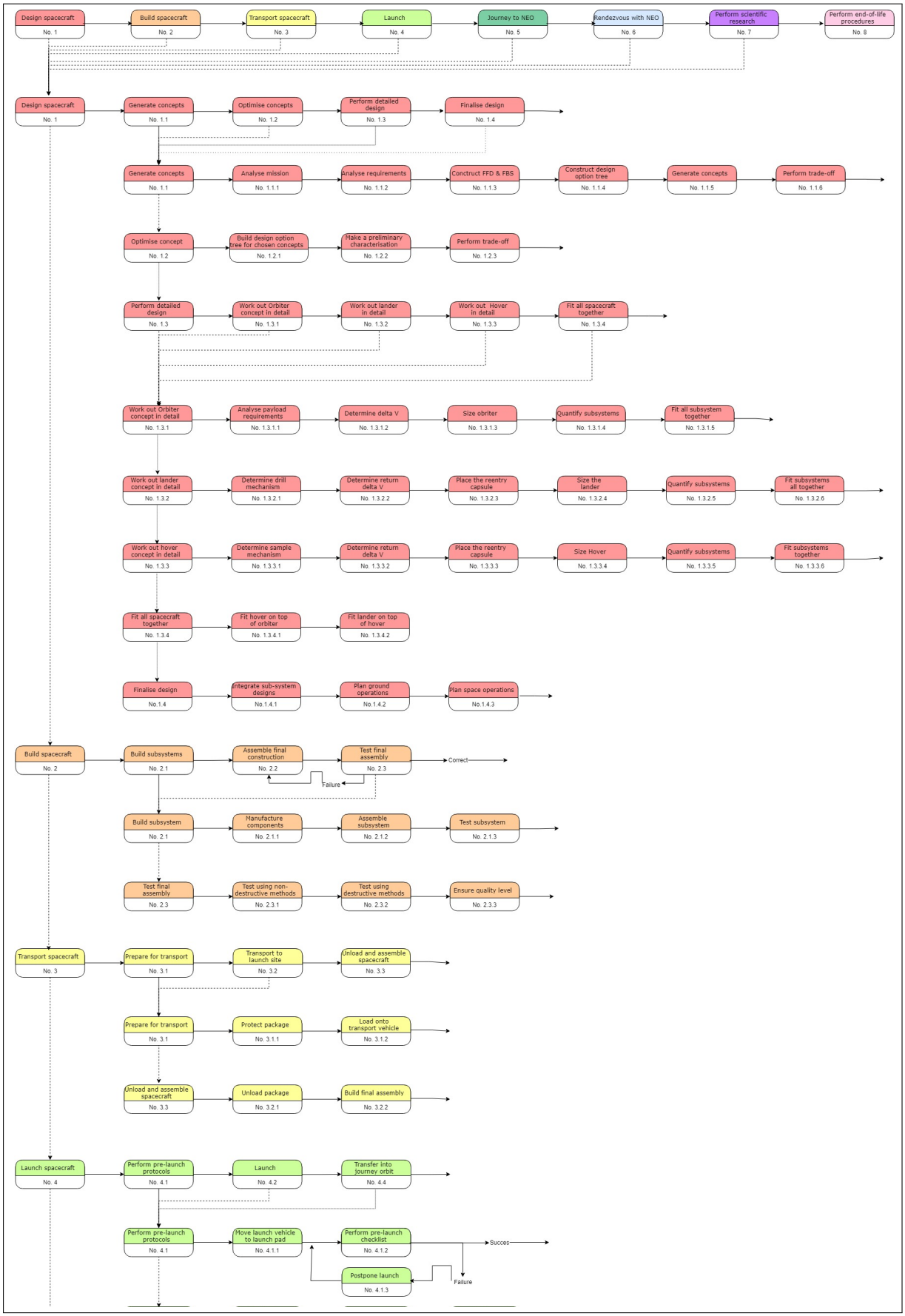

Figure A-1: Functional flow diagram of the Piazzi mission.

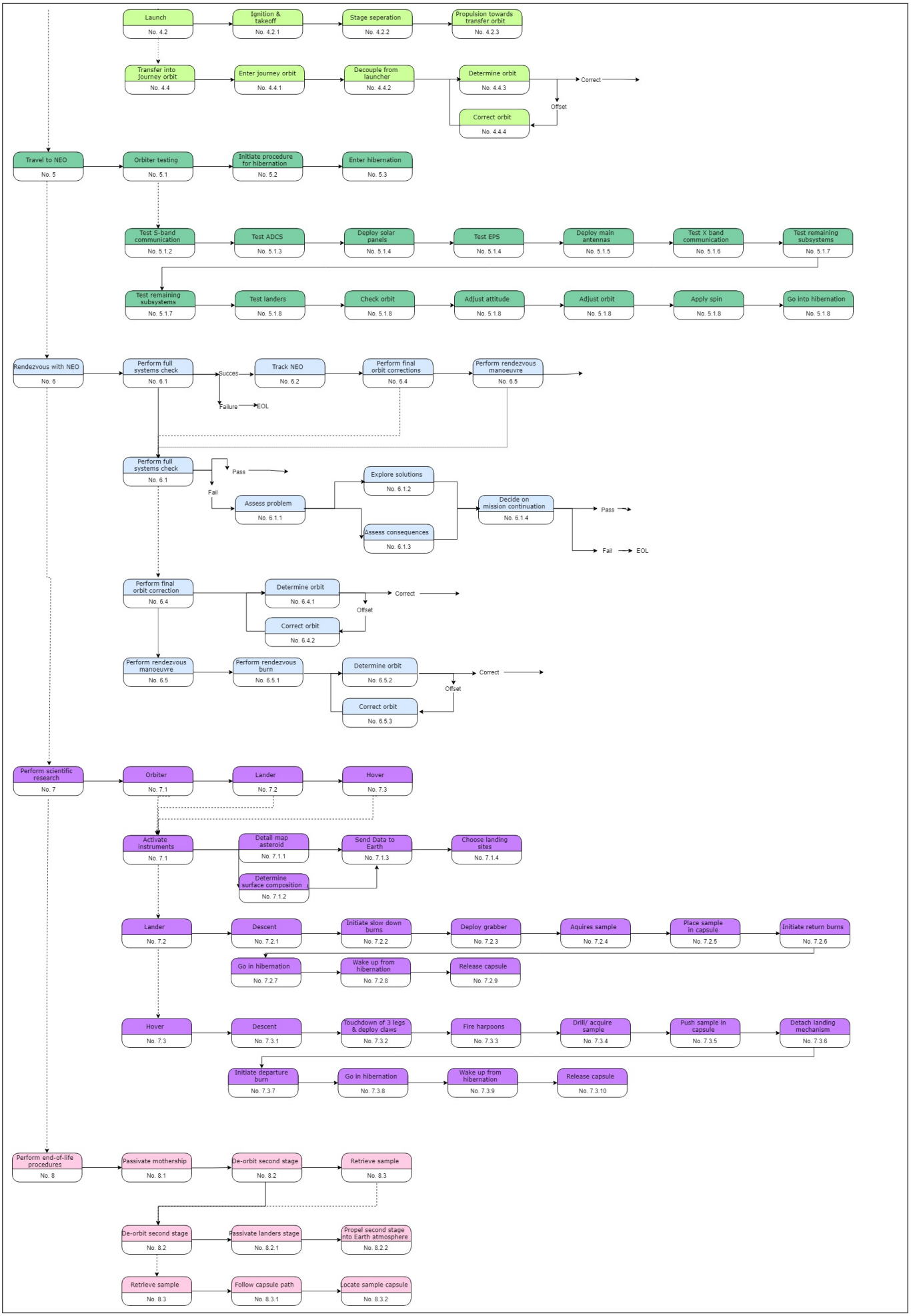

Figure A-2: Functional flow diagram of the Piazzi mission.

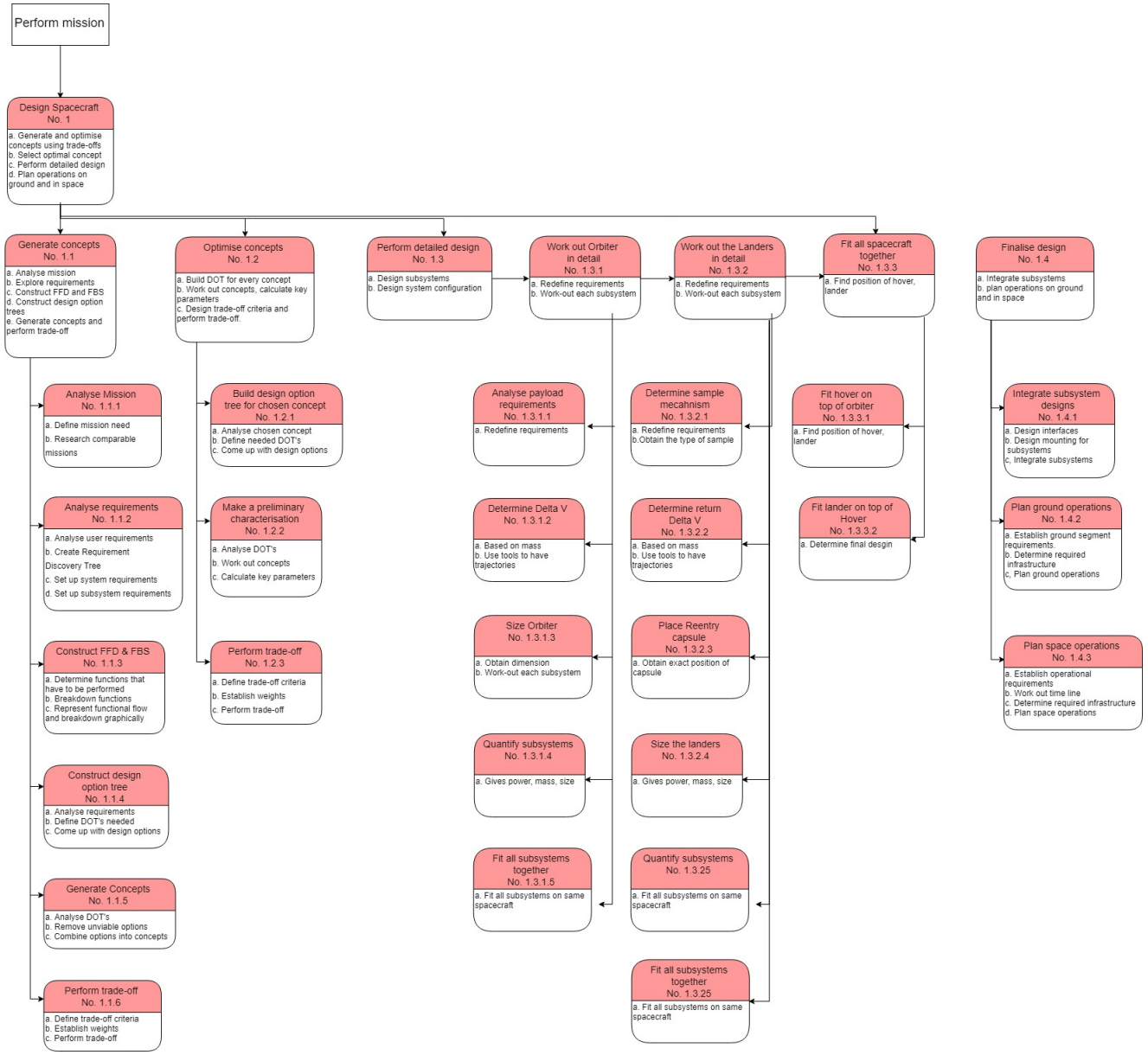

Figure A-3: Functional breakdown structure of the design of the spacecraft.

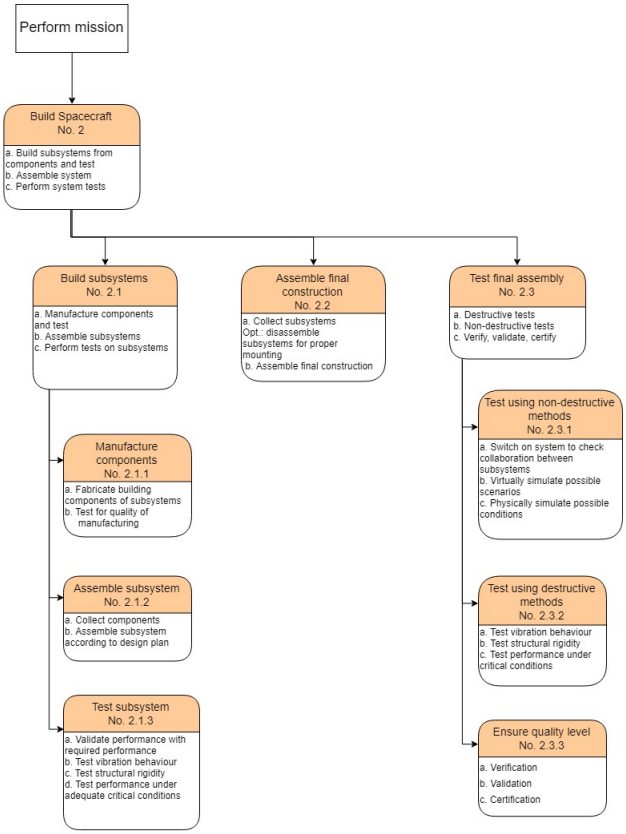

Figure A-4: Functional breakdown structure of the manufacturing process of the spacecraft.

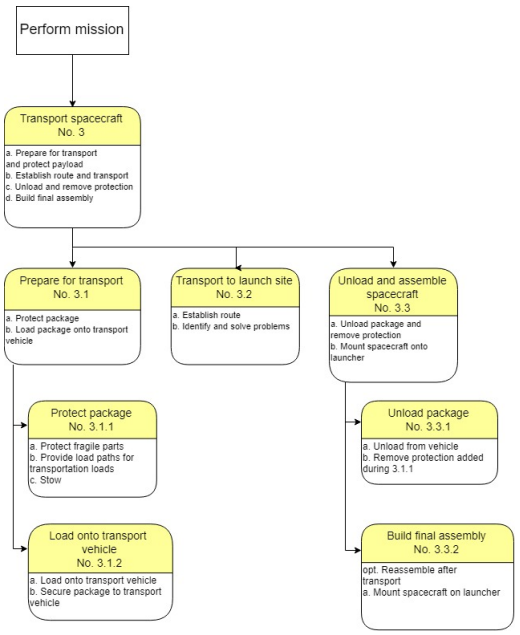

Figure A-5: Functional breakdown of the transport process of the spacecraft.

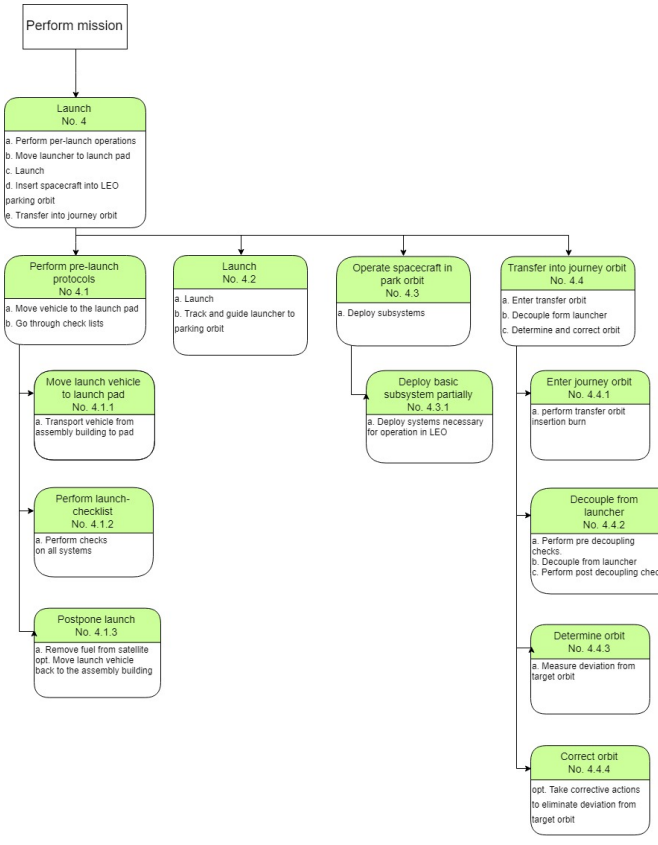

Figure A-6: Functional breakdown of the launch of the spacecraft.

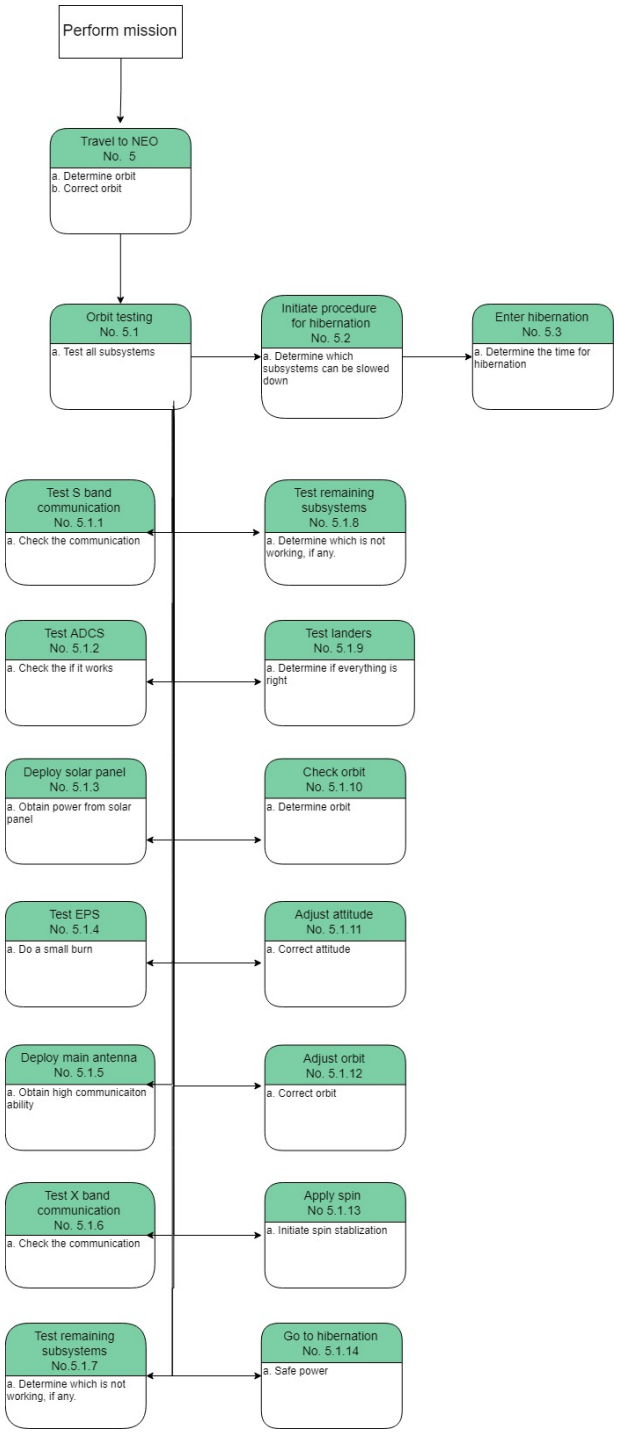

Figure A-7: Functional breakdown of the travel process of the spacecraft to the asteroid.

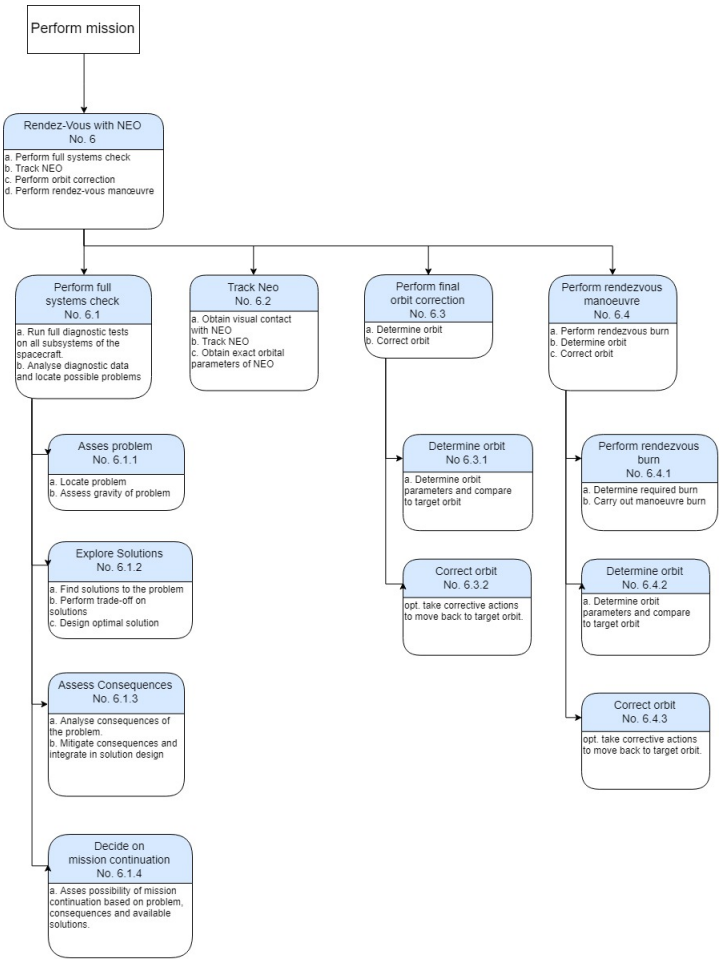

Figure A-8: Functional breakdown of the rendezvous phase of the spacecraft.

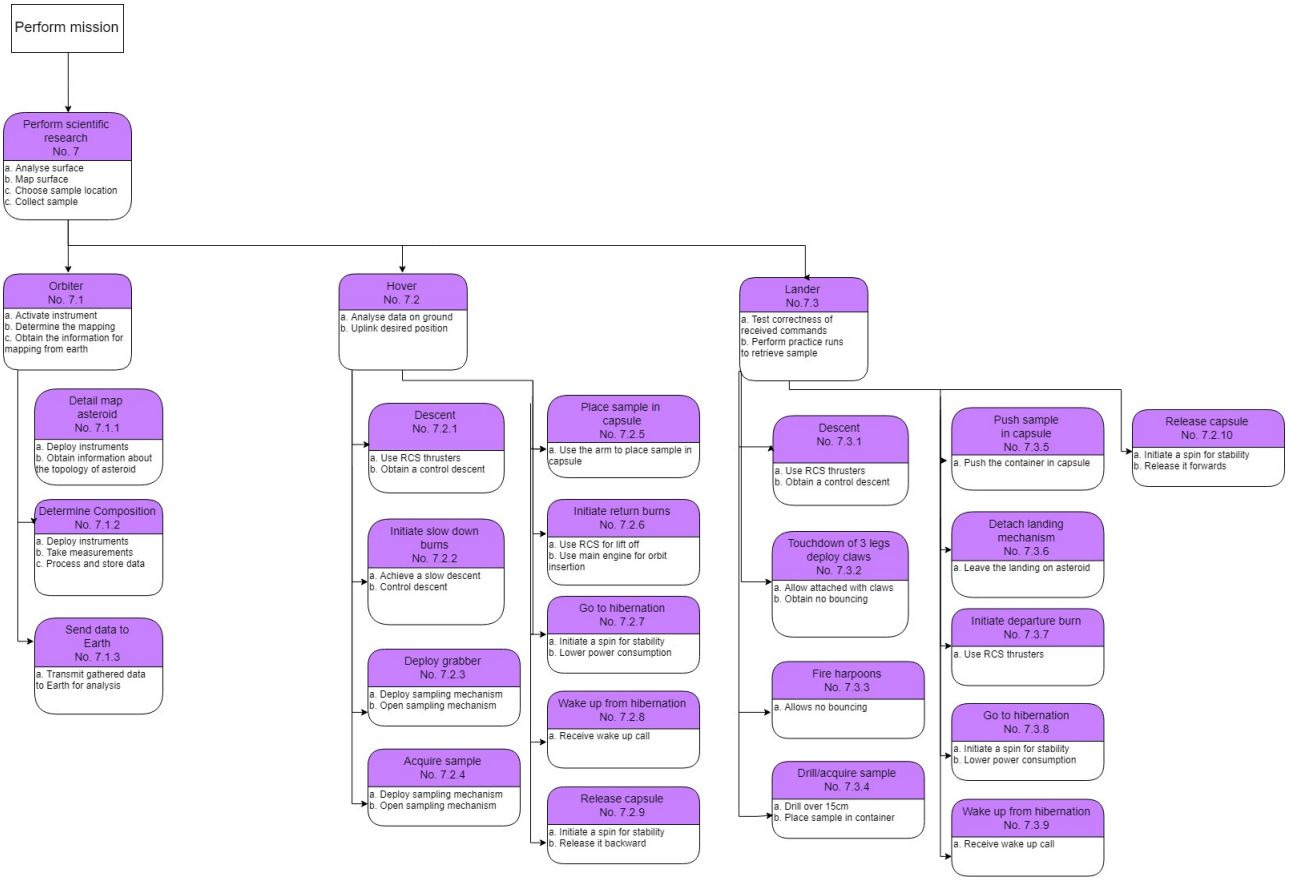

Figure A-9: Functional breakdown of the scientific research.

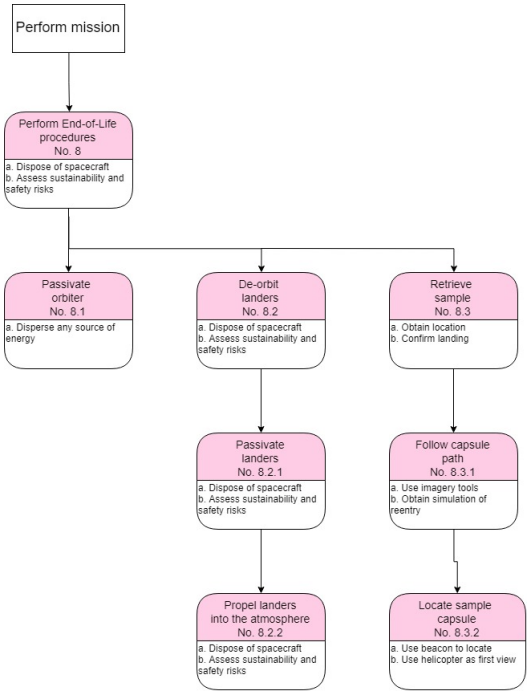

Figure A-10: Functional breakdown of the end of life process of the spacecraft.

B
Work division

Chapter	Section	Completed by
Preface	-	Koen
Summary	-	Koen
Introduction	-	Lex
Market Analysis	-	Andreas
Sustainability	-	Valentin
Project Overview and System Design	Project Mission	Koen
Project Overview and System Design	Concept Trade-Off Midterm Phase	Koen
Project Overview and System Design	Asteroid 1989 UQ	Koen
Project Overview and System Design	Verification & Validation	Koen, Stefan
Project Overview and System Design	Compliance Matrix	Lex
Final Design Overview	Functional Analysis	Valentin
Final Design Overview	Technical Budgets	Koen
Final Design Overview	Cost Analysis	Koen, Lex
Mission Overview	Timeline	Koen
Mission Overview	Astrodynamics	Arthur, Bert
Mission Overview	Asteroid Mapping Phase	Bruno, Koen, Arthur
Mission Overview	Launcher	Arthur
Mission Analysis	Reentry	Koen, Bruno
Spacecraft	Orbiter	Stefan, Andreas
Spacecraft	Observation Instruments	Koen, Bruno
Spacecraft	Lander	Zalan, Bert, Lex
Spacecraft	Hover	Valentin , Arthur, Wouter
Subsystems	Structural	Andreas
Subsystems	EPS	Wouter
Subsystems	Propulsion	Andreas , Stefan
Subsystems	ADCS	Stefan
Subsystems	Thermal	Zalan
Subsystems	TT&C	Wouter
Subsystems	CD&H	Zalan, Bruno
Risk Assessment	-	Lex
RAMS Analysis	-	Arthur
Operations & Production	Logistics	Valentin
Operations & Production	Production Plan	Valentin
Operations & Production	Operations	Bert
Project Design & Development	Project Design & Development Logic	Koen, Lex
Project Design & Development	Gantt Chart for post DSE phases	Koen
Conclusion & Recommendations		Stefan
Sensitivity Analysis	-	Valentin
Visualisation	CATIA & Renders	Andreas
Visualisation	Poster & Front page renders	Bruno